SYNTHESIS AND CHARACTERIZATION OF PANI/PEANI CONDUCTING POLYMERS-Au/Ag NANOPARTICLE COMPOSITES

A THESIS

Submitted for the Degree of

Doctor of Philosophy

2013

Sujata Vohra

Roll No. 950809004

School of Chemistry and Biochemistry

Thapar University

Patiala

CERTIFICATE

Certified that the thesis entitled "SYNTHESIS AND CHARACTERIZATION OF PANI/PEANI CONDUCTING POLYMERS-Au/Ag NANOPARTICLE COMPOSITES" being submitted by Ms. Sujata Vohra to the School of Chemistry and Biochemistry, Thapar University, Patiala (Punjab), India in fulfillment of the requirement for the award of degree of Doctor of Philosophy is a record of bonafide research work carried out by her. The matter presented in this thesis does not incorporate any material previously published or written by any other person except where due reference is made in the text.

The results obtained in this thesis have not been submitted in part or full to any other institute or university for the award of degree or diploma.

Madan Lal Singla

Supervisor
Dr.M L Singla
Ex-Chief Scientist & Head Agrionics
Central Scientific Instruments Organisation
Sector 30, Chandigarh

Susheel Mittal 5.5.14

Supervisor
Dr. Susheel Mittal
Senior Professor
School of Chemistry & Biochemistry
Thapar University, Patiala

DECLARATION

Certified that the thesis is entirely my own and that the ideas and references cited herein have been duly acknowledged.

Sujata

(SUJATA VOHRA)

Attestation by Supervisors

Madan Lal Singla

Supervisor
Dr.M L Singla
Ex-Chief Scientist & Head Agrionics
Central Scientific Instruments Organisation
Chandigarh

Susheel Mittal 5.5.14

Supervisor
Dr. Susheel Mittal
Senior Professor
School of Chemistry & Biochemistry
Thapar University, Patiala

ACKNOWLEDGEMENTS

First of all, I would like to acknowledge the Almighty for blessing me with strength and wisdom throughout my research work.

Completion of this doctoral dissertation was possible with the support of several people. This thesis has been kept on track and been seen through to completion with the support and encouragement of my well wishers, my friends, colleagues and various institutions. At this juncture, it is a very pleasant task to express thanks to all those who made it possible for me to complete this thesis with their contribution in different ways.

I am extremely indebted to my supervisors **Dr. ML Singla**, Ex- Chief Scientist & Head Agrionics Division, Central Scientific Instruments Organisation (CSIO) Chandigarh and **Dr. Susheel Mittal**, Senior Professor, School of Chemistry & Biochemistry, Thapar University, Patiala for their valuable guidance, scholarly inputs and consistent encouragement which I have received throughout the research work. **Dr. Singla,** despite his busy schedules, has always made himself available to clarify my doubts which provided good and smooth basis for my Ph.D. I have learnt a lot from him at all stages of this thesis. I would also like to thank him for being an open person to ideas, and for encouraging and helping me to shape my interest and ideas. **Dr. Mittal** has also been very supportive and I consider it as a great opportunity to complete my doctoral programme under his guidance. I simply could not wish for better supervisors. Under their guidance I successfully overcame many difficulties and learned a lot.

I take this opportunity to sincerely acknowledge the Central Scientific Instruments Organisation, Chandigarh for allowing me to use the facilities available in one of the most prestigious laboratory of the country.

I gratefully acknowledge the Director, Thapar University and School of Chemistry & Biochemistry, Thapar University for the support provided for my research work.

I am grateful to Dean of Research, Thapar University for the support towards my research work. I am extremely thankful to my Doctoral Committee Chairman **Dr.**

Satnam Singh, Expert members **Dr Bonamali Pal** & **Dr. Rajeev Mehta** for their hard questions, valuable comments and encouragement during my progress report presentations.

The thesis would not have come to a successful completion, without the help I received from the staff of CSIO. I would like to thank **Sh Manish Jharwal, Ms Pooja Devi, Ms Suman Singh and Sh Sukesh Kumar** for their help. My thanks also go to **Sh Narinder Singh & Sh Sunil Dutt** for their help in my research study.

SPECIAL ACKNOWLEDGEMENT

I dedicate this dissertation to my husband, **SANJEEV**, for his remarkable patience, unwavering love and support he has been providing right from the beginning of the course till the completion of my research work. Without his encouragement and motivation it would not have just been possible for me to complete this research work.

Last but not the least; I would like to thank my family, especially my children ARNAV & VAISHNAVI, my parents, mother in law, my loved ones AKSHIT, ANANYA & ANAKH, for their continuous love and support.

Thanks again to all those who helped me whether directly or indirectly.

SUJATA VOHRA

TABLE OF CONTENTS

LIST OF FIGURES

LIST OF TABLES

List of Abbreviations/Symbols

A	Absorbance
Å	Angstrom
AgNPs	Silver nanoparticles
CPs	Conducting polymers
CV	Cyclic voltammetry
d	Interplanar distance
DSC	Differential Scanning Calorimetry
EB	Emeraldine base
ES	Emeraldine salt
eV	Electron volt
FTIR	Fourier Transform Infrared
g	Gram
GNPs/AuNPs	Gold nanoparticles
ICPs	Intrinsically conducting polymers
ITO	Indium tin oxide
K	Kelvin
LEB	Leucoemeraldine base
M	Molarity
ml	Milliliter
NPs	Nanoparticles
nm	Nanometer
N	Normality
PANI	Polyaniline

PEAN I	Polyethylaniline
PANI/Au NC	Polyaniline gold nanocomposite
PANI/Ag NC	Polyaniline silver nanocomposite
PEANI/Au NC	Polyethylaniline gold nanocomposite
PEANI/Ag NC	Polyethylaniline silver nanocomposite
PNB	Perigraniline base
R	Resistance
rpm	Rotation per minute
S/cm	Siemen per centimetre
SEM	Scanning electron microscopy
SPR	Surface Plasmon resonance
t	Time
T_g	Glass transition temperature
TGA	Thermal Gravimetric Analysis
TEM	Transmission electron microscopy
UV-Vis	Ultraviolet-visible
XRD	X-Ray Diffraction
Xe	Xenon
μm	Micrometer
ρ	Resistivity
σ	Conductivity
ε	Extinction coefficient
λ	Wavelength
°C	Degree Celsius

LIST OF CHEMICALS USED

S No	NAME OF CHEMICAL	CHEMICAL FORMULA	MOLAR MASS	SOURCE OF PROCUREMENT
1	Aniline	$C_6H_5NH_2$	93.13	Spectrochem Ltd Mumbai
2	Hydrochloric Acid	HCl	36.46	Merck Specialities Ltd Mumbai
3	Ammonium peroxodisulphate (APS)	$(NH_4)_2S_2O_8$	228.20	Spectrochem Ltd Mumbai
4	Sulphuric Acid	H_2SO_4	98.07	Loba Chemicals Ltd Mumbai
5	Trisodiumcitrate (TSC)	$Na_3C_6H_5O_7$	258.06	Loba Chemicals Ltd Mumbai
6	Hydrogen peroxide	H_2O_2	34.01	Merck Specialities Ltd Mumbai
7	2-Ethylaniline	$C_8H_{11}N$	121.18	HiMedia Ltd Mumbai
8	Para-Toluene sulphonic acid (PTSA)	$CH_3C_6H_4SO_3H$	190.22	Sigma Aldrich Chemicals
9	N-methyl-2-pyrrolidone (NMP)	C_5H_9NO	99.13	Merck Specialities Ltd Mumbai
10	Ortho-Phosphoric acid (PA)	H_3PO_4	98.0	Merck Specialities Ltd Mumbai
11	Polyvinyl pyrrolidone (PVP)	$(C_6H_9NO)n$	~40000	Spectrochem Ltd Mumbai
12	Hydrazine hydrate	$N_2H_4.H_2O$	50.06	Loba Chemicals Ltd Mumbai
13	Cetyltrimethylammonium bromide (CTAB)	$C_{19}H_{42}NBr$	366.45	Loba Chemicals Ltd Mumbai
14	Ascorbic acid (AA)	$C_6H_8O_6$	176.12	Sigma Aldrich Chemicals
15	Chloroauric acid	$HAuCl_4.3H_2O$	393.83	Central Drug House Ltd Delhi
16	Sodium borodydride	$NaBH_4$	37.83	Spectrochem Ltd Mumbai
17	Ethylene glycol (EG)	$C_2H_6O_2$	62.07	S D Fine Chem Ltd Mumbai
18	Silver Nitrate	$AgNO_3$	169.87	Spectrochem Ltd Mumbai
19	Ethanol	CH_3CH_2OH	46.08	Changshu Yangyuan Chemicals, China

CHAPTER 1

INTRODUCTION

The clubbing of polymers and nanoparticles is opening a new pathway for engineering flexible composites that exhibit advantageous electrical, optical and mechanical properties. Recent advances reveal routes to exploit both enthalpic and entropic interactions so as to direct the spatial distribution of nanoparticles and thereby, control the microscopic performance of the material. For tailoring the particle coating and variation in size, researchers are creating self healing materials for improved sustainability and self corralling rod for photovoltaic applications. A challenge in studies is to create hierarchically structure composites contributing to distinct function to yield mechanically integrated multifunctional materials (1).

The nanosized materials and their composites/hybrid materials have drawn attention of material scientists due to the unique properties (2). In last few years; synthesis of organic/inorganic nanocomposites has become the subject of extensive studies. The nanocomposites having organic polymers and inorganic nanoparticles in nanoscale regime provide a completely new class of materials with novel properties (3-5). Conducting polymers (CPs) are the interesting materials in modern technology because of their potential applications in sensors, electromagnetic radiation shielding, antistatic coating devices and insulator to conducting properties depending upon the type of dopants added (6-7). In CPs, polyaniline (PANI), polypyrrole (PPy), polythiophene (PTh) and several others and their derivatives have been extensively investigated due to variation in their characteristics for applied applications in electronics and sensing devices. PANI and its derivatives are the unique families of the conjugated polymers due to their ease of synthesis, reversible control of conductivity both by charge-transfer doping and protonation. It has now become possible to synthesize these materials in the form of micro as well as nanosize having conjugated fibres grown in 2D or 3D (8). PANI is generally insoluble in aqueous state and made to dissolve in solvents like N-Methyl-2-pyrrolidone (NMP) and can be casted into flexible films. However, their bulk conductivity alters due to separation of reduced and oxidized units present in polymer chains (9). A number of studies have

reported that both electrical and mechanical properties of CPs can be improved by incorporation of metal nanoparticles for details of which have been covered in literature survey in Chapter 2.

Our study focuses on the synthesis and characterization of both PANI/Au, PANI/Ag as well as polyethylaniline/gold, polyethylaniline/silver (PEANI/Au,PEANI/Ag) nanocomposites and their comparison. To the best of my knowledge, so far no such study has been reported on PEANI-metal (Au, Ag) nanocomposite which has yielded interesting properties. Further in this study, PANI- metal composites have also been generated through different routes.

1.1 CONDUCTING POLYMERS :

Until about 35 years ago all carbon based polymers were rigidly regarded as insulators. The idea that plastics could be made to conduct electricity would have been considered to be absurd. They were utilized as inactive packaging and insulating material. This very narrow perspective is rapidly changing as a new class of polymer known as intrinsically conductive polymer or electroactive polymers are being discovered. The potential uses of these materials are quite significant. Since then it has been found that about a dozen different polymers and polymer derivatives undergo this transition when doped with a weak oxidising or reducing agent or with acid-base doping resulting in various conjugated polymers.

The **intrinsically conducting polymers (ICPs)**, more commonly known as “synthetic metals”, refer to the large class of organic polymers which possess not only the mechanical properties and processibility of conventional polymers, but also unique electrical, electronic, magnetic, and optical properties of metals, which conventional polymers do not have (10). Figure 1.1 represents the chemical structure of some of the commonly known conducting polymers (11).

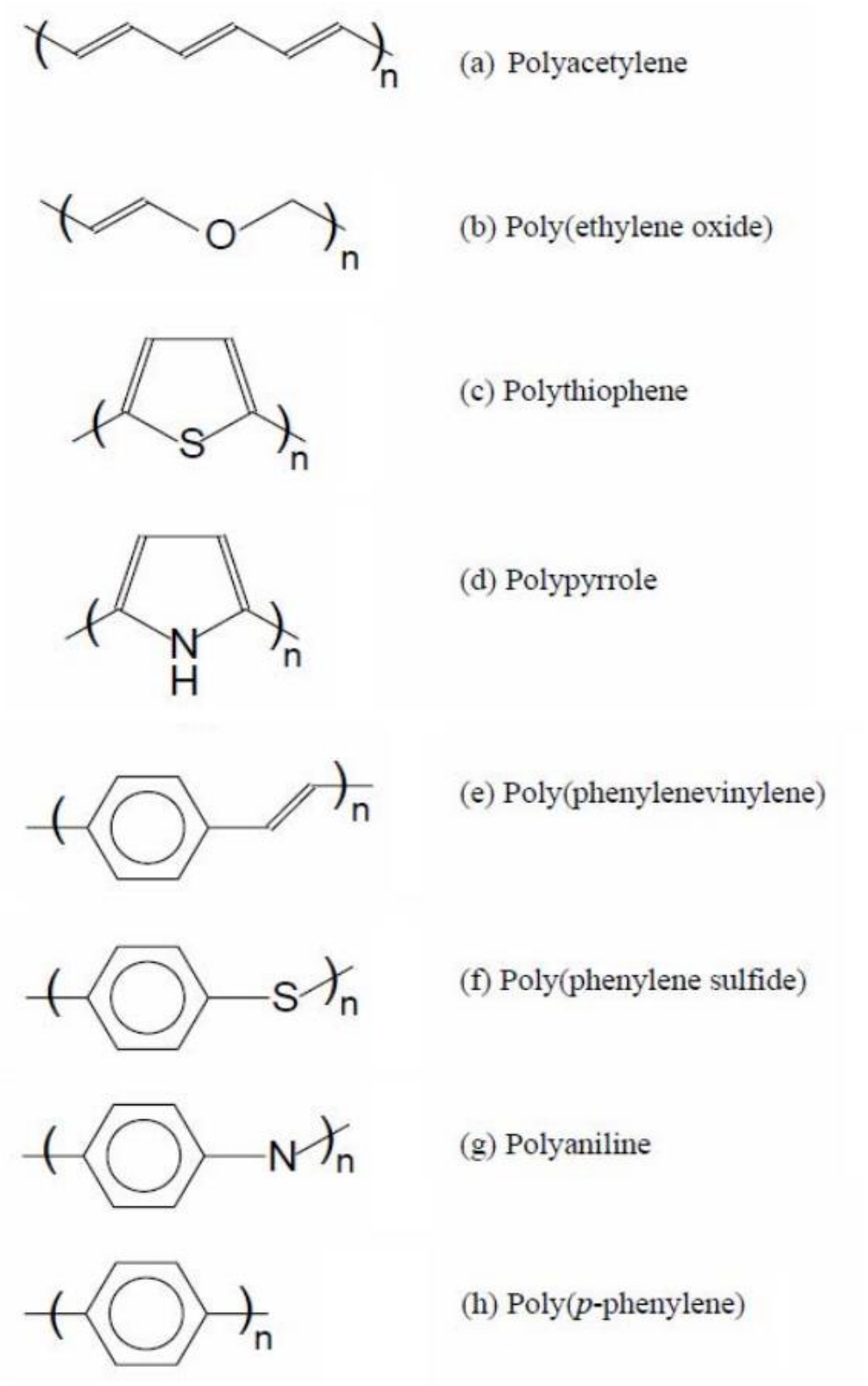

Fig 1.1: Structural formulae of some of the commonly known conducting polymers

A conducting polymer has π conjugated double bonds where the overlapping π-electrons fairly extend and delocalize along the polymer backbone. They can

provide the conduction of electric charges through movement of electrons in unoccupied energy states or movement of holes in filled energy states. These conductive holes and electrons arise from chemical oxidation or reduction, i.e. p-type or n-type doping. During the chemical oxidation or reduction, the conductive polymer is doped with anionic specie which is the electron acceptor, or with cationic specie which is the electron donor (12, 13). Therefore, it is important to understand the principle that conductive polymers can alternatively behave as a metal, semiconductor, or insulator. Free electron model is introduced first and extended in further to band model to comprehensively explain the properties of conductive polymers. Finally, chemical doping also is given to illustrate briefly the conductivity of conductive polymers.

1.1.1 Free Electron Model

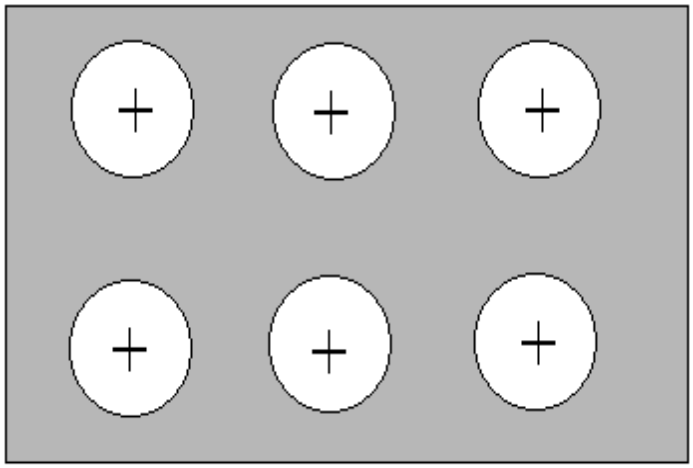

Fig 1.2: Schematic illustration of the free electron model applied to sodium metal

The free electron model describes that valence electrons move freely through the volume of the metal. The forces are neglected between conduction electrons and the ion cores. As shown in figure 1.2, sodium cores with positive charge share the moving electrons with each other. The moving electrons come from valence electron of sodium from 3s orbital. Thus, sodium atomic core (Na^+ions) are dispersed in the sea of conduction electrons (14). However, this model fails to explain the difference between metals, semiconductors, and insulators, why some chemical elements crystallize to form good conductors, and why conductive polymers have the conduction of electrical charges. Therefore, band model is given here.

1.1.2 Band Model

Based on the invention of quantum mechanics, the band model refines the previous model. It introduces that a band gap exists between the valence band and the conduction band. As shown in Figure 1.3, in metals conduction band overlaps the valence band. There is no evidence of the band gaps between them. Electrons can move freely in the conduction band. In semiconductors, the valence band and the conduction band are separated by enough small band gaps where electrons in valence band can jump to conduction band through thermal or optical excitation energy. In insulators, there exists a large band gap between the valence band and the conduction band (15).

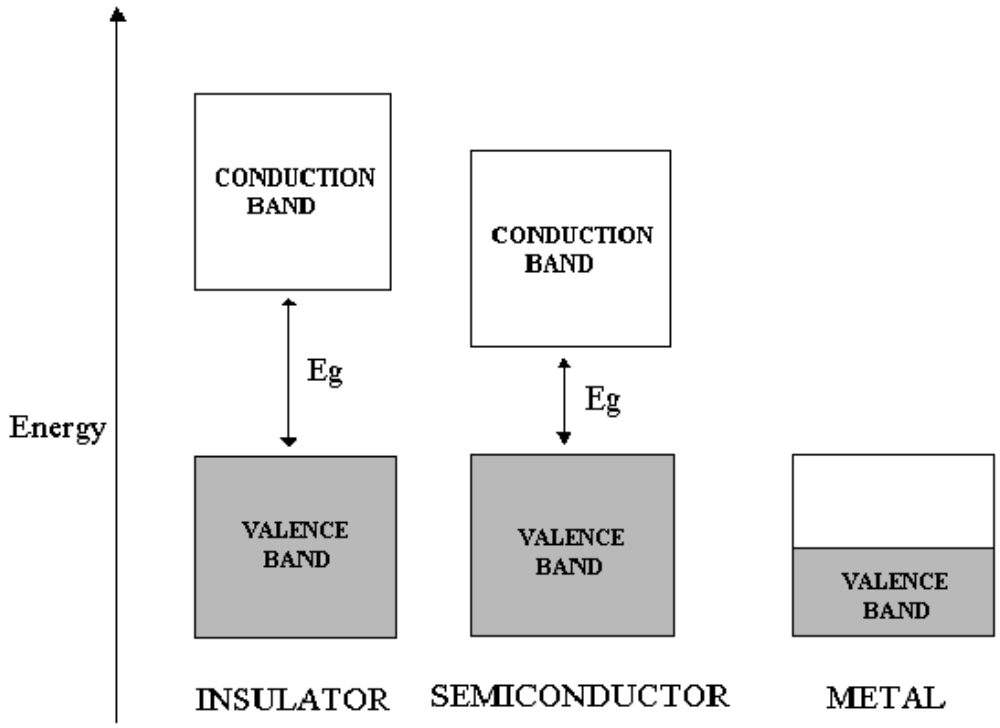

Fig 1.3: Schematic band model

The band model is also quite appropriate to explain why conductive polymers can be conductors, semiconductors, or insulators. Conductive polymers exhibit π conjugation where the overlapping π -electrons fairly extend and delocalize along a polymer backbone. The band gap can be decreased gradually by extending the π chain length of the molecules. A dimer has the largest band gap. In addition, a

polymer can be as conductive as a metal when the band gap is removed, a semiconductor (e.g. silicon) when the band gap is small enough, or an insulator as polyethylene when the band gap is large.

1.1.3 Doping

In a conductive polymer, electrons are removed (or added) by chemical methods to form positive (or negative) charge on the polymer chain. Also, negative (or positive) ions bond together to form polymer salt. This process is called "*doping*" by which the conductivity of these polymers can be increased to several orders of magnitude, such as polyacetylene doped with iodide ion. The conductivity of doped polyacetylene is 9 orders of magnitude higher than that of an undoped one (12). In a p-type conductive polymer, the concentration of holes in the valence band is greater than that of electrons in the conduction band. Most conductive polymers are p-type, such as polyaniline, polypyrrole, and polythiophene. However, n-type conductive polymers still can be found, such as poly (benzobisimidazobenzophenanthroline) (BBL), in which the concentration of electrons in the conduction band is higher than that of holes in the valence band. In addition, some polythiophene derivatives can be doped n-type. Polyacetylene can be doped p-type or n-type. The schematic band diagram of p-type and n-type doped polymers are shown in Figure 1.4.

In solid-state physics terminology, the use of an oxidizing agent corresponds to p-type doping and that of a reducing agent to n-type doping. The doping reaction is usually summarized as:

$$CP_{Neutral\ chains} + n(A^-)_{aq} + mS \rightarrow [CP^{+n}A_n^-S_m] + ne \quad [1]$$

$$CP_{Neutral\ chains} + n(C^+)_{aq} + ne + mS \rightarrow [CP^{-n}C_n^-S_m] \quad [2]$$

Where the different symbols mean: aqueous (aq), anion (A^-), cation (C^+), electron (e), solvent (S) and "m" and "n" are stoichiometric coefficients.

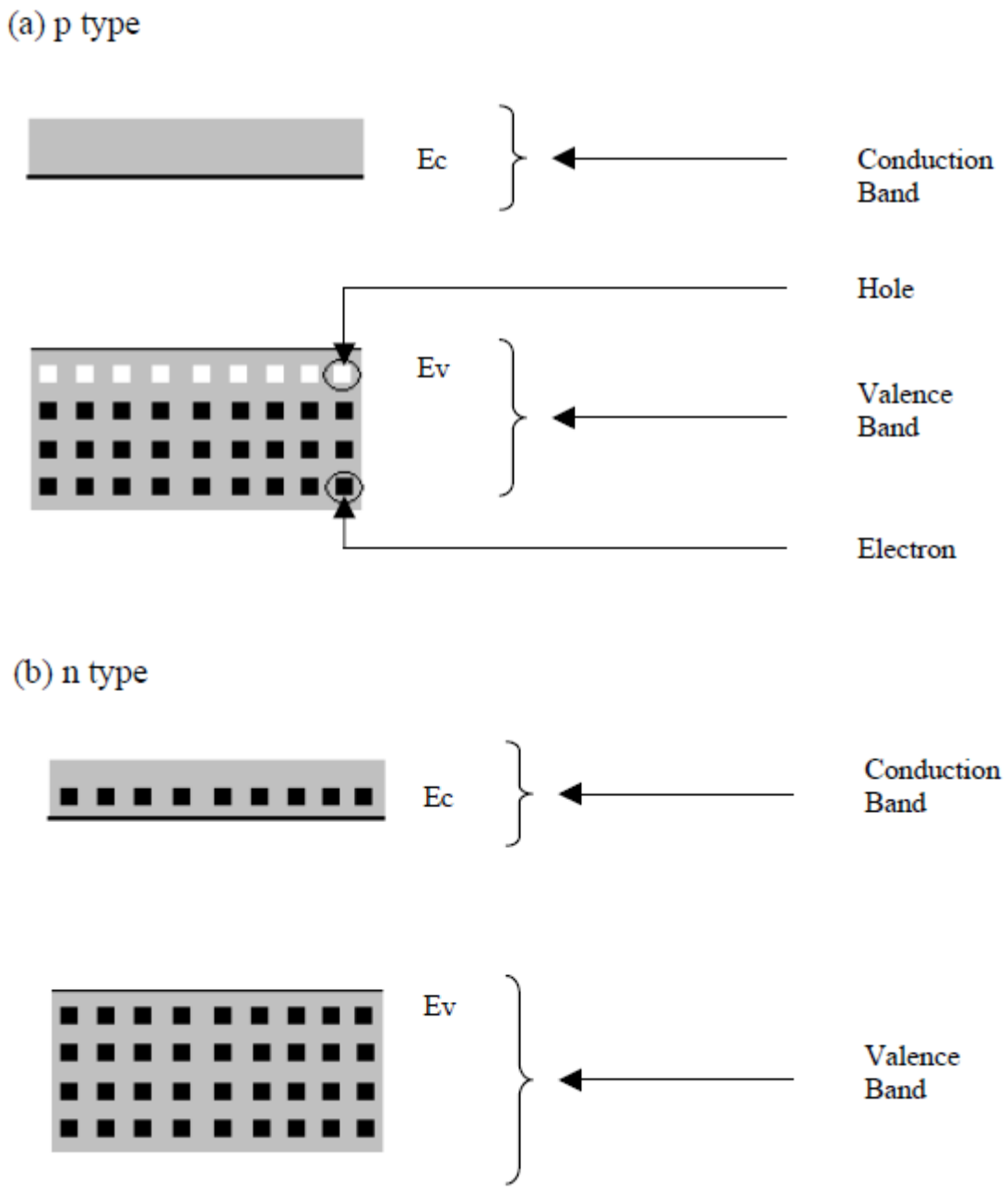

Fig 1.4: Schematic band diagram of p-type and n-type doped polymers

The important feature of the doping is that the process is reversible i.e. the conducting polymer can be made neutral through 'de-doping' process. In the doped state, conduction occurs through solitons (generally free radical), polarons (free radical and cation pair) or bi-polarons (di-cation) charge carriers. These charge carriers are nothing but the defects in the conjugated backbone, which span across few monomer units; yet treated as a 'single particle' for convenience. The formation of the type of charge carriers depends upon backbone chain, its

degeneracy and degree of doping. The process of doping is illustrated in Fig 1.5 for iodine doped polyacetylene.

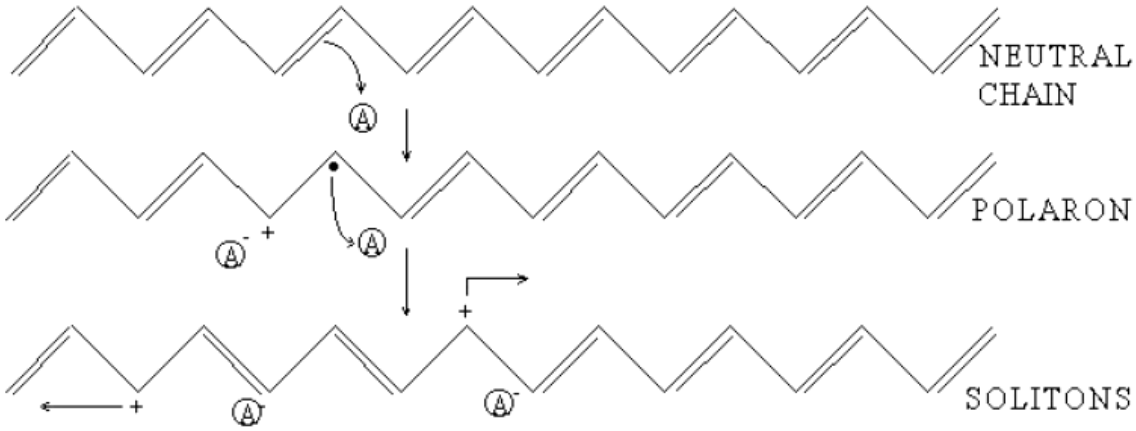

Fig 1.5: Polaron and solitons formation in p-doped polyacetylene.

Table 1.1: Typical properties of solitons, polarons and bipolarons

Defect	**Spin**		**Charge**
Solitons	Neutral	½	0
Solitons	Charged	0	+e or –e
Polarons	Charged	1/2	+e or –e
Bipolarons	Charged	0	+2e or -2e

When poly-acetylene is doped with iodine, the backbone is oxidized and gives an electron to the dopant species. This reaction creates a positively charge radical and a cation pair termed as polaron (at low doping level). While the radical can travel easily along the chain, the cation's movement is restricted due to electrostatic interaction with dopant specie. Therefore presence of more negative ions along the backbone is necessary to allow the movement of free radical along the backbone. Conjugated polymers with a degenerate ground state have a slightly different mechanism. As with polypryyole, polarons and bipolarons are produced upon oxidation. However, because the ground state structure of such polymers are two fold degenerate, the charged cation are not bound to each other by a higher energy bonding configuration and can freely

separate along the chain. The effect is that the charged defects are independent of one another and can form domain walls that separate two phases of opposite orientation and identical energy. These are called solitons and can sometimes be neutral. Solitons produced in polyacetylene are believed to be delocalized over about 12 CH units with the maximum charge density next to the dopant counterion. The bonds closer to the defect showed less amount of bond alternation than the bonds away from the centre. Soliton formation results in the creation of new localized electronic states that appear in the middle of the energy gap. At high doping levels, the charged solitons interact with each other to form a soliton band which can eventually merge with the band edges to create true metallic conductivity.

This requirement explains the need for a large amount of dopant for the conducting polymers (16). The presence of these charge carriers creates new energy levels between conduction band and valence band thus 'narrowing' the band gap in conducting polymers. This is illustrated in Fig 1.6.

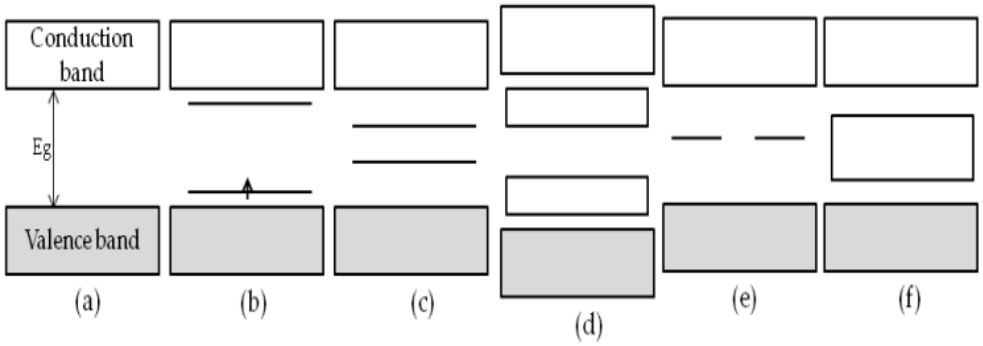

Fig 1.6: Schematic representation of the energy gap in (a) neutral polymer (b) polaron (c) bipolaron (d) bipolaron bands and (e) soliton and (f) soliton band resulting at different levels of doping.

In heterocyclic polymers (polypyrrole, polyaniline) from moderate to high doping levels [(b) to (d) in Figure. 1.6] polaron and bipolaron type charge carriers are largely responsible for the conduction. At very high doping levels, bipolaron forms continuous band [refer (d), Figure. 1.6] but at the expense of the valence and conduction band edges resulting in increase in the band gap. With further increase in doping, the bipolaron band finally merges with the valence and conduction band respectively, which render metallic conductivity.

In degenerate ground-state conducting polymer like polyacetylene, at high doping level the movement of the charge carriers (mostly solitons) is independent of each other. At very high doping level solitons starts to interact with each other resulting in the 'soliton band' [refer (f), Figure. 1.6]. Thus formed soliton band merges with the valence and conduction band respectively giving true metallic conductivity to the doped polyacetylene. The complete explanation of the transport mechanism is still one of the major goals in the area of conducting polymers (17).

1.2 PROPERTIES, APPLICATIONS AND LIMITATIONS OF CONDUCTING POLYMERS

1.2.1 Properties

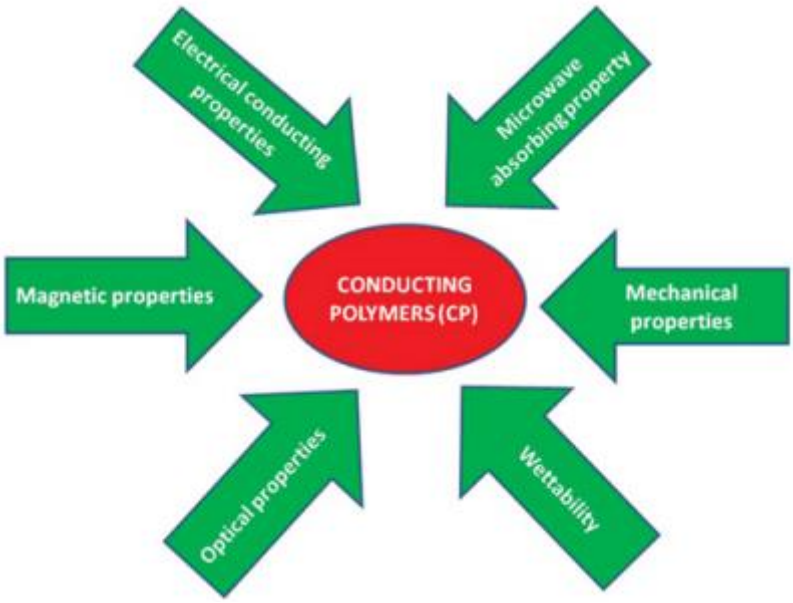

Fig 1.7: Properties of conducting polymers

In order to understand the potential of conducting polymers it is important to recognise some of the principal properties commonly exhibited by them:

- They possess stiff, conjugated backbones (in their doped, conductive form).
- They can act as electronic switches by suitable changes in their level of oxidation or pH.
- They may display changes in their optical spectra with oxidation and reduction or with changes in pH.

- The conductivity, solubility and other properties of the polymers can often be 'tuned' by the synthesis of substituted polymers or by the incorporation of different counterions.
- Organic conducting polymers are of much lower density than metals.

1.2.2 Potential Applications of Conducting Polymers

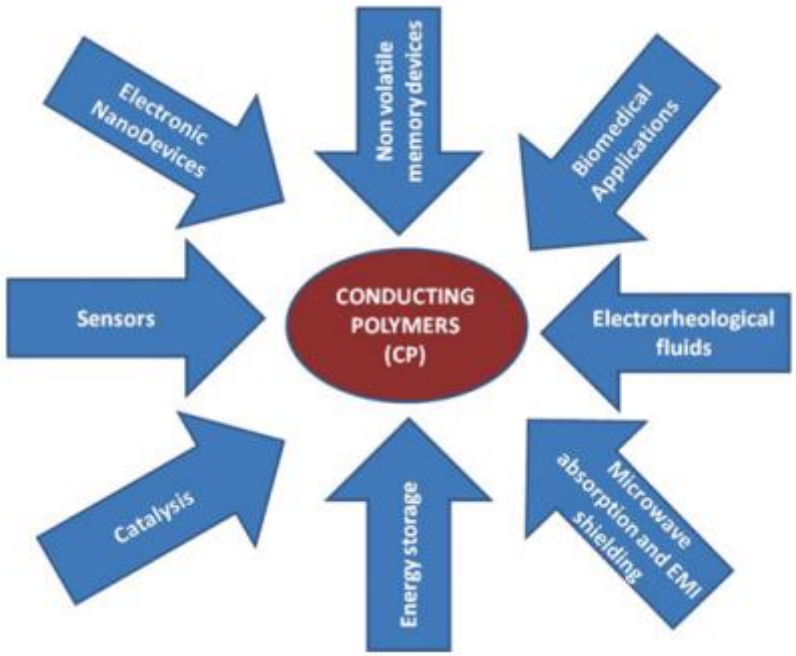

Fig 1.8: Applications of conducting polymers

The conducting polymers have important applications in molecular electronics (18), electrochromic displays (19), electromagnetic shielding (20-21), printed circuit boards (22), rechargeable batteries (23), solid electrolytes and optical computers (24-25). Other potential applications of these conducting polymers are in chemical, biochemical and thermal sensors (26-28), artificial nerves, drug release system (29-30), ion exchange membranes (31), electromechanical actuators (32) and 'smart' structures (33). Major interest in conducting polymers has its origin in the possible commercial applications of these materials. The commercial applications are based on the promise of a novel combination of light weight, processibility and electrical conductivity. Some of conducting polymers can change their optical properties on applications of current or voltage and therefore may find useful applications as heat shutter and light emitting diodes (LEDs) (34).

1.2.3 Limitations

The use of conducting polymers in actual applications has certain limitations by the very nature of the polymers. Polymers with a conjugated backbone generally have an inherent susceptibility to aerial oxidation, and, in fact, polyaniline is the only known conducting polymer to show complete resistance to oxidative degradation under ambient conditions. Appropriate choice of dopant counter-ion can increase polymer stability; otherwise it is often necessary to exclude oxygen and water if the conductivity of the polymer is to remain constant during use. An even greater obstacle to the use of these polymers is their lack of processability. Conductive polymers possess stiff backbones, such polymers tend not to melt or dissolve easily, and this behaviour can be attributed to three main factors. Firstly, these linear or planar polymers can pack efficiently, this maximises the inter-chain forces and so they can exhibit significant crystallinity. These strong forces must be weakened for melting to take place and this requires high temperatures, often above the temperature at which the polymer degrades. For dissolution to occur a very strong interaction between polymer and solvent is essential if the inter-chain forces are to be overcome. Secondly, the doped forms of conducting polymers are charged and this leads to electrostatic interactions between chains which are much stronger than the Van der Waals interactions present between chains in conventional polymers. Lastly, there is little entropic gain in the melting or dissolution of macromolecules with stiff chains because these processes do not produce a large increase in conformational freedom. As well as these factors cross-linking renders some of these polymers intrinsically insoluble (e.g. polypyrrole).

1.3 PROCESSIBILITY

Conjugated polymers may be made by a variety of techniques, including cationic, anionic, radical chain growth, co-ordination polymerization, step growth polymerization or electrochemical polymerization. Electrochemical polymerization occurs where monomers are electrochemically oxidized to create an active monomeric and dimeric species which react to form a conjugated polymer backbone. The main problem with electrically conductive plastics stems from the very property that gives it its conductivity, namely the conjugated

backbone. This causes many such polymers to be intractable, insoluble films or powders that cannot melt. There are two main strategies to overcome these problems: either modify the polymer so that it may be more easily processed, or to manufacture the polymer in its desired shape and form. There are, at this time, four main methods used to achieve these aims.

The first method is to manufacture a malleable polymer that can be easily converted into a conjugated polymer. This is done when the initial polymer is in the desired form and then, after conversion, is treated so that it becomes a conductor. The treatment used is most often thermal treatment. The precursor polymer used is often made to produce highly aligned polymer chain which is retained upon conversion. These are used for highly orientated thin films and fibres. Such films and fibres are highly anisotropic, with maximum conductivity along the stretch direction (35).

The second method is the synthesis of copolymers or derivatives of a parent conjugated polymer with more desirable properties. This method is the more traditional one for making improvements to a polymer. What is done is to try to modify the structure of the polymer to increase its processibilitywithout compromising its conductivity or its optical properties. All attempts to do this on polyacetylenehave failed as they always significantly reduced its conductivity. However, such attempts on polythiophenes and polypyrroles proved more fruitful. The hydrogen on carbon 3 on the thiophene or the pyrrole ring was replaced with an alkyl group with at least four carbon atoms in it. The resulting polymer, when doped, has a comparable conductivity to its parent polymer whilst be able to melt and it is soluble. A water soluble version of these polymers has been produced by placing carboxylic acid group or sulphonic acid group on the alkyl chains. If sulphonic acid group groups are used along with built-in ionisable groups, then such system can maintain charge neutrality in its oxidized state and so they effectively dope themselves. Such polymers are referred to as "self-doped" polymers (36).

The third method is to grow the polymer into its desired shape and form. An insulating polymer impregnated with a catalyst system is fabricated into its desired form. This is then exposed to the monomer, usually a gas or a vapour.

The monomer then polymerizes on the surface of the insulating plastic producing a thin film or a fibre. This is then doped in the usual manner. A variation of this technique is electrochemical polymerization with the conducting polymer being deposited on an electrode either the polymerization stage or before the electrochemical polymerization. This cast may be used for further processing of the conducting polymer. For instance, by stretching aligned bends of polyacetylene/polybutadiene the conductivity increase 10 fold, due to the higher state of order produced by this deformation (37).

The final method is the use of Langmuir-Blodgett trough to manipulate the surface active molecules into a highly ordered thin films whose structure and thickness which are controllable at the molecular layer. Amphiphilic molecules with hydrophilic and hydrophobic groups' produces monolayers at the air-water surface interface of a Langmuir-Blodgett trough. This is then transferred to a substrate creating a multilayer structure comprised of molecular stacks which are normal about 2.5 nm thick. This is a development from the creation of insulating films by the same technique. The main advantage of this technique is its unique ability to allow control over the molecular architecture of the conducting films produced. It can be used to create complex multilayer structures of functionally different molecular layers as determined by the chemist. By producing alternating layers of conductor and insulator it is possible to produce highly anisotropic film which is conducting within the plane of the film, but insulating across it (38).

Table 1.2: Stability and processing attributes of some conducting polymers

POLYMER	CONDUCTIVITY (Scm^{-1})	STABILITY (doped state)	PROCESSING POSSIBILITIES
Polyacetylene	10^3- 10^5	poor	limited
Polyphenylene	1000	poor	limited
PPS	100	poor	excellent
PPV	1000	poor	limited
Polypyrroles	100	good	good
Polythiophenes	100	good	excellent
Polyaniline	10	good	good

1.4 POLYANILINE (PANI)

1.4.1 Introduction

Polyaniline is unique among conducting polymers in its wide range of electrical, electrochemical and optical properties as well as good stability. Polyaniline can be doped to highly conducted state by protonic acids or by electrochemical methods and show moderate conductivity upon doping. The electrical and sensing properties of the polyaniline may be increased by formation of composites with various types of particles. It is one of the so-called doped polymers, in which conductivity results from a process of partial oxidation or reduction. Polyaniline compounds can be designed to achieve the required conductivity for a given application. The resultant blends can be as conductive as silicon and germanium or as insulating as glass. Another advantage is that it is both melt and solution processable. This means that the compound can be easily mixed with conventional polymers and that it is easy to fabricate polyaniline products into required shapes.

1.4.2 Structure of PANI

Polyaniline is a typical phenylene-based polymer having a chemically flexible -NH- group in a polymer chain flanked either side by a phenylene ring. It is a unique polymer because it can exist in a variety of structures depending on the value of (1-y) in the general formula of the polymer shown in Figure 1.9 (a) (39,40).

The electronic properties of PANI can be reversibly controlled by protonation as well as by redox doping. Therefore, PANI could be visualized as a mixed oxidation state polymer composed of reduced {-NH-B-NH-} and oxidized {-N=Q=N-} repeat units where -B- and =Q= denote a benzenoid and a quinoid unit respectively.

Depending upon the oxidation state of nitrogen atoms which exist as amine or imine configuration, PANI can adopt various structures in several oxidation states, ranging from the completely reduced leucoemeraldine base state (LEB) (Fig 1.9(b)), y-1 = 0, to the fully oxidized pernigraniline base state (PNB) (Fig .1.9

(e)), where 1-y = 1. The "half" oxidized (1-y = 0.5) emeraldine base state (EB) (Fig 1.9 (c)) is a semiconductor and is composed of an alternating sequence of two benzenoid units and a quinoid unit. The protonated form is the conducting emeraldine salt (ES) (Fig 1.9(d)).

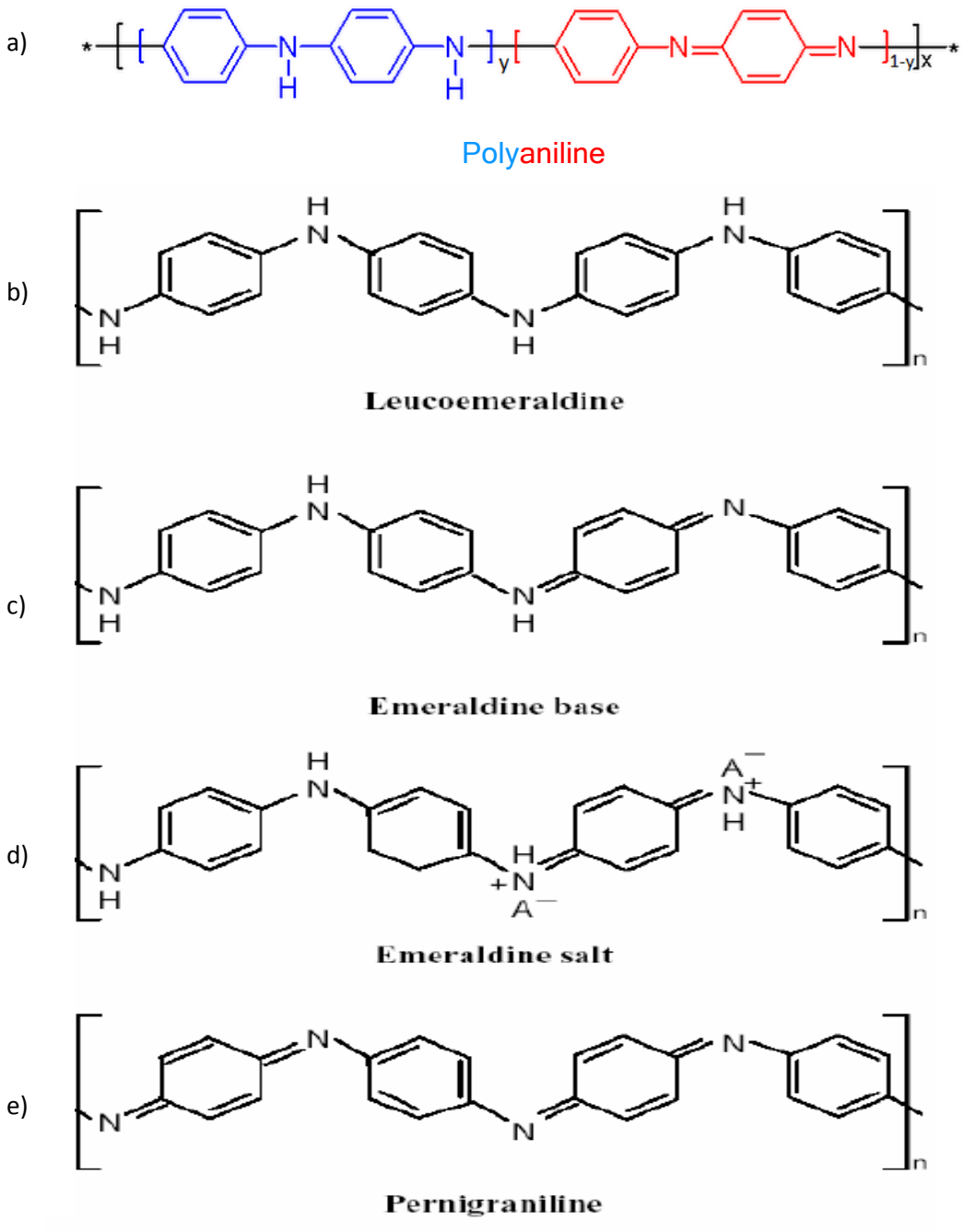

Fig 1.9: Oxidation States of Polyaniline [Adapted from reference (39, 40)]

The electronic structure and excitations of these three insulating forms (LEB, PNB, EB) are contrasted. However, the LEB form can be *p*-doped (oxidatively doped), the EB form can be protonic acid doped and the PNB form can be *n*-

doped (reductively doped) to form conducting ES systems.

The EB, intermediate forms of PANI can be non-redox when doped with acids to yield the conductive emeraldine salt state of PANI as demonstrated in Figure 1.10. It can be rendered conductive by protonating (proton doping) the imine nitrogen, formally creating radical cations on these sites.

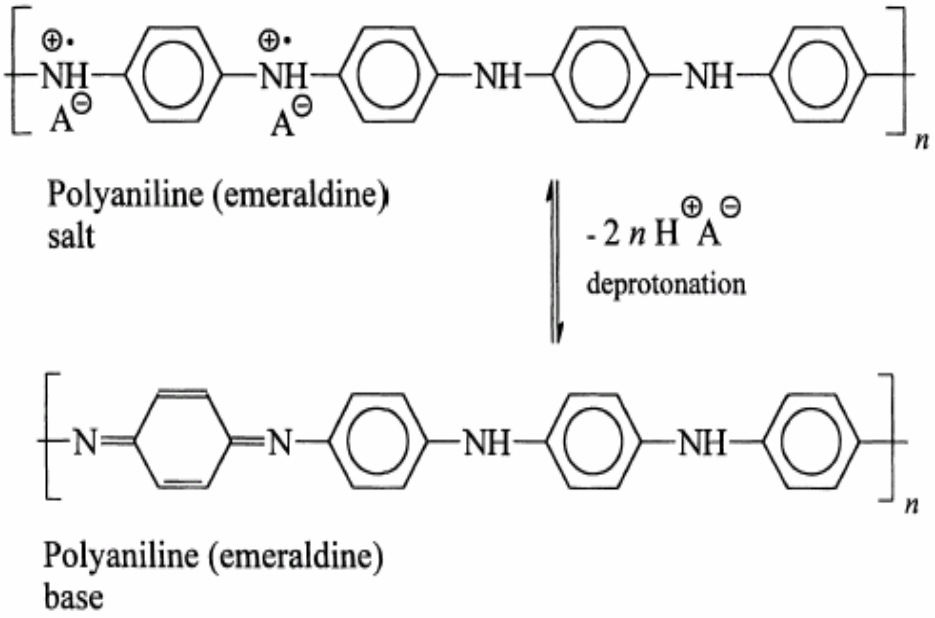

Fig 1.10: PANI (emeraldine) salt is deprotonated in the alkaline medium to PANI (emaraldine base), A is an arbitrary anion

Similar electronic behaviour has been observed for other non-degenerate ground state systems as for protonic acid doped PANI. That is, polarons are important at low doping levels. For doping to the highly conducting state, a polaron lattice (partially filled energy band) forms. In less ordered regions of doped polymers, polaron pairs or bipolarons are formed.

During doping all the heteroatoms in polymer, namely the imine nitrogen atoms of the polymer become protonated to give a polaronic form where both spin and charge are delocalized along the entire polymer backbone. The conductive emeraldine salt state can be converted back to the insulating emeraldine base state through treatment with a base, indicating that this process is reversible.

This protonated emeraldine salt form is electronically conducting, the magnitude of increase in its conductivity varies with proton (H^+ ion) doping level (protonic acid doping) as well as functionalities present in the dopant (41). In the doping

acid, the functional group that present, its structure and orientation can influence the solubility of a conducting form of PANI or for obtaining aqueous dispersion and compatibility with other polymers.

1.5 POLY (2-ETHYLANILINE) (PEANI)

1.5.1 Introduction

There are several limitations in enginerred use of PANI due to its poor solubility in different solvents. In view of this, several derivatives of PANI are investigated which have some different characteristics than PANI. Incorporation of long and flexible alkyl chains in the polymer backbone is a common technique to prepare PANI-type polymers which are soluble in water and/or organic solvents but limitations are then imposed on the conductivity of polymer produced.

Poly (2-ethylaniline), which is a derivative of Polyaniline, is also one of the important conductive polymers. PEANI, besides its high solubility, provide opportunities to study the dependence of electrical properties on chain confirmation, which in turn will depend, at least in part, on the size of ethyl group substituent. The substitution of ethyl group on the phenyl ring increases the steric repulsion between the rings in the polymer chain. It causes an increase in the torsional angle and a decrease in conjugation in PEANI when compared to PANI.

1.5.2 Structure of Poly(2-ethylaniline)

Poly (2-ethylaniline) refers to ortho-ethyl substituted aniline polymer which can exist like PANI in 3 different discrete oxidation states, in both their doped and undoped forms. It can be considered as being derived from a polymer, the base formed of which has the generalised composition (42-43):

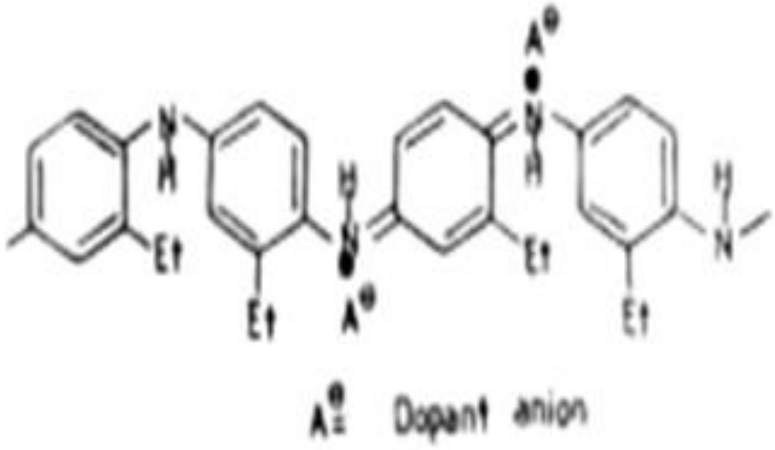

Fig 1.11: Structure of poly (2-ethyl aniline)

1.6 METAL NANOPARTICLES

Nanoparticles (particles of 1-100 nm in diameter or length) exhibit unique electronic, optical, photonic and catalytic properties and are an ideal size for use as nanotechnological building blocks (44-47). These are composed of any material including metals, semiconductors, ceramics, organic polymers and others (48-56). These particles display properties intermediate between bulk and quantum materials (57-58) because of nanometric size and large surface area-to- volume ratios. Nanoparticles of different sizes and shapes exhibit different optical properties. They represent metastable clusters exhibiting the fundamental properties to aggregate. Thus, the stabilization of nanoparticles against aggregation is a pre-requisite in nanotechnology which is being carried out by using different stabilizing agents. The stabilization of nanoparticles may be accomplished by the capping of the nanoparticles with weakly, electrostatically – bound ions, by molecular ligands, and the protection of the nanoparticles in polymer matrices or micellar assemblies. Nanoengineering of nanoparticles surfaces i.e. layer- by- layer deposition of organic modifiers, allows fine control of the shell size and structure.

The ability to selectively synthesize metal nanoparticles of any desired shape or size generates significant opportunities in chemistry because catalytic, optical, magnetic and electronic activities are dimensionally sensitive.

1.7 GOLD

1.7.1 Properties of Gold

Gold is a chemical element with the symbol **Au** and atomic number 79. It is a dense, soft, malleable, and ductile metal with an attractive, bright yellow color and luster that is maintained without tarnishing in air or water. Chemically, gold is a transition metal and a group 11 element. The electronic configuration is [Xe] $4f^{14}5d^{10}6s^{1}$. The gold melts at 1064.18°C and vapourizes at 2856°C. Common oxidation states of gold include +1 (aurous compounds) and +3 (auric compounds). Gold ion in solution is readily reduced and precipitated out as gold metal by any other metal as reducing agent. The added metal is oxidized and dissolved allowing the gold to be displaced from the solution and be recovered as solid precipitates (59).

1.7.2 Gold Nanoparticles

Although gold is the subject of one of the most ancient themes of investigation in science, its renaissance now leads to an exponentially increasing number of publications, especially in the context of emerging nanoscience and nanotechnology with nanoparticles and self-assembled monolayers (SAMs). AuNPs are the most stable metal nanoparticles, and they present fascinating aspects such as their assembly of multiple types involving materials science, the behaviour of the individual particles, size-related electronic, magnetic and optical properties (quantum size effect), and their applications to catalysis and biology (60-63). Their promises are in these fields as well as in the bottom-up approach of nanotechnology, and they will be key materials and building blocks in the 21st century.

1.8 SILVER

1.8.1 Properties of Silver

Silver is a soft, white, lustrous transition metal, it has the highest electrical conductivity of any element and the highest thermal conductivity of any metal. The metal occurs naturally in its pure, free form as an alloy with gold and other metals. The atomic number is 47 and atomic mass is 108 $gmol^{-1}$.Electronic configuration is [Kr] $4d^{10}$ $5s^{1}$. The melting and boiling point are 961.78°C and 2162°C respectively (64).

Silver has long been valued as a precious metal, and it is used to make ornaments, jewellery, high-value tableware, utensils (hence the term silverware), and currency coins. Today, silver metal is also used in electrical contacts and conductors, in mirrors and in catalysis of chemical reactions. Its compounds are used in photographic film and dilute silver nitrate solutions and other silver compounds are used as disinfectants and microbiocides. While many medical antimicrobial uses of silver have been supplanted by antibiotics, further research into clinical potential continues.

1.8.2 Silver Nanoparticles

Silver nanoparticles have been synthesised in various shapes and sizes because as the size decreases from bulk to nano, the properties of silver nanoparticles changes drastically and it behaves completely different from their conventional size. Thus silver nanoparticles are being used for an ever-growing number of applications.

Over the last decades silver nanoparticles have found applications in catalysis, optics, electronics and other areas due to their unique size-dependent optical, electrical and magnetic properties. Currently most of the applications of AgNPS are in antibacterial/antifungal agents in biotechnology and bioengineering, textile engineering, water treatment, and silver-based consumer products (65). There is also an effort to incorporate silver nanoparticles into a wide range of medical

devices, like bone cement, surgical instruments, surgical masks, wound dressings and treatment of HIV-1. "In the first-ever study of metal nanoparticles", silver nanoparticles of sizes 1-10 nm attached to HIV-1 and prevented the virus from bonding to host cells. The study, published in the Journal of Nanotechnology, was a joint project between the University of Texas, Austin and Mexico University, Nuevo Leon. Samsung has created and marketed a material called Silver Nano, which includes silver nanoparticles on the surfaces of household appliances (66).

1.9 CONCUCTING POLYMER COMPOSITES WITH NOBLE METAL NANOPARTICLES

Incorporation of metals, metal oxides, and organometallic species such as metallocenes in intrinsically conductive polymers can enhance electron transfer through a direct or mediated mechanism with improved conductivity and enhanced stability (67-68). For these systems the electron-rich polymer often acts as a chemical receptor or scaffold for the secondary component. The electron density of the conductive polymer is important, providing stability to species that may be electron deficient. However, it has also been suggested that the polymer provides stability through exclusion of surface contaminants that may interfere with the surface chemistry of the deposit. The structure of the conductive polymer plays a role in the dispersion of the species, their aggregation, and formation of the composite materials. The polymer is used to provide high surface, protection against the fouling of the metal catalyst, and a scaffold for high dispersion and anchoring of the metal particles. The conductivity of the composite allows the electron density of the polymer to be controlled through the applied thermodynamic potential which influences chemical reactions at the metal surface. The ability to finely disperse the secondary species in the polymer ensures high surface area and possible enhancement of the unique characteristics of the composite. The synthetic method employed is an important factor to consider with regard to the homogeneous distribution of the secondary component.

There are multiple methods used to prepare the ICP composite materials with metallic species distributed at the polymer surface in the vicinity of the electrode/polymer interface or throughout the bulk of the polymer. The approach

used to introduce the metallic species typically determines the degree of dispersion or deposition. For example, dispersion of the polymer using pulsed deposition and relaxation (spontaneous reduction of the species) or co-deposition of the ICP with the active species using cyclic voltammetry has been utilized to introduce metal species (69). One common approach involves the chemical reaction and uptake of a species by the conductive polymer. In this case the species are introduced by controlled reduction of metallic anions such as $AuCl_4^-$, $PtCl_4^{2-}$, and $PtCl_6^{2-}$ by manipulating the redox sites within the ICP (70-72). The uptake of the negatively charged anion of interest is based on the oxidation of the polymer and the need to maintain charge neutrality in the system. Reduction of the anion occurs as the potential is switched to negative values. In contrast, the oxidized form of the metal species can be introduced to the polymer using metal salts followed by the electrochemical, chemical, or spontaneous reduction of the metallic species. The most common metals incorporated into the ICPs include gold, platinum, and palladium as nano or microparticles.

In many cases formation of the metal nanoparticles occurs prior to incorporation into conductive polymer matrix. In such cases, the preformed clusters of metal, metal oxides or metallocenes are dispersed in solution containing the ICP precursor. Chemical oxidation of the precursor results in encapsulation of the metal species to form the ICP composite (73-76). The resulting materials can then be cast onto substrates for subsequent applications. However, in certain metal-polymer synthesis, metal ions are often reduced in presence of pre-formed polyaniline. In such case, metal NPs are not effectively dispersed into polymer matrix and NPs react with imino group of polymer and reduce at the point of contact (77-78). Recently, the direct chemical synthesis of composite materials using polymer precursors and oxidizing anions such as $AuCl_4^-$ and $PtCl_4^{2-}$ has was reported (79-81). Each of the methods discussed has its advantages and disadvantages that must be weighed before they are used to prepare composite materials.

There has been very limited study on simultaneous oxidation of monomer and reduction of metal ion to form PANI/Au or Ag nanocomposites to get large surface area and better properties. No study has been reported till date on the composite

of PEANI/Au or Ag which has been discussed in the present study. Thus the objectives of my study are:

1. Chemical synthesis of PANI, PEANI and addition of different dopants.
2. Characterization of these materials for structure, stability and morphology by using FTIR, SEM and TGA.
3. Synthesis of gold and silver nanoparticles less than 10nm having different capping agents.
4. Characterization of nanomaterials using UV-vis spectrophotometer, TEM & XRD.
5. Synthesis of composites of PANI/Au or Ag nanoparticles and PEANI/Au or Ag nanoparticles. Their characterization for morphology, crystallinity, thermal and optical behaviour.

REFERENCES:

1. A.C.Balazs, T.Emrick, T.P.Russell, Science 314, 1107, 2006
2. J.W.G.Wildoer, L.C.Venema, A.G.Rinzler, R.E.Dekker, Nature 59, 391, 1998
3. H.S.Nalwa, R.Gangopadhyay, Handbook of Organic-Inorganic Hybrid Materials and Nanocomposites; A.De; ed.; American Scientific Press; New York, 2003
4. R. Gangopadhyay, A.De, Chem. Mater.12, 608, 2000
5. Y.Ma, N.Li, C.Yang, X.Yang, Colloids Surf. A 1, 269, 2005
6. V.E.Gul, Structure and properties of conducting polymer composites; VSP: Utrecht, The Netherlands, 1996
7. A.N.Shipway, I.Willner, Chem. Commun. 2035, 2001
8. A.B.Afzal, M.J.Akhtar, M.Nadeem, M.M.Hassan, J.Phys.Chem.C 113,17560,2009
9. H.T.Lee, K.R.Chuang, S.A.Chen, P.K.Wei, J.H.Hsu, W.Fann, Macromolecules 28, 7645, 1995
10. T.A.Skothein, Handbook of Conducting Polymers, 1&2, Marcel Dekker, NY, 1986
11. J.Margolis, Conductive Polymers and Plastics, Chapman and Hall, 121, 1989
12. The Noble Prize in Chemistry, Conductive Polymers, 2000
13. P.Chandrasekhar, Conducting Polymers Fundamentals and Applications:A Practical Approach, K.A. Publishers,1999
14. C.Kittel, Introduction to Solid State Physics, John Wiley &Sons, vol.7, 1996
15. B.G.Streetman, Solid State Electronic Devices, Prentice Hall, 1990
16. B.Norden, E.Krutmeijer, Advanced Information: Nobel Prize in Chemistry, 2000, Royal Swedish Academy of Sciences
17. H.S.Nalwa, Handbook of Advanced Electronics and Photonic Materials and Devices 8,35,2001
18. Rajesh, T.Ahuja, D.Kumar, Sensors and Actuators B 136, 275, 2009
19. J.C.Lacroix, K.K.Kanazawa, A.Diaz, J. Electrochem. Soc. 136(5), 1308, 1989
20. D.C.Trivedi, S.K.Dhawan, Synth. Met. 59, 267, 1993

21. V.G.Kulkarni, W.R.Mathew, J.C.Campbell, C.J.Dinkins, P.J.Durbin, J.Vinyl Tech. 14(2), 123, 1992
22. S.Gottesfeld, F.A.Uribe, S.P.Armes, J. Electrochem. Soc. 14, 139, 1992
23. F.Cheng, W.Tang, C.Li, J.Chen, H.Liu, P.Shen, S.Dou, Chem.Eur. J. 12, 3082, 2006
24. K.S.Park, S.B.Schougaard, J.B.Goodenough, Adv.Mater. 19, 848, 2007
25. W.H.Meyer, Adv. Mater. 10, 439, 1998
26. J.T.Mabeck, G.G.Malliaras, Anal.Bioanal. Chem. 384, 343, 2006
27. D.Lakshmi, A.Bossi, M.J.Whitcombe, I.Chianelle, S.A.Piletsky, E.V.Pilestky, S.A.Flower, Anal. Chem. 81, 3576, 2009
28. H.Yoon, J.Jang, Adv. Funct. Mater. 19, 1567, 2009
29. Z.Zhang, M.Rouabhia, Z.Wang, C.Roberge, G.Shi, P.Roche, J.Li, L.H.Dao, Artif. Organs 31, no.1, 2007
30. N.Gomez, C.E.Schmidt, Journal of Biomedical Materials Research Part A doi 10.1002/jbm.a
31. T.Xu, Journal of Membrane Science 263, 1, 2005
32. E.Smela, Adv. Mater. 15, 481, 2003
33. A.A.Entezami, B.Massoumi, Iranian Polymer Journal 15(1), 13, 2006
34. N.C.Billingham, P.Calvert, Adv.Polym.Sci. 1,90,1989
35. M.Ian, Introduction to Synthetic Polymers, Oxford Science Publications, Chapter 10, 1994
36. Richard B.Kaner and Alan.G.MacDiarmid, Scientific America, 60, February 1988
37. Luis Alcacea, Conducting Polymers, D.Reidel Publishing Company, 1987
38. M.F.Rubner, Molecular Electronics, Research Studies Press, Chapter 2, 1992
39. A.Drury, S.Chaure, M.Kroll, V.Nicolosi, N.Chaure, W.J.Blau, Chem. Mater. 19, 4252, 2007
40. J. E. de Albuquerque, L.H.C. Mattoso, R.M. Faria, J.G. Masters and A.G. MacDiarmid, Synth. Met. 146, 1, 2004
41. J.Stejskal, R.G.Gilbert, Pure Appl. Chem. 12, 608, 2008
42. M.V.Kulkarni, A.K.Viswanath, Polym. Eng. Sci. 47, 1621-1629, 2007
43. R.A.Misra, S.Dubey, B.M.Prasad, D.Singh, Indian Journal of Chemistry, 38A, 141-149, 1999

44. L.N.Lews, Chem.Rev. 93, 2693, 1993
45. M.Kralik and A.Biffis, Mol.Catal. A 177, 113, 2001
46. A.P.Alivisatos, Science 271, 933, 1996
47. D.L.Feldheim and C.D.Keating, Chem. Soc.Rev. 27, 1, 1998
48. P. Khullar, V. Singh, A. Mahal, H. Kaur, V. Singh, T.S. Banipal, G. Kaur, M. S. Bakshi, The Journal of Physical Chemistry C 115(21), 10442, 2011
49. W.P.McConnel, J.P.Nowak, L.C.Brousseau, III, R.R.Fuierer, R.C.Tenet, and D.L.Feldheim, J.Phys.Chem.B 104, 8925, 2000
50. Praveen Kumar, M. Tuteja, M. Kesaria, U.V. Waghmare, S.M. Shivaprasad, Applied Physics Letters 101(13), 131605, 2011
51. K.Grieve, P.Mulvaney, F.Grieser, Curr.Opin.Colloid Inter.Sci 5, 168, 2000
52. R. Garjonyte, A. Malinauskas, Biosens. Bioelectron. 15, 445, 2000
53. S.C.Farmer and T.E. Patten, Chem. Mater.13, 3920, 2001
54. J.H.Hodak, A.Henglein, and G.V.Hartland, J.Chem.Phys. 114, 2760, 2001
55. M.Wan, R.R. Yadav, K.L. Yadav, S.B. Yadaw, Experimental Thermal and Fluid Science 41, 158, 2012
56. X.J.Xu, P.Y.Chow, and L.M.Gan, J. Nanoscience Nanotechnol. 2, 61, 2002
57. A.Henglein, Chem. Rev. 89, 1861, 1989
58. G.D.Stucky, J.E.MacDougall, Science 247, 669, 1990
59. AZoM.com, The A to Z of Materials, 2001
60. A.S.M. Giasuddin, K.A.Jhuma, A.M.Mujibul, Bangladesh J. Med. Biochem. 5(2), 56, 2012
61. S.Jain, D.G. Hirst, J.M. O'Sullivan, The British J. Radiology 85, 101, 2012
62. M.V.Yigit, Z.Medarova, Am. J. Nucl. Med. Imaging 2(2), 232, 2012
63. K.Saha, S.S.Agasti, C.Kim, X.Li, V.M.Rotello, Chem. Rev. 112, 2739, 2012
64. www.lenntech.com/periodic/elts/ag.htm.s
65. R.A.Khaydarov, R.R.Gapurova, J. Nanoparticle Research 11, 1193, 2009
66. en.wikipedia.org/wiki/Silver nanoparticles
67. D.N.Muraviev, J.Macanas, M.Farre, M.Munoz, S.Alegret, Sens.Actuators B 118, 408, 2006
68. D.N.Muraviev, M.I.Pividory, J.L.M.Sotto, S.Alegret, Solv. Extract. Ion Exchange 24, 731, 2006
69. H.S.Li, M.Josowicz, D.R.Baer, M.H.Engelhard, J.J.Janata, Electrochem. Soc. 142 (3), 798, 1995

70. M.Kinyanjui, J.Hanks, D.W.Hatchett, A.J.Smith, M.J.Josowicz, Electrochem.Soc. 151, D113, 2004
71. A.P.O'Mullane, S.E.Dale, T.M.Day, N.R.Wilson, J.V.Macpherson, P.R.Unwin, J.Solid State Electrochem. 10, 792, 2006
72. L.Niu, Q.Li, F.Wei, S.Wu, P.Liu, X.Cao, J.Electroanal.Chem. 578, 331, 2005
73. A.N.Grace, K.Pandian, Electrochem.Commun. 8, 1340, 2006
74. T.Amaya, D.Saio, T.Hirao, Tetrahedron Lett. 48, 2729, 2007
75. S.Baranton, C.Coutanceau, P.Capron, Electrochim. Acta 51, 517, 2005
76. C.Bian, Y.Yu, G.Xue, J.Appl.Polym.Sci. 104,21,2007
77. J.A. Smith, M.Josowicz, J.Janata, J.Electrochem.Soc. 150: E 384, 2003
78. S.K.Pillalamarri, F.D.Blum, A.T.Tokuhiro, M.F.Bertino, Chemical Mater. 17, 5941, 2003
79. J.M.Kinyanjui, J.Hanks, D.W.Hatchett, Macromolecules 37, 8745, 2004
80. P.R.Selvakannan, S.Mandal, R.Pascricha, M.Sastry, J.Colloid Interface Sci. 279, 124, 2004
81. Z.Guo, Y.Zhang, L.Huang, M.Wang, J.Wang, J.Sun, L.Xu. N.Gu, J. Colloid Interface Sci. 309, 518, 2007

CHAPTER 2

LITERATURE REVIEW

This chapter covers the brief details of the research work reported in the area of this study. Literature review is confined to conducting polymers [with special reference to polyaniline and poly (2-ethylaniline)], noble metal nanoparticles [with special reference to gold and silver] and their nanocomposites.

2.1 CONDUCTING POLYMERS

Polymers have been long thought of and applied as insulators. But in the 1970s, somewhat surprisingly, a new class of polymers possessing high electronic conductivity in the oxidised state was discovered. Three collaborating scientists, J.Heeger, MacDiarmid and Shirakawa, played a major role in this breakthrough and received the Noble Prize in Chemistry in 2000 " for the discovery and development of electronically conducting polymers" (1-4).

The use of conducting polymers is being increasingly going up as their physico-chemical properties can be tailored for numerous applications. These applications are based on their variable electrical conductivity and electroactivity. Yuan et al. (5) showed that polyaniline (PANI) can be used as coating on a glass surface for reflecting infrared radiations. Similar application of PANI coating on fabric to shield from electromagnetic radiation has been reported by Dhawan et al. (6).Li et al. (7) have demonstrated that conducting polymer adhesives can be prepared to glue conducting surfaces together. This enables the electric current to pass through them. Jonas and Schrader proposed that coating insulating materials with conducting polymer 3, 4-polyalkylenedioxythiophene enables them to absorb radiowave and microwave radiations which may cause malfunctions in other electrical devices placed nearby. McCullough (8) reviewed the application of polythiophenes and stated that urethane-substituted polythiophene could be used as electromagnetic radiation shielding as well as antistatic coating. The conducting polymer coating can also be sued to prepare printed circuit boards which are being used in electrical appliances (9-10). Foitzik et al. (11) demonstrated that a woven woollen fabric when coated with cross-linked poly (α,ω-bis (3-pyrrolyl) alkanes) provided low surface resistance, high color fastness and stability to it. Hu et al. (12) have shown that coating an aircraft with

conducting polymer will prevent buildup of static charge on it. Widge et al. (13) have shown that conducting polymer can act as artificial nerve as they can transport small electrical signals through the body.

It has been further shown by Xu et al. (14) that redox states can be altered by selectively using suitable dopant ions. The conducting polymers being intensely coloured, only a very thin layer is required for devices with a high contrast and large viewing angle. Wang and MacDiarmid (15) have shown that doped polypyrrole, poly (3, 4-ethylenedioxythiophene) and polyaniline improved the mechanical flexibility of electrical display devices. Bedioui et al. (16) had proposed that film of polypyrrole and other conducting polymers can play an important role as support for electrocatalytic metal complexes. Pickup (17) has shown that the electronically conducting ion exchange polymer poly-(3-methylpyrrole-4-carboxylic acid) has potential to bind large cations reversibly. The chemical, structural, thermal, optical, biological, electrical properties of conducting polymers make them desirable material for their use in different types of sensors (18).

2.2 POLYANILINE (PANI) – Development and Synthesis

Among conducting polymers, PANI is one of promising material due to environmental stability, tunable doping & de-doping chemistry and excellent optical & electrical behaviour (19-20). It has been known since 1862 as aniline black (21). Willstatter and co-workers in 1907 &1909 regarded aniline black as an 8-nuclei chain compound (22-23). However in 1910 Green & Woodhead were able to report various forms of PANI (24).

Singh et al. have reviewed research on PANI type conducting polymers. According to them, process development with high accuracy of product results had the direct relationship with structure and properties (25). PANI nanostructures such as nanotubes, nanofibres, coreshell material have resulted in enhanced performance in various opto-elctronic sensing applications (26). Edward Song and Jin-Woo Choi have synthesized one-dimensional PANI nanowires which can be used as an active layer for sensors whose conductivity change can be used to detect chemical or biological species (27). By interfacial polymerization method, Jiaxing has been able to produce pure nanofibres. With

this nanofibres morphology, the dispersibility and processibility of PANI has improved. They can also serve as a template to grow inorganic/PANI nanocomposites (28).

The morphological and structural changes of PANI films after their exposure to higher temperatures were revealed by Peikertova et al. (29). It was observed that the increasing of temperature influences the colour of PANI thin films, which passes from green to blue. The colour change may indicate the transition of PANI to its non-conductive form.

2.2.1 Chemical Synthesis

According to the IUPAC Technical Report as prepared by J. Stejskal (30), eight persons from five institutions in different countries carried out polymerizations of aniline following the same preparation protocol. In a "standard" procedure, aniline hydrochloride was oxidized with ammonium peroxydisulfate in aqueous medium at ambient temperature. The yield of polyaniline was higher than 90 % in all cases. The electrical conductivity of polyaniline hydrochloride thus prepared was 4.4 ± 1.7 Scm^{-1} (average of 59 samples), measured at room temperature. A product with defined electrical properties could be obtained in various laboratories by following the same synthetic procedure. The influence of reduced reaction temperature and increased acidity of the polymerization medium on polyaniline conductivity were also addressed. The conductivity changes occurring during the storage of polyaniline were monitored. The average conductivity of corresponding polyaniline bases was 1.4×10^{-8} S cm^{-1}. Additional changes in the conductivity take place during storage. Aging is more pronounced in powders than in compressed samples. As far as aging effects are concerned, their assessment is relative. The observed reduction in the conductivity by about 10 % after more than one-year storage is large but, compared with the low conductivity of corresponding polyaniline (PANI) base, such a change is negligible. For most applications, an acceptable level of conductivity may be maintained throughout the expected lifetime (30).

The number of different nanostructures (flowers, fibres, spheres, rods etc) produced from the chemical oxidation of aniline into polyaniline have been shown by H. D. Tran et al. (31). The small and subtle changes in reaction parameters

resulted in their formation. These changes can often result in drastic differences in the polymers nano scale morphology. Rosa Veera et al. have shown that the morphological differences of the polymeric films as a function of the chemical nature of the monomers influenced their behaviour as barrier effect against the aggressive media (32). Kulkarni et al. have synthesized and characterised PANI by rapid liquid-liquid interfacial polymerization technique using trichloroethane as organic media and APS as an oxidising agent (33). Singla et al. has used PANI in several applications (34-35).

2.2.2 Electrochemical Synthesis

Jianbing Zang et al. have electropolymerised PANI on undoped nanodiamond (ND) powder in presence of sulphuric acid. The results showed that the PANI growth rate increased with the increasing concentration of aniline monomer and sulphuric acid but it decreased when the monomer concentration was higher than 0.3 M (36).

According to the study of Bekir Sari et al. conductive homopolymers of o-chloroaniline, p-bromoaniline and N-methylaniline were synthesized electrochemically in perchloric acidic solution and their properties were analyzed. Initially, the maximum oxidation potential values of these monomer solutions were determined by Cyclic Voltammetry (CV). These conductive polymers were synthesized under a nitrogen atmosphere using a potentiostat (37).

Majidi et al. worked out that the synthesis of optically active polyaniline salt films via the enantioselective electro polymerization of aniline on indium-tin-oxide (ITO)-coated glass electrodes in the presence of sulphonic acid. They found the similar results as were obtained under potentiostatic, galvanostatic and potentiodynamic conditions. Results suggest that chiral holes might be formed in the polymer matrix during both redox and chemical re-doping cycles of polyaniline salt films (38). Hager et al. electropolymerised aniline over grapheme immobilized on glassy carbon substrate potentiostatically in a three-electrode-one compartment cell. The results revealed that the presence of graphine enhances the electrochemical of PANI (39). Ralph et al. used the platinum tip of a scanning tunnelling microscope to direct the electropolymerization of aniline on nanometer-

scale regions of a graphite surface which was emerged in an aqueous aniline containing electrolyte (40).

2.3 POLY (2-ETHYLANILINE) (PEANI)

2.3.1 General Information:

Poly (2-ethylanilne) is another derivative of PANI conducting polymer. Patricia Enzel et al. have succeeded in synthesis of PEANI upto the length of 0.1 μm long in Zeolite host (41). Andreia L. Schemid et al suggest that, depending on the size of the counterion, the presence of an alkyl group in the ortho position will influence the participation of this anion in the ionic exchange process due to steric hindrance. The electron-donating effect of the ethyl substituent is completely disregarded as compared with the steric effect that produces an increase of the torsion angle between phenyl rings (42).

2.3.2 General Synthesis

Poly(2-ethylanilne) aniline is prepared by the oxidation of aniline in solution. The oxidation can be achieved either chemically or electrochemically as proposed by R.A. Misra (43).

2.3.2.1 Electrochemical Synthesis:

The electrochemical synthesis of poly (2-ethyleaniline) was carried out by the anodic oxidation of monomer 2-ethyleaniline in solution by Andreia L Schemid et al.(42). PEANI films were electropolymerised on to platinum substrate by applying triangular potential sweeps (0.01 Vs^{-1}). The polymerisation was carried out in a 0.5 mol/L monomer and 1 mol/L HCl electrolytic solution.

The electrochemical method has the advantage that the electrolyte (and hence the dopant species) can be selected and also that the applied potential can be altered in order to provide polymers with a spectrum of physical and chemical properties. The oxidation level of the polymer can easily be altered in these studies to provide clues as to the chemical structure of the polymer under different redox conditions. Electrochemical synthesis produces a more homogenous polymer because the oxidation of the monomer is carried out with no additional chemical oxidant. Therefore, the composition of oligomeric materials into the polymer matrix is minimized relative to PEANI produced using

chemical synthesis methods. Electrochemistry of conducting polymers-persistent model was reviewed by Jurgen et al. (44).

2.3.2.2 Chemical Synthesis and other methods

Poly (2-ethylaniline) emeraldine salt was also synthesized by the oxidative polymerisation of 2-ethylaniline in aqueous acidic media by using a variety of oxidizing agents, the most commonly used oxidant being APS. The synthetic strategy and reaction mechanism for PEANI is similar to those of PANI (45-46).

Enzymatic synthesis of poly (2-ethylaniline)/SPS complex was reported by Mohammad Reza Nabid et al. They prepared a water-soluble and conducting poly (2-ethylaniline) in the presence of sulphonated polystyrene (SPS). The polymerization of 2-ethylaniline was performed with horseradish peroxidase (HRP) as a catalyst to form conducting poly (2-ethylaniline)/SPS complex with moderate electrical conductivity (47).

Ethyl and ethoxy substituted PANI with poly (styrenesulfonic acid) has been synthesized by Der-Shyu Lin and Sze-Ming Yang. The complexes were prepared by chemical polymerisation of monomer with PSSA using an oxidant of APS in 1M HCl (48). PEANI films were chemically deposited onto gold electrodes using oxidant in the presence of surfactants (sodium dodecylsulphate and tetradecyltrimethylammonium bromide) by Aysegul Uygun (49).

2.4 NOBLE METAL NANOPARTICLES

2.4.1 Historical Perspective

The materials in nanometer range were already in use since the 4th century A.D., in the form of Lycurgus Cup which had nanoparticles of gold and silver that imparted interesting optical properties to the material. But this preparation was most probably adventitious and the detailed knowledge of the presence of ‘nanomaterial’ inside the glass was not there. Similarly, churches of Middle Ages had aesthetically pleasing ruby-colored glasses. These were prepared by adding the gold salts in the glass-precursor mixture. At the high temperatures required for glass formation, the gold salt decomposed to nascent gold that was trapped in its colloidal state within the matrix of glass. Variation of the synthesis conditions resulted in the formation of glass of different lines and colors (due to the formation

of nanoparticle of different sizes). Another example of inadvertent use of nanoparticles was the 'Aurum potabile'. This was colloidal gold sol in aqueous medium, and was thought to have powers for manydiseases, including venereal diseases and arthritis (50).

A detailed experimental study of gold sols was undertaken by Michael Faraday in the 1850s (51). He was the first to systematically study this 'hydrosol of gold. Boosted by the newer methods for the synthesis of colloids with low polydispersity, further experiments by Zsigmondy and others established the use of finely divided gold nanoparticles (52). The 'ultramicroscope' of Zsigmondy utilized a very important property of matter in colloidal state – scattering of light. This effect is known as "Tyndall effect" and is a unique property of material in micron and submicron regime. Around that time, a detailed theoretical description of the optical properties of nanoparticles was provided by Mie. In 1915, Ostwald wrote his famous book "The World of Neglected Dimensions" in which he discussed about colloids and interfaces. Then, in 1931, Knoll and Ruska developed the electron microscope giving the ability to visualize material in nanometer range. Another landmark in the development of Nanotech was the famous lecture by Feynman in 1960 that ignited people to look into the 'small' matter closely. His lecture was titled "There is plenty of room at the bottom" and highlighted the potential applications/properties of nanomaterials (53). Turkevich and Frens developed methods for simple and reproducible preparation of gold sols with low particle dispersity (54-55). Alongside, Stober developed the procedure for preparation of highly monodisperse silica nanoparticles. In the year 1974, Prof. Taniguchi of Japan was the first to coin the term 'Nanotechnology'. The advent of Scanning Tunneling Microscope during the early 1980s was another milestone in the development of Nanotech. These instruments allowed the imaging and manipulation of atoms and gave tremendous insights into the structures of nanomaterials.

2.4.2 Present status

Metal nanoparticles are now attracting investigators due to their unique size dependent physio-chemical properties (56-57) and their use in areas such as sensors (58) and optoelectronics (59) and many more.

Several physical and chemical methods have been used for synthesis and stabilizing nanoparticles (60-61). The most common approach for their synthesis is chemical reduction using organic/inorganic reducing agents such as citrate, ascorbate, sodium borohydride and polyol process (62). Different types of surfactants such as thiols, amines, acids and alcohols have been used to stabilize the surfaces.

The presence of surfactants (hexamine, TEAB, CTAB and PVP) on the surface of zinc oxide nanoparticles resulted variation in their optical properties.The optical properties of each surfactant capped ZnO nanoparticles were investigated by Singla et al. (63). In our laboratory, Suman Singh et al. have synthesized and studied the conjugates of gold nanoparticles and semiconductor quantum dots (CdS/T) with bovine serum albumin using wet chemistry (64).

Simple and effective route for synthesis of crystalline silver nanorods and nanowires for electro applications, electronic and photonic devices depending upon size and shape has been discussed by several authors (65). Temperature dependent size control and nucleation of gold nanoclusters was reported by Mona B Mohamed (66). Wires, plates, flowers, needles and coreshell diverse nanostructures of gold using PANI templates were proposed by Sajanlal etc (67).

2.4.3 Gold Nanoparticles (GNPs)

Gold nanoparticles are an important object of their chemical stability and specific optical (68-70), physical and biological (71-72) behaviours.

One of the important characteristic of gold nanoparticles is a phenomenon called **Surface Plasmon Resonance (SPR)**. According to SPR, when light is shone on GNPs of different sizes, shapes or compositions, they appear of different colours. Because of this property, GNPs are commercially used in rapid testing arrays like pregnancy tests and other bio-molecule detectors (73-74).

Gold nanoparticles are used as **catalysts** in number of chemical reactions. The surface of a GNP can be used for selective oxidation or in certain cases the surface can reduce a reaction.

L.Prati and A.Villa have been able to prepare active gold catalysts by different methods like impregnation, coprecipitation etc (75). Z. Zhong et al. have

identified the subtle, atomic-scale structural transformation that can activate and deactivate GNPs catalysts which may lead to longer lasting hydrogen fuel cells (76). Mark Turner et al. have been able to do selective oxidation of styrene with dioxygen by GNPs catalysts derived from 55-atom clusters (77).

Gold nanoparticles are used in variety of **sensors**. J.P.Lafleur et al. have demonstrated the vast potential of GNP-based microfluidic sensors for detection of 2 important classes of environmental contaminants-heavy metal and pesticides (78). Breath testing using GNPs sensors as a fast and reliable diagnostic test for early detection of chronic kidney disease have been reported by O.Marom et al. (79). A simple colorimetric technique for detection of small concentrations of aqueous heavy metal ions using functionalized GNPs have been suggested by Y.K. Robert et al.(80).

Gold nanoparticles are used in **electronics** as conductors from printable inks to electronic chips. Two dimensional arrays of GNPs with sulphur containing fullerene nanoparticles were self assembled through the formation of Au-S covalent bonds by S.M. Shih et al. The assembled arrays have potential applications as nanoelectronics (81). The Langmuir-Blodgett deposition of organically passivated GNPs is reported by S.Paul et al. A monolayer of these particles has been incorporated into a metal-insulator-semiconductor (MIS) structure. The MIS device exhibits a hysteresis in its capacitances vs voltage characteristic, the magnitude of which is dependent on the voltage sweep conditions (82).

Gold nanoparticles having appropriate size scale exhibits unique **optical properties** and are a lot of interest in biology and medicine. They have immense potential in applications like cancer diagnosis and therapy because of their SPR enhanced light scattering and absorption (83). P.K. Jain et al. have discussed the plasmonic photothermal therapy of cancer achieved by using the strongly enhanced plasmon resonance absorption of gold nanospheres and nanorods (84). Colleen L. Nehl et al. have reported the synthesis, structure and optical properties of 100 nm star shaped GNPs. Single particle spectroscopy measurements revealed that these nanoparticles have multiple plasmon resonances resulting in polarization dependent scattering with multiple spectral peaks, which correspond to the different tips on the star shaped structure. The

plasmon resonances were also found to be extremely sensitive to the local dielectrical environment (85).

2.4.4 Silver Nanoparticles: History and Applications

Silver nanomaterials are fine particles of metallic silver that have at least one dimension less than 100 nm. Nanosilver is not a new discovery; it has been known for over 100 years. Previously, nanosilver or suspensions of nanosilver were referred to as colloidal silver. Before the invention of penicillin in 1928, colloidal silver had been used to treat many infections and illnesses. By converting bulk silver into nanosized silver, its effectiveness for controlling bacteria and viruses was increased multifold, primarily because of the nanomaterials' extremely large surface area when compared to bulk silver, thus resulting in increased contact with bacteria and fungi.

In 1951, Turkevich et al. (54) reported a wet chemistry technique to synthesize nanosilver using silver nitrate as a silver ion source and sodium citrate as the reducing agent for the first time. Recent advances in nanomaterials science in the last two decades have enabled scientists to engineer silver nanomaterials by controlling their size, shape and surface properties. This has been motivated by the unique chemical, physical and optical properties of nanosilver and allows for their utilization in various scientific & industrial applications.

Applications

Metallic nanoparticles, including nanosilver, exhibit **surface plasmon resonance (SPR) and surface enhanced Raman scattering (SERS)**. As a consequence of the SPR and SERS, silver nanomaterials are used for detection of DNA sequences (86), colorimetric sensors for Histidine (87), determination of fibrinogens in human plasma (88), real-time probing of membrane transport in living microbial cells (89), colorimetric sensors for measuring ammonia concentration (90), biolabeling and optical imaging of cancer (91) and glucose sensors for medical diagnostics (92).

The high surface area to volume ratio of silver nanomaterials provides high surface energy, which promotes surface reactivity such as adsorption and **catalysis**. This has resulted in the use of silver nanomaterials and silver nanocomposites to catalyze many reactions in industrial processes such as CO

oxidation, benzene oxidation to phenol, photodegradation of gaseous acetaldehyde and the reduction of the p-nitrophenol to p-aminophenol.

Silver nanoparticles immobilized on silica spheres can be used to catalyze the reduction of dyes by sodium borohydride ($NaBH_4$) have been reported by Nikolaj et al. (93).According toYan et al., Ag nanoparticles synthesized in polyethylene glycol with simple bubbling of H_2 gas can been used to catalyze the three component coupling reaction of aldehyde, alkyne, and amine with good to excellent yields in one reaction vessel, thus saving time and materials (94).

The high electrical and thermal conductivity of nanosilver along with the enhanced optical properties result in various applications in electronics. Nanosilver is used in electronic equipments, mainly in solder for circuit connections as reported by DiRienzo (95).According to Kim et al., silver nanowires are used as nanoconnectors and nanoelectrodes for designing and fabricating nanoelectronic devices (96). Roldan et al.have also reported that siver nanoparticles are used in the preparation of active waveguides in optical devices, inks for printed circuit boards, optoelectronics, nanoelectronics (such as single-electron transistors, and electrical connectors), subwavelength optics and data storage devices (97).

2.5 CONDUCTING POLYMER COMPOSITES WITH NOBLE METAL NANOPARTICLES

The mixing of polymer and nanoscale inorganic particle has been recognized as a potential and economic method of producing new materials with better mechanical/electrical or catalytic behavior and also with new functions (98-99).

Composites of PANI

Already some composites of PANI with inorganic materials have been investigated for their use in catalysis, sensors and selectively for vapour sensors (100) & other similar applications (101-102).

Among the inorganic nanoparticles NPs, silver halides are photosynthetic material and extensively used as source material in photographic films, photo catalyst and ionic semiconductors (103-107). In 2004, Sui et al. put the first attempt to synthesis AgCl/PANI nanocompiste using reverse micelle method

(108). Zhu and Coworkers synthesised core shell PANI/AgCl nanocomposites with enhanced electroactivity (109-110). More recently Huagi and Jiping (111) have synthesized silver halide/PANI nanocomposites with different PANI morphology. Ag@AgCl nanocomposite was synthesized for photocatalyst under visible light and biosensors (112-114).

K Majid et al. have synthesized composite of PANI with finely graded (45μM) Mn_3O_4. The study shows the potential of the composite to act as NTC material for thermistor applications and continuous thermocouple (115). M.Sideeq Rather et al. have prepared PANI nanocomposite with photoadduct of potassium hexacyanoferrate and pyridine through ball milling, photochemical route and by oxidative polymerisation technique using APS as an oxidizing agent (116). The PANI/Mn_3O_4 composite doped with perchloric acid, sulphuric acid, acetic acid, o-phosphoric acid have been characterised as sensing material to detect relative humidity in the range of 20-90 % by Singla et al. (117) in our laboratory.

R.Del Riao et al. synthesized the composite of PANI and carbon black using electrochemical technique. The potential of Pt- electrode was varied and the electrode was dipped in the solution containing aniline and carbon black suspension. Sodium dodecyl sulphate (SDS) was used as an additive. It is shown that the rate of polymerization is enhanced by the presence of both carbon black and SDS by a factor of 5 (118).

Y.N. Qi et al. synthesised Polyaniline/Al_2O_3 (PANI/Al_2O_3) composites by in-situ polymerization in the presence of HCl as dopant by adding Al_2O_3 nanoparticles into aniline solution. The results showed that Al_2O_3 nanoparticles were connected with the PANI chains and affected the absorption characteristics of the composite through the interactions between PANI and nano-sized Al_2O_3. The PANI/Al_2O_3 composites were more thermal stable than the pure PANI (119). The PANI/manganese oxide composites were synthesized in an acidic medium using oxidative polymerisation method. The composite after dedoping with ammonia was doped with acetic acid and acrylic acid. The influence of energy deposition by gamma rays was investigated by Sajeela et al. (120). J. Jaczewska et al. developed the polyaniline film using spin coating technique. The polymers were dissolved in analytical- grade common solvents (chloroform, THF, and cyclohexanone) to form solutions of pure polymers (with a concentration of 30

mg/mL) and symmetric (1:1 w/w) polymer blends (with a constant concentration of 20 mg/mL). The pure polyaniline films were prepared using the solution of PANI in solvent and spin coated onto Si/SiO_2 substrate at a speed of 3000 rpm (121).

Nanocomposites based on conducting polymers combine the mechanical flexibility, optical and electrical properties of conducting polymers with electrical conductivity and magnetic properties of metal nanoparticles.Controlling the shape, size, morphology is very important for defining their properties (122-123).

Sarma and co-workers have synthesized PANI coated gold composite with higher electrical conductivity (124). Interactions between natural organic matter and gold nanoparticles stabilized with different organic capping agents have been discussed by Dylan P. Stankus (125). One step electrochemical synthesis of gold nanoparticles-polypyrrole composite for application in catechin electrochemical biosensors by Suman Singh has been reported (126). Fabrication of a nanostructured gold polymer composite material has been characterized with Raman, UV-vis and other characterization techniques by K.Mallick (127). Composite of sol gel and PVP stabilized gold nanoparticles has been synthesized chemically and used as an immobilization matrix for tyrosinase enzyme by M.L.Singla et al.(128). Y.Wang et al. have demonstrated a facile route to the synthesis of PANI nanofibres by polymerization of aniline using chloroaurate acid as the oxidant. The reduction of $AuCl_4^-$ is accompanied by oxidative polymerization of aniline, leading to uniform PANI nanofibres and aggregated gold nanoparticles which can precipitate from the liquid phase during the reaction. It is found that the gold aggregates are capped with polyaniline and the conductivity of the fibre is around 0.16S/cm (129). A glucose biosensor based on composite of Au nanoparticles–conductive polyaniline nanofibres was developed by Y.Xian et al.Immobilized with glucose oxidase (GOx) and nafion on the surface of nanocomposite, a sensitive and selective biosensor for glucose was successfully developed by electrochemical oxidation of H_2O_2. It indicates excellent reproducibility and good operational stability (130). An electrochemical sensor was fabricated by electrodeposition of gold nanoparticle on pre-synthesized polypyrrole (PPy) nanowire, forming an Au/PPy composite matrix on glassy carbon electrode (Au/PPy/GCE) by Jing Li and X.Lin. As an

electrochemical sensor, the Au/PPy/GCE exhibited strongly catalytic activity toward the oxidation of hydrazine and hydroxylamine. In addition, the sensor showed excellent sensitivity, selectivity, reproducibility and stability properties (131).

Neelgund et al. prepared composites of polyaniline derivatives–polyaniline, poly (2, 5-dimethoxyaniline) and poly (aniline-2, 5-dimethoxyaniline) and silver nanoparticles through simultaneous polymerization of aniline derivative and reduction of $AgNO_3$ in the presence of poly(styrene sulfonic acid) (PSS). $AgNO_3$ was used as one of the initial components (1) to form the silver nanoparticles and (2) as an oxidizing agent for initiation of the polymerization reaction. UV-visible spectra of the synthesized nanocomposites revealed the synchronized formation of silver nanoparticles and polymer matrix. The morphology of the silver nanoparticles and degree of their dispersion in the nanocomposites were characterized by transmission electron microscopy. Thermogravimetric analysis and differential scanning calorimetry results indicate an enhancement of the thermal stability of the nanocomposites compared to the pure polymers. The electrical conductivity of the nanocomposites is in the range 10^{-4} to 10^{-2} S cm^{-1} (132).

Polyaniline/Ag nanocomposites have been synthesized via in situ chemical oxidation polymerization of aniline in silver salt by sonochemical method using H_2O_2 as an external medium (133). H_2O_2 was used to reduce $AgNO_3$ to Ag nanoparticles as well as to polymerize aniline to polyaniline in the same pot. The ultrasound radiation as an energy source was applied to facilitate the reaction by reducing the reaction time. Reduction of the silver salt in aqueous aniline leads to the formation of silver nanoparticles which in turn catalyze oxidation of aniline to polyaniline. The research on the structures and properties of the composites showed the individual or aggregated silver nanoparticles are dispersed in the matrix of polyaniline. The composites possess a higher degradation temperature than polyaniline alone, and their electrical conductivity are raised morethan 200 times. The cyclic voltammetry and impedance spectroscopy results showed that the polyaniline/Ag film exhibits considerably higher electroactivity compared with polyaniline film without Ag particles. Pooja Devi et al. have synthesized and characterized silica-coated silver core shell nanostructures and their sensing

behaviour when deposited on glass carbon electrode for nitrobenzene detection (134). Ag@AgCl-A highly efficient and stable photocatalyst under visible light has been reported by Peng Wang et al (135). Silver doped with acidic-basic polymers–novel, reactive metallic composite has been proposed by Hanna Behar -Levy (136). Optical humidity sensing characteristic of Ag-PANI nanocomposite was discussed by Fuke et al. (137). PANI/Ag nanocomposite was synthesised by using aniline as dispersant and stabilizer of nanosilver sol (138).

There has not been any study on the composite material of PEANI with gold, silver which may become an interesting study for several applications such as sensing and opto-electronic devices. A highly conductive PEANI/kaolinite composite was suggested by Anakli et al. The composite was prepared by chemical polymerisation in aqueous HCl medium in the presence of kaolinite particles by using potassium chromate as an oxidant (139). Electrorheological (ER) properties of various polyaniline derivatives, namely: poly (*o*-toluidine) (POT), poly(*N*-methyl aniline) (PNMAn), poly(*N*-ethyl aniline) (PNEAn), and poly(2-ethyl aniline) (P2EAn) were investigated. Effects of various parameters such as; particle size, particle conductivity, suspension's sedimentation stability, flow times, concentration, electric field strength, shear rate, frequency and temperature onto ER activity of these polyaniline derivatives/silicone oil (SO) suspensions were investigated by B.Gercek (140).

Chemical synthesis of substituted PANI/Chitosan (Ch) composites was reported by A.G.Yavuz et al.The PEANI/Ch composite exhibited higher thermal stability than the other composites (141). The same team synthesized substituted PANI/Ch composites electrochemically in 0.1M H_2SO_4 acid medium. Glucose oxidase was immobolised on to the surface of these composites by physical adsorption and was used for glucose sensing (142). Conducting polymers of alkylanilines and their conducting composites were synthesized with KIO_3as an oxidant by B.Sari et al.The highest conductivity was obtained with PEANI with a value of $4x10^{-5}$ Scm^{-1} (143). Z.W.He et al.have fabricated nitrogen containing carbon nanospheres via pyrolysis of lignosulfonate/PEANI composite nanospheres at 600-800°C (144).

REFERENCES:

1. H.Shirkawa, E.J.Louis, A.G.MacDiarmid, A.J.Heeger, J.Chem.Soc.Chem. Commun. 579, 1977
2. H.Shirakawa, Angew Chem. Int. Ecl. 40, 2574, 2001
3. A.G.MacDiarmid, Angew Chem. Int. Ed. 40, 2581, 2001
4. A.J.Heeger, Angew Chem. Int. Ed. 40, 2591, 2001
5. T.Yuan, Y.Huang, S.Dong, T.Wang, M.Xie, Polymer Testing 21, 641 2002
6. S.K.Dhawan, N.Singh, S.Venkatachalam, Synth. Metal 125, 389, 2001
7. Y.Li, C.P.Wong, Materials Science and Engineering 1,51,2006
8. R.D.McCullough, Adv. Mater. 10,93,1998
9. O.Zabihi, A.Khodabandeh, S.M.Mostafavi, Polymer Degradation and Stability, 3,97,2012
10. H.Meyer, R.J.Nichols, D.Schroer, L.Stamp, Electrochimica Acta 39, 1325, 1994
11. R.C.Foitzik, A.Kaynaka, F, M. Pfeffer, Synth.Metal 157, 534, 2007
12. J.Hu, Y.Zhu, H.Huang, J.Lu, Prog. Polym. Sci. 37, 1720, 2012
13. A.S.Widge, M.Jeffries-El, X.Cui, C.F.Lagenaur, Y.Mastsuoka, Biosensors and Bioelectronics 22, 1723, 2007
14. C.Xu, J.Zhao, J.Yu, C.Cui, Electrochimica Acta 82,96,2013
15. P.C.Wang, A.G.MacDiarmid, Displays 28, 101, 2007
16. F.Bedioui, C.Bongars, J.Devynck, C.Bied-Charreton, C.Hinnen, J.Electroanal. Chem. 87, 207, 1986
17. P.G.Pickup, J.Electroanal. Chem. 225, 273, 1987
18. T.Patois, J.B.Sanchez, F.Berger, J.Y.Rauch, P.Fievet, B.Lakard, Sensors & Actuators B 431,171-172, 2012
19. A.G.MacDiarmid, Syn. Metals 27, 84, 1997
20. S.Bhandra, D.Khastgir, N.K.Singha, J.H.Lee, Prog. Polym. Sci. 34, 783, 2009
21. H.Lethebey, J.Am. Chem.Soc. 2215, 161, 1862

22. Willstatter and Moore, Ber. 40, 2665, 1907

23. Willstatter and Dorogi, Ber. 42, 2147, 4118, 1909

24. A.G.Green and A.E.Woodhead, J.Chem.Soc. 97, 2388, 1910

25. Yuvraj Singh Negi and P.A.Adhyapak, J.Macromolecular Sc. 42, 35, 2002

26. D.Li, J.Huang, R.B.Kaner, Acc. Chem. Res. 42, 135, 2009

27. Edward Song and Jin-Woo Choi, Nanomaterials 3, 498, 2013

28. Jiaxing Huang, Pure Appl. Chem. 78, 15, 2006

29. P.Peikertova, V.Matejka, L.Kulhankova, J.Tokarsky, Nanocon 9, 21, 2011

30. J.Stejskal, Pure App.Chem. 74, 857, 2002

31. Henry D.Tran, Julio M.D.Arcy, Yue Wang, Veronica A.Strong, J.Mater Chemistry 21,3534, 2010

32. R.Veera, H.Romero, A.J.Eduardo, J.Chil.Chem.Soc. 48,23,2003

33. M.Kulkarni, B.Kale, S.Apte, S.Naik, U.Malik J.Chem. and Chem. Tech. Vol. 5, No. 1, 2011

34. M.L.Singla, J.Singh, A.P.Bhondekar, A.Sharma, Appl. Mater. Interface 5, 5346, 2013

35. M.L.Singla, V.S.Pandey, Defence Science Journal 57, 255, 2007

36. Jianbing Zang, Yanhui Wang, Xiyan Zhao, Shubing Ren, Int. J.Electrochem. Sc. 7, 1677, 2012

37. S.Bekir, M.Talu, Turk. J.Chem. 22, 301, 1998

38. M.R.Majidi, A.P.Leon, K.Magvire, G.W.Gordon, Anstranan Journal of Chemistry 5(1), 23, 2002

39. Hagar K.Hassan, Nada F. Atta, Ahmed Golal, Int. J.Electrochem.Sci. 7, 11161, 2012

40. Ralph M.Nyffenegger and Reginald M.Penner, J.Phys. Chem. 100(42), 17041, 1996

41. P.Enzel, T.Bein, Am.Ins. Phy. Conf. Proc. 93, 262, 1992

42. A.L.Schemid, S.I.Cordoba, A.N.Bassetto, I.A.Carlos, J.Braz. Chem. Soc. 11, 317, 2000

43. R.A.Misra, S.Dubey, B.M.Prasad, D.Singh, Indian Journal of Chemistry 38A, 141, 1999

44. J.Heinze, B.A.Frontar-Uribe, S.Ludwigs, Chem. Rev. 110, 2010

45. E.M.Genies, A.Boyle, M.Lapkowski, C.Tsintavis, Syn.Metals 35, 159, 1990

46. F.Lux, Polymer 35, 2915, 1994

47. M.R.Nabid, A.A.Entezami, Iranian Polymer Journal 12, 401, 2003

48. Der-Shyu Lin and Sze-Ming Yang, J. of App. Polymer Sc. 98(3), 1198, 2005

49. Aysegul Uygun, J.Macromolecular Sc. 47(7), 633, 2010

50. A.J.Lewis, D.T.Walz, Prog. Med. Chem. 19, 1, 1982

51. M.Faraday, Philos. Trans. 147, 145, 1857

52. R.Zsigmondy, The Chemistry of Colloids, 1&2, John Wiley & Sons, NY, 1917

53. R.P.Feynman, Eng.Sci. 22, 1960

54. J.Turkevich, P.Stevenson, J.Hiller, Discuss Faraday Soc. 11, 55, 1951

55. G.Frens, Nature: Phys. Sci. 241, 20, 1973

56. C.Jeyaprabha, S.Sathiyanarayanan, G.Venkatachari, J.Appl. Polym. Sci 101, 2144, 2006

57. R.H.Friend, R.W.Gymer, A.B.Holmes, R.N.Marks, C.Taliani, D.D.C.Bradley, D.A.Dos Santos, W.R.Salaneck, Nature 121, 397, 1999

58. M.D.Levi, Y.Gofer, D.Aurbach, Polymers for Advanced Technologies 13, 697, 2002

59. S.K.Dhawan, N.Singh, D.Rodrigues, J.Sci. and Technol. Adv. Mater 4, 105, 2003

60. A.Lopez-Miranda, A.Lopez-Valdivieso, G.Viramontes-Gamboa, J.Nanopart. Res. 14, 1101, 2010

61. Yugang Sun, Younan Xia, Science 298, 2177, 2002

62. E.A.Sanches, J.C.Soares, R.M.lost, V.S.Marangoni, G.Trovati, T.Batista, J.Nanomaterials, doi: 10.1155/2011/697071

63. M.L.Singla, M.M.Shafeeq, Manish Kumar, J. of Luminescence 129, 434, 2009

64. Suman Singh, Rajnish Kaur, Pooja Devi, D.V.S.Jain, M.L.Singla, J. of Luminescence 141, 53, 2013

65. Jiang-Qiang Hu, Qing Chen, Zhao-Xiong Xie, Guo-Bin Han, Adv. Fun. Material 2, 14, 2004

66. Mona B.Mohamed, Zhong L.Wang, Mostafa, A.El Ssyed, J.Phys. Chem. A 103, 10255, 1999

67. P.R.Sajanlal, T.S.Sreeprasad, A.Sreekumaran Nair, T.Pradeep, Langmuir 24, 4607, 2008

68. J.P.Novak, L.C.Brousseau, F.W.Vance, R.C.Johnson, B.I.Lemon, J.T.Hupp, D.L.Feldheim, J.Am. Chem. Soc. 122, 12029, 2000

69. M.Bruct, D.Bethell, C.J.Kiely, D.J.Schiffrin, Langmuir 14, 5425, 1998

70. R.M.Tilakia, Iraji Zads, M.Madhav, Appl. Phys. A.84, 215, 2006

71. P.K.Jain, K.S.Lee, I.H.El-Sayeed, M.A.El-Sayeed, J.Phys.Chem. B 110, 7238, 2006

72. A.J.Haes, D.A.Stuart, S.Nie, R.P.V. Duyne, Journal of Fluorescence 14, 355, 2004

73. A.Sugunan, J.Dutta, J. of Physics Sc. and Ielea No. 1 & 2, 4, 2004

74. A.Gole, J.W.Stone, W.R.Genmill, C.J.Murphy, Am.Chem. Soc. 24, 6232, 2008

75. Laura Prati and Alberto Villa, Catalysts 2, 24, 2012

76. Z.Zhong, Xu Li, Stella See Soon Fang, J.Teo, Ming Lin, Catalysis 2(3), 360, 2012

77. Mark Turner, V.B.Golovko, P.Abdulkin, A.B.Murcia, M.S.Tikhov, Nature 454, 981, 2008

78. J.P.Lafleur, Silija Senkbeil, T.G.Jensen, Lab. Chip 12, 4651, 2012

79. O.Marom, F.Nakhoul, Ala Shiban, Hossan Haick, Nanomedicine 7, 639, 2012

80. Y.Kim, Robert C.Johnson, J.T.Hupp, Nano Letters 1(4), 2001

81. S.M.Shih, W.F.Su, Y.L.Lin, C.D.Chen, Langmuir 18, 332, 2002

82. S.Paul, C.Pearson, A.Molloy, M.A.Cousins, Nano Letters 3(4), 533, 2003

83. I.Safarik, Mirka Safarikova, Chemical Monthly 133, 737, 2002

84. P.K.Jain, X.Huang, M.A.Sayed, Nanomedicine 2(5), 681, 2007

85. Collen L.Nehl, Hongwei Liao, Jason H.Hafuer, Nano Letters 6(4), 683, 2006

86. J.A.Jacob, H.S.Mahal, N.Biswas, S.Kapoor, Langmuir 24,528, 2008

87. D.Xiong, M.Chen, H.Li, Chem. Commun. 880, 2008

88. J.ZhiLiang, C.Yuan, L.AiHui, Z.FuXin, T.NingLi, Sci. China Ser. B 50, 345, 2007

89. X.Xu, W.J.Brownlow, Q.Wan, J.J.Viola, Biochem. 43,10400,2004

90. S.T.Dubas, V.Pimpan, Talanta 76,29,2008

91. B.J.Wiley, Y.Chen, J.M.McLellan, D.Ginger, Y. Xiong, Nano Lett. 7, 1 032, 2007

92. Y.K.Mishra, S.Mohapatra, D.Kabiraj, B.Mohanta, N.P.Lalla, D.K.Avasthi, Scr. Mater, 56, 629, 2007

93. L.Nikolaj, R.E.Anderson, R.Peterson, T.L.Roge, Inst. for Physics and Nanotech. - Aalborg Univ

94. W.Yan, R.Wang, Z.Xu, L.Lin, J.Mol.Cat. 255,81,2006

95. M.DiRienzo, 2006. New Applications for Silver: The LBMA Precious Metals Conference 2006, Montreux

96. S.H.Kim, B.S.Choi, K.Kang, I.Y.Yang, J.Alloys and Compounds 433, 261, 2007

97. M.V.Roldan, A.Frattini, N.Pellegri, Appl.Surf.Sc. 254, 281, 2007

98. L.Qi, H.Colfen, M.Antonietti, Nano Letters 1, 65, 2001

99. H.Zhao, E.P.Douglas, B.S.Harrison, K.S.Schanze, Langmuir 17, 8423, 2001

100. Z.F.Li, F.D.Blum, M.F.Bertino, C.S.Kim, Sensors & Actuators B 161, 390, 2012

101. Q.Wu, Z.Xue, Z.Qi, F.Wang, Polymer 41, 2029, 2000

102. F.Klasovsky, J.Hohmeyer, A.Bruckner, M.Bonifer, J.Arras, M.Steffan, M.Lucas, J.Radnik, C.Roth, P.Claus, J.Phys.Chem. C 112, 19555, 2008

103. Q. Wu, Y. Xu, Z. Yao, A. Liu, G. Shi, ACS Nano 4, 1963,2010

104. D. Schurch, A. Currao, S. Sarkar, G. Hodes, G. Calzaferri, J. Phys. Chem. B 106,12764,2002

105. Y. Tian, T. Tatsuma, J. Am. Chem. Soc. 127, 7632, 2005

106. J. Bai, Y. Li, M. Li, S. Wang, C. Zhang, Q. Yang, Appl. Surf. Sci. 254, 4520, 2008
107. C. Zhang, Q. Liu, N. Zhan, Q. Yang, Y. Song, L. Sun, H. Wang, Y. Li, Colloids Surf. A 353,64,2010
108. X. Sui, Y. Chu, S. Xing, C. Liu, Mater. Lett. 58, 1255, 2004
109. J. Zhu, X. Feng, Y. Liu, C. Lu, W. Hou, Nanotechnology 17,3578,2006
110. J. Zhu, W. Yan, X. Feng, X. Chen, X. Li, Bioelectrochemistry 72, 21,2008
111. H. Yin, J. Yang, Macromol. Mater. Eng. 297, 203, 2012
112. C. Ozdemir, F. Yeni, D. Odaci, S. Timur, Food Chem. 119, 380, 2010
113. Q. Zhang, F. Liu, L. Li, G. Pan, S. Shang, J. Nanopart. Res. 13, 415, 2011
114. S. Zhou, M. Xie, X. Yuan, F. Zeng, W. Zou, D. Yuan, Am. J. Anal. Chem. 3, 385, 2012
115. K.Majid, S.Awasthi, M.L.Singla, Sensors and Actuators 135, 113, 2007
116. M.S.Rather, Kowsar Majid, R.K.Wanchoo, M.L.Singla, Chemical Physics 61,16681,2013
117. M.L.Singla, S.Awasthi, A.Srivastava, D.V.S.Jain, Sensors and Actuators A 136, 604, 2007
118. R.Del Riao, J.H.Zagal, G.de T.Andrade, S.R.Biaggiv, J. of Applied Chem. 29, 759, 1999
119. Y.N.Qi, F.Xu, H.J.Ma, L.X.Sun, J.Zhang, T.Jiang, Journal of Thermal Analysis and Calorimetry 91, 219, 2008
120. S.Awasthi, P.Aggarwal, S.K.Tripathi, T.V.Singh, M.L.Singla, A.Srivastava, Int. J. Of Chem. 1(4), 472, 2012
121. J.Jaczewska, A.Budkowski, I.Bernasik, J.Raptis, D.Raczkowska, M.Rysz, Journal of Applied Polymer Science 105 (1), 67, 2007
122. A.P.Alivisatos, Science 271, 933, 1996
123. J.Huang, R.B.Kaner, J.Am. Chem. Soc. 126, 851, 2004
124. T.K.Sarma, A.Chattopadhyay, J.Phy.Chem.A 108, 7837, 2004
125. Dylan P.Stankus, Samuel E.Lohse, James E.Hutchison, Jeffery A.Nason, Environ. Sci. Technol. 45, 3238, 2011

126. Suman Singh, D.V.S. Jain, M.L.Singla, Anal. Methods 5, 1024, 2013

127. K.Mallick, M.Witcomb, M.Scurrell, The European Physical Journal E 20, 347,2006

128. M.L.Singla, Suman Singh, D.V.S.Jain, Sensors & Actuators B 182, 161, 2013

129. Y.Wang, Z.Liu, B.Han, Z.Sun, Y.Huang, G.Yang, Langmuir 21, 833, 2005

130. Y.Xian, Y.Hu, F.Liu, Y.Xian, H.Wang, L.Jin, Biosens. Bioelectron. 21,10,2006

131. Jing Li and Xiangqi Lin, Sensors & Actuators B 126, 527, 2007

132. Gururaj M. Neelgund, Erika Hrehorova, Margaret Joyce, Valery Bliznyuk, Poly Int. 57, 1083, 2008

133. Zhihua Li and Yanwei Wang, Polym. Compos. 31, 1662, 2010

134. Pooja Devi, P.Reddy, Swati Arora, Suman Singh, C.Ghanshyam, M.L.Singla, J.Nanopart.Res. 14, 1172, 2013

135. Peng Wang, Baibiao Huang, Xiaoyan Qin, Ying Dai, Angeio Chem. Int. Ed. 47, 7931, 2008

136. Hanna Bahar-Levy, David Avnir, Adv. Funct. Mater 15, 1141, 2005

137. M.V.Fuke, A.Vijayan, P.Kanikar, R.C.A.Iyer, IEEE Sensors Journal 9,2009

138 Z.Li, Y.Li, J.Lu, F.Zheng, J.Laven, A.Foyet, J.App.Polym.Sci. 2012 doi 10.1002/APP 38618

139. D.Anakli, S.Cetinkaya, Curr. Appl. Phys. 10, 401, 2012

140. B.Gercek, M.Yavuz, H.Yilmaz, Bekir Sari, H.I.Unal, Colloids and Surfaces A 299, 124, 2007

141. A.G.Yavuz, A.Uygun, V.R.Bhethanabotla, Carbohydrate Polymers 75, 448, 2009

142. A.G.Yavuz, A.Uygun, V.R.Bhethanabotta, Carbohydrate Polymers 81, 712, 2010

143. B.Sari, A.Gok, D.Sahin, J.Appl. Polym. Sci. 101, 241, 2006

144. Z.W.He, Q.F.Lu, Q.Lin, Bioresour. Technol. 127, 66, 2013

CHAPTER 3

CHARACTERIZATION TECHNIQUES

This chapter provides a brief overview of the techniques used for characterization of polymers, nanomaterials and their composites such as Fourier Transform-Infra Red (FTIR) spectroscopy, Ultraviolet-Visible spectroscopy (UV-Vis), Powder X-Ray Diffraction (XRD), Thermo-Gravimetric Analysis (TGA), Differential Scanning Calorimetry (DSC), Transmission Electron Microscopy (TEM)/Scanning Electron Microscopy (SEM) and resistivity/conductivity measurements.

3.1 Ultraviolet - visible (UV-Vis) Spectroscopy

Ultraviolet-Visible spectroscopy involves the spectroscopy of photons in the UV-Visible region. It uses light in the visible and adjacent near ultraviolet (UV) and near infrared (NIR) ranges. In this region of energy space molecules undergo electronic transitions. Absorbance of ultraviolet and visible radiation in molecules is restricted to certain functional groups (chromophores) that contain valence electrons of low excitation energy (1, 2). The possible electronic transitions in organic molecule are shown in figure 3.1.

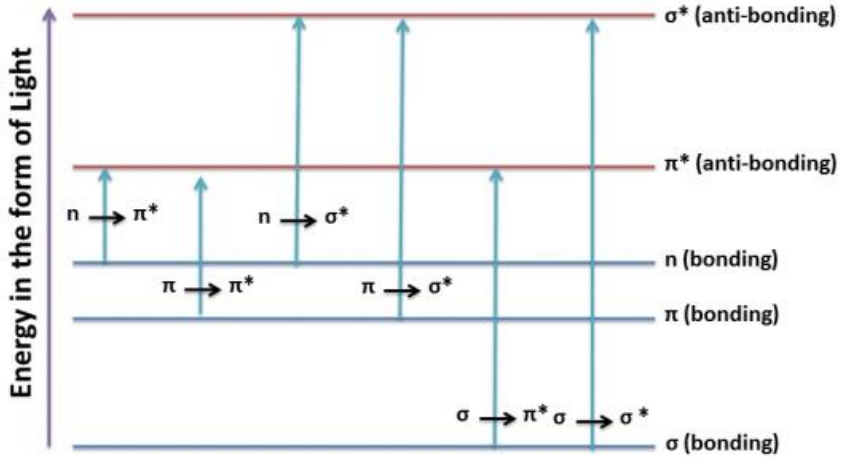

Fig 3.1: Possible electronic transitions between energy levels

The n-π^* and π-π^* transitions require lesser energy in comparison to other electronic transitions. Therefore such transitions appear at longer wavelength.

Beer-Lambert law

The method is most often used in a quantitative way to determine concentrations of an absorbing species in solution, using the Beer-Lambert law :

$$A = -\log_{10}(I/I_0) = \varepsilon \cdot c \cdot L$$

Where A is the measured absorbance, I_0 is the intensity of the incident light at a given wavelength, I is the transmitted intensity, L the path length through the sample, and c the concentration of the absorbing species. For each species and wavelength, ε is a constant known as the molar absorptivity or extinction coefficient.

The instrument used in ultraviolet-visible spectroscopy is called a UV-Vis spectrophotometer. It measures the intensity of light passing through a sample (I), and compares it to the intensity of light before it passes through the sample (I o). The ratio I /I o are called the transmittance, and is usually expressed as a percentage (%T). The absorbance, A, is based on the transmittance:

$$A = -\log (\%T)$$

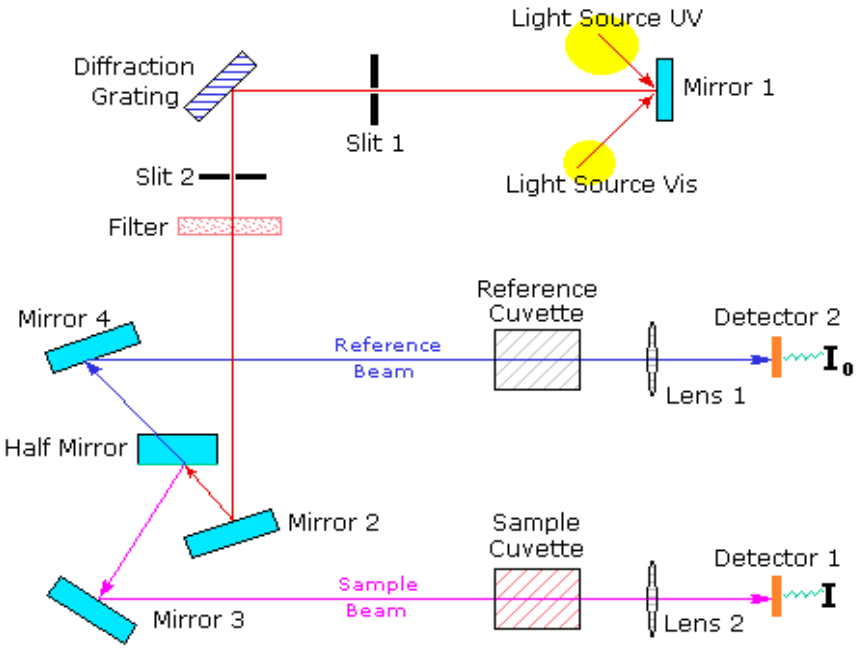

Fig 3.2: Diagram of a UV- Vis spectrophotometer

A spectrophotometer can be either single beam or double beam. In a single beam instrument, all of the light passes through the sample cell. Io must be measured by removing the sample. This was the earliest design, but is still in common use in both teaching and industrial labs.

In a double-beam instrument, the light is split into two beams before it reaches the sample. One beam is used as the reference; the other beam passes through the sample. Some double-beam instruments have two detectors (photodiodes), and the sample and reference beam are measured at the same time. In other instruments, the two beams pass through a beam chopper, which blocks one beam at a time. The detector alternates between measuring the sample beam and the reference beam.

Samples for UV/Vis spectrophotometer are most often liquids, although the absorbance of gases and even of solids can also be measured. Samples are typically placed in a transparent cell, known as a cuvette. Cuvettes are typically rectangular in shape, commonly with an internal width of 1 cm. This width becomes the path length, L, in the Beer-Lambert law. The best Cuvettes are made of high quality quartz, although glass or plastic cuvettes are common. Glass and most plastics absorb in the UV, which limits their usefulness to visible wavelengths.

Instrument Used

UV/Vis spectra of the colloidal nanoparticles, PANI, PEANI and their composites were carried by JASCO V-530 UV/Vis spectrophotometer, in the range 200 nm to 800 nm. The photograph of UV/Vis spectrophotometer is given in figure 3.3.

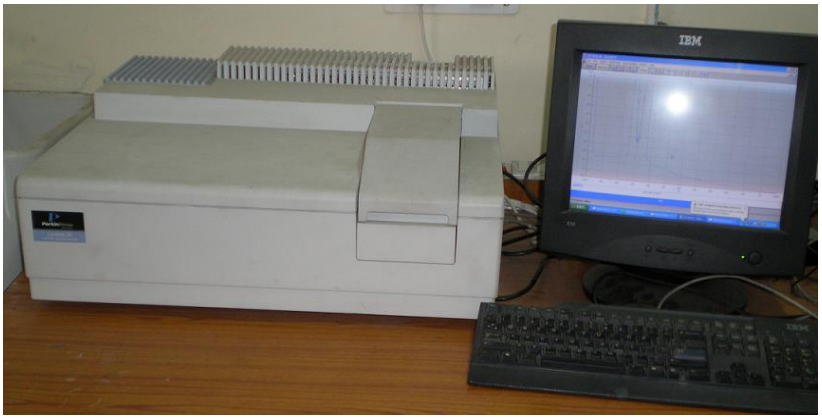

Fig 3.3: UV-Visible spectrophotomer

3.2 Fourier Transform Infra Red (FTIR) Spectroscopy

Molecules consist of atoms bound together by chemical bonds. When a molecule gets disturbed from its equilibrium state, the molecular vibrations set in. A vibrating molecule will interact with electromagnetic radiations. The radiation with frequency same as one of the normal modes of vibration of molecule will be absorbed. The energy absorbed will later be lost by the molecule either by re-radiation or by transfer of energy to other molecule of material in the form of heat (3). IR spectroscopy is quite useful to predict the presence of certain functional groups which absorb at definite frequencies in polymers.

An infrared absorption spectrum of a material is obtained by passing infrared radiations through the sample and determining the fraction of radiation being absorbed at each frequency. Figure 3.4 shows the schematic setup of an IR spectrophotometer.

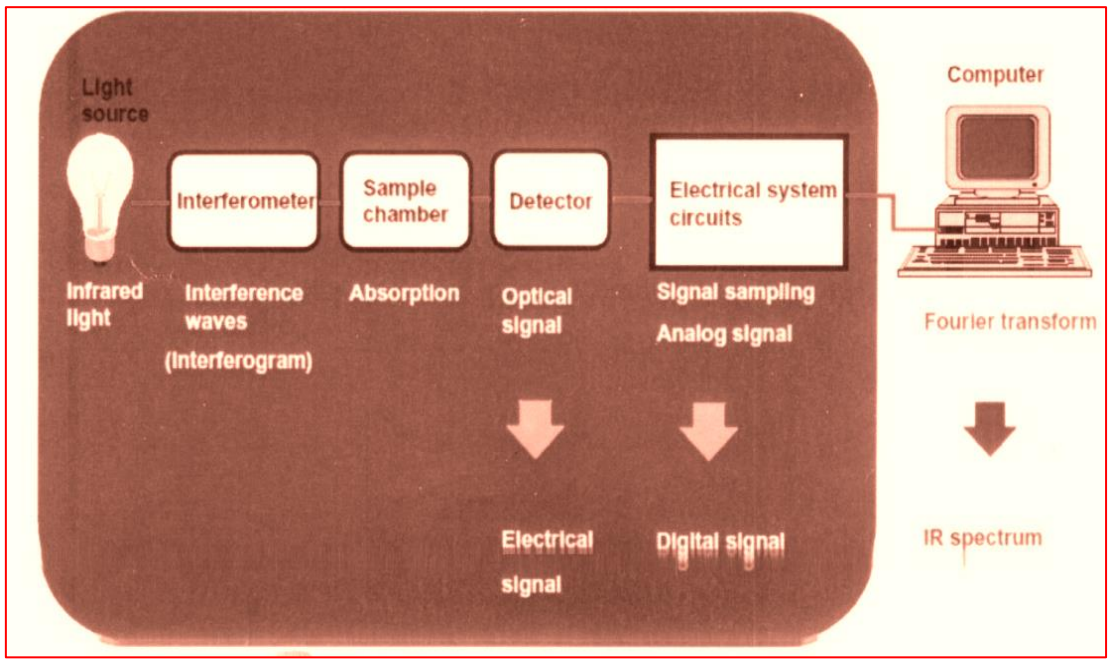

Fig 3.4: Schematic setup of an IR spectrophotometer

For chemical studies, the vibrational portion of infrared region i.e. radiation with wavelength (λ) between 2.5 μm is important. As wavelength is inversely proportional to energy so in order to simplify, radiation is referred in terms of wavenumber ($\overline{\nu}$), which is the reciprocal of wavelength (1/ λ). The complex lower region below 1000 cm^{-1} in IR spectrum is called 'fingerprint region'. Each organic

compound gives an identical pattern every time in this region. Therefore its identity can be confirmed by comparing the spectrum of the lower region (4).

$$\% \text{ transmission } (\%T) = \frac{\text{Intensity of sample beam } (I_t)}{\text{Intensity of reference beam } (I_o)} \times 100$$

Each interatomic bond within a molecule may vibrate in stretching or being mode; depending on the number of IR frequencies absorbed by an individual bond (5). Stretching absorptions of a bond appear at high frequencies (higher energies) as compared to the being absorption of the same bond. It is also important to note that non-polar molecules do not cause absorption of IR radiation. The factors determining that a chemical bond is IR active are the type of atoms joined by the bond and their bond order. The presence of electron donating group and conjugation lower the wave number of absorption while the presence of electron attracting groups raises the wave number of absorption. Hydrogen bonding lowers the wave number of absorption. Lowering in wave number and broadening of band are significant in case of intermolecular hydrogen bonding.

Instrument used

A Fourier transform infrared spectrophotomer (Varian 670 – IR system) was used to identify the chemical structure of polymeric materials. The FTIR spectra were obtained using powder samples which were grinded with KBr and then pressed into pellet form. IR spectra were recorded in the range 4000-400 cm^{-1}. The photograph of one of the FTIR spectrophotometer used in the present study is shown in Fig 3.5.

Fig 3.5: FTIR spectrophotomer

3.3 X-Ray Diffraction (XRD)

X-ray diffraction is a versatile, non-destructive analytical method for identification and quantitative determination of various crystalline forms, known as phases of compound present in powder and solid samples. Diffraction occurs as waves interact with a regular structure whose repeat distance is about the same as the wavelength. The phenomenon is common in the natural world, and occurs across a broad range of scales. For example, light can be diffracted by a grating having scribed lines spaced on the order of a few thousand angstroms, about the wavelength of light. It happens that X-rays have wavelengths on the order of a few angstroms, the same as typical inter-atomic distances in crystalline solids. That means X-rays can be diffracted from minerals which, by definition, are crystalline and have regularly repeating atomic structures. When certain geometric requirements are met, X-rays scattered from a crystalline solid can constructively interfere, producing a diffracted beam (6).

From research to production and engineering, XRD is an indispensable method for materials characterization and quality control. X-ray diffraction has been in use in two main areas, for the fingerprint characterization of crystalline materials and the determination of their structure. Each crystalline solid has its unique characteristic X-ray powder pattern which may be used as a “fingerprint” for its identification. Once the material has been identified, X-ray crystallography may be used to determine its structure, i.e. how the atoms pack together in the crystalline state and what are the interatomic distance and angle etc. The size and the shape of the unit cell for any compound can be determined easily using the diffraction of X-rays (7).

X-ray diffraction peaks are produced by constructive interference of monochromatic beam scattered from each set of lattice planes at specific angles. X-rays source have wavelengths Kα = 1.5405A. Cu-Kα beam is used as incident X-ray source. In 1912, W. L. Bragg recognized a predictable relationship among several factors (8-9).

1. The distance between similar atomic planes in a mineral (the interatomic spacing) which we call the d-spacing and measure in angstroms.

2. The angle of diffraction which we call the theta angle and measure in degrees. For practical reasons the diffractometer measures an angle twice that of the theta angle. Not surprisingly, we call the measured angle '2-theta'.
3. The wavelength of the incident X-radiation, symbolized by the Greek letter lambda and, in our case, equal to 1.54 angstrom.

Bragg's Law is:

$$n\lambda = 2dSin\theta$$

Where,
n is an integer,
θ is the angle between the planes in the atomic lattice,
λ is the wavelength of X-rays, moving electrons, protons and neutrons and
d is the spacing between the planes in the atomic lattices

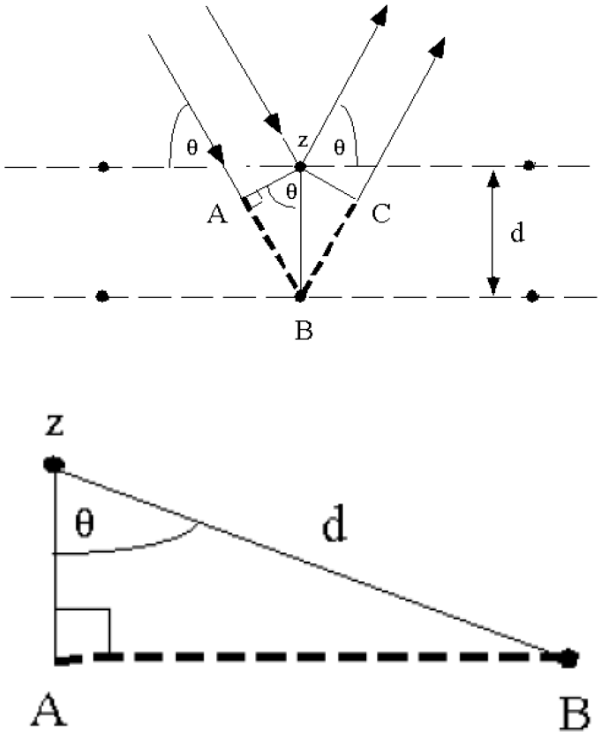

Fig 3.6: Bragg's diffraction

Here XRD was done by the X-ray diffraction of the as milled powder samples were performed using the diffractometer. X-Ray diffraction patterns were

recorded from 0° to 80° range with a X-Ray diffractometer using Cu Kα (λ=1.549A) with an accelerating voltage of 30 KV. Data were collected with a counting rate of 4°/min. The Kα doublets were well resolved. From XRD, the crystallite size can be found out by using the Scherrer's formula,

$$P = \frac{0.89\lambda}{\beta cos\theta}$$

Where,

P – Crystallite size

λ – Wavelength (0.154 nm),

β - Full width at half maxima,

θ- Diffraction angle

Instrument Used

XRD patterns were recorded with a X'PERT PANALYTICAL diffractometer using Cu (K∝) radiation having wavelength, λ=1.54 Å. The photograph of X-Ray diffractometer used in the present study is shown in figure 3.7.

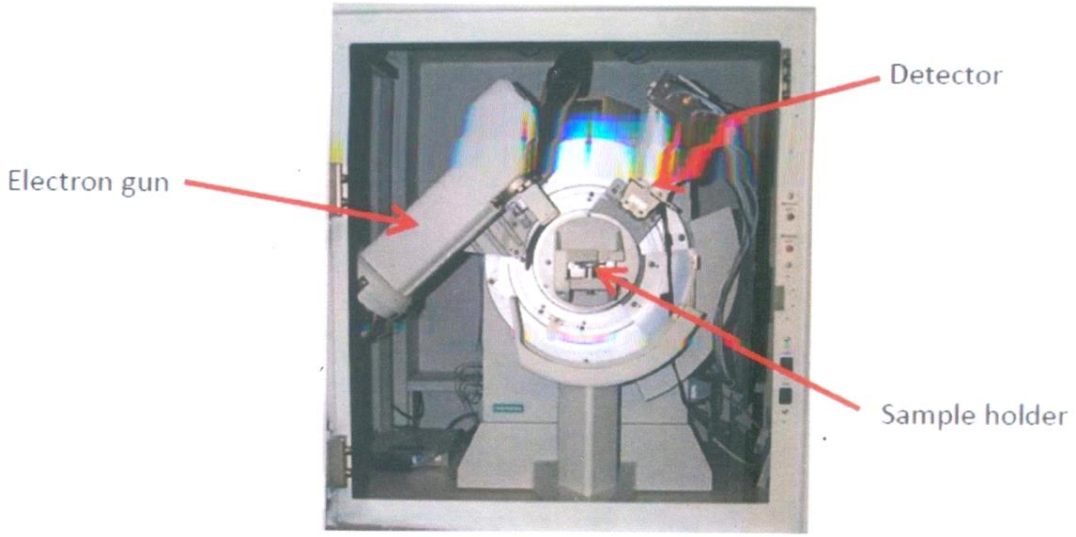

Fig 3.7: X-Ray Powder Diffractometer

3.4 Thermal Analysis (TGA-DSC)

Thermal analysis methods are based on the measurement of changes in chemical or physical properties of material as a function of temperature in a

controlled atmosphere. Thermal gravimetric analysis (TGA) technique works on the principle of change in weight of sample as a function of temperature (10). Differential scanning calorimetry (DSC) is a technique in which difference in the amount of heat required to increase the temperature of a sample with respect to reference is measured as a function of temperature.

3.4.1 Thermal gravimetric analysis (TGA)

The thermal gravimetric analyzer consists of:

- A balance with high-precision
- Oven which can be heated electrically connected to a thermocouple for accurate temperature measurement
- Inert atmosphere to prevent oxidation
- Computer to control the instrument

TGA data provides information such as:

- Thermal stability of the initial sample and of the amount of residue (if any)
- Possible pathway of degradation of the initial sample can be predicted

3.4.2 Differential Scanning Calorimetry (DSC)

There are two identical pans; one contains the material to be tested and the other acts as reference pan. During experiment both the pans kept in a furnace are heated gradually and simultaneously. The pan containing the sample requires a different amount of heat to maintain a constant temperature rise when compared to the reference pan because additional heat is required by the former to heat up. This is directly related to the heat capacity of the sample, which is the amount of heat required to raise the temperature by one degree per unit mass (11). The results are obtained in the form of plot between heat flow (W) and temperature (°C).

Instrument Used

TGA-DSC analysis was carried out using Universal V4.1D TA instrument. The ramping rate was kept 5°C/min in nitrogen flow in the temperature range of 30-1000°C. Figure 3.8 shows the photograph of the instrument used in the present study.

Fig 3.8: Thermal gravimetric analyzer

3.5 Semiconductor characterization

I-V characteristics of thin films of PANI, PEANI and their composites were measured using KEITHLEY 2400 SEMICONDUCTOR CHARACTERISATION UNIT. The photograph of the instrument is given below. The thin film was placed on the probe table. The silver paste was applied at the two ends of the film. The tungsten probe was made to touch these contacts, and the current through the film was measured at different voltages. This measurement was used to calculate the resistivity and hence the conductivity of the thin film.

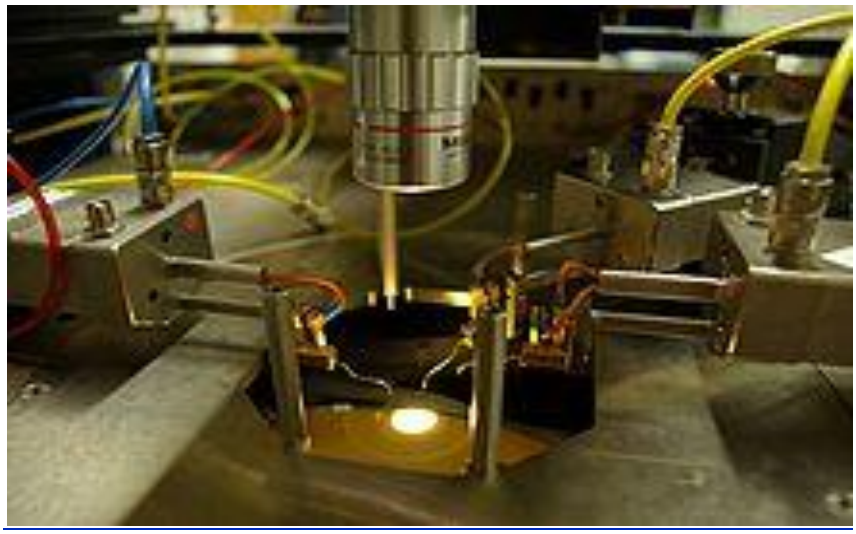

Fig 3.9: Probe station used to probing the sample

3.6 Scanning electron microscopy (SEM)

The scanning electron microscope (SEM) is a type of electron microscope that images the sample surface by scanning it with a high-energy beam of electrons in a raster scan pattern. The electrons interact with the atoms that make up the sample producing signals that contain information about the sample's surface topography, composition and other properties such as electrical conductivity. The types of signals produced by an SEM include secondary electrons, back scattered electrons (BSE), characteristic X-rays, light (cathodoluminescence), specimen current and transmitted electrons. These types of signal all require specialized detectors that are not usually all present on a single machine. The signals result from interactions of the electron beam with atoms at or near the surface of the sample. In the most common or standard detection mode, secondary electron imaging or SEI, the SEM can produce very high-resolution images of a sample surface, revealing details about 1 to 5 nm in size. Due to the way these images are created, SEM micrographs have a very large depth of field yielding a characteristic three-dimensional appearance useful for understanding the surface structure of a sample (12).

Instrument Used

The morphological investigations were carried out by using scanning electron microscopy SEM; model no-HITACHI S-4300SE/N FE-SEM. Figure 3.10 shows the photograph of SEM instrument used in the present study.

Fig 3.10: Scanning Electron Microscope

3.7 Transmission Electron Microscopy:

3.7.1 Instrument Used

TEM measurements were performed using a Hitachi H-7500 instrument operated at 120 kV (shown in figure 3.11). This instrument was used to see the smaller features of the composite material and the nanoparticles.

Fig 3.11 : Transmisson Electron Microscope

3.7.2 Sample preparation

For preparation of samples for TEM analysis, a portion of composite film was scratched and was dispersed in an ethanol solution and deposited on carbon-coated Cu-TEM grids. The film on the TEM grid was allowed to stand for some time to allow the liquid to evaporate. After drying, the specimen was transferred in the microscope column for imaging at different magnifications and the electron diffraction patterns were recorded (13).

3.7.3 Working

Transmission Electron Microscopy (TEM) is a technique where an electron beam interacts and passes through a specimen. The electrons are emitted by a source and are focused and magnified by a system of magnetic lenses. The electron beam passes through the condenser aperture and "hits" the sample surface. The electrons that are elastically scattered consists the transmitted beams and pass through the objective lens. The objective lens forms the image display and the following apertures, the objective and selected area aperture are used to choose the elastically scattered electrons that will form the image of the microscope. Finally, the beam goes to the magnifying system which consists of three lenses- the first and the second intermediate lenses (which control the magnification of the image) and the projector lens. The formed image is shown either on a fluorescent screen or on monitor or both and is printed on a photographic film (14).

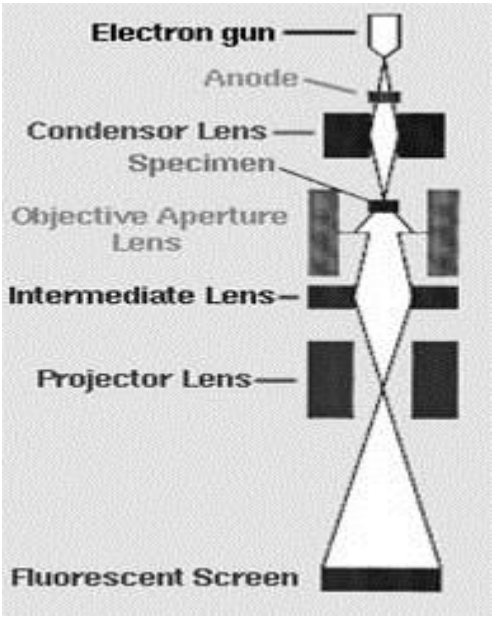

Fig 3.12: Schematic diagram of TEM

REFERENCES:

1. W.Kemp, Spectroscopy of Organic compounds, ed. W.H.Freeman, New York, 1991
2. S.K.Al-Ani, I.Al-Hassany, Z.Al-Dahan, J.Material Science 30, 3720, 1995
3. P.C.Painter, M.M.Coleman, J.L.Koeng, The Theory of Vibrational Spectroscopy and its Application to the Polymeric Materials, John Wiley & Sons, Chichester, 1982
4. J.L.Koeng, Spectroscopy of Polymers, Elsevier, Amsterdam, 1999
5. The Electromagnetic Spectrum, Infrared Spectroscopy, Theory, online edition (http://orgchem.colorado.edu/Spectroscopy/irtutor/IRtheory.pdf)
6. Suryanarayan and M.G.Norton, X-ray Diffraction-A Practical Approach, 207, 1999
7. C.Hammond, The basics of crystallography and diffraction, 2nd edition, OUP, 2001
8. F.J.Balta-Calleja and C.G.Vonk, X-ray scattering of synthetic polymers, Elsevier, Amsterdam, 1989
9. L.E.Alexander, X-ray Diffraction in Polymer Science, Wiley, London, 1969
10. V.A.Bershtien, Differential Scanning Colorimetry of Polymers, Ellis Horwood, 1994
11. M.Subramanium, Polymer testing New Instrumental Methods, Momentum press, 2012
12. J.Goldstein, Scanning Electron Microscopy and X-ray Microanalysis, Springer, 3rd edition, 2003
13. P.J.Goodhew, F.J.Humphreys, Electron Microscopy and Analysis, Imperial College, London, 1997
14. P.E.Champness, Electron Diffraction in the Transmission Electron Microscope, Garland Science, 2001

CHAPTER 4 (Part A)

SYNTHESIS AND CHARACTERIZATION OF GOLD NANOPARTICLES

This chapter comprises of two parts. This first part of the chapter is about study of gold nanoparticles and second part is about silver nanoparticles. Though several studies have been reported on these metal nanoparticles, but due to fast changes occurring in the properties by altering experimental conditions, it has been possible to design advanced/fast track materials of the choice.

4.1 GOLD NANOPARTICLES (GNPs)

4.1.1 Synthesis of gold nanoparticles

To generate gold nanoparticles of variable size, shape and monodisperse, different synthetic routes were followed. Several studies have already been reported for synthesis of gold nanoparticles/nanorods using different reducing agents and capping agents (1-4) in which nanoparticles have been synthesized by reducing Au (III) in presence of suitable stabilizer and reducing agent. Various reducing agents capable of Au (III) reduction in aqueous medium include citrate, ascorbate, tartarate, hydrazine hydrate, hydrogen peroxide (5-6).Other ways of reducing Au(III) can be high temperature decomposition/ultrasonic or microwave reduction (7-8). Various strategies of Au (III) reduction in non-aqueous medium have also been reported (9).

In the present study, GNPs have been synthesised by varying the precursor concentration in aqueous medium and other reagents (reducing and capping agents) as per table 4.1. Their respective ratios helped in controlling size, shape and distribution of synthesised Au nanoparticles.

Table 4.1 Starting materials for synthesis of goldnanoparticles and nanorods

Sr. No.	Reducing agent	Capping agent	Shape(from TEM)
1.	Hydrazine hydrate/ Hydrogen peroxide	PVP	Nearly spherical shape PVP capped AuNPs
2.	$NaBH_4$/Ascorbic acid	CTAB	Well defined spherical shape CTAB capped AuNPs
3.	$NaBH_4$/Ascorbic acid	TSC/CTAB	High aspect ratio nanorods (Seed Growth Process)

1) Synthesis of PVP capped gold nanoparticles – It has been possible to generate gold nanoparticles of desired size by reducing gold chloride with hydrazine hydrate/hydrogen peroxide in presence of PVP, in which dimensional control is possible by the reaction conditions.

In a typical experiment, 5 mL of 0.25 M $HAuCl_4.3H_2O$ was added to PVP solution (0.05 g dissolved in 20 mL water) and stirred for 20 to 30 minutes. 1 mL of hydrazine hydrate was added to the above solution dropwise with constant stirring. The wine red solution formed indicated the formation of GNPs. This wine red solution was centrifuged at 25000 rpm for about 15 minutes for 3-4 times. The nanoparticles obtained after centrifugation were washed with DI water in repeated steps and finally with ethanol and dried in the vacuum rotavapor. The same procedure was followed with hydrogen peroxide as reducing agent in place of hydrazine hydrate.

2) Synthesis of CTAB capped gold nanoparticles- CTAB capped GNPs were synthesized by seed-growth method in two steps procedure.

a) Seed solution was prepared initially by reducing $HAuCl_4.3H_2O$ (0.25M, 1mL) with the addition of freshly prepared ice-cold $NaBH_4$ (0.1M, 2mL) in the presence of CTAB (0.1M, 2mL) with constant stirring. The mixture turns into light brown suspension and was used as seeds for further synthesis of GNPs after about 2 hrs aging. The size of seeds was found to be 3-5 nm.

b) Growth solution was prepared by the reduction of $HAuCl_4.3H_2O$ (0.25M, 5mL) with freshly prepared ascorbic acid (0.1M, 10mL) in the presence of CTAB (0.1M, 5mL). Then controlled quantity of the prepared seed solution was dropped into the growth solution using microejector. The resultant solution turned red-wine in colour (10-11). To remove the reaction products formed during the reaction, the above solution was centrifuged at 10000 rpm for 30 minutes and washed with DI water. This process was repeated 3-4 times.

3) Synthesis of high aspect ratio gold nanorods- In this synthesis, Au nanorods were separated from the final product using the seed mediated synthetic method.

The aspect ratio of gold nanorods can be controlled by varying the amount of gold nanoparticles seeds with respect to the gold precursor. Gold nanorods can also be produced in quantitative yields by using silver nitrate as an additive (12).

a) Seed solution- An aqueous solution (20mL) containing $4x10^{-4}$M $HAuCl_4.3H_2O$ and $4x10^{-4}$M tri-sodium citrate was prepared in a dried clean flask. Then, 1 mL of freshly prepared 0.1M sodium borohydride was added into the solution under stirring. The solution colour turned to orange immediately and stirring was continued for about 5 minutes after adding the reductant. The as-prepared gold seed solution was used in 2-8 hrs after preparation.

b) Growth solution- For nanorods growth, 10 mL growth solution consisting of $4x10^{-4}$M $HAuCl_4.3H_2O$ and 0.1M CTAB were mixed with 5 mL of 0.1M ascorbic acid solution. Ascorbic acid as a mild reducing agent changed growth solution colour from brown-yellow to colourless. Next controlled quantity of seed solution was added without further stirring. Within 5-10 minutes, the solution colour changed to red-wine. The concentration of the rods in the solution can be enhanced by shape specific separation. This can be done by centrifuging at different speeds in a centrifuging machine. The heavier materials settle down leaving rods dispersed in the solution which can be separated easily.

4.1.2 Results and Discussion

The nanoparticles prepared using PVP and CTAB and nanorods were characterized for their shape, size, optical properties and crystal structure. Shape and size distribution was studied using TEM, whereas optical properties were studied using UV-visible spectroscopy and crystal structure was studied using XRD analysis.

4.1.2.1 CHARACTERISATION OF PVP CAPPED GOLD NANO PARTICLES

Morphological Study (TEM analysis):

The samples for TEM images were prepared by drop-casting the dispersed particle solution on copper grid coated carbon membrane. TEM images show size variation of gold nanoparticles with very low monodispersity. The shape of nanoparticles was generally nearly spherical with the size distribution of 8 nm to

14 nm; however, some particles were of quasi-spheroid shape. There was also some overlapping of particles.

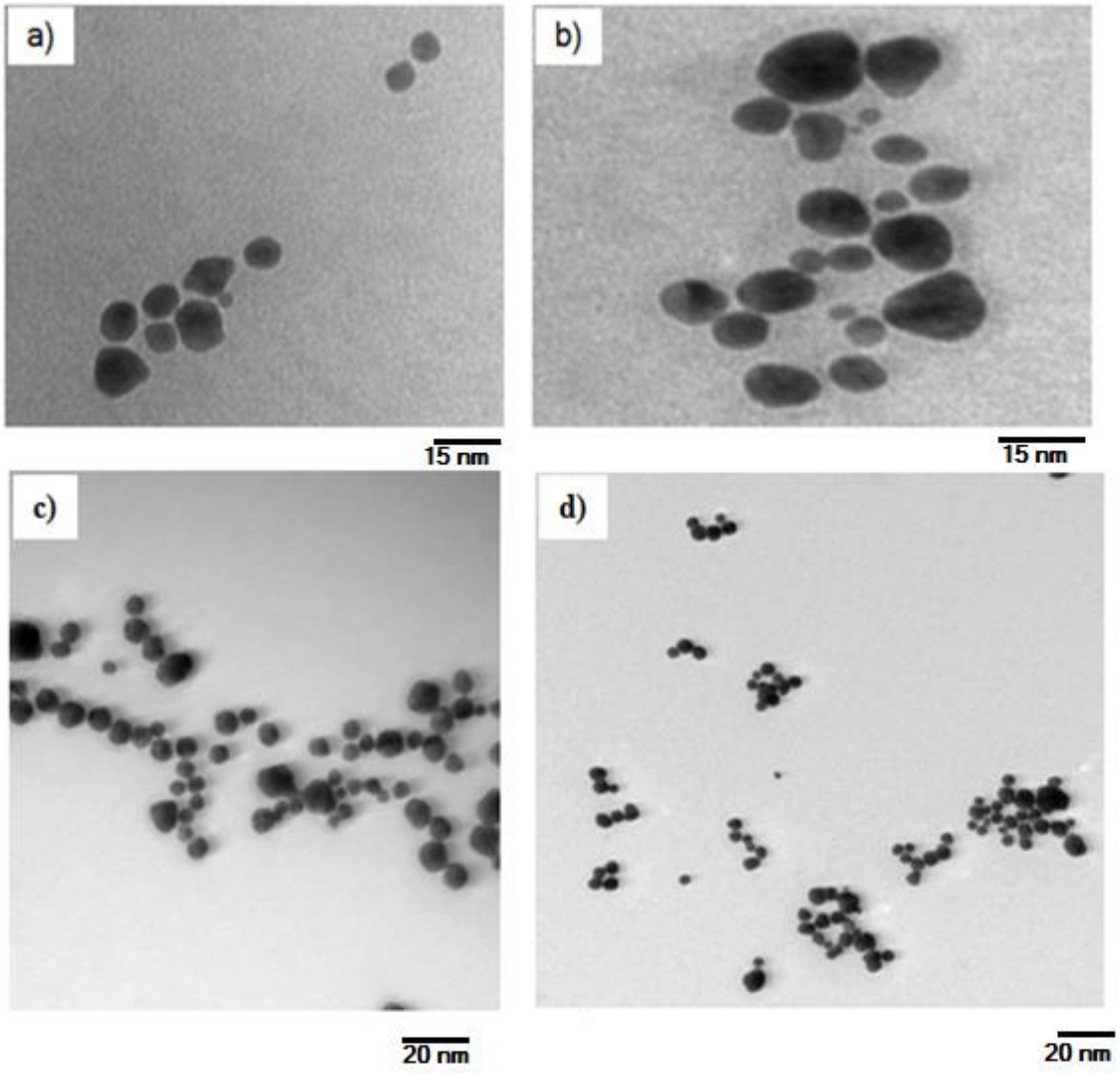

Fig 4.1: TEM image of PVP capped gold nanoparticles-a, b (using hydrazine hydrate) & c, d (using hydrogen peroxide)

Optical Study (UV-Visible Spectroscopy):

The UV-Vis spectra of PVP capped gold nanoparticles synthesised with hydrazine hydrate and hydrogen peroxide are shown in figure 4.2a and 4.2 b respectively.

The gold nanoparticles are characterized by one of the highest extinction coefficient. The total extinction of such a system depends on many factors like size and shape of the particles and dielectric constant of the dispersion medium. The absorption in visible region for gold is due to surface plasmon resonance.

The surface plasmon band is highly sensitive to the particle size and shape. As the particle size is increased, the absorption intensity increased and absorption maximum get red shifted.

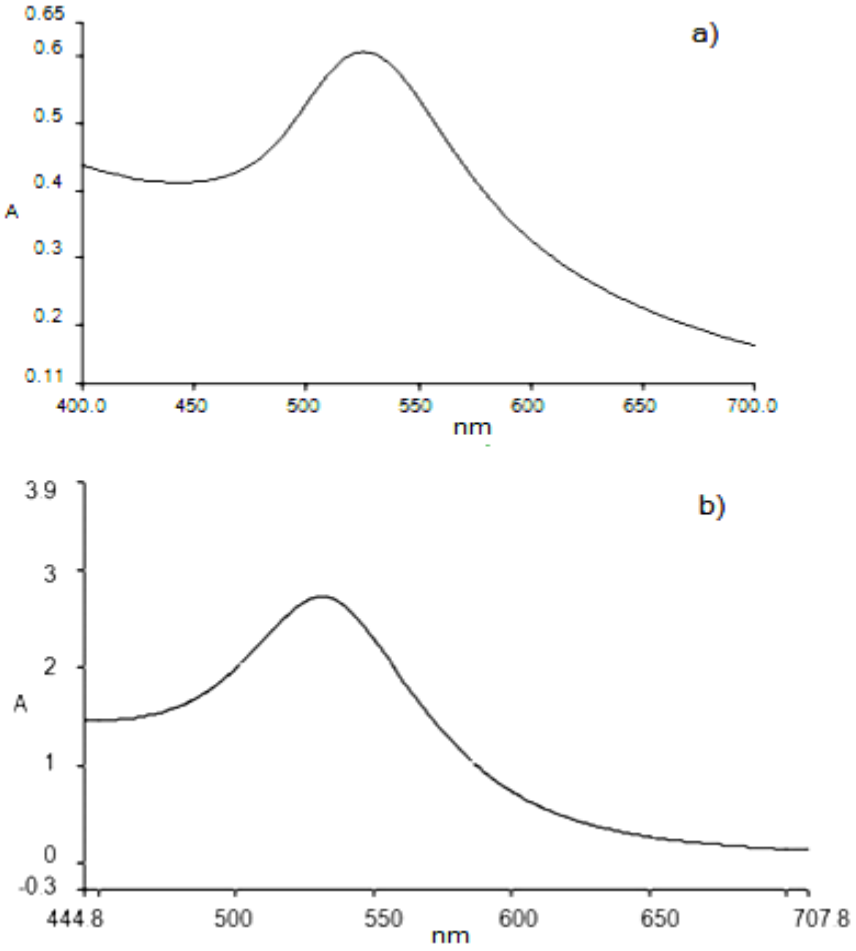

Fig 4.2: UV-vis spectrum of PVP capped gold nanoparticles-- a) hydrazine hydrate b) hydrogen peroxide

As can be seen from the figure 4.2a & 4.2b, PVP capped gold nanoparticles showed absorption peak at 525 nm and 528 nm respectively. The results are in agreement to spectra of colloid which generally displayed a Surface Plasmon Resonance (SPR) band at 530nm (13). There is a blue shift in the spectral absorption indicating the smaller size of nanoparticles.

Structural Study (X-Ray Diffraction Analysis):

XRD is a useful method for analyzing the crystal structure of the powdered nanoparticles. The sharp peaks prove the sample to be crystalline with each peak specifying the family of planes constituting crystal structure.

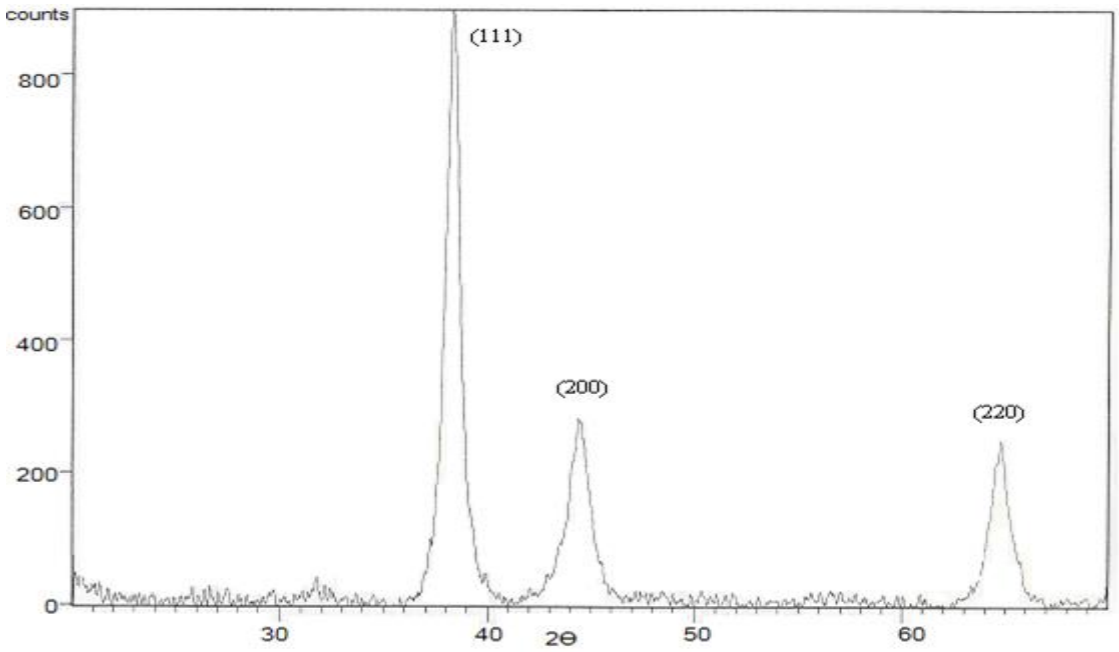

Fig 4.3: The XRD pattern of PVP capped gold nanoparticles

The PVP capped gold nanoparticles powder sample was scanned from 20° to 70°, where three major peaks were detected. The first peak with relative intensity 100 % was detected at 38.2°. The second peak with intensity 27.7% at 44.4° and the third peak with intensity 25.52 % was present at 64.7°. The comparison from reference scans shows that the three peaks corresponds to (111), (200), (220) planes of the face centered cubic structure respectively (14). The peaks also demonstrate that the prepared product is pure crystalline gold with fcc structure (JCPDS-04-0784).

The particle size was calculated for the most intense peak at 38.2° using Scherrer's formula

$$\text{Particle size} = \frac{0.9\,\lambda}{(\text{FWHM})\,\cos\theta} = 12.5 \text{ nm}$$

Where λ= 1.54 Å

FWHM= Full width at half maximum

The size comes out to be 12.5 nm, which is nearly in agreement to the particle size measured from TEM studies.

4.1.2.2 CHARACTERISATION OF CTAB CAPPED GOLD NANOPARTICLES

Morphological Study (TEM Analysis):

The samples were prepared by concentrating the aqueous solution of CTAB capped gold nanoparticles with centrifuge equipment. The copper grid coated carbon membrane was used to deposit the solution droplet for TEM analysis.

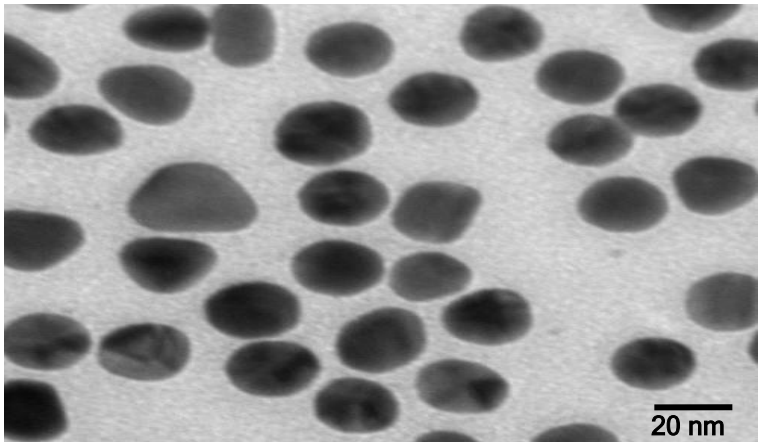

Fig 4.4: TEM image of CTAB capped gold nanoparticles

The micrograph indicates that majority of particles have quasi-spheroid or hexagon shape with average size in the range of 15-25 nm and quasi-spherical particles are polyhedron in nature. Kim and co-authors have reported icosahedral gold particles in ethylene glycol at a high temperature of 280°C (15). However in the present study it is much easier to produce such regular shapes following this procedure.

Optical Study (UV-Visible Spectroscopy):

The UV-Visible spectrum showed broad absorption peak with maxima at about 535 nm. This characteristic resonance corresponds to the excitation of Surface Plasmon vibrations in AuNPs. In comparison to PVP capped nanoparticle spectrum, CTAB capped particles show red shift which may signify bigger nanoparticle size of CTAB capped nanoparticles. The red to pink color was observed which is the characteristic of AuNPs solution and the results are in agreement to already reported study (16).

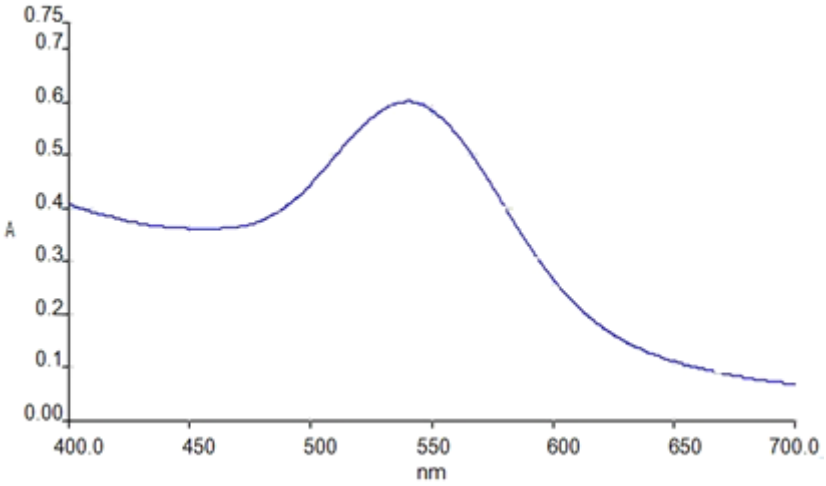

Fig 4.5: UV-Visible Spectrum of CTAB capped gold nanoparticles

UV-Visible spectrum of seed solution:

The UV-Visible spectrum was recorded for seed solution also (Figure 4.6). Spectrum was recorded immediately after preparation of seed solution. The seed solution showed no absorption peaks because of the negligible seed size of around 1-2 nm. However, the seed solution after aging for few hours which have been used in the present growth solution, showed an absorption peak at about 522.8 nm indicating that the size has increased between 3-5 nm.

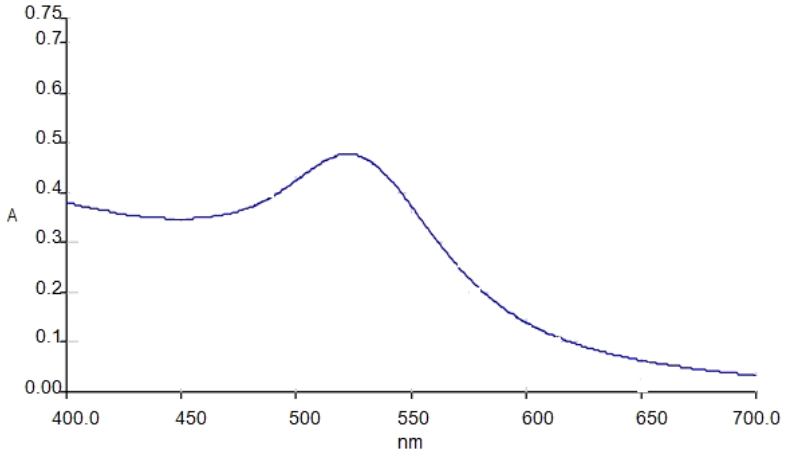

Fig 4.6: UV-Visible spectrum of Au seed solution aged for few hours

The results indicate the role of aging time also. During aging process, small nanoparticles agglomerate to comparatively bigger nanoparticles. Figure 4.7 below shows the absorbance recorded for seed and growth solution together. As can been seen, intensity of absorbance increased in growth solution. And this increase in absorbance can be attributed to the increase in size as well as number of gold nanoparticles formed.

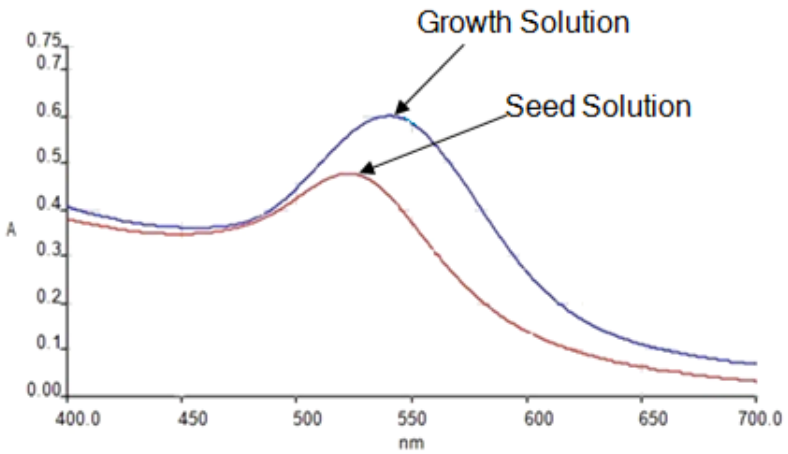

Fig 4.7: UV-Visible spectrum of seed and growth solution of Au NPs

Structural Study (X-Ray Diffraction Analysis):

In XRD analysis, the powder sample was scanned from 30^0 to 70^0 and its spectra is given in figure 4.8. Three prominent diffraction peaks were observed at 38.1^0, 44.5^0 and 64.7^0. The comparison with standard graphs show that the three peaks correspond to (111), (200), and (220) family of planes of the face centered cubic structure respectively. The average particle size derived from data is 16 nm. The XRD scan for PVP capped and CTAB capped nanoparticles show nearly no difference except for the intensity and width of peaks. For both the scans, the peaks are obtained at the same respective angles.

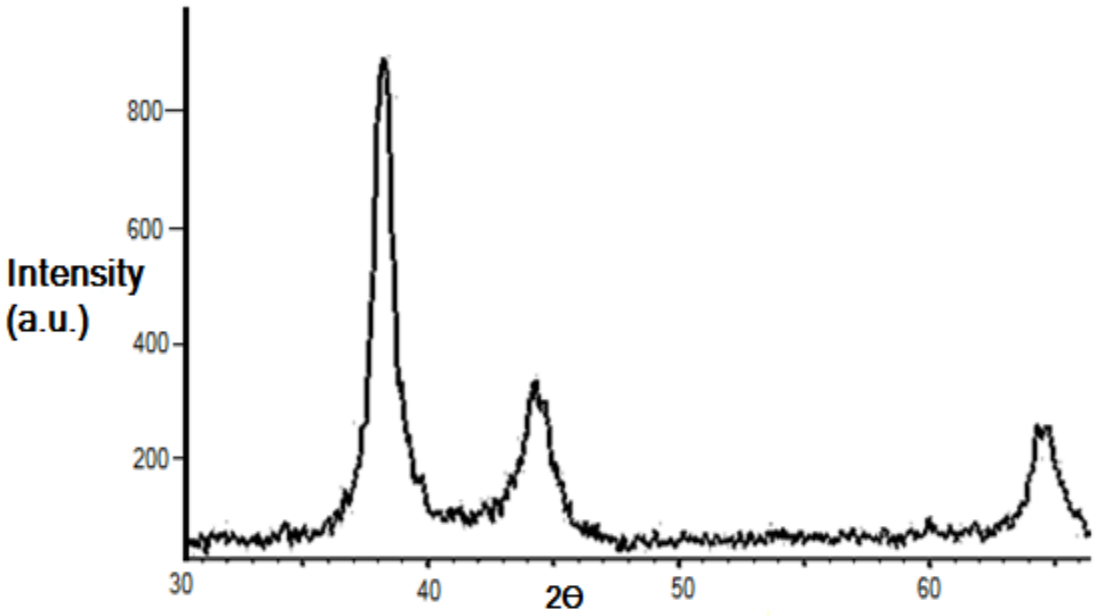

Fig 4.8: The XRD pattern of CTAB capped gold nanoparticles

The particle size slightly differs from TEM analysis as actual size is seen in TEM whereas average size was observed in XRD.

4.1.2.3 CHARACTERISATION OF GOLD NANORODS

Morphological Study (TEM Analysis): The copper grid coated carbon membrane was used to deposit the solution for TEM analysis.

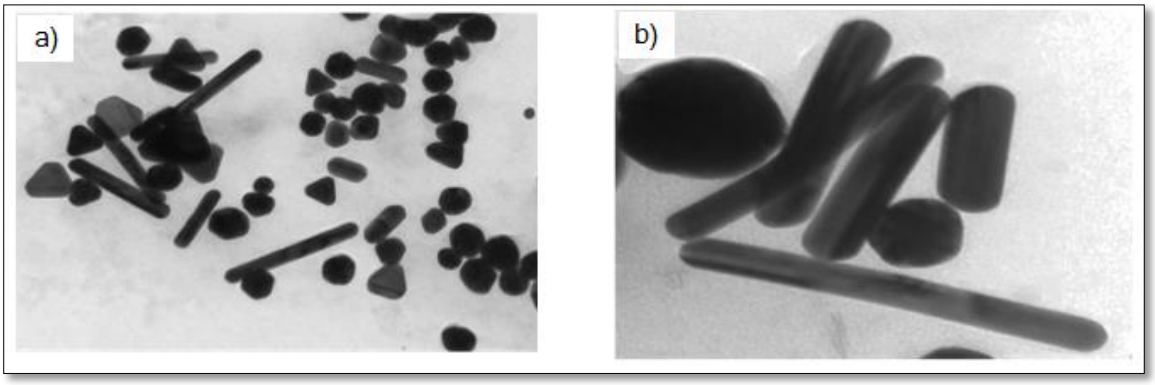

Fig 4.9: TEM images of high aspect ratio gold nanorods

TEM image (Fig 4.9 a) shows the formation of mixture of nanorods, spherical and quasi-spherical nanoparticles. Monodispersed high aspect ratio gold nanorods with the length varying between 100 to 150 nm were separated by centrifugation (Fig 4.9b). Aspect ratio is defined as the length to diameter ratio of the nanorods. The average diameter is nearly 20 nm. The aspect ratio distribution is from 5 to 8. The maximum length of rods detected in the image is 150 nm. Along with rods, many large sized hexagonal and triangular plates have also been detected. The yield of nanorods is very low with nearly 7 nanorods for every hundred particle i.e. 7% yield.

The concentration of CTAB is critical for nanorod growth: 0.1M concentrations are required, even though the critical micelle concentration for CTAB is far less than that. One of the auothor has reported higher yield of gold nanorods in presence of Ag^+ ions (17). The reaction conditions are also important as slight alteration results in variable shapes. In nanorod formation, CTA^+ ion stabilizes certain face of nanoparticle than the other plane (18). However, it is also possible to alter the carbon chain length in CTAB to change the morphology of nanorods. The mechanism of nanorod growth starts with the single crystalline seed particles. Then, surface binding groups preferentially bond to certain crystal faces of the

seed or growing nanorod in presence of CTAB.

Optical Study (UV-Visible Spectroscopy):

The UV-Visible spectrum of high aspect ratio gold nanorods usually shows two absorption peaks; one at shorter wavelength corresponding to absorption and scattering of light along the short axis of the nanorod (transverse plasmon band), and the other band at longer wavelength corresponding to absorption and scattering of light along the long axis of the nanorod (longitudinal plasmon band). The longitudinal surface plasmon resonance peak depends on the aspect ratio of the gold nanorods and show peaks at higher wavelength i.e. in Near Infra Red region (NIR) (19-20).

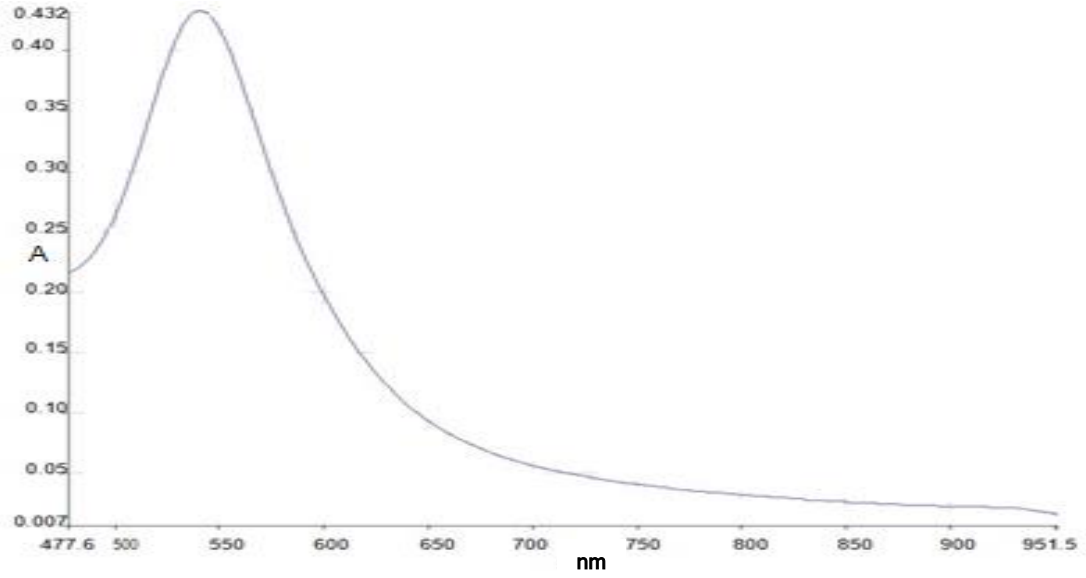

Fig 4.10: UV-Visible Spectrum of gold nanorods (the second absorption peak is expected beyond 1000nm)

In the above spectrum (Fig 4.10), transverse Surface Plasmon Resonance peak at about 541 nm is found and the other longitudinal Surface Plasmon resonance peak is expected beyond 1000 nm in the NIR region.

Structural Study (X-Ray Diffraction Analysis) :

The Fig 4.11 shows the XRD of powder sample scanned from 35^0 to 85^0. The XRD pattern of high aspect ratio gold nanorods showed five diffraction peaks, with most intense peak at 37.90 ^{0}.

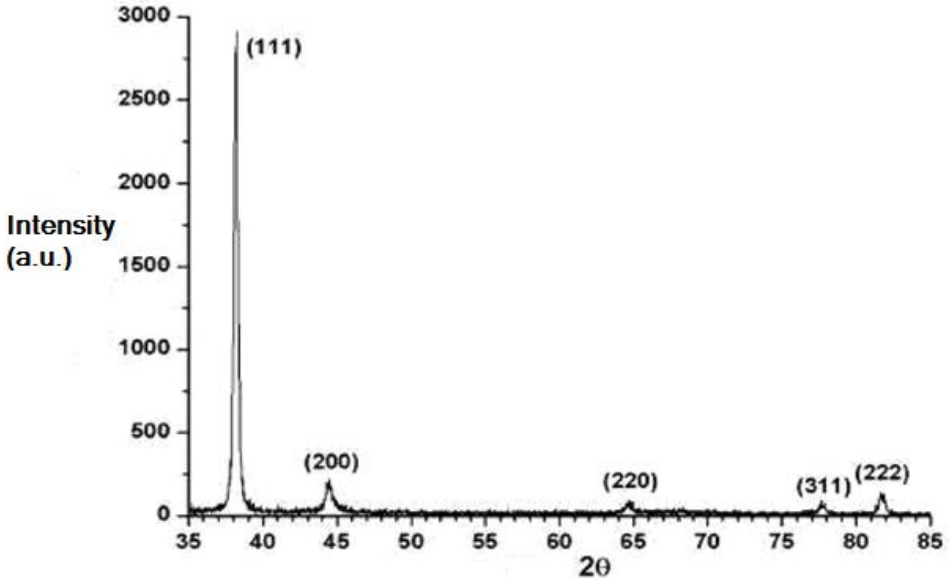

Fig 4.11: XRD Pattern of high aspect ratio gold nanorods

Other peaks were obtained at 44.8^0, 64.5^0, 77.7^0, 82.0^0. The comparison from standard XRD pattern shows that peaks correspond to (111), (200), (220), (311) and (222) family of planes. The average particle size comes out to be 42 nm from Scherrer's formula.

The fine gold particles with nanometer –scale dimensions are of great interest due to their unusual properties. Indeed, gold nanoparticles of size about 100 nm appear red when suspended in transparent media like alcohol (21-23) and those of size less than 5nm can catalyze chemical reactions. In addition to this, nanometallic rods have properties of strength, stiffness, ductility and have applications in electronics, photonics, chemical sensing and imaging (24-29). The optical properties of these nanoparticles are tunable throughout the visible and near-infrared region, as a function of size, shape and aggregation (30-35). Surface-enhanced plasmon resonance with metal nanoparticles is large in case of nanorods when the molecule is about 10-100 nm away from the metal surface (36). These nanoparticles have been combined with conducting polymers (PANI & PEANI) for better applications in catalysis, sensors and memory devices (37). Optimization of particle size and stability are important for the performance of bistable memory devices. The investigation involves the synthesis of PANI-Au nanoparticles together with hydrogen peroxide and synthesis of PEANI-Au nanoparticles using APS and hydrazine hydrate.

4.2 SILVER NANOPARTICLES

4.2.1 Synthesis of silver nanoparticles

Several methods have been employed to synthesize silver in nano-metric sizes. The most widespread and common ones are chemical reduction methods. The physicochemical methods (e.g. ultrasound, templates and milling process) and 'green' synthesis using microorganisms, enzymes, plants or plant extracts are equally effective, but sometimes they require complex apparatus. Chemical reduction in aqueous and non-aqueous solutions is the most common method for the synthesis of nanoparticles due to its convenience, facility, being not time-consuming and having a high yield of nanoparticles produced. Additionally, nanoparticles obtained by chemical route can be stored for a long time without stability loss (38-39).

In the present study, silver ions in aqueous medium have been reduced using sodium borohydride/ ethylene glycol in presence of PVP (surfactant acting as capping agent) resulting in the formation of silver precipitates.

Synthesis of silver nanoparticles using sodium borohydride (Method A)

In a typical experiment, 0.5 g PVP was added to 10mL of 0.1M sodium borohydride taken in a beaker, which was placed in an ice bath. The mixture was stirred on a magnetic stirrer. 5mL of 0.2M $AgNO_3$ was then added dropwise to the above solution with continuous stirring. A transparent solution changed into the characteristic yellow-brown colour, which indicated the formation of silver nanoparticles.

Synthesis of siver nanoparticles using ethylene glycol (Method B)

For the synthesis of silver nanoparticles in the presence of ethylene glycol (EG), 10mL of EG was heated to about 110°C. To this hot solution, 1mL of 0.2 M silver

nitrate solution was added dropwise while maintaining the temperature. The transparent solution becomes golden-brown in colour which was the confirmation of formation of silver nanoparticles. EG has acted both as a reducing and a stabilizing agent. It has been possible to alter the shape and size by altering the precursor's ratio, minor change in temperature and reaction time.

4.2.2 Results and Discussion

The nanoparticles prepared using sodium borohydride and ethylene glycol were characterized for their shape, size, optical properties and crystal structure. Shape and size distribution was studied using TEM, whereas optical properties were studied using UV-visible spectroscopy and crystal structure was studied using XRD analysis.

Optical Study (UV-visible Spectroscopy):

Method A

UV-vis spectroscopy is one of the most widely used techniques for structural characterisation of silver nanoparticles (40-41). The absorption spectrum of the pale yellow-brown silver colloids prepared by using sodium borohydride is shown in figure 4.12

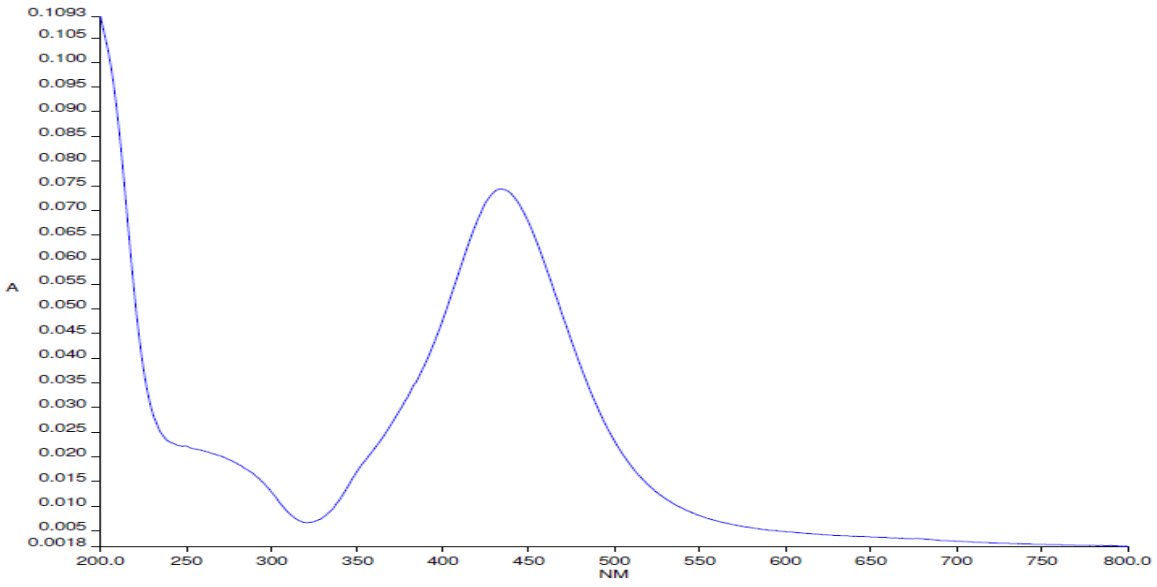

Fig 4.12: UV-Vis spectrum of silver nanoparticles (Method A)

It showed a Surface Plasmon absorption band at 431.1 nm with a sharp peak indicating the formation of nearly monodispersed silver nanoparticles. Then, absorption spectra during synthesis were recorded with a time interval of 5 min and the observed spectra is shown in Figure 4.13.

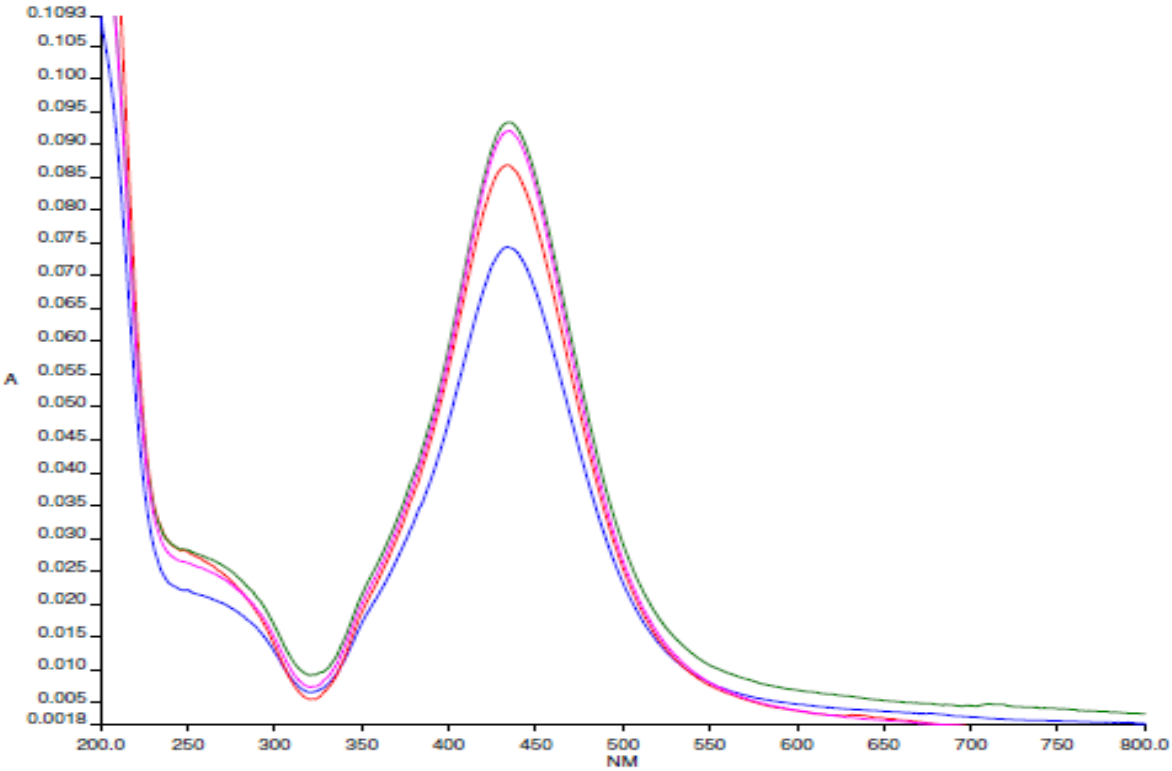

Fig 4.13: UV-Vis spectrum, this implies the growth of silver nanoparticles (Method A)

The so formed silver nanoparticles showed the surface plasmon resonance (SPR) band at 431.59 nm. A monotonic increase in the absorption band at 431.59 nm is due to the growth of silver nanoparticles which occurred during the reduction of silver ions by sodium borohydride. The position of the SPR band observed at 431.59 nm did not change with time, although a gradual increase in the absorbance was observed.

Method B:

The physical appearance of the reaction mixture turning from yellow to brown is due to the surface plasmon resonance (SPR) of the silver nanoparticles, which is considered to be the primary signature of nanoparticle formation. UV-vis spectroscopy is a versatile technique to understand the reduction mechanism of silver ions into silver nanoparticles. An observed peak at 433.5nm (Fig 4.14) is

assigned to the surface plasmon resonance band (longitudinal vibration) of the silver nanoparticles, which is comparable with the literature values and exhibits continuous rise in intensity without any change in the peak position as a function of time (42-43).

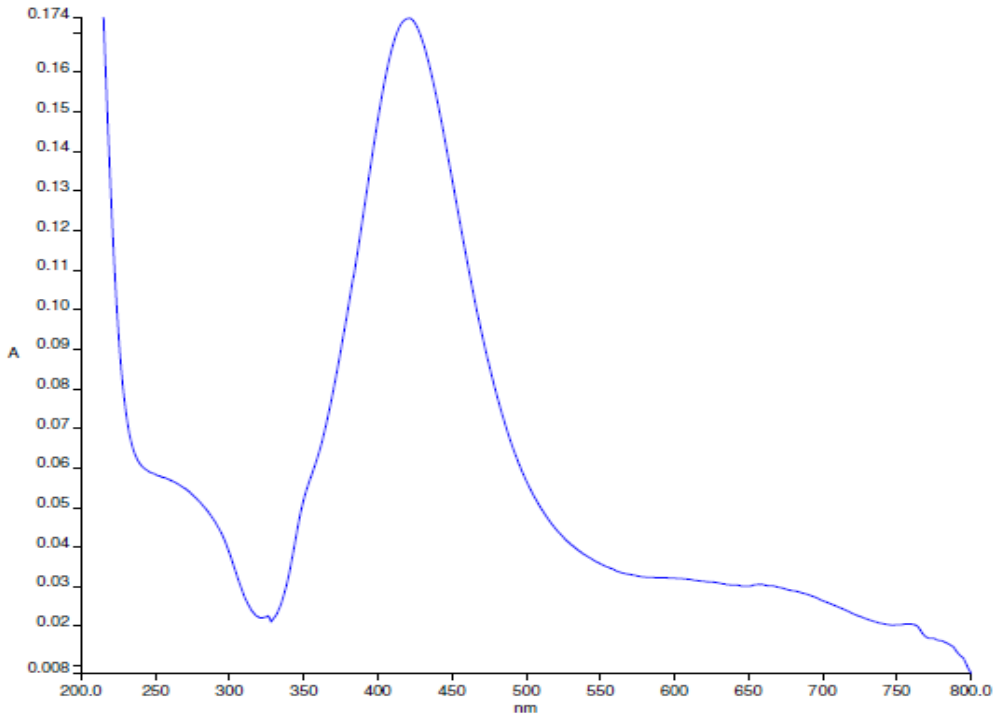

Fig 4.14: UV-vis spectrum of silver nanoparticles (Method B)

The UV-vis spectra of the reaction mixture recorded as a function of time, is shown in Figure 4.15. During initial period, the absorption peak was weak and broad, which indicates the smaller size of silver nanoparticles. As time elapsed, the gradual increase in the absorbance was observed, which is due to the increasing concentration of silver nanoparticles as well as the particles' growth in size although the position of the SPR band did not change.

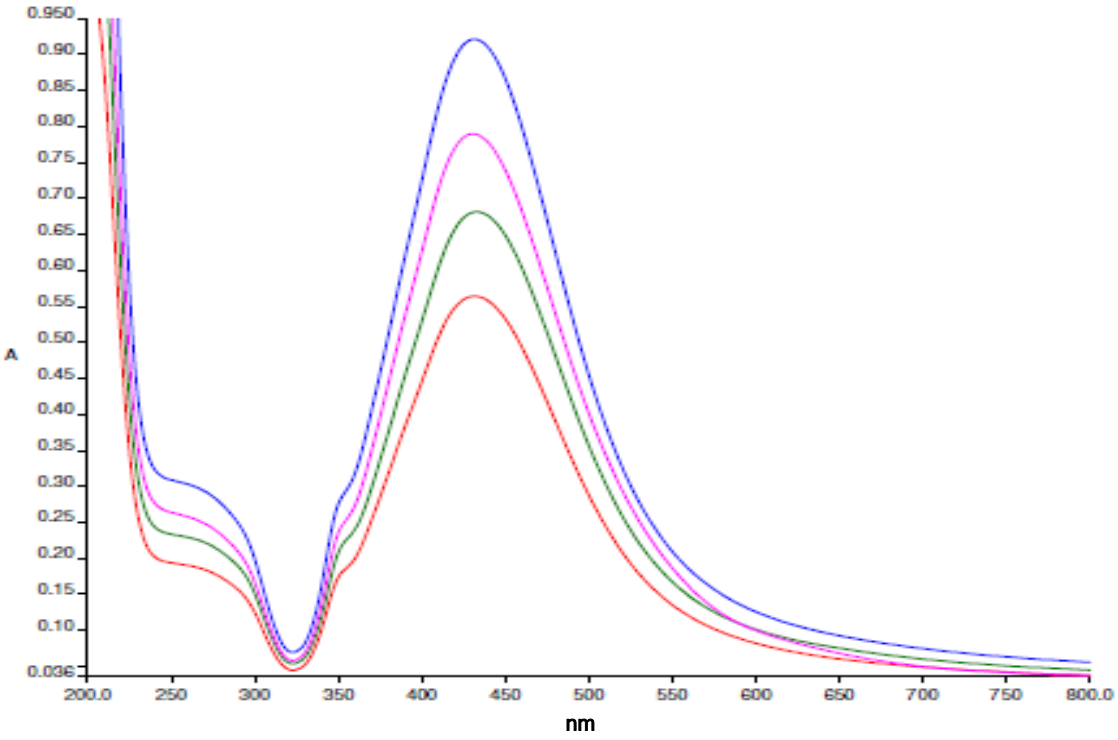

Fig 4.15: UV-Vis spectrum, this implies the growth of silver nanoparticles (Method B)

Structural Study (X-ray Diffraction Analysis):

The crystalline structure of the synthesized silver nanoparticles (both by Method A and Method B) was investigated by XRD analysis and the obtained X-ray diffraction patterns are shown in Figure 4.16 and 4.17 respectively.

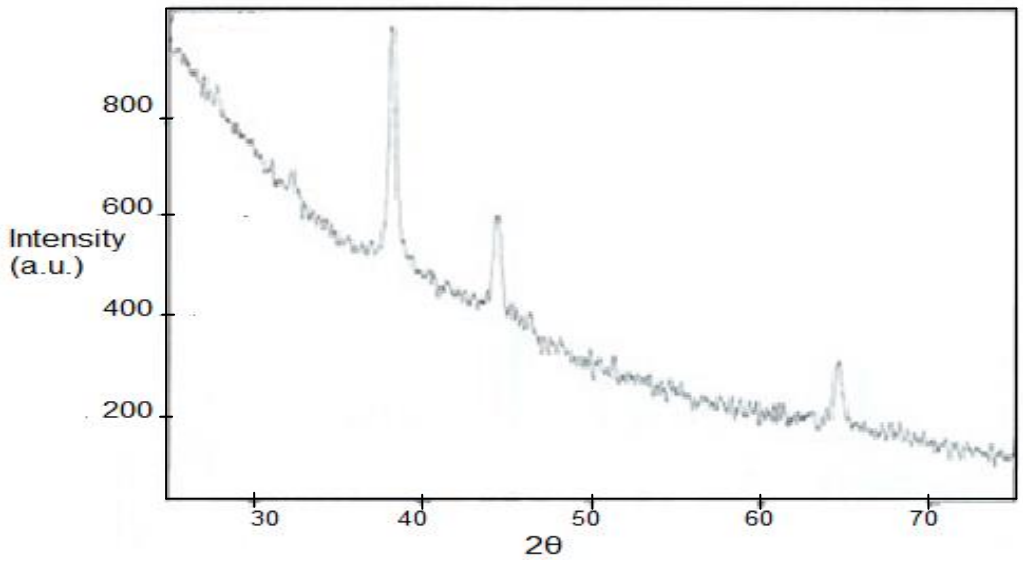

Fig 4.16: X-ray diffraction of silver nanoparticles (Method A)

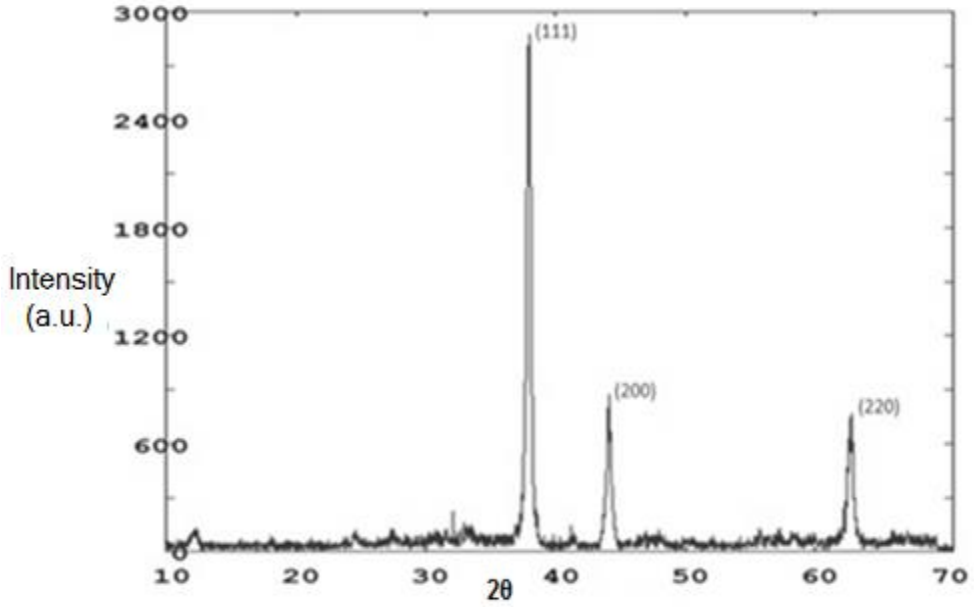

Fig 4.17: X-ray diffraction of silver nanoparticles (Method B)

The obtained diffraction peaks were observed at 38.1°, 44.3°, 64.4°(MethodA) and 37.9°.44.1°,63.7° for Method B are respectively assigned to (111), (200), (220) crystalline planes, which indicates that the synthesized silver nanoparticles are crystallized in face centered cubic (fcc) symmetry (JCPDS- 04-0783). No additional diffraction peaks were observed other than the characteristic peaks of the silver structure that reflects the purity of synthesized silver nanoparticles. It is very well clear from the figures that intense peaks correspond to 38.1° and 37.9° 2Θ angles, indicating that silver nanoparticles are dominantly ruled by (111) planes. The formation of NPs with essentially (111) facets may be the result of lower free energy of the (111) planes (44-45) leading to better stability.

The mean crystallite size was calculated by Debye-Scherrer's equation using the FWHM (Full Width at Half Maximum) of the (111) reflections. It has been found to be about 38 nm (Method A) and about 25nm (Method B), which is comparable with the particle size as obtained from TEM analysis. However the size in method B can be altered by changing the reaction time (lower the time smaller the particles & higher the time larger the particles).

Morphological Study (TEM Analysis):

For TEM images, the reaction product was centrifuged and washed with deionized water and ethanol several times. The concentrated residue obtained

after washing was then dissolved in deionized water/ethanol and sonicated for about 20 minutes. Finally the drop of this solution was placed on copper grid and allowed solvent to evaporate in air. Representative TEM images of Ag NPs synthesised by both methods are shown in figure 4.18.

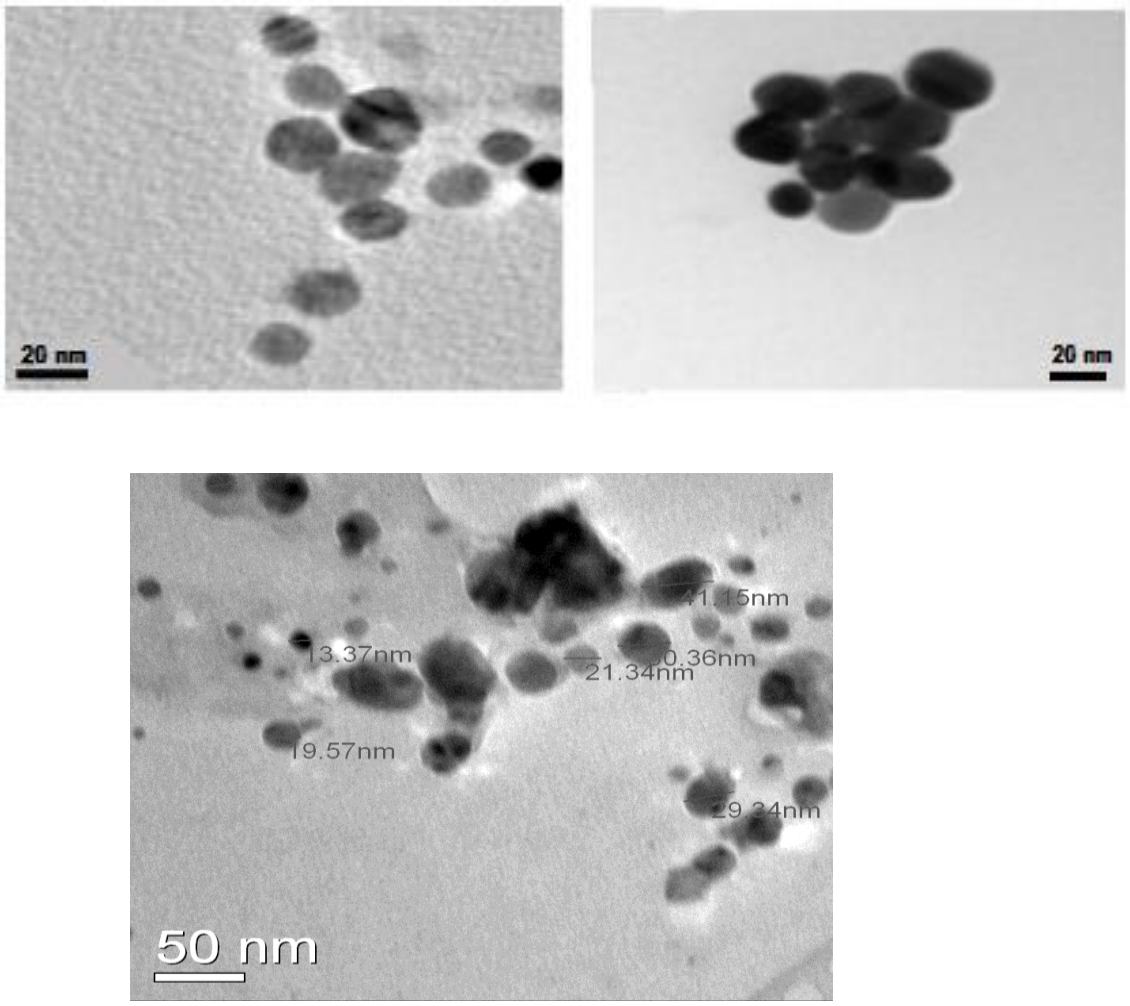

Fig 4.18: TEM images of silver nanoparticles

It shows that the Ag nanoparticles are spherical in shape with a smooth surface morphology. The diameter of the nanoparticles is found to be approximately 20 to 30 nm. TEM images also show that the produced nanoparticles are more or less uniform in size and shape. However at certain places overlapping of the particles was observed when synthesis was done with ethylene glycol.

REFERENCES:

1. R.Jin, Y.Cao, C.A.Mirkin, K.L.Yely, G.C.Schatz, J.G.Zhang, Science 294, 1901-1903, 2001
2. J.Kimling, M.Maier, B.Okerve, V.Kotaidis, H.Ballot, A.Plech, J.Phys.Chem. B 110(32), 15700-1507, 2006
3. B.Nikoobakht, M.A.El-Sayed, Chem. Mater. 15(10), 1957-1962, 2003
4. P.D.Jadzinsky, G.Calero, C.J.Ackerson, D.A.Bushnell, R.D.Komberg, Science 318, 430-433, 2007
5. K.S.Mayya, N.Jain, A.Gole, D.Langevim, M.Sastry, J.Coll.Interface Sci, 270, 133-139, 2004
6. C.L.Chang, J.Coll.Interface Sci. 239, 334-341, 2001
7. D.A.Fleming, M.E.Williams, Langmuir 20, 3021-3023, 2004
8. F.K.Liu, C.J.Ker, Y.C.Chang, F.H.Ko, T.C.Chu, B.T.Dai, Jpn. J. Appl. Phys. 42, 4152-4158, 2003
9. M.Y.Han, C.H.Quck, W.Huang, C.H.Chew, L.M.Gon, Chem. Mater. 11, 1144-1147, 1999
10. Yi Wang Lai Zhan, Chang Zhi Huang, RSC, 2010
11. T.K.Sau, C.J.Murphy, Langmuir 21(7), 2923-2929, 2005
12. Z.C.Xu, C.M.Shen, C.W.Xiao, T.Z.Yang, S.T.Chen, H.L.Li, H.J.Gao, Chem. Phys. Letters 432, 222-225, 2006
13. C.S.Tudoran, V.Pasricha, B.Fricke, J.Anton, W.D.Sepp, T.Jacob, Eur.Phy.JD 24,65-68,2003
14. A.Suguman, C.Thanachayanont, J.Dutta, J.G.Hilborn, Sc. and Tech. of Adv. Mat. 6, 335-340, 2005
15. F.Kim, S.Connor, H.Song, T.Kuykendall, P.Yang, Angew.Chem. 43,3673-3677,2004
16. S.Mandal, Sujatha K.Arumugam, S.D.Adyanthaya, Renu Pasricha, M.Sastry, J.Mater.Chem. 14,43-47,2004
17. C.J.Murphy, T.K.Sau, A.M.Gole, C.J.Orendroff, J.Gao, L.Gou, S.E.Hunyadi, Tan Li, J.Phy.Chem.B 109,13857-13870,2005
18. P.L.Gai, M.A.Harmer, Nano Lett. 2,771-774,2002
19. B.D.Burbee, S.O.Obare, C.J.Murphy, Adv. Mat. 15, 414-416, 2003

20. H.L.Ulu, C.H.Chen, Michael H.Huang, Chem. Mater. 21(1), 110-114, 2009
21. M.A.El-Sayed, Acc.Chem.Res. 34,257-264,2001
22. Metal nanoparticles:Synthesis, Characterisation and Applications, D.L.Feldheim, C.A.Foss, Marcel Dekker: New York, 2002
23. M.C.Daniel, D.Astruc, Chem.Rev. 104,293-346,2004
24. T.E.Mallouk, N.I.Kovtyukhova, Chem.Eur.J. 8,4354-4363,2002
25. M.Law, D.J.Sibuly, J.C.Johnson, J.Goldberger, P.Yang, Science 305,1269-1273,2004
26. H.Fan, Y.Lu, A.Stump, S.T.Reed, T.Baer, R.Schunk, C.J.Brinker, G.P.Lopez, Nature 405,56-60,2000
27. B.H.Ji, H.J.Gao, J.Mech.Phys.Solids 52,1963-1990,2004
28. D.A.Schultz, Curr.Opin.Biotechno. 14,13-22,2003
29. A.K.Salim, P.C.Searson, K.W.Leong, Nature Mater. 2,668-671,2003
30. S.Link, M.A.El-Sayed, J.Phys.Chem.B 103,8410-8426,1999
31. J.J.Mock, M.Barbie, D.R.Smith, D.A.Schultz, S.Schultz, J.Chem.Phys. 116,6755-6759,2003
32. J.P.Kottman, O.J.F.Martin, D.R.Smith, S.Schultz, Chem.Phys.Lett. 341,1-6,2001
33. S.Nie, S.R.Emory, Science 275,1102-1106,1997
34. A.Tao, F.Kim, C.Hess, J.Goldberger, R.He, Y.Sun, Y.Xia, P.Yang, Nano Lett. 3,1229-1233,2003
35. P.Hanarp, M.Kall, D.S.Sutherland, J.Phys.Chem.B 107, 5768-5772, 2003
36. J.R.Lakowicz, C.D.Geddes, J.Malicka, Z.Gryzczynski, K.Aslan, J.Lukomski, E.Matveera, J.Zhang, R.Badugn, J.Huang, J.Fluorescence 14,425-441,2004
37. C.O.Baker, B.Shedd, R.J.Tseng, A.A.Martinez-Morales, C.S.Ozkan, M.Ozkan, Y.Yang, R.B.Kaner, ACS Nano 5,3469-3474,2011
38. W.Zhang, X.Qiao, J.Chen, Mater. Sci. Eng. B 142, 1-15, 2007
39. J.P.Abid, A.W.Wark, P.F.Bravet, H.H.Girault, Chem. Comm. 7, 792-793,2002
40. A.Hangelin, J.Phys.Chem. 97, 5457-5471,1993

41. M.Sastry, K.S.Mayya, K.Bandyopadhyay, Colloids Surf. A 127, 221-228, 1997
42. B.L.He, J.J.Tan, Y.L.Kong, H.F.Liu, J.Mol.Catal. A.Chem. 22, 121-126, 2004
43. M.P.Zheng, M.Y.Gu, Y.P.Jin, G.L.Jin, Mater. Res. Bull. 36, 853-859, 2001
44. R.Pasricha, M.Sastry, Bull. Mater. Sci. 28(5), 503-510, 2005
45. L.Baia, M.Baia, W.Kiefer, J.Popp, S.Simon, Chem. Phys. 63, 327, 2006

CHAPTER 5 (PART A)

SYNTHESIS AND CHARACTERIZATION OF POLYANILINE/GOLD NANOCOMPOSITES

The Chapter 5 comprises of three parts (A, B and C). This part (part A) is about study of PANI and its nanocomposite with gold, the part B is about PANI/AgCl nanocomposite and the part C deals with PANI/Ag nanocomposite.

5.1 Synthesis of PANI:

Synthesis of PANI has been reported by several others in which solution pH has varied from 1 to 4, in different mineral acids like HCl, H_2SO_4 with different oxidants like APS, H_2O_2 and potassium chromate. However, it has been observed that the most preferred method for synthesis is to use either HCl or H_2SO_4 (pH=2) with APS as an oxidant (1-3).

In the present study, we have synthesized PANI in HCl/ H_2SO_4 medium mainly using H_2O_2. The use of H_2O_2 has been deployed since it has dual function where it works as an oxidant for the polymerisation of aniline and reductant for reducing noble metal. Moreover, to improve the conductance level of the polymer, we have added ferrous chloride ($FeCl_2$) as catalyst (4). In a typical experiment, 5 mL of aniline monomer was added to 100 mL of 2M HCl ice-cooled solution in a glass beaker. The solution was continuously stirred to make a uniform solution. To this solution, 1 mL of $FeCl_2$ and 10 mL of H_2O_2 was slowly added with continuous stirring (1hr) till green coloration is formed. The solution was allowed to stir for about 3 hours more till the green precipitates appear which indicated the polymerisation of aniline. The solution was kept as such overnight for complete precipitation to occur. After keeping overnight, the precipitates were filtered, washed with deionised water and dried at about 60°C. A portion of this green colored polymer was kept for further characterisation and labelled as 'A'. The other portion (B) was dissolved in 100 mL of 1N NH_4OH solution. The color of the precipitates turned blue due to reduction which is an insulating state and called as emeraldine base. A portion of this compound was stored as such after drying(C) and the remaining portion was treated with 0.1N HCl solution to make it in

conducting state(emeraldine salt) and named as PANI. Some of the materials were characterised for morphology, chemical structure, conducting and optical behaviour using TEM/XRD/FTIR/UV-VIS & I-V techniques.

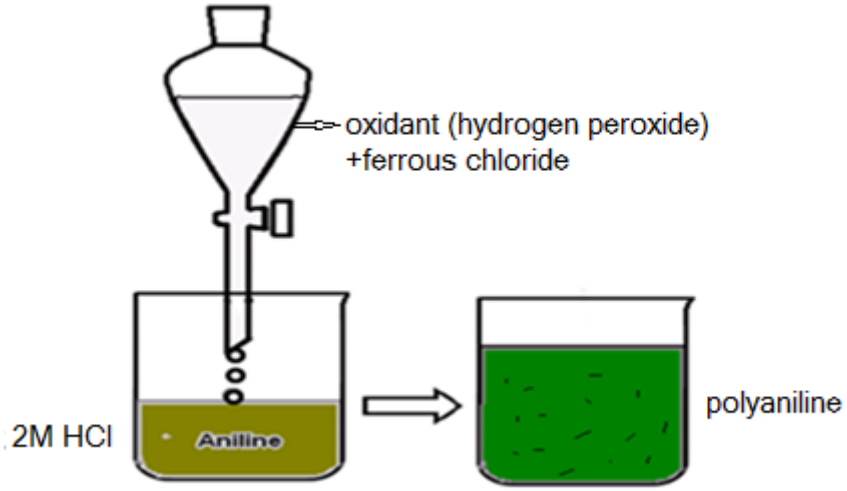

5.2 Synthesis of PANI/Au nanocomposite:

Several studies have been reported on synthesis of PANI/Au nanocomposites where cumbersome methods have been adopted (5-8). Few reports have also appeared for synthesis of this composite using hydrogen peroxide where high temperature has been used. However, limited results have been reported on one step chemical synthesis of PANI/Au nanocomposites using hydrogen peroxide redox chemistry (9-10).

In the present study, we have tried to synthesize the nanocomposite using aniline monomer, gold ion solution and hydrogen peroxide which acts both as oxidant and reductant in the temperature range of 0-5°C in presence of a catalyst.

In a typical experiment, each 1 mL of aniline and 0.1mL of 1M $FeCl_2$ was mixed into 5 mL (S-1), 10 mL (S-2), 20 mL (S-3) and 50 mL (S-4) of 0.1 M $HAuCl_4.3H_2O$ aqueous solution respectively in separate glass containers. Each reaction mixture was injected to the dispersion of 50 mL of 2 M HCl with 0.1 g PVP (which was already ice cooled and stirred for 15 minutes on a magnetic stirring to make a uniform dispersion). 5mL of H_2O_2 was added drop wise to each solution with continuous stirring till turned green in colour and the reaction product was kept as such for overnight at room temperature. Each precipitated residue was separated from the reaction mixture by high speed centrifugation, followed by washing with

dilute HCl and DI water till free from acid. The precipitates were dried in oven at 60^0C. Throughout the experiment, the molar ratio of aniline to HCl was kept same.

5.3 Results and Discussion

Structural Study of PANI & PANI/Au nanocomposite (XRD Analysis):

Crystallinity and orientation of composite material is of interest because more highly ordered systems display a metal like conductivity state. XRD patterns of both nanocomposite powder and PANI are given in Fig 5.1.

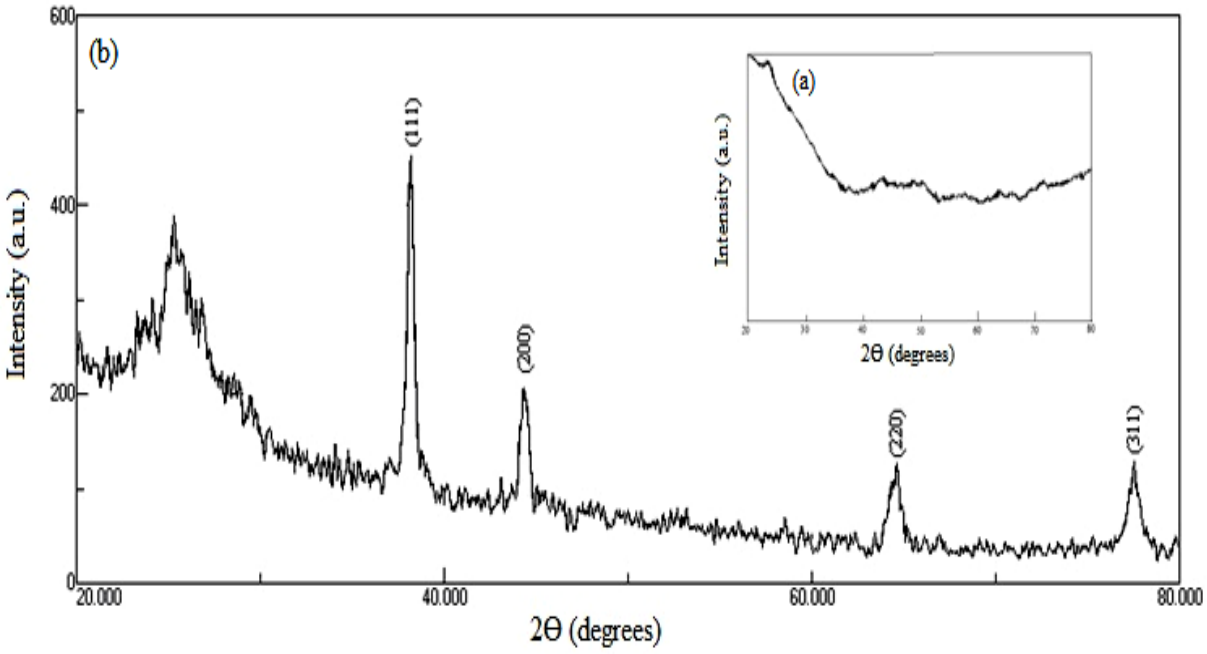

Fig 5.1: XRD pattern of a) PANI b) PANI/Au nanocomposite

No sharp peak in the XRD pattern of PANI (Fig- 5.1a, insert), shows that PANI is amorphous in nature and the broad hump at $2\Theta=22\text{-}24^0$ is in agreement with reported result in the literature (11). The characteristic Bragg diffraction peaks for Au at 2θ = 37.4°, 43.5°, 64.8 °and 78.1° in XRD diffraction in Fig 5.1 b corresponds to face centered cubic (fcc) phase of (110, 200, 220, 311) planes respectively. The results showed that observed diffraction peaks are those expected for face centered cubic gold based on bulk lattice constants [JCPDS-04-0784] and broadened in contrast to bulk due to finite size. Controlled size of AuNPs in composite was due to its surface capping by PVP surfactant and surrounding environment provided by polymer chains. The diffraction peak due to PANI in composite which appeared at about 24.5^0 becomes sharp broad hump

indicating polymer interactions with AuNPs. The average crystallite size calculated from the width of (111) Bragg reflection, using Debye –Scherrer equation is about 12nm.

Scanning Electron Microscope (SEM) Analysis:

The scanning electron microscopy was used for morphological investigation by using HITACHI S-4300SE instrument. The micrograph of PANI showed randomly grown circular polymer chains interlinking each other leaving several voids. However, the magnified view of composite film depicts gray and white patches in which gold nanoparticles have been trapped which are not visible.

a)

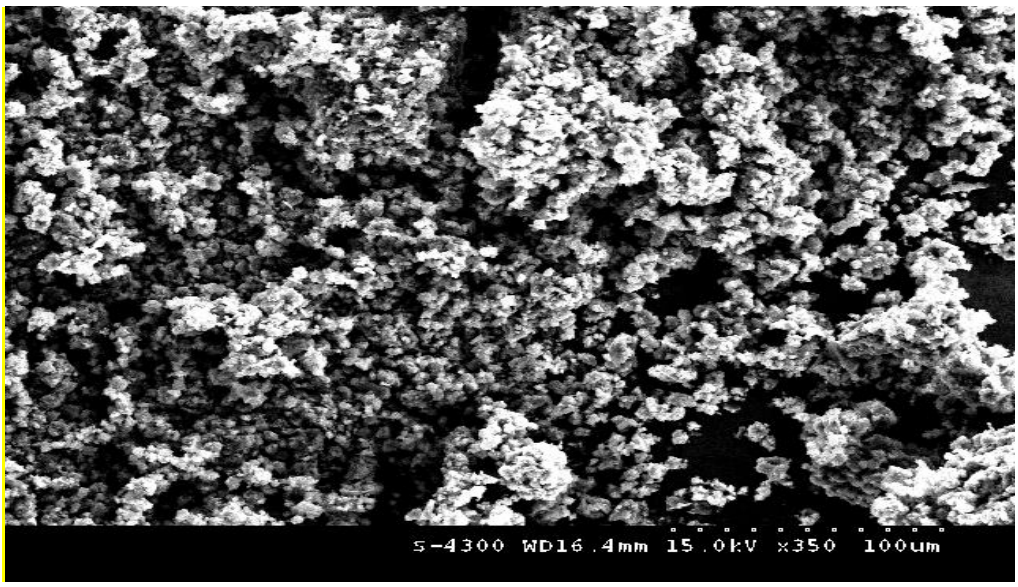

b)

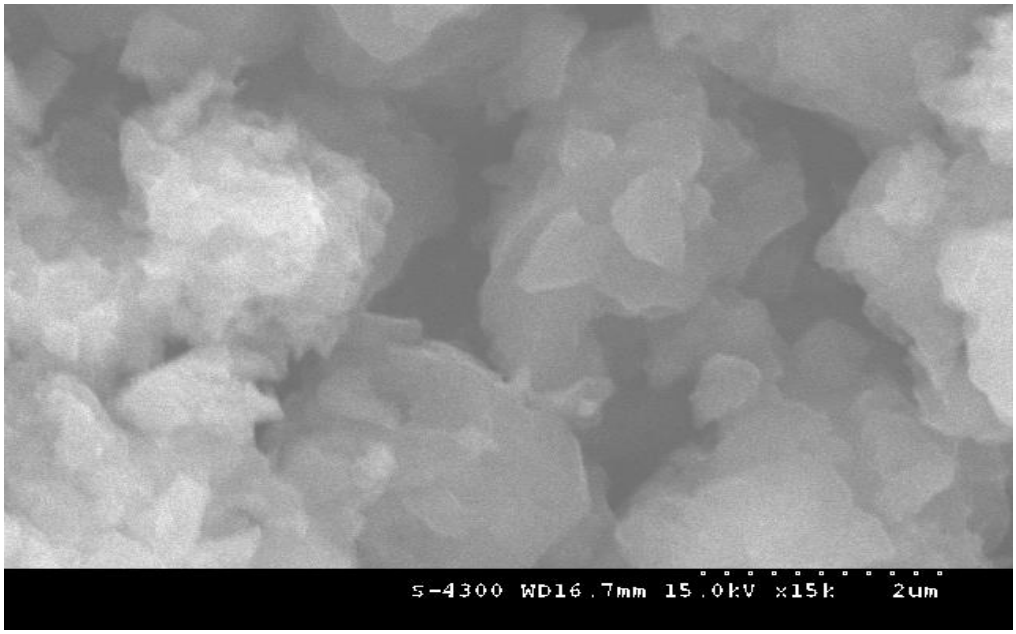

Fig 5.2: SEM micrograph of a) PANI b) PANI/Au nanocomposite

Morphological Study of PANI & PANI/Au nanocomposite (TEM Analysis):

The morphology of AuNPs dispersed in the matrix of polymer was examined using TEM. The micrograph of gold nanoparticles (Fig 5.3a) shows that particles are nearly spherical, monodispersed and have size around 10±2 nm. The figure 5.3 (b to d) represent images of PANI/Au nanocomposites using different concentrations of gold chloride solution. They clearly show that AuNPs are of regular size and are randomly distributed through out the matrix. The diameter of the particle was found to be around 12nm. No region containing only polymer or AuNPs agglomeration was detected from analysis of several TEM images taken from different portions of the sample. The reason for limited growth size of AuNPs in composite material and its random distribution may be due to following reasons: (i) sufficient numbers of electrons were available during the synthesis process resulting in quick formation of seeding nanoparticle thus restricting the faster growth (ii) the reaction temperature was kept low which may not have allowed faster growth. Moreover, presence of PVP in the reaction mixture also resulted in stabilizing the AuNPs. Since PVP is an amphiphilic and non-ionic surfactant, it forms polymer coils in aqueous solutions. These coils may be encircling AuNPs through charge transfer interactions between PVP functional group and the surface atoms of Au (12-13). From TEM images, it can be seen that no core-shell type configuration was observed as reported for iron oxide nanoparticles coated with PANI (14). It appears that polymerization process was initiated in presence of hydrogen peroxide, continuously propagated while entrapping AuNPs and finally completed in the reaction solution.

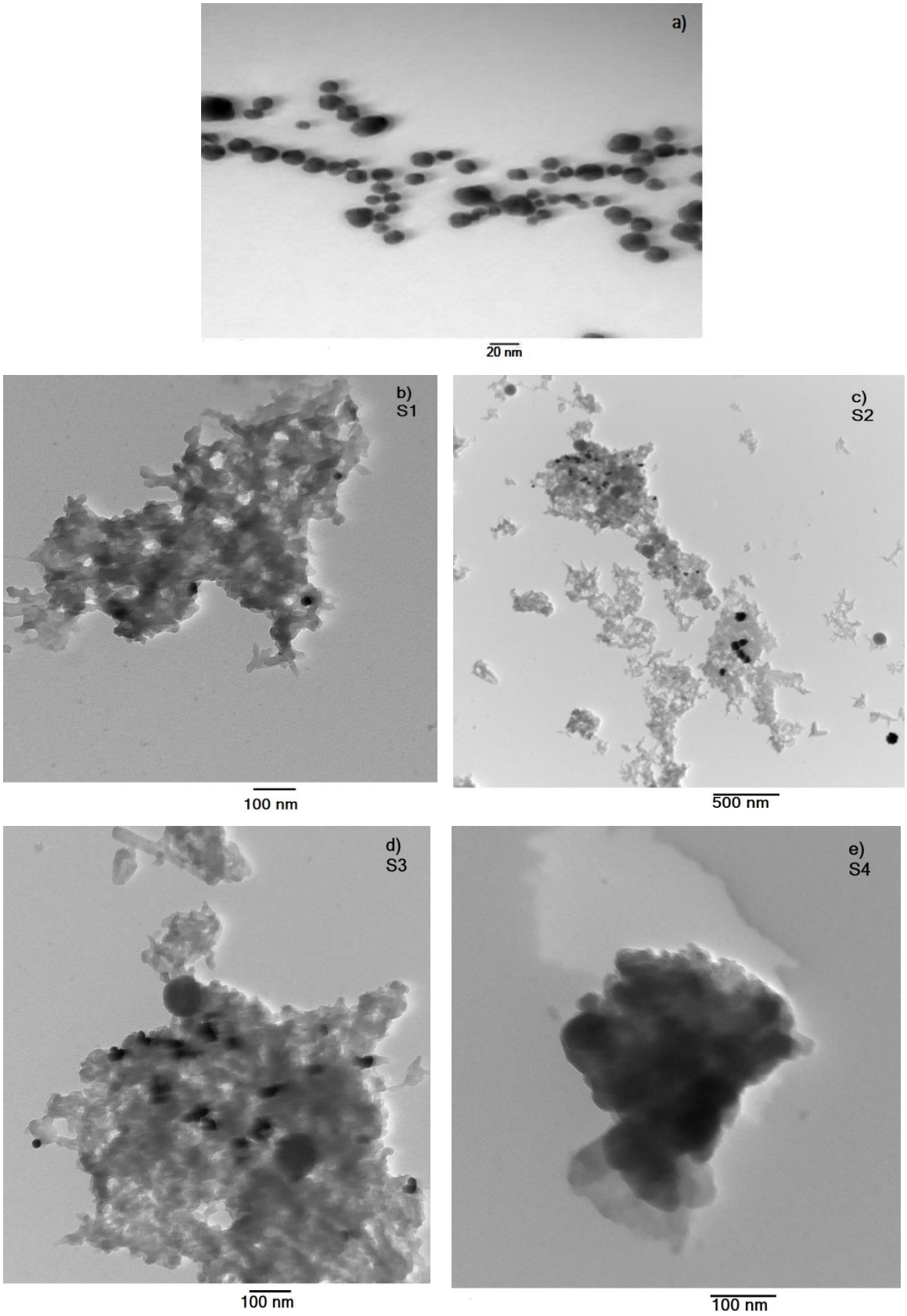

Fig 5.3: TEM micrograph of a) Au NPs b-e) PANI/Au nanocomposite (S1, S2, S3, S4)

FTIR Spectral Analysis of PANI & PANI/Au nanocomposite:

The FT-IR spectra of PANI and PANI/Au nanocomposite are shown in figure 5.4 and 5.5 respectively.

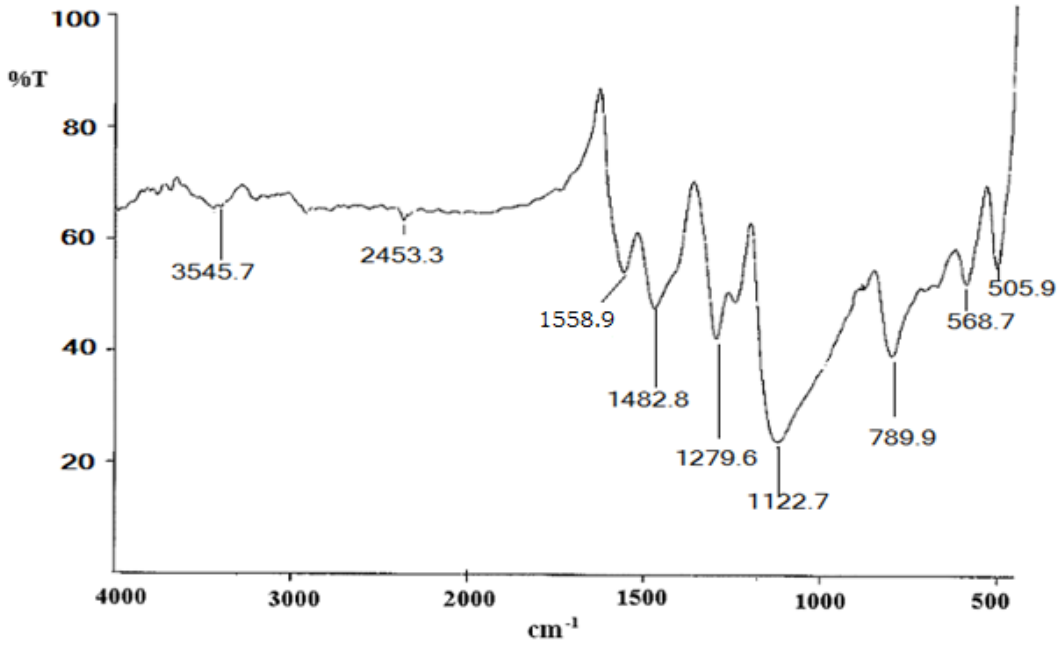

Fig 5.4: FTIR spectra of PANI

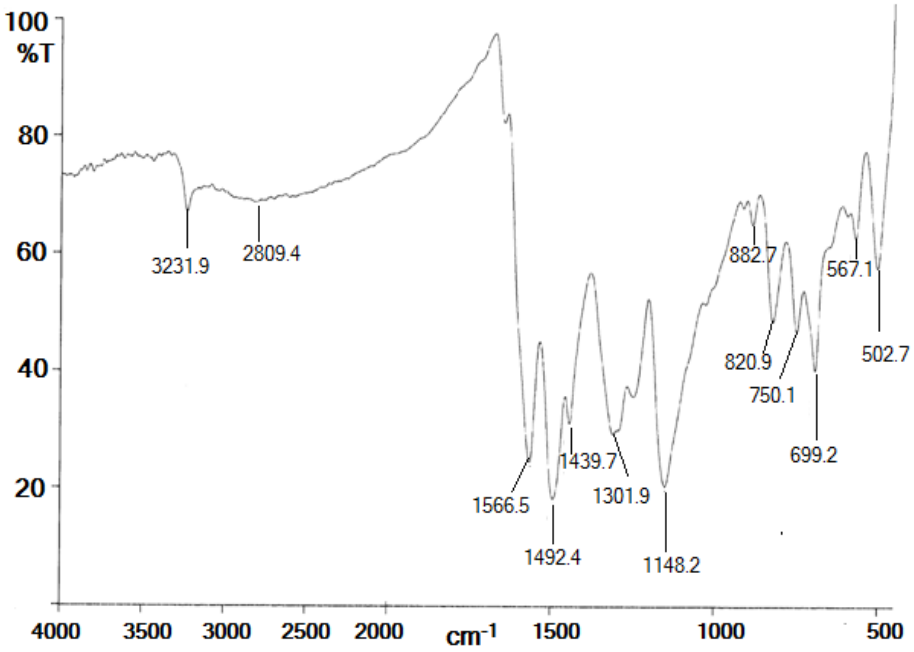

Fig 5.5: FTIR spectra of PANI/Au nanocomposite

In FTIR spectra of these samples, 3500-3300 cm^{-1} absorption is related to the characteristic N-H stretching vibration suggesting the presence of NH- groups.

This hump shows a significant shift of about 200 cm^{-1} in case of composite. The peak at 1558.9 cm^{-1} in PANI is due to stretching vibration of quinoid (N=Q=N) ring which occured at 1566.5 cm^{-1} in composite (15-16). The band occurring at 1482.8 cm^{-1} due to benzenoiod ring (N-B-N) in PANI has shifted to 1492.4 cm^{-1} in composite. The peak at 1279.6 cm^{-1}, characteristic of the conducting form of PANI (ES) is also observed, it has been interpreted as originated from bipolaron structure related to C-N^{+} stretching vibration (17) which has been shifted to 1301.9 cm^{-1} in case of composite. These results indicate that both PANI and composite are in doped state. The existence of strong absorption peak at 1122.7 cm^{-1} in case of PANI, which has been interpreted as originating from the C-H (18) in plane bending vibration, has appeared at 1148.2 cm^{-1} in composite. The band appearing at 789.9 cm^{-1}, which is assigned to out of plane deformation of C-H in PANI, has shifted to 820.9 cm^{-1} in composite. The results suggest that there is not much difference in structure between PANI and PANI/Au nanocomposite except absorption bands shifting towards higher frequency (blue shift). Apart from these, a peak corresponding to 882.7cm^{-1} in composite is due to C-H out of plane deformation (benzene ring). It means that during interaction between AuNPs, there is deformation of the bonds of polymer molecules.

The overlay of FTIR spectras' of PANI/Au nanocomposites with different amounts of gold chloride solution (S1, S2, S3 & S4 in Fig 5.6) show nearly similar pattern with some variations in the absorption bands.

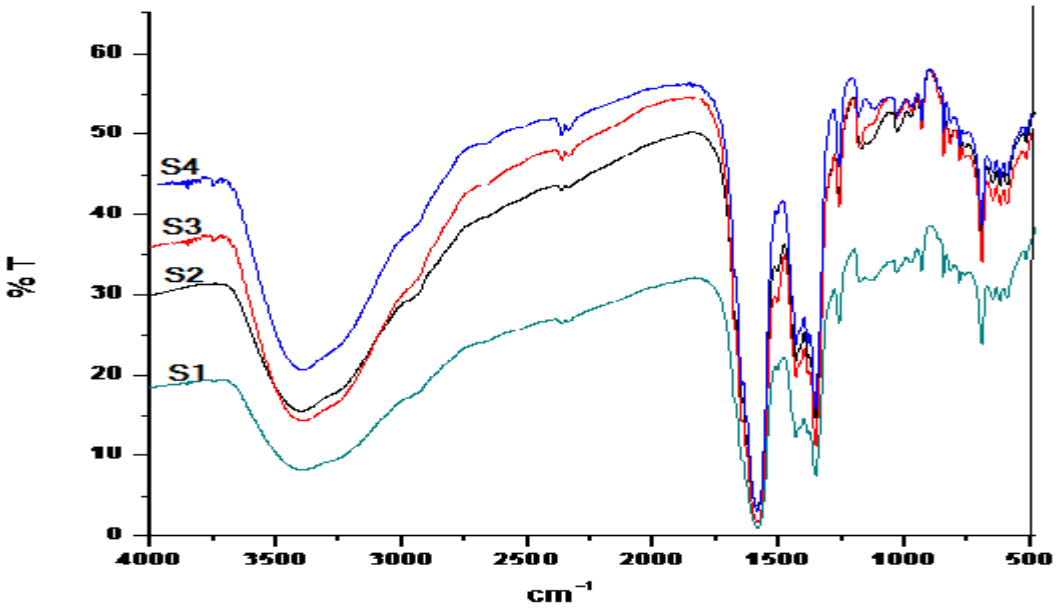

Fig 5.6: Overlay of FTIR spectras' of PANI/Au NCs with different amounts of gold ion solution

Thermal Study (TGA Analysis):

The TGA/DSC thermogram of PANI (Fig 5.7a) and composite (Fig 5.7b) were recorded from 25 – 1000 ^{0}C at heating rate of 5 ^{0}C min^{-1} with N_2 as the purge gas.

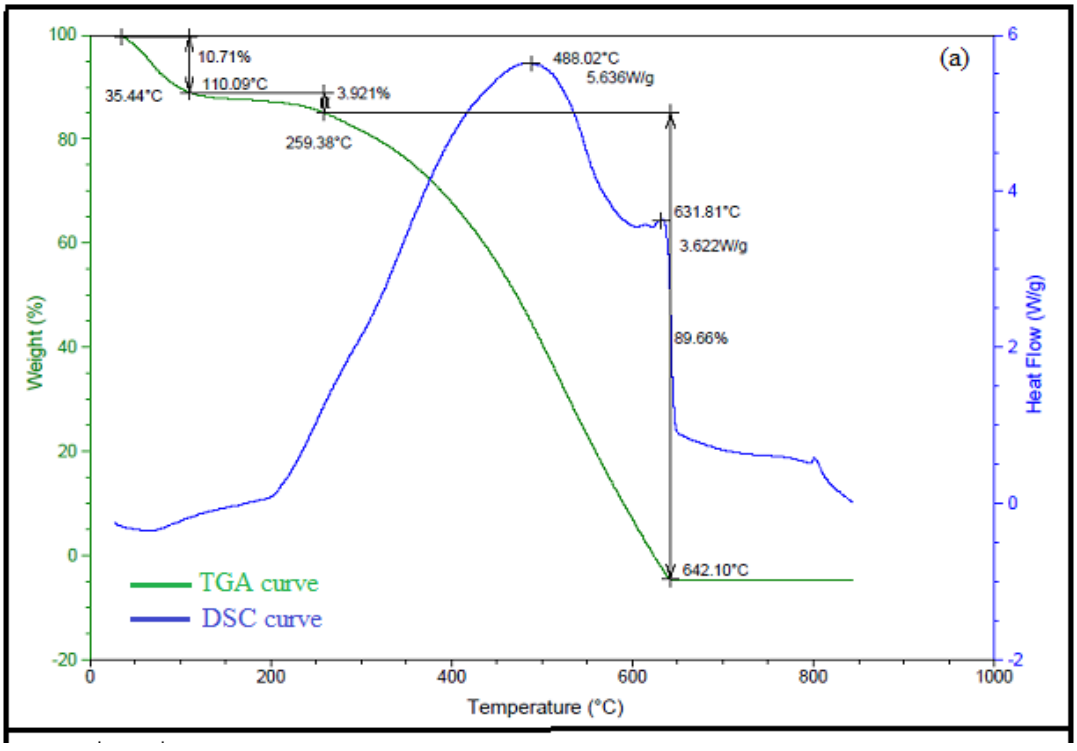

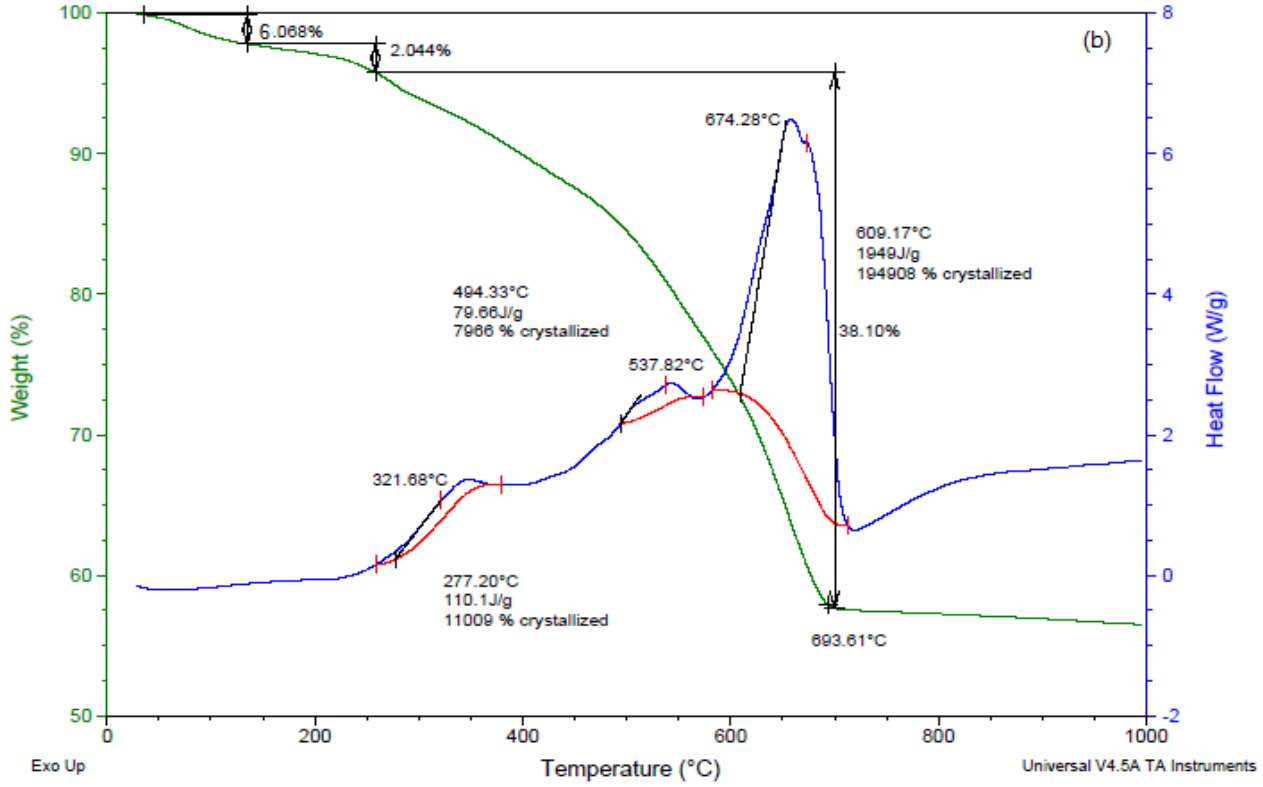

Fig 5.7: TGA/DSC thermogram of a) PANI b) PANI/AuNC (S4)

The TGA curve showed initial weight loss of 10% upto 110°C in case of PANI and about 6% in case of composite. It means that PANI alone has retained more water molecules than the composite; it may be due to their morphological differences (19). The presence of AuNPs in composite may be acting as water repellent due to spherical shape of NPs. The second weight loss of 3.92% and 2.04% upto 250°C for PANI & composite respectively is for removal of HCl dopant and small oligomers. In the third step upto 640°C, a slow and somewhat gradual weight loss profile was observed due to the complete degradation of PANI polymer. However, decomposition of polymer chains in composite lasted upto 693.61°C with residual weight of about 50% in S4 sample which may be due to the presence of GNPs in the PANI polymer indicating successful incorporation of GNPs. From DSC curves, it can be seen that heat flow for the decomposition of PANI in composite is 6.5Wg^{-1} whereas it is 5.63Wg^{-1} for PANI alone indicating the better stability of composite (20).

Optical Study (UV-Visible absorption spectra)

The characteristic absorption spectra of PANI, gold nanoparticles and PANI/Au nanocomposite is shown in the figure 5.8 a, b, c respectively.

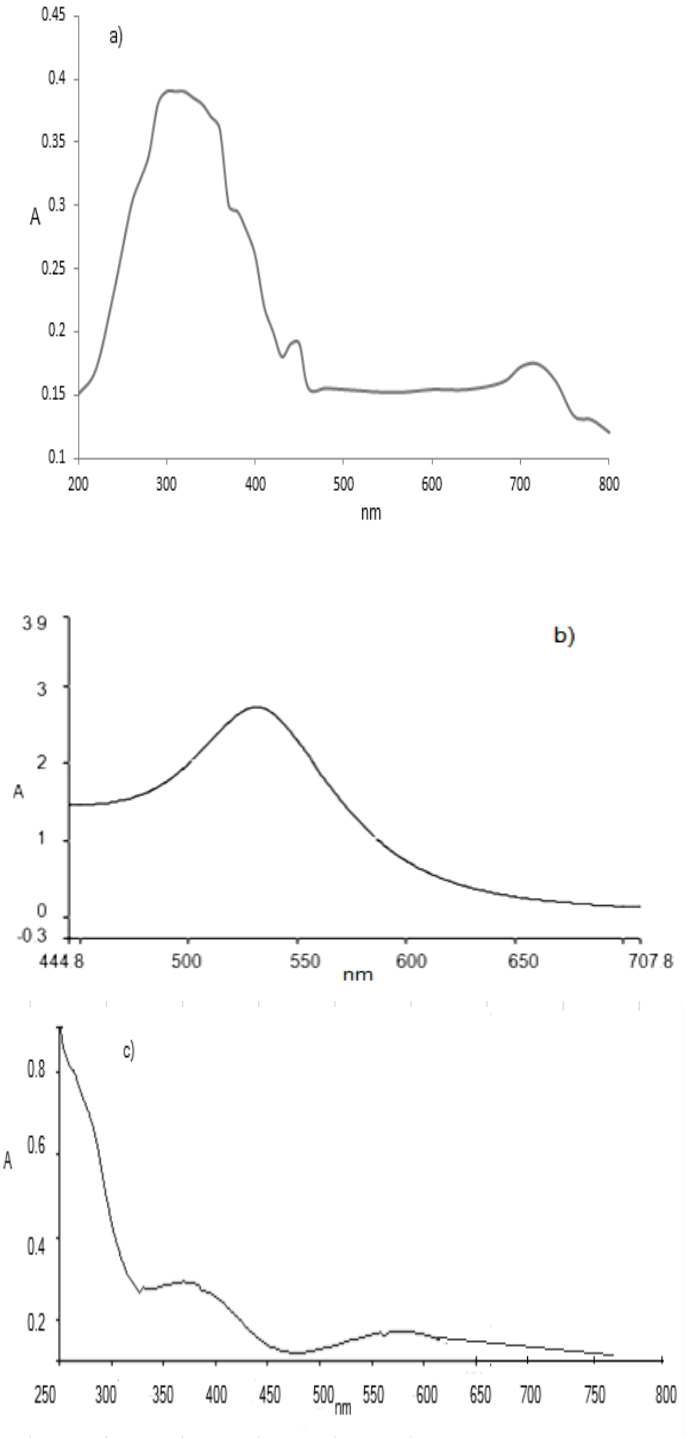

Fig 5.8: UV-vis spectra of a) PANI b) AuNPs c) PANI/Au nanocomposite

The spectra of PANI (Fig 5.8 a) shows 3 characteristic absorbance peaks. They are the π-π^* transition located between 300-320nm, the polaron-π^* transition at ~440nm and polaron-π transition between 700-750 nm, indicating emeraldine state of PANI (21). PANI/Au nanocomposite (Fig 5.8 c) showed an absorption band at about 350-400 nm which may be due to over lapping of π-π^* and polaron-π^* transition. However, it did not exhibit the surface plasmon resonance band of AuNPs {Fig 5.8(b) from Chapter 4 Fig 4.2b}. This may be due to the reason that AuNPs are deeply incorporated into the polymer chain and they are unable to exhibit the SPR band at 528 nm (Chapter 4 fig 4.2b). In addition, broad absorption band in the range of 550-600 nm may be regarded as an indication of somewhat elongation of the particles under the influence of the radiation field (23).

Electrical Characterisation of PANI & PANI/Au nanocomposite

The electrical conductivity of PANI and its nanocomposites was calculated from the current-voltage characteristic recorded using two electrode scheme in the planar ITO coated substrate. Representative I-V curves obtained for PANI & the composite (S-2) are shown in Fig 5.9.

a)

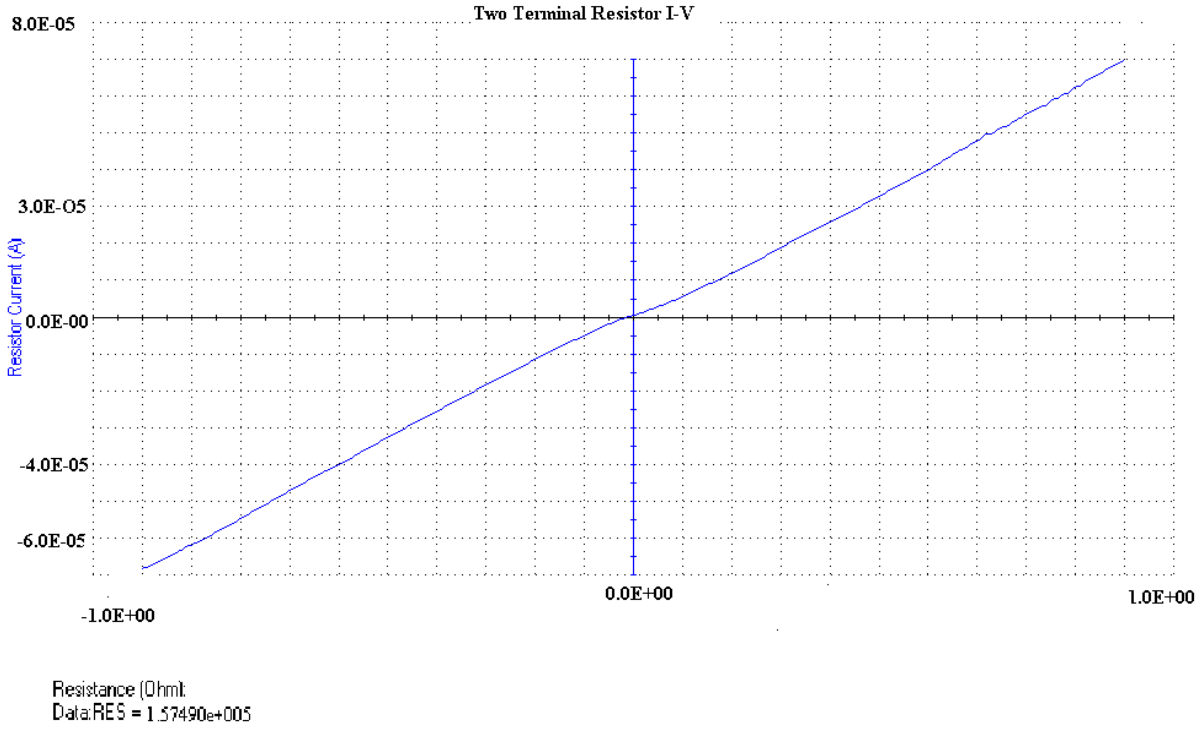

b)

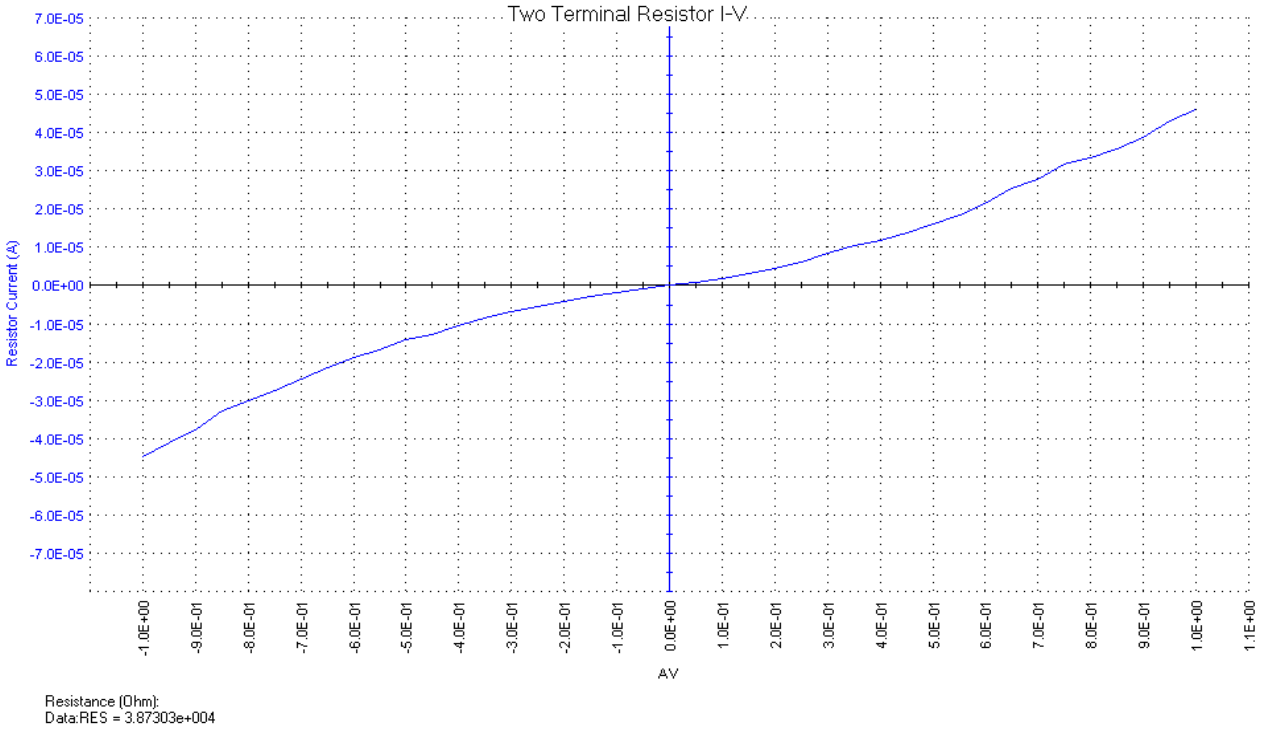

Fig 5.9: I-V Characterisation of a) PANI b) PANI/Au nanocomposite

From these curves, it can be seen that electrical properties of the composite are different from the individual component. I-V characteristic of PANI displayed ohmic behaviour, whereas S-2 displayed a diode like curve which depends on voltage. From the resulting data, conductivity values were calculated and are given in table 5.1.

Table 5.1: Conductivities of PANI and PANI/Au nanocomposites

Sample name	Length of the thin film(cm)	Cross sectional area(cm^2)	σ (S/cm)
PANI	1.2	1.107	6.8×10^{-3}
S-1	1.2	1.107	4.3×10^{-2}
S-2	1.2	1.107	2.1×10^{-1}
S-3	1.2	1.107	2.9×10^{-1}

The conductivity value of PANI film is of the order of 10^{-3} S cm^{-1} which is much lower than the value reported for its synthesis using ammonium persulphate as oxidant and keeping other experiment conditions same. Moreover, the conductivity values of the composite films have shown many times fold increase that of PANI. Similar conductivity values were observed when repeated measurements were made. The electrical conductivity of conducting polymers results from mobile charge carriers introduced into π electronic system through doping. The insertion of AuNPs in conducting polymer has further enhanced its mobility with uniform dispersion (24).

CHAPTER 5 (PART B)

SYNTHESIS AND CHARACTERIZATION OF POLYANILINE/SILVER CHLORIDE NANOCOMPOSITES

Among the inorganic nanoparticles, silver halides are photosynthetic material and extensively used as source material in photographic films, photo catalyst and ionic semiconductors (25). Very few studies have been reported for the synthesis/fabrication of PANI /AgCl nanocomposites for exploration of material with different properties. Since PANI is being synthesized in different morphologies, therefore the addition of light sensitive silver halides open new possibilities with improved performance. As such no study has been reported for the fabrication of thin films on a solid surface with PANI/AgCl nanocomposite and their electrical behaviour. Here, we report a facile route for synthesis of PANI/AgCl nanocomposite, in which PVP has been used for capping the AgCl NPs and bridge PANI and AgCl, through weak Vander Waal forces or hydrogen bonding. Presence of PVP in polymer matrix also enhances the bonding with a solid surface to make thin film of uniform thickness. PANI/AgCl nanocomposite has been characterized for their morphological, structural, thermal and electrical properties. This is a new strategy to generate materials of different properties for better processability.

5.4 Synthesis of PANI/AgCl nanocomposites

PANI/ AgCl nanocomposites were synthesized by polymerization of aniline monomer in aqueous HCl solution in presence of H_2O_2 oxidant with simultaneous precipitation of AgCl in polymer matrix. In a typical experiment, 0.5 mL of aniline was mixed into 1 mL (S-1), 2 mL (S-2), 5 mL (S-3) and 10 mL (S-4) of 0.2 M $AgNO_3$ solution in already marked cuvettes. Each solution was injected into a separate 200 mL glass flask containing 100 mL of 2 M HCl with 0.05 g PVP. To make a uniform dispersion, reaction bath was stirred for 15 min on a magnetic stirrer continuously followed by ice cooling in the controlled temperature bath. To each of reaction mixture 10 mL H_2O_2 was added drop wise with continuous stirring, till a green colored solution formed. These were allowed to stand as such for an over-night at ambient temperature. Precipitated residue was separated

from the reaction mixture by high speed centrifugation, followed by washing with dilute HCl and DI water till free from acid. Vacuum drying of the residue was carried out at 60°C. A portion of S-4 was used for TEM, XRD, TGA and FTIR characterization. Each left out nano composite power was used for thin film casting on ITO coated glass surface. Throughout the experiment, the molar ratio of aniline to HCl was retained same. AgCl NPs were also synthesized in the presence of PVP keeping similar experimental conditions.

To make solution film, a portion of each; PANI, S-1, S-2 & S-3 & S-4 powder was dispersed in 50 mL of 1 % ammonia solution in a separate glass container and allowed to stand for 6 hours. The blue colored residue was separated using centrifugation method followed by washing with DI and ethanol. After vacuum drying, a known amount of powder (0.1 g) was dissolved in NMP (2 mL). The solution was stirred into make it completely soluble. To remove any insoluble particle, it was again centrifuged till a clear solution was formed. Thin films were fabricated by solution spin casting technique on the ITO coated glass substrates using each of this solution. The rotation speed of the spin casting machine was initially taken 600 rpm for 30 s, and raised to 1,000 rpm for another 20 s. Each film was allowed to dry at room temperature. It was again dipped in 20 mL of 0.1 M HCl solution for about 6 h for acid doping, washed with DI water/ethanol and air dried. Thickness of each film was measured using mechanical profilometer. Electrical characterization was done on film surfaces having thickness of 5.0 ± 0.2 μm.

5.5 Results and discussion

Structural Study (XRD analysis):

XRD patterns of PANI and S-4 (AgCl/PANI) nanocomposite powder are given in Fig 5.10.

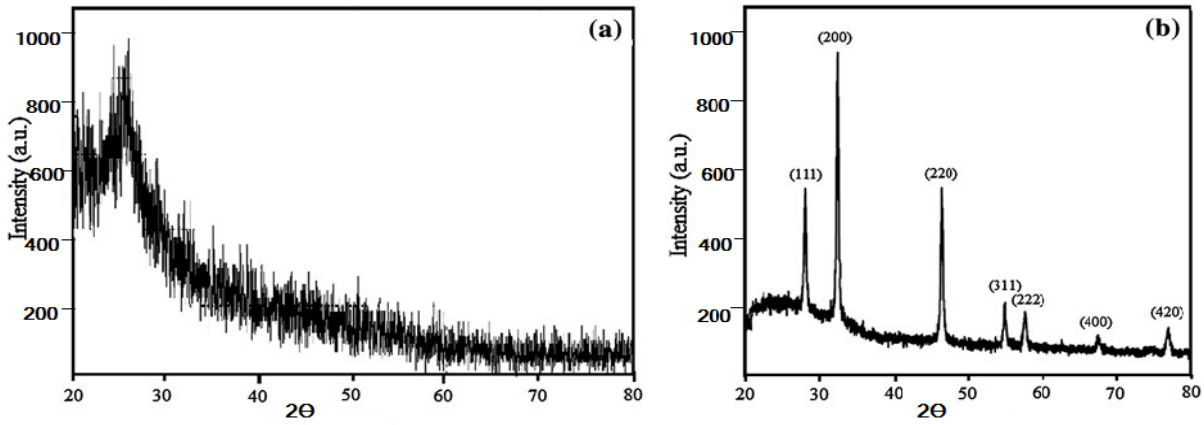

Fig 5.10: a) XRD pattern of pure HCl doped PANI b) XRD pattern of PANI/AgCl nanocomposite

The diffraction pattern of PANI powder in Fig 5.10 a exhibited one broad hump at a position of 2Θ = 22° is ascribed to the periodicity parallel to polymer chains. However in S-4 composite (Fig 5.10b), the intensity of the broad diffraction hump of PANI gradually diminished. Other seven sharp diffraction peaks at 2Θ = 27.70°, 32.00°, 46.05°, 54.70°, 57.32°, 67.40° and 76.70° could be assigned to the characteristic diffraction peaks for AgCl (111), (200), (220), (311), (222), (400), and (420) facets respectively. These diffraction patterns are in good agreement with the reported data (JCPDS No. 06-0480) (26-27). The typical diffraction peaks of silver were absent in the XRD pattern of composite indicating complete precipitation of AgCl from its precursor $AgNO_3$ due to the significant amount of chloride ions availability in the reaction mixture during synthesis. It also indicates that PVP has only stablized AgCl NPs, and has not reduced metal ion though it acts as weak reducing agent.

Morphological Study (TEM analysis):

Figure 5.11 reveals the typical TEM image of PANI/ AgCl (S-4) nanocomposite. From TEM image, it can be seen that most of AgCl NPs have irregular spherical shape and randomly distributed in the polymer matrix.

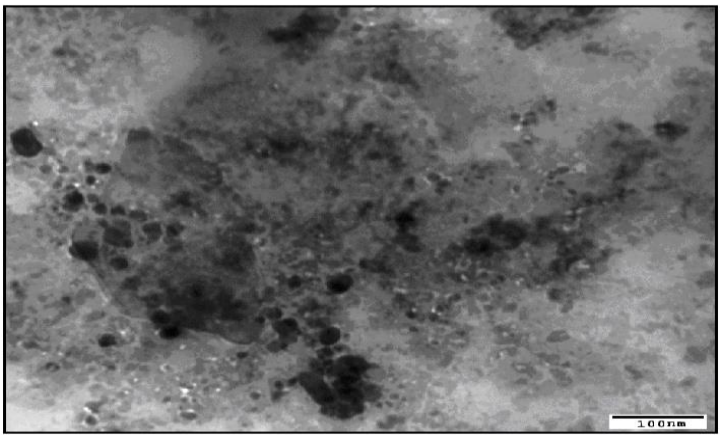

Fig 5.11: TEM image of PANI/AgCl nanocomposite

The diameter of these particles was found to be in the range of 10–20 nm. No region containing only polymer or nanoparticles agglomerations alone was seen though several TEM images of the same sample were taken at different positions indicating the presence of both PANI and AgCl NPs in close vicinity. The reason for the same is the availability of a sufficient number of chloride ions in the synthesis process resulting in fast nucleation of tiny AgCl particles. The controlled growth of these particles was possible due to low temperature (0°C to ambient) during synthesis and quick entrapment of AgCl in polymer chains, polymerization of aniline in composite being in situ. PVP was also added at the beginning of the precipitation reaction, being nonionic surfactant, it forms coils in dilute aqueous solution and encapsulates nanoparticles through charge transfer interactions from the oxygen atom of carbonyl end in PVP. The nucleophile character of oxygen stabilizes AgCl NPs, silver being electro positive in character (28). It may also be possible that the nonpolar end of PVP get mingled within PANI polymer chains through hydrogen bonding. From TEM image, it can be said that PANI has not been coated on the surface of AgCl NPs; however core-shell nano structures were also reported by Feng et al (29). The formation of the existing morphology of composite may be due to the reaction condition employed and oxidant used. Thus the polymerization process was initiated with hydrogen peroxide along with entrapping AgCl NPs in it. PVP has stabilized AgCl NPs which may be an inter-linker among the polymer and nanoparticles.

FTIR Spectral Analysis:

FTIR is a useful technique to examine the structural transformations in materials.

Figure 5.12 represents the FT-IR absorption spectrum of S-4 powder in the frequency range of 500- 4,000 cm^{-1} which showed major characteristic peaks of PANI.

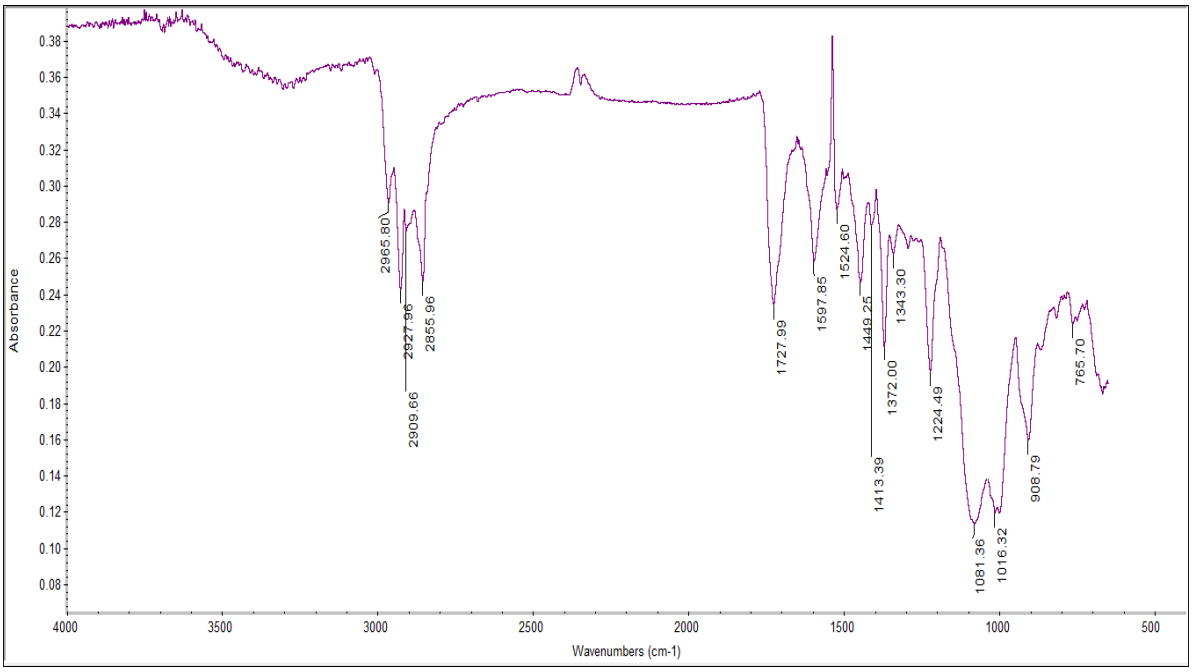

Fig 5.12: FTIR spectra of PANI/AgCl nanocomposite

The main band at 1,597.0 cm^{-1} is due to stretching of N=Q=N (Q represents a quinoid ring), where as band appearing at 1,524.6 cm^{-1} due to stretching of N-B-N (B represents a benzenoid ring) are the fingerprint of PANI in nano composite. However the absorption band of benzenoid ring in composite has shifted in higher frequency than PANI (emeraldine salt) at 1,492.0 cm^{-1} (30) indicating NPs interactions with polymer chains. Another absorption band at 1,224.49 cm^{-1} is due to protonated chain vibrations $Q=NH^{+}$-B or B-NH^{+}-B which can hydrogen bond to the -NH- or =N- group in PANI which was also reported as 1,189.0 cm^{-1}. FTIR analysis of PANI fibrils made by Wang et al. (31) showed a stretching vibration mode due to C-N bond link at 1,124 cm^{-1} which has been missing in this composite. Absorption peaks at 1,081.36 and 765.70 cm^{-1} were related to C-H in plane bending and C-H out of plane bending in PANI (32, 33). The band at 1,081.36 cm^{-1} may be associated with high electrical conductivity and high degree of electron delocalization (33). A strong absorption band at 1,727.99 cm^{-1} is of a carbonyl group stretching of PVP indicating its presence in the composite which is capped AgCl NPs. A red shift in this absorption peak to the already reported results at 1,661.0 cm^{-1} for pure PVP, 1,669.0 and 1,671.0 cm^{-1} for AgCl/PVP

system (26) indicates that there are interactions within PVP and PANI chains in composite. Feng et al. (29) reported this carbonyl stretching peak of at 1,651.0 cm^{-1} for core shell PANI/AgCl NPs composites. Other peaks of PVP are at 2,965.80, 1,449.25 and 1,343.30 cm^{-1} corresponding to C-H, C=C & C-N respectively. A strong C-H symmetric and asymmetric stretch between 2,800.0 and 3,000.0 cm^{-1} of PVP was also present in composite. From IR analysis it can be interpreted that PVP has interacted with both AgCl NPs and PANI in the composite.

Thermal study (TGA-DSC Analysis)

TGA/DSC thermograms of S-4 composite powder and PANI are given in Fig 5.13.

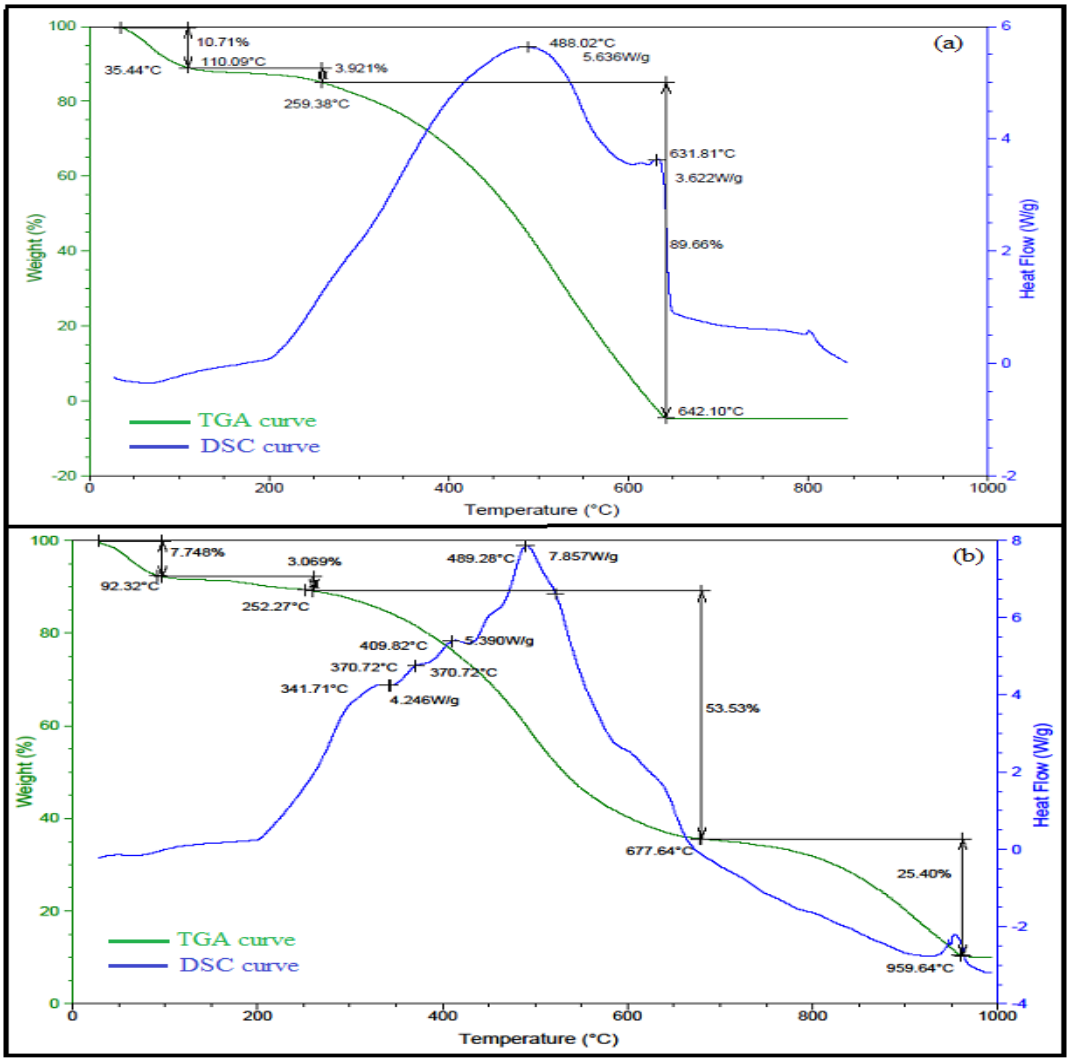

Fig 5.13: TGA/DSC thermograms of a) HCl doped PANI b) PANI/AgCl nanocomposite

TGA curve of S-4 (Fig 5.13b) showed initial weight loss of 7.74 % which is due to the evaporation of moisture as PANI present in composite is a hygroscopic polymer. Several studies reported the endo-thermic effect registered in the ambient to 140 °C due to evaporation of water (34, 35). Moisture can interact with the polymer chains during synthesis as well as storage. The second weight loss of 3.06 % up to 252.27°C is for removal of HCl dopant. No weight loss was seen till 300°C followed by a steep weight loss of 53.53 % up to the temperature of 677.64°C due to the degradation of both PANI and PVP. Decomposition of PVP has been reported in the temperature range of 250 –600°C depending on its molecular mass (36). However no separate curve was seen in TGA for the decomposition of PVP, reason being both PANI and PVP are simultaneously disintegrating into their moieties in the same temperature profile. Degradation of PANI alone has already reported by several authors in the temperature range of 300-620°C with 0 % residue depending on dopant and gas flow (37, 38). Similar results have been found in the present study for PANI alone in Fig 5.13a. However, decomposition of polymer chains in composite lasted up to 670°C with 30 % residue of AgCl. Enhancement of polymer degradation temperature in composite showed higher stability. AgCl NPs has acted as filler material in polymer chains which has extremely high surface to volume ratio leading to good dispersion. It changes the nature of the original matrix and made it more rigid. The final weight loss occurred in the temperature range of 800 – 959.6°C due to the decomposition of the AgCl (29). The DSC curve in Fig 5.13b showed one main peak due to the decomposition of PANI and three minor peaks. A peak at 341.7 °C is due to cross linking reaction within polymer chain from coupling of two neighbour quinoid and benzenoid ring similar to reported in PANI and emeraldine salt (39-40). There are other two peaks at 370.72°C and 409.82°C which may be due to the decomposition of PVP molecules and removal of small agglomeration polymer moieties respectively. Main peak at 489.28°C is due to the disintegration of PANI chains into its C, H & N moieties (41). From DSC curves, it can be seen also that heat flow for the decomposition of PANI in composite is 7.85 W g^{-1} (Fig 5.13b) whereas it is 5.63 W g^{-1} for PANI alone (Fig 5.13a) indicating the better stability of composite. These results have been supported by XRD and FTIR data also.

Electrical characterisation

Current-voltage (I-V) characterization was carried out by a linear potential scan method in the potential range of 0 to ±5 V at ambient temperature.

Table 5.2: Conductance data of HCl doped PANI, PANI/AgCl nanocomposite and AgCl NPs alone

Sample name	Length of the thin film (cm)	Cross sectional area (cm^2)	Conductivity (S cm^{-1})
PANI	1.2	1.107	$6.8x10^{-3}$
S-1	1.2	1.107	$2.9x10^{-3}$
S-2	1.2	1.107	$1.05x10^{-3}$
S-3	1.2	1.107	$2.9x10^{-2}$
S-4	1.2	1.107	$4.6x10^{-5}$
AgCl NPs	1.2	1.107	$6.5x10^{-6}$

From the resulting data, conductivity values were calculated which were found to be different than PANI alone. An increase in conductance values was seen in composite samples with the increase of nanoparticle concentration up to a certain level as per Table 5.2. The reason for this change can be interpreted as total conductivity of a composite material is a combination of both microscopic and macroscopic conductivity. The microscopic conductivity is the level of nanoparticles/ nanofiller present in the composite, its shape, size distribution and nature of interactions with the polymer chains. On the other hand macroscopic conductivity depends upon grain boundary, inhomogeneity and its compactness. PANI/AgCl nanocomposites are inhomogeneous because of nanoparticle dispersion in polymer matrix. In the synthesis of composite material in situ polymerization and AgCl nanoparticle precipitation occurred together, thus both modes of conductivity will change due to physical behaviour of composite including compactness, orientation and concentration level of NPs in it. The orderness gives rise to more compactness in polymer chains, higher thermal stability and different conductivity. PANI itself is less compact as microscopic particles are randomly distributed and linkage between polymer particles through the grain boundaries is not strong enough. The conductance value of thin film samples shows several fold variation which is due to above reasons (Table 5.2).

However, as AgCl NPs concentration in the composite is the order of 30 % or higher, conductance values begin to decrease. The reason for the same is that AgCl compound is an insulator and possesses conductivity of the order of 10^{-7} S cm^{-1}. However with the presence of increased amounts of AgCl NPs in composite, its surface is now rich with nanoparticles, thus turning into an insulator with less conductivity. The presence of PVP also affects the conductivity due to its interactions with AgCl or PANI. PVP appears to inhibit charge transfer between the PANI chains and AgCl NPs which creates a barrier in for alteration of conductivity.

SYNTHESIS AND CHARACTERIZATION OF POLYANILINE/SILVER NANOCOMPOSITES

Polyaniline/Ag nanocomposites have been obtained by reduction of silver salt by the already formed polyaniline(42), polymerisation of aniline in a silver nanoparticles containing medium (43), using templates for growing both silver nanoparticles and polyaniline (44), a photoredox mechanism (45) and an electrochemical method (46). However, multistep reactions are involved or a complex set for sequential reactions is required in the foregoing methods. Single-pot methods are considered to be beneficial to obtain uniform and molecularly defined composite materials. Herein, one step chemical synthesis of PANI/Ag nanocomposites has been carried using silver nitrate and aniline as raw materials. H_2O_2 was used both as an oxidizing agent and a reducing agent.

5.6 Synthesis of PANI/Ag nanocomposite:

In a typical procedure, to ice- cooled 50 mL of 2M sulphuric acid or PTSA solution,

2 mL of aniline and 5 mL of 0.2M silver nitrate was added with continuous stirring. 5mL of hydrogen peroxide solution was then added as an oxidant for aniline and reductant for silver ions.Green precipitates started to appear which indicated the polymerization of monomer unit. The stirring was done overnight, so that the polymerization may complete. Next day, the residue formed was separated by centrifugation, washed till free from acid and was vacuum dried.

In another study, in place of hydrogen peroxide, a mixture of APS and sodium borohydride was used.

5.7 Results and discussion:

Structural Study (XRD Analysis):

Fig 5.14 shows the XRD pattern of PANI/Ag nano composite powder.

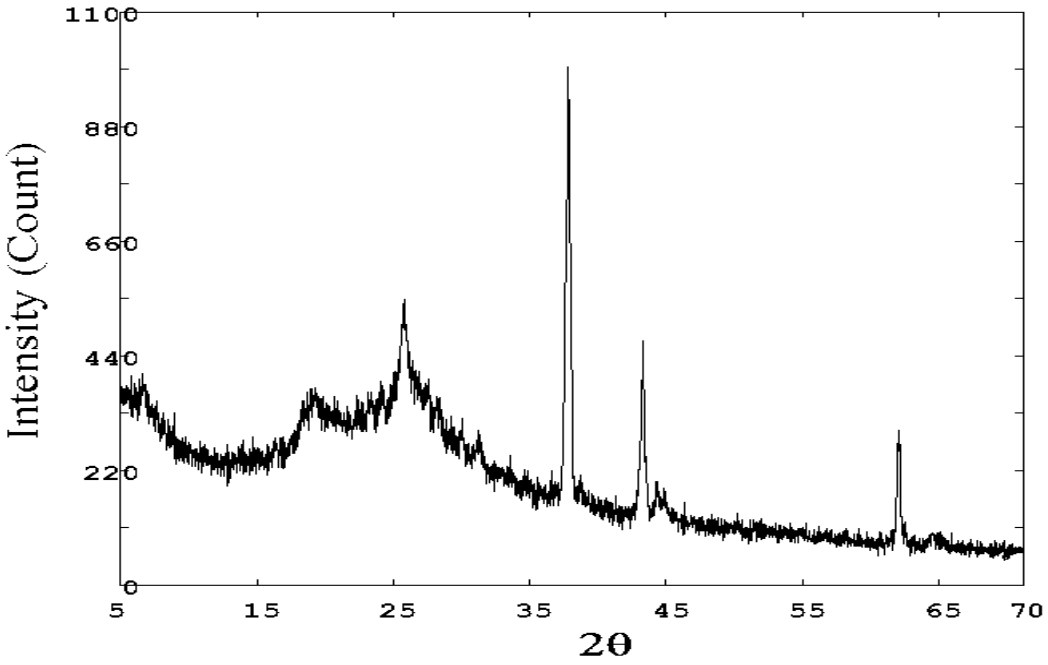

Fig 5.14: XRD pattern of PANI/Ag nanocomposite

The XRD diffraction peaks of PANI/Ag composite were found to shift to lower 2θ values as compared to the Ag nanoparticles (as explained in the section-XRD analysis of Chapter 4-Part B). The peak at 38˚ of Ag is shifted to 37.8˚, 44˚ is shifted to 43.3˚ and peak at 63.8˚ is shifted to 62.1˚. The peak shifting to lower angle in PANI/Ag composite than the Ag nanoparticles indicates the tensile stress in the composite. It might be attributed to the attachment of the nanoparticles with polymer chains.

The peak which is at 24.5˚ in PANI/Ag composite may be explained on the basis of the attachment of the polymer chains of PANI with the Ag nanoparticles. The polymer chains during the interaction may attach to the nanoparticles along this plane. This will increase the reflection intensity of the light. The average size of the PANI/Ag NPs was 41nm, which shows an increase in the crystallite size when compared to the size of silver nanoparticles. This shows the formation of PANI/Ag nanocomposite.

Morphological Study (TEM Analysis)

The TEM images of the PANI/Ag composites are shown in the Fig 5.15 (a), (b), (c) and (d) at different magnifications.

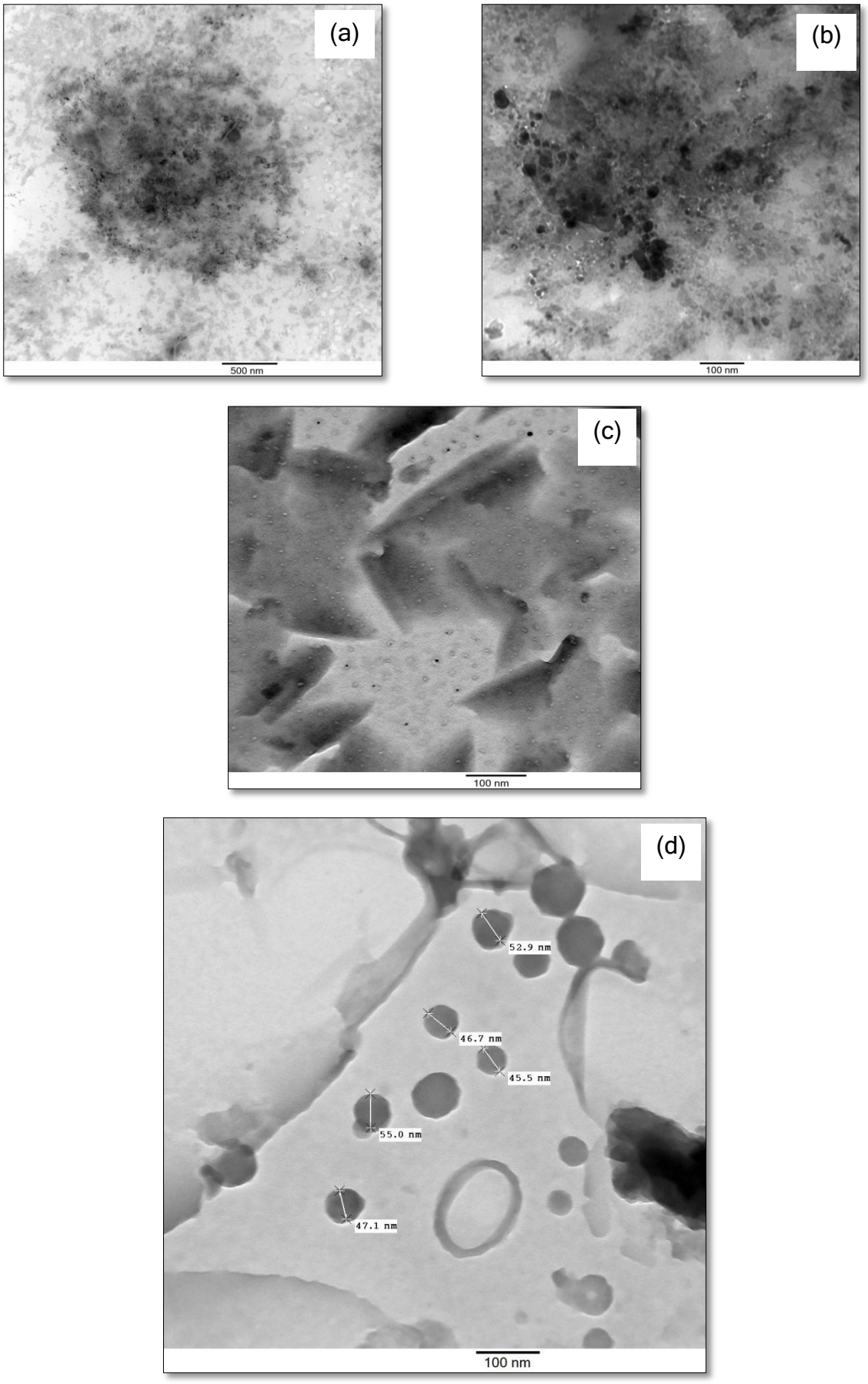

Fig 5.15: TEM images of PANI/Ag nanocomposites at different magnifications

It is clear that the nanoparticles are attached to the polymer molecules as clearly indicated by the Fig 5.15. In the images, the dark portion which is spherical in nature represents nanoparticles and the gray areas show the polymer chains. Hence, it is clear from the micrographs that the polymer molecules have been adsorbed on the surface of the nanoparticles. The molecules of the PANI and the nanoparticles are hence bonded by weak bonds and are forming the composite. Fig 5.15(d) shows that Ag nanoparticles are trapped in PANI and the average size of PANI/Ag nanocomposite is 47 nm which is in agreement with XRD analysis.

FTIR Spectral Study

The FTIR spectras of the pure PANI and the composite material are shown in Fig 5.16 and 5.17 respectively. The two peaks at 3545.7 and 2453.3 cm^{-1} in the spectra of PANI are due to the N-H stretching and C=N stretching. The peaks at 1558.9 cm^{-1} and 1482.8 cm^{-1} are attributed to the stretching vibrations of N=Q=N ring and N-B-N ring respectively. The peak at 1279.6 cm^{-1} corresponds to C-N^{+} stretching vibration. The peaks at 1122.7 and 789.9 cm^{-1} can be assigned to bands characteristic of B-NH-Q or B-NH-B bonds, and out-of-plane bending vibration of C-H of benzene rings (where B refers to the benzene-type ring and Q refers to the quinonic-type ring) (47-48).

FTIR spectra of composite shows more peaks than the polymer sample. The peaks which are corresponding to polyaniline are shifted towards higher wave number. The peaks at 1558.9, 1482.8, 1279.6, 1122.7 and 789.9 cm^{-1} are shifted to 1576.5, 1504.1, 1339.7, 1169.8 and 830.2 cm^{-1} respectively. This may be due to the interaction between the polymer and the nanoparticles. Apart from these two peaks corresponding to 1276.9 and 896.2 cm^{-1} are due to C-H out of plane deformation (benzene ring). It means that during interaction between Ag nanoparticles there is deformation of the bonds of the polymer molecules.

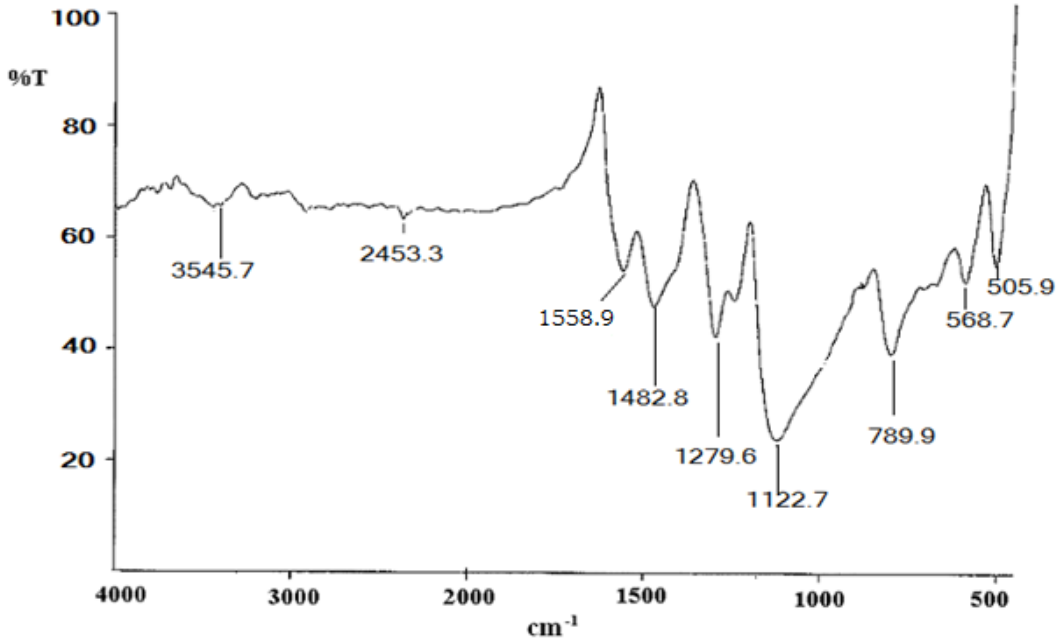

Fig 5.16: FTIR spectra of PANI

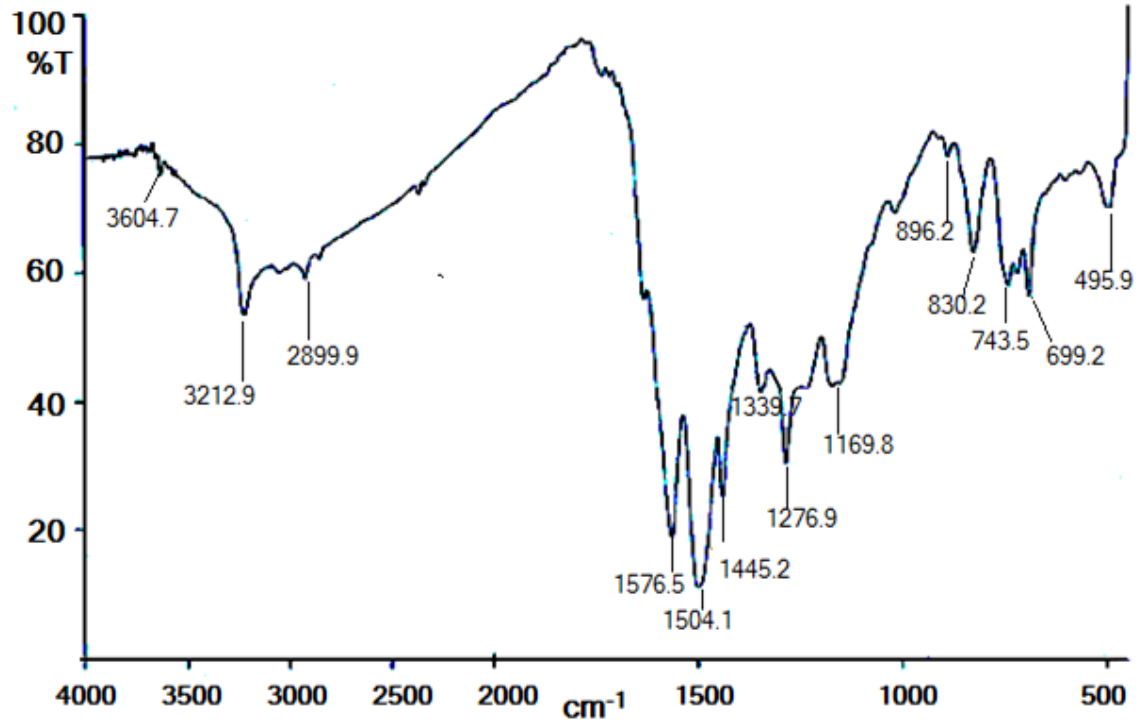

Fig 5.17: FTIR spectra of PANI/Ag nanocomposite

Optical Study (UV-Vis Spectroscopy):

The optical study was conducted at room temperature for Polyaniline/Ag nanocomposite and the absorption spectra is shown in Fig 5.18.

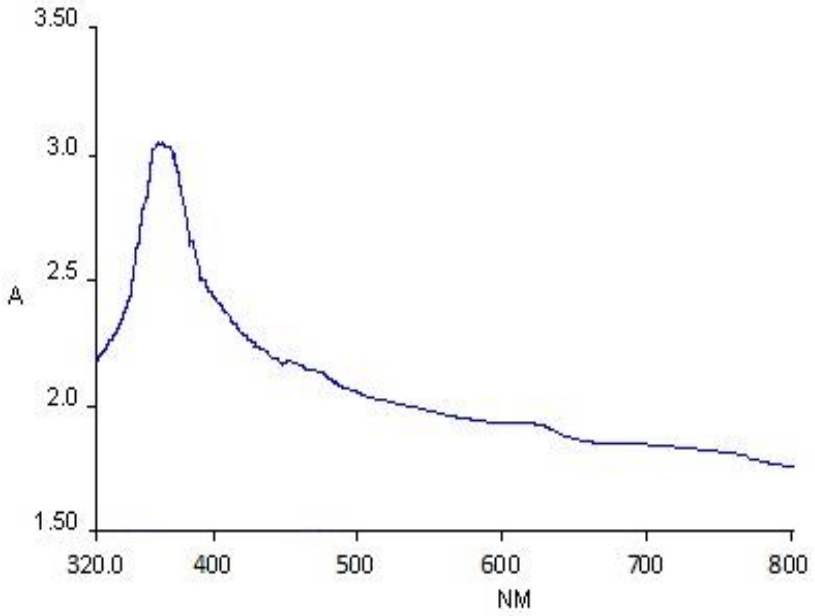

Fig 5.18: Absorption spectra of PANI/Ag nano composite

The UV spectra of the synthesized silver nanocomposite shows the presence of characteristic absorption peak at about 360 nm, which corresponds to the π-π^* transitions of PANI (as explained in fig 5.8a Section B of this chapter). There is shifting of the absorbance edge towards higher wavelength which indicates a decrease in band gap, thereby increasing the conductivity. There may also be the possibility of aggregation of Ag NPs which results in the increase in their size. The spectra did not show the characteristic SPR absorption band of Ag nanoparticles which may be due to the reason that NPs are deeply embedded in the polymer matrix.

Electrical Characterisation of PANI & PANI/Ag Nanocomposite

I-V characteristics of the thin films of PANI and PANI/Ag nano composites were observed to find the value of resistance for the films. I-V curves shown in the Fig 5.19 and 5.20 indicate that the resistance of the PANI film is greater than the composite thin film.

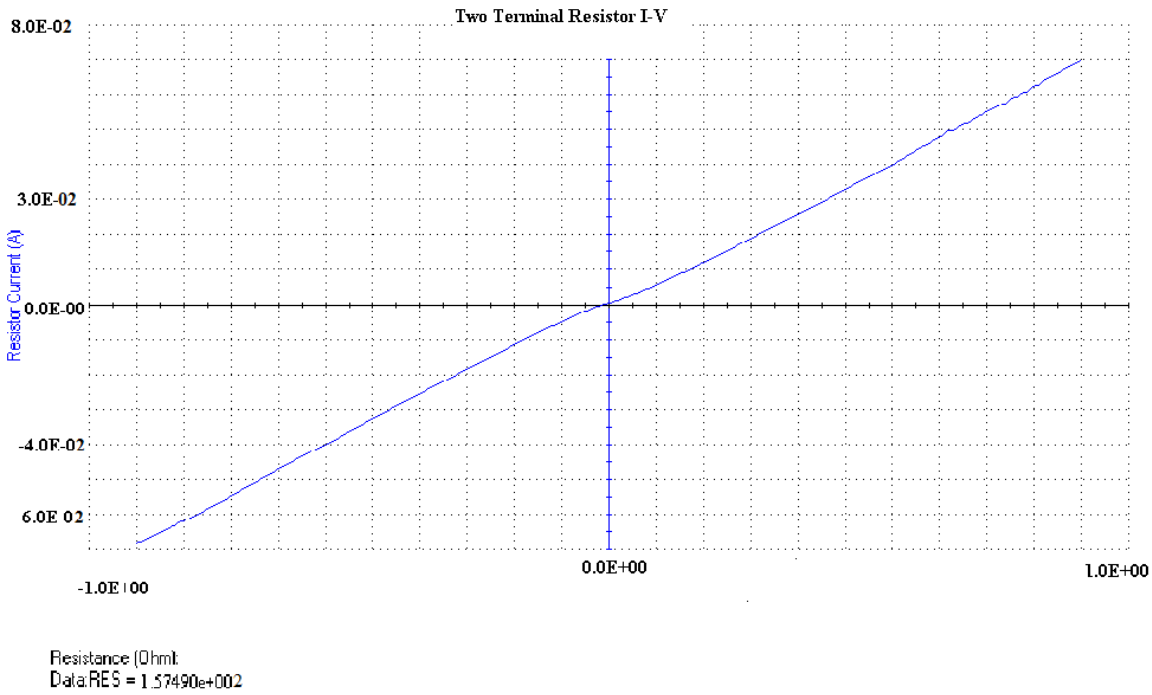

Fig 5.19: I-V Characteristic of the thin film of PANI

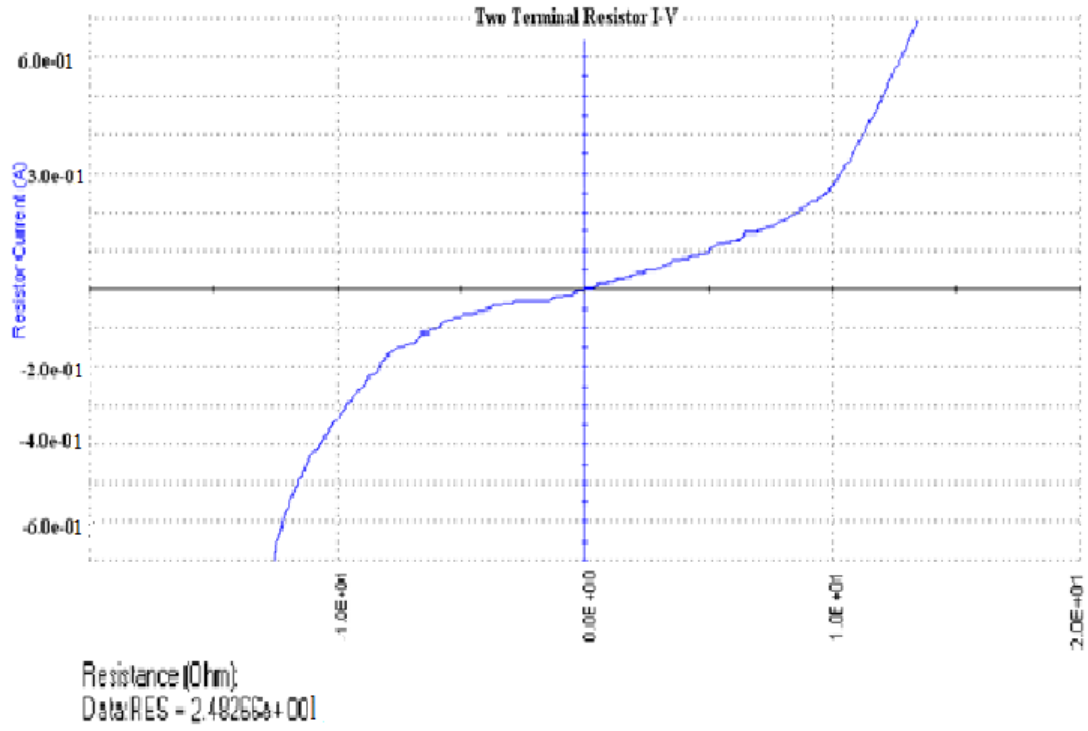

Fig 5.20: I-V Characteristic of the thin film of PANI/Ag nano composite

I-V characteristic curve for PANI displayed ohmic behavior. The PANI/Ag nano composite curve displayed a diode like behavior. From the resistance value we can easily calculate the conductivity of the thin films. The conductivities of both the samples are given in the table 5.3.

Table 5.3: Conductivities of PANI and PANI/Ag nanocomposite

Sample name	Length of the thin film(cm)	Cross sectional area(cm^2)	σ (S/cm)
PANI	1.2	1.107	$6.8x10^{-3}$
PANI/Ag nanocomposite	1.2	1.107	$3.1x10^{-2}$

The conductivity of PANI/Ag nanocomposite is four times higher than PANI polymer. It can be explained on the basis of change of ordering of the sample and silver is very good conductor. The enhancement of the conductivity in the composite is possible due to metallic nanoparticles in the polymer. It has been also reported in the literature (49). From the I-V characteristics, it is clear that the current is not flowing uniformly through the thin film. In real systems, there are trapped charges near the nanoparticles which would lead to a random offset charge disorder. In the presence of such disorder, current does not flow uniformly through the nanoparticles film. In fact it is possible that there may be a few energetically favorable paths that carry most of the current (50).

5.8 CONCLUSION:

PANI has been successfully synthesized in presence of hydrogen peroxide as oxidant and ferrous chloride as a catalyst which has helped to increase the conductance though yield is somewhat low. The synthesis was also carried with Cl^-, SO_4^{2-} ion dopants.

Gold nanoparticles in different amounts were incorporated into PANI polymer matrix which was confirmed from the thermal study. It also shows that composite is more stable than PANI. TEM analysis also confirms the presence of AuNPs of regular sizes and randomly distributed in the polymer.

While synthesizing silver nanoparticles in presence of HCl, silver chloride nanoparticles (AgCl NPs) were generated and got incorporated into PANI polymer chains, which have technological importance. The presence was

confirmed from XRD patterns and thermal stability. The conductance level decreases with the increase of AgCl concerntration.

In presence of PTSA solution, silver nanoparticles were formed and got embedded into the polymer matrix as confirmed from TEM studies. The PANI/Ag nanocomposite material synthesized showed better conductance and higher thermal stability than the polymer PANI.

REFERENCES:

1. S.P.Armes and J.F.Miller, Synth.Metals 22,385,1988
2. G.E.Asturias, A.G.MacDiarmid, A.J.Epstein, Synth.Metals 29,E157,1989
3. Y.Cao, A.Andreatta, A.J.Heeger, P.Smith, Polymer 30,2305,1989
4. Z.Sun, Y.Geng, Ji.Li, X.Wang, X.Jing, F.Wang, J.App.Polym.Sci. 72,1077-1084,1999
5. K.Mallick, M.J.Witcomb, M.S.Scurrell, J.Mater.Sci. 41,6189-6192,2006
6. J.A.Smith, M.Josowicz, J.Janata, J.Electrochem.Soc. 150E,384-388,2003.
7. A. Saheb, J.A.Smith, M.Josowicz, J.Janata, D.R.Baer, M.H.Engelhard, J.Electroanal.Chem. 621,238-244,2008
8. E.Granot, E.Katz, B.Basnar, I.Wliiner, Chem.Mater. 17,4600-4609,2005
9. T.K.Sarma, D.Chowdhary, A.Paul, A.Chattopadhyay, Chem.Commun. 1048-1049
10. J.M.Kinyanjui, D.W.Hatchett, J.A.Smith, M.Josowicz, Chem.Mater. 16,3390-3398,2004
11. Y.B.Moon, Y.Cao, P.Smith, A.J.Heeger, Polym.Commun. 30,196-199,1989
12. M.Tsuji, K.Matsumoto, N.Miyamae, T.Tsuji, X.Zhang, Cryst.Growth Des. 7,311-320,2007
13. Y.Borodko, S.M.Humphrey, T.D.Tilley, H.Frei, G.A.Somoraji, J.Phys.Chem.C 111,6288-6295,2007
14. S.Xuan, Y.Xiang, J.Wang, K.C.F.Leung, K.Shu, J.Phys.Chem. C 112,18804-18809,2008
15. K.Majid, S.Awasthi, M.L.Singla, Sensors and Actuators A 135,113-118,2007
16. T.K.Sarma, A.Chattopadhyay, J.Phys.Chem. A 108,7837-7842,2004
17. P.S.Khiew, N.M.Huang, S.Radiman, M.S.Ahmad, Mater.Lett. 58,516-521, 2004
18. Y.Sun, A.G.MacDiarmid, A.J.Epstein, J.Chem.Soc.Chem.Commun. 529-531, 1990
19. M.C.Gupta and S.S.Umare, Macromolecules 25,138-142,1992
20. P.S.Rao, D.N.Sathyanarayana, S.Palaniappan, Macromolecules 35,4988-4996,2002

21. Y.Cao, P.Smith, C.Yang, Synth.Met. 69,191-192,1995
22. P.V.Kamat, J.Phys.Chem. B 106,7729-7744,2002
23. P.Sawant, E.Kovalev, J.T.Klug, S.Efrima, Langmuir 17,2913-2917,2001
24. M.M.Oliveira, E.G.Castro, C.D.Canestraro, D.Zanchet, D.Ugarte, L.S.Roman, A.J.G.Zarbin, J.Phys.Chem. B 110,17063-17069,2006
25. K. Matsubara, T.Tatsuma, Adv.Mater. 19, 2802,2007
26. H. Yin, J. Yang, Macromol. Mater. Eng. 297, 203,2012
27. J. Bai, Y. Li, L. Sun, C. Zhang, Q. Yang, Bull. Mater. Sci. 32,161,2009
28. Y. Borodko, S.M. Humphrey, T.D. Tilley, H. Frei, G.A. Somoraji, J.Phys. Chem. C 111, 6288-6295,2007
29. X.Feng, Y. Liu, C. Lu, W. Hou, J. Zhu, Nanotechnology 17, 3578,2006
30. E. Marie, R. Rothe, M. Antonietti, K. Landfester, Macromolecules 36, 3967, 2003
31. R.C. Wang, Z. Wang, M. Li, H. Li, Chem. Phys. Lett. 341, 431,2001
32. A. Drury, S. Chaure, M. Kroll, V. Nicolosi, N. Chaure, W.J. Blau, Chem. Mater. 19, 4252,2007
33. M. Wan, J. Li, J. Polym. Sci. A Polym. Chem. 38, 2359,2000
34. G.C. Li, Z.K. Zhang, Macromolecules 37, 2683,2004
35. E.T. Kang, K.G. Neoh, K.L. Tan, Prog. Polym. Sci. 23, 277,1998
36. Y. Wei, G.W. Jang, K.F. Hsueh, E.M. Scherr, A.G. MacDiarmid, A.J. Epstein, Polym. Mater. Sci. Eng. 61, 916,1989
37. S.A. Chen, H.T. Lee, Macromolecules 26, 1569,1993
38. M. Kumar, A. Phatak, M. Singh, M.L. Singla, Thin Solid Films 519,1445,2010
39. M.L.Singla, S.Awasthi, A.Srivastava, D.V.S.Jain, Sens. & Actuators A 136, 604,2007
40. C. Chen-Ho, J. Appl. Polym. Sci. 89, 2142,2003
41. R.J.Tseng, J.Huang, J.Ouyang, R.B.Kaner, Y.Yang, Nano Lett. 5,1077-1080,2005
42. W.Li, Q.X.Jia, H.Wang, Polymer 47,23,2006
43. M.M.Oliveira, D.Zanchet, D.Ugarte, A.J.G.Zarbin, Prog.Colloid.Poly.Sci. 128,126,2004
44. A.Drury, S.Chaure, M.Kroll, V.Nicolosi, N.Chaure, W.J.Blau, Chem. Mater. 19,4252,2007

45. R.A.Barros, W.M.Azevedo, F.M.Aguiar, Mater.Charact. 50,131,2003
46. S.Ivanov and Tsakova, Electrochim. Acta 28(50),5616,2005
47. J.Laska, J.Widlarz, Polymer 46,1485,2005
48. X.R.Zeng, T.M.Ko, Polymer Physics 35,1993,1997
49. Z.Peng, L.Guo, Z.Zhang, B.Tesche, T.Wilke, S.Hu, Langmuir 22,10915,2006
50. C.Reichhardt and C.J.Olson Reichhardt, Phys.Rev.Lett. 90,46802,2002

SYNTHESIS AND CHARACTERIZATION OF POLYETHYLANILINE

This chapter of thesis comprises of synthesis and characterisation of polyethylaniline (PEANI) polymer. In this study, ethylaniline monomer has been oxidised in presence of a suitable oxidant for polymerisation and doped with various anions to alter physical and chemical properties. The process which was followed after experimental trials is discussed below:

6.1 Synthesis of PEANI - In this synthesis, ethylaniline monomer has been dissolved in certain amount of organic solvent (methanol / ethanol) as this monomer is not directly soluble in water. In a typical experiment, monomer solution (1mL of ethylaniline dissolved in 10mL of ethanol) was mixed to ice cooled solution of 40mL of 2 M HCl (dopant acid). Here we have used APS for the oxidation of monomer as the polymer yield with hydrogen peroxide was not upto level. 2g of APS (dissolved in 10 mL of 2M HCl) was cooled and added dropwise to above solution. After continuous stirring, green coloration was formed which turns into green precipitates with time. The reaction mixture was kept as such for overnight for complete precipitation. The green colored residue was separated after filtration using suction pump, followed with washing with DI water and ethanol. The green colored residue was vacuum dried at about 60°C and named as PEANI A. The yield of polymer was found to be 80 %, showing that the polymerisation process has been almost complete.

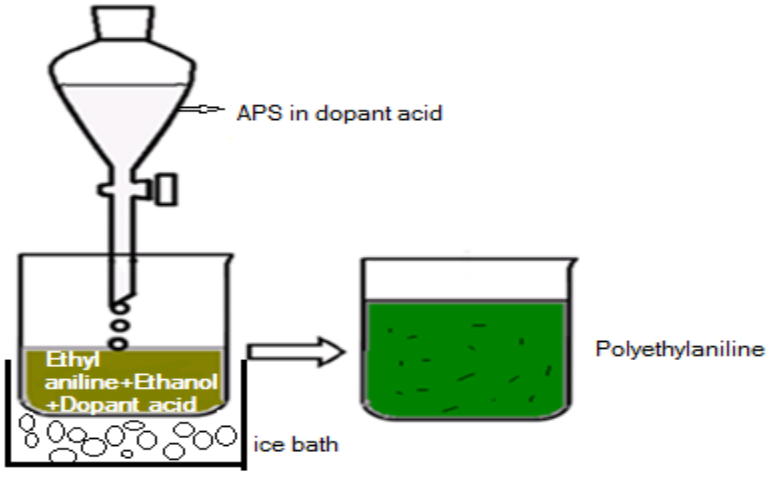

Similarly three more sets of experiments were conducted with different dopant acids (p-toluene sulphonic acid, sulphuric acid & o-phosphoric acid) and polymers so obtained were named as PEANI B, C & D respectively as shown in table 6.1.

Table 6.1 Polymers synthesised using different dopant acids

Dopant Acid used	Name of polymer formed
• hydrochloric acid (HCl)	PEANI A
• p-toluene sulphonic acid (PTSA)	PEANI B
• sulphuric acid (SA)	PEANI C
• o-phosphoric acid (PA)	PEANI D

6.2 RESULTS AND DISCUSSION

6.2.1 Characterisation of Polyethylaniline with different dopant acids:

Structural Study (X-Ray Diffraction Analysis): All the four synthesised PEANI polymers (A, B, C&D) were selected for XRD analysis and their individual X-ray diffractograms are shown in Fig 6.1.

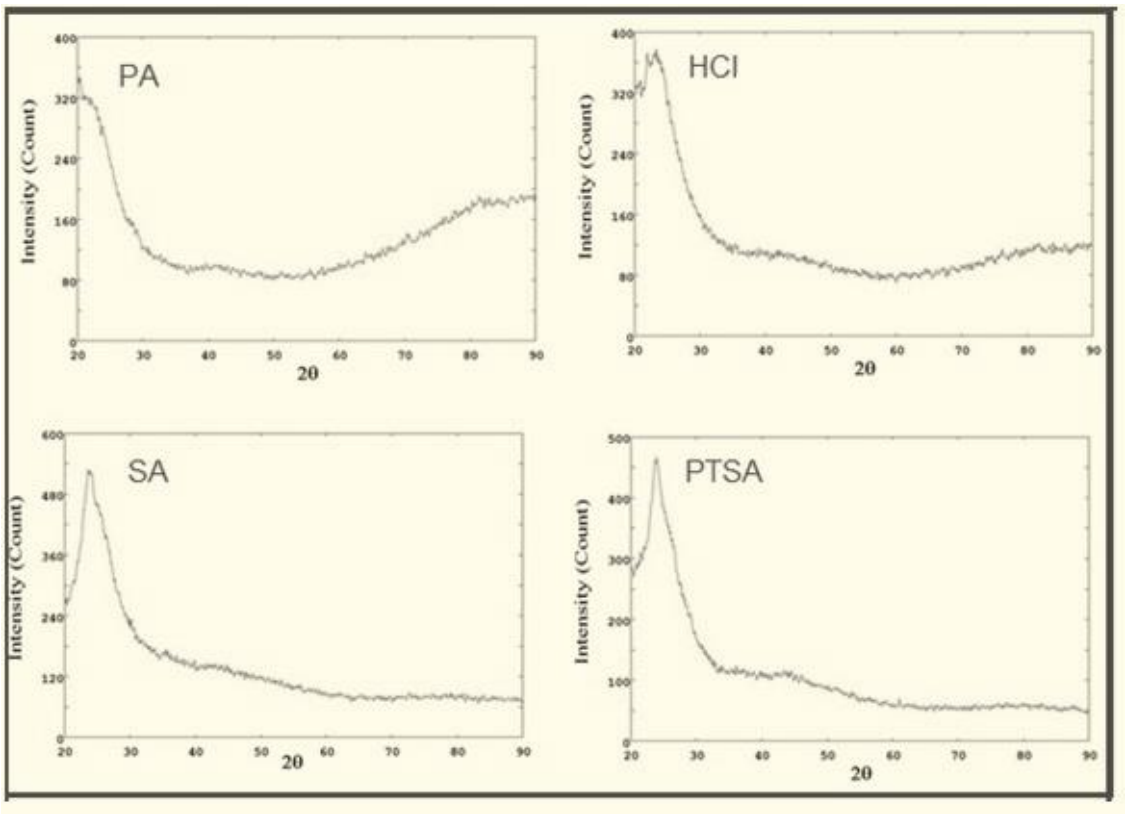

Fig 6.1: Individual XRD patterns of PEANI with different dopant acids

The analysis of XRD pattern from these figures is given in Table 6.2.

Table 6.2 Description of XRD broad band patterns of PEANI A, B ,C & D

Polymer	2Θ peak angle	d (A°)	Height	Area	FWHM
PEANI A	23.315	3.81225	378.2	4536.6	0.2040
PEANI B	23.884	3.72273	466.7	5133.5	0.1870
PEANI C	23.623	3.76324	528.2	6852.5	0.2210
PEANI D	20.412	4.34744	347.0	5200.4	0.2550

In case of polymer A (doped with HCl), intense broad band is centered at 2Θ~ 23.315°, polymer B (PTSA doped polymer) shows an intense broad band at 2Θ ~23.884° and polymer C (doped with SA) at 2Θ~ 23.623°. 2Θ values for polymers A, B & C lie in the range of 23.3° to 23.9°, however, the PA doped polymer shows the broad band peak at 20.4°, indicating blue shift as compared with other anion dopant polymers. The reason for the same may be that o-phosphoric acid may not be completely dissociated into phosphate ions, where its mono or di-hydro ions may be present which can alter the chain configuration of polymer.

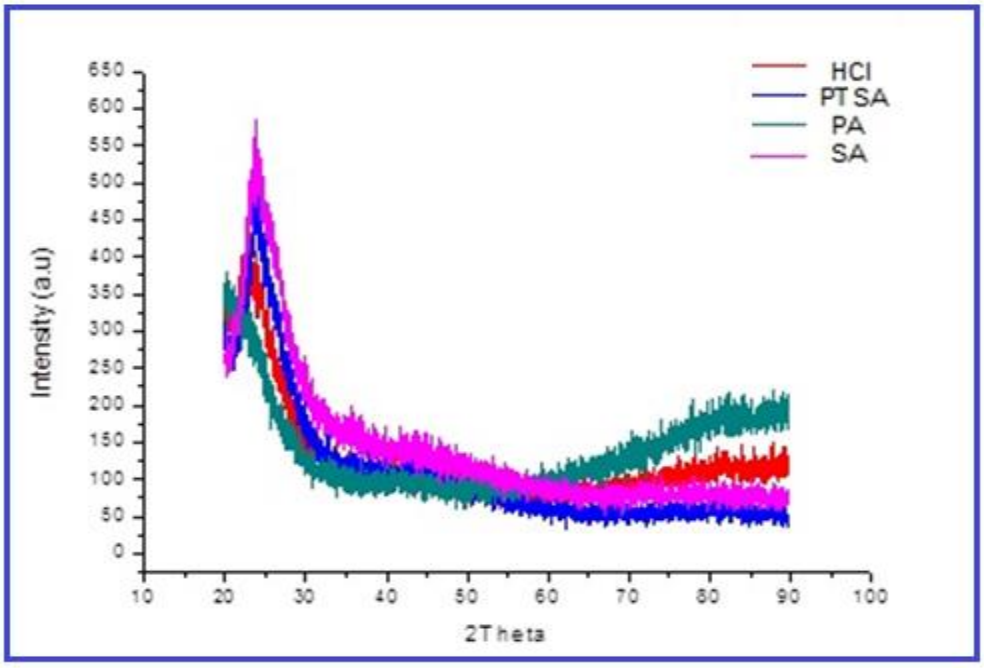

Fig 6.2: Overlay of XRD patterns of PEANI with different dopant acids.

The overlay of X-ray diffractograms of all the four PEANI polymers (A, B, C &D) is shown in figure 6.2. All these polymers show nearly similar patterns, with little variation in the intensity broad bands also showing that each of these PEANI polymers is partially crystalline. The diffraction patterns are similar to that obtained by Andreia et al (1).

FTIR Spectral Study of PEANI polymers doped with different acids:

FTIR studies were conducted using KBr powder to study the finger prints of each polymer synthesised. Figures 6.3, 6.4, 6.5 & 6.6 represent FTIR spectras of PEANI A, B, C & D respectively. The peak positions related to the corresponding chemical bonds are listed in Table 6.3.

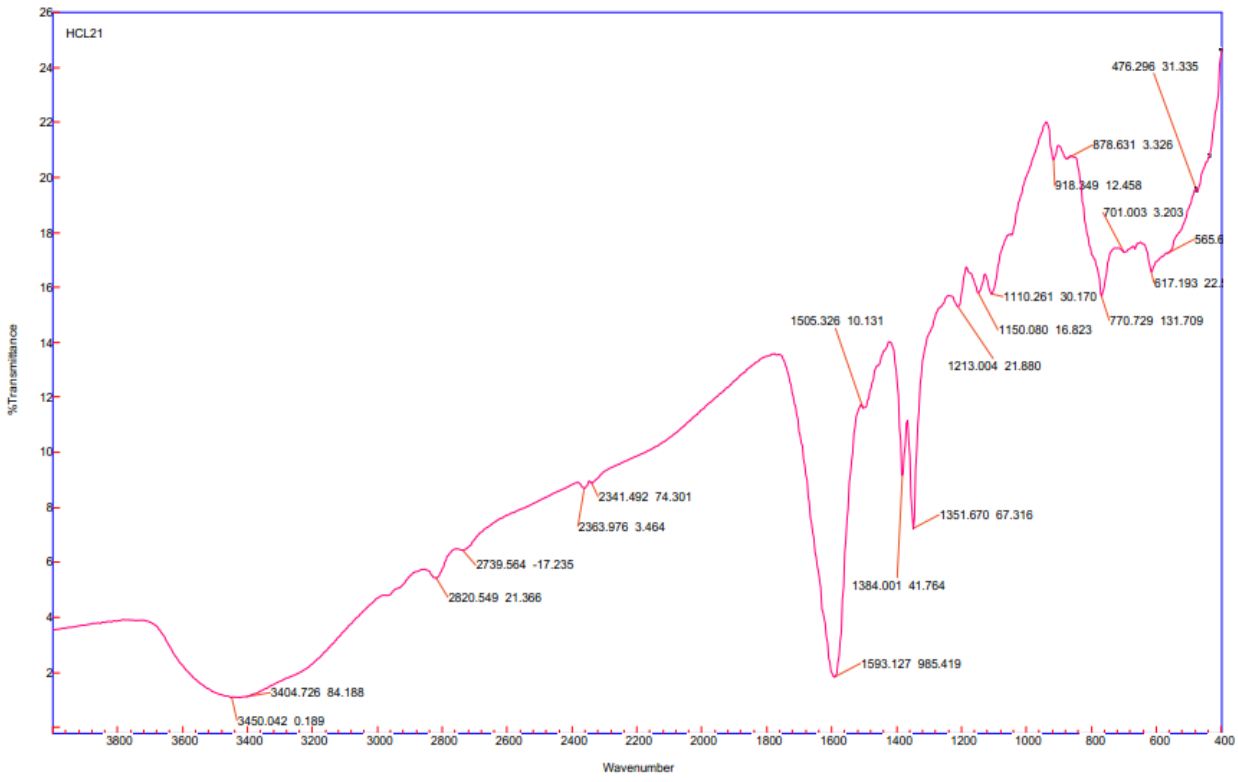

Fig 6.3: FTIR spectra of HCl doped PEANI (PEANI A)

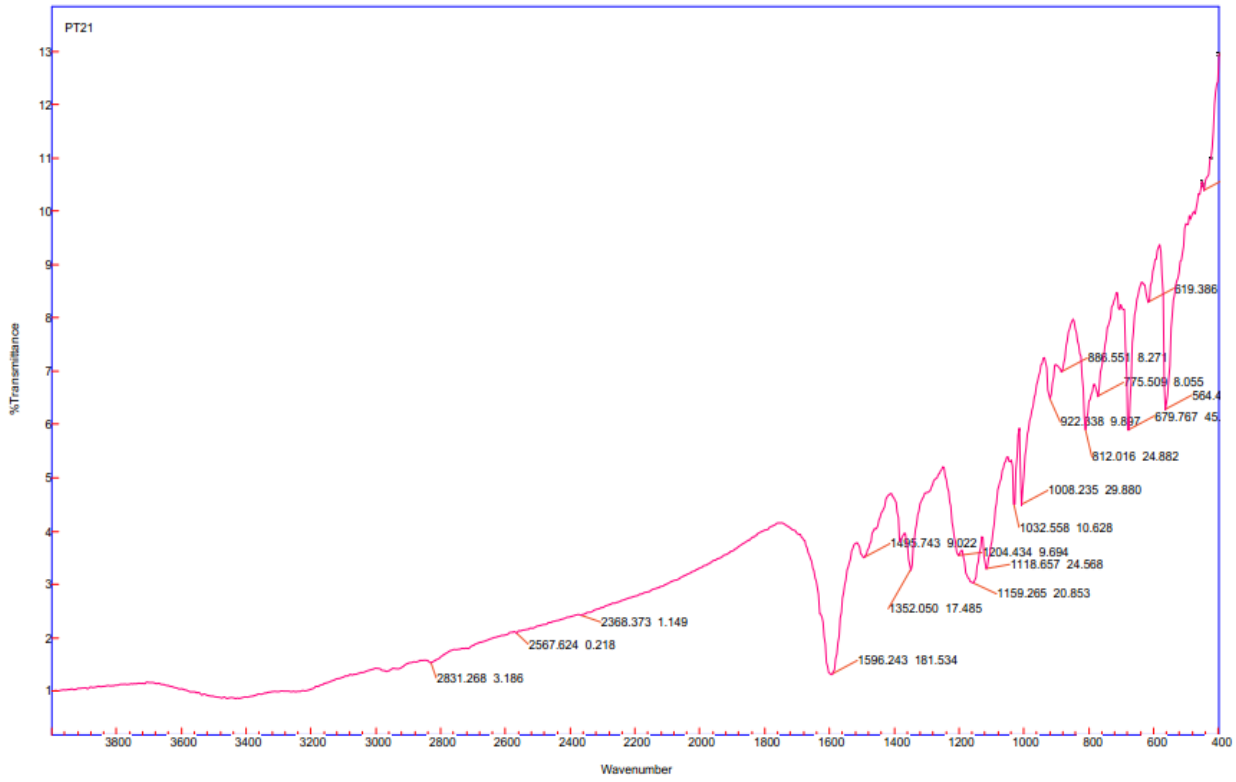

Fig 6.4: FTIR spectra of PTSA doped PEANI (PEANI B)

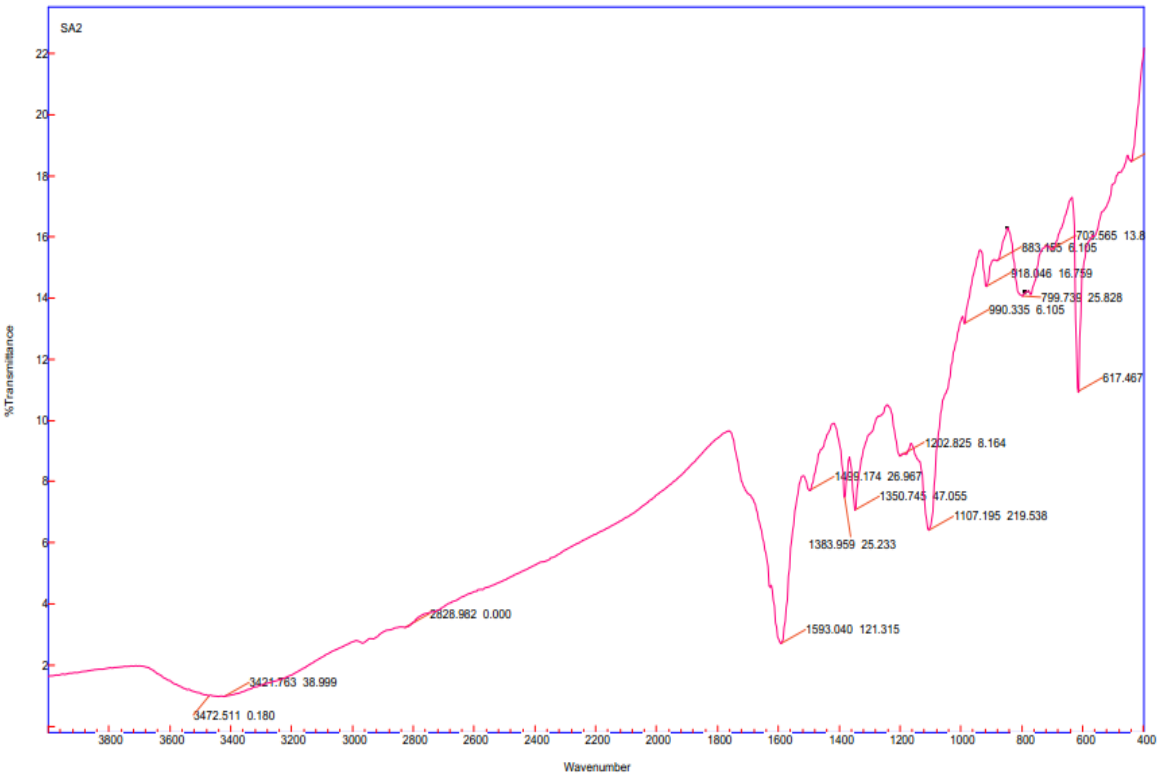

Fig 6.5: FTIR spectra of SA doped PEANI (PEANI C)

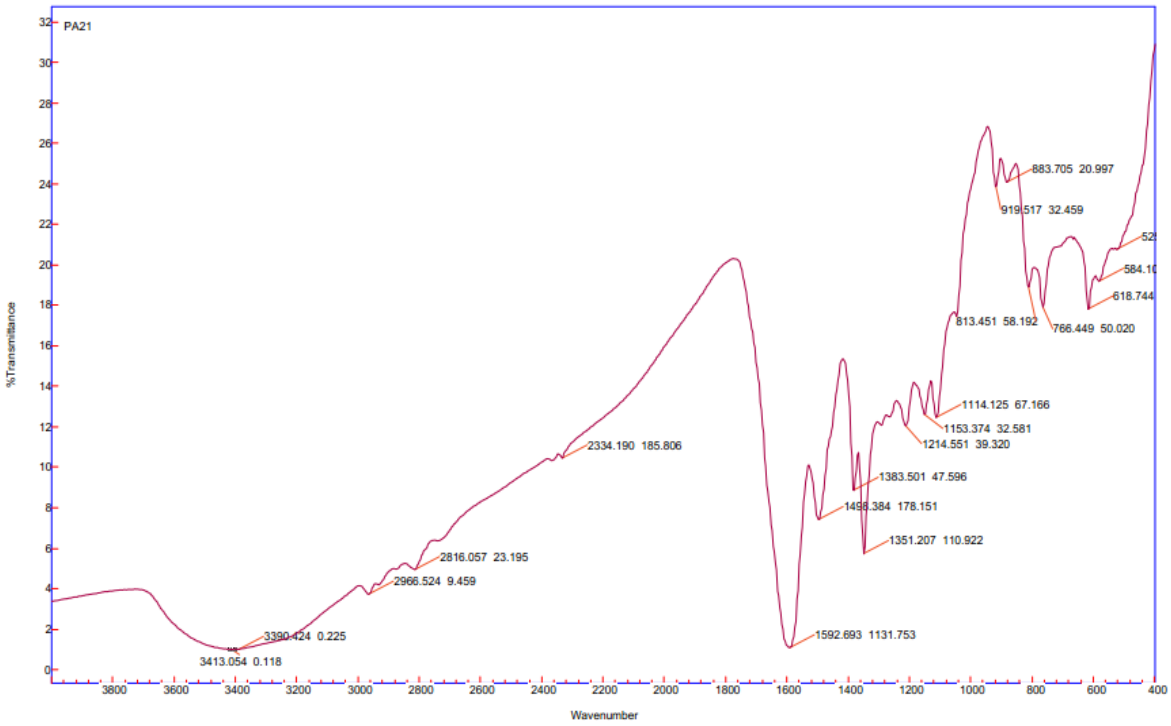

Fig 6.6: FTIR spectra of PA doped PEANI (PEANI D)

Table 6.3: FT-IR absorption bands of PEANI with different dopant acids

	PEANI A cm^{-1}	PEANI B cm^{-1}	PEANI C cm^{-1}	PEANI D cm^{-1}
Quinoid	1593	1596	1593	1593
Benzenoid	1505	1495	1499	1498
C-H in-plane bending	1110	1119	1107	1114
C-H out of plane bending	770	775	799	766
$C\text{-}N^{+}$ stretching vibration	1213	1204	1202	1214
Paradisubstituted aromatic ring	808	812	800	813
C-H stretching of ethyl group	2820	2831	2828	2816

The presence of two bands in the vicinity of 1500 and 1600cm^{-1} are due to the benzenoid and quinoid ring units which are the signatures of these polymers. Similar results have been reported for polyaniline and its derivatives earlier thus

confirming the polymerisation process (2). The higher frequency vibrations at about 1600 cm^{-1} has a major contribution from the quinoid rings (N=Q=N), while the lower frequency modes at about 1500 cm^{-1} depicts the presence of benzenoid (N-B-B) ring units. The absorption bands at 1110, 1109,1107, 1114 cm^{-1} and at 770, 775, 799, 766 in all four polymers are the characteristic to C-H in plane bending and C-H out of plane bending vibrations (3). The band characteristic of the conducting protonated form is observed near 1200 cm^{-1} in all these polymers and interpreted as a $C\text{-}N^{+}$ stretching vibrations in the polaron structure (4). The absorption bands in the region of 800-880 cm^{-1} for these acid doped PEANI polymers confirm that the monomer units were linked to para position and head to tail coupling of ethylaniline occurred during polymerization (5). Symmetric and asymmetric aliphatic C-H stretching vibrations are observed at 2831, 2820, 2828 and 2816 cm^{-1} for PTSA, HCl, SA and PA doped PEANI and are due to the substituent ethyl group present on the nitrogen atom (6). These vibrations are observed exclusively in PEANI and are absent in polyaniline. The overlay of FTIR spectras' of PEANI using different dopant acids is shown in Figure 6.7.

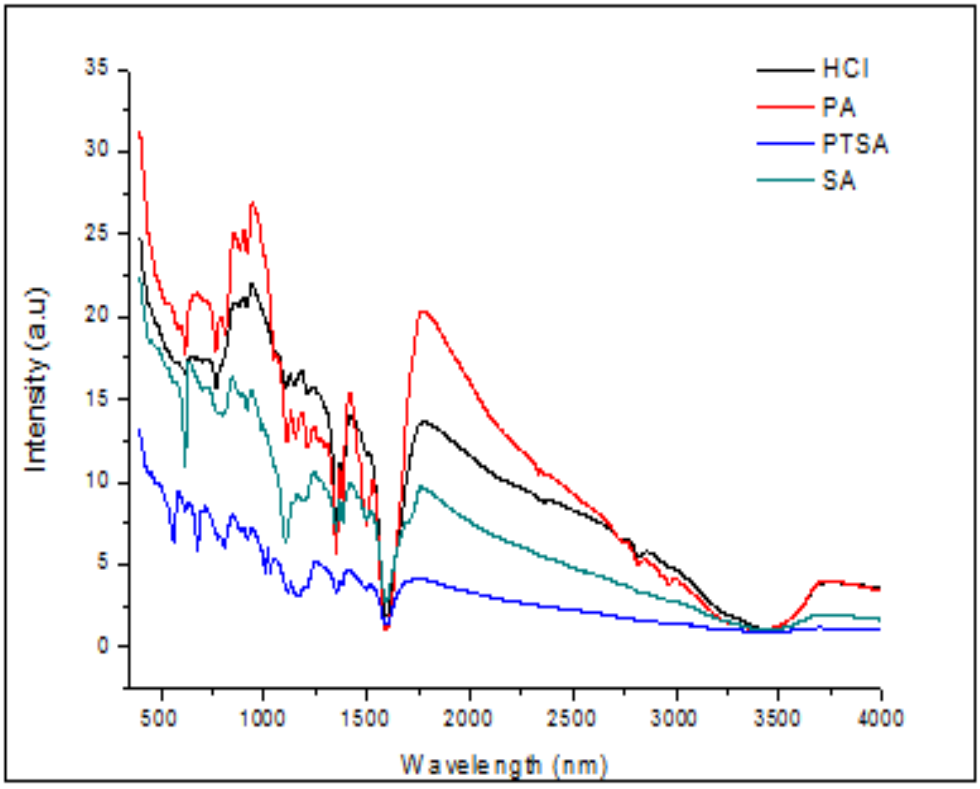

Fig 6.7: Overlay of FTIR spectras' of PEANI using different dopant acids.

From IR spectra and its analysis, it is confirmed that the structure of PEANI is almost similar to that of the polyaniline with characteristic modes of the polyaniline backbone with certain shift in the absorption peaks. The results have already been presented in Chapter 5.

Thermal study (TGA-DSC Analysis):

The thermal analysis of all the four PEANI polymers was carried out. Each polymer powdered sample was loaded in aluminium oxide crucibles for its analysis and allowed to undergo heating cycle from 25 to 800°C. Nitrogen was used as purge gas with flow rate of 10mL/min.

Thermal Study of PEANI A (doped with HCl): The TGA-DSC curves of HCl doped PEANI polymer is shown in Figure 6.8.

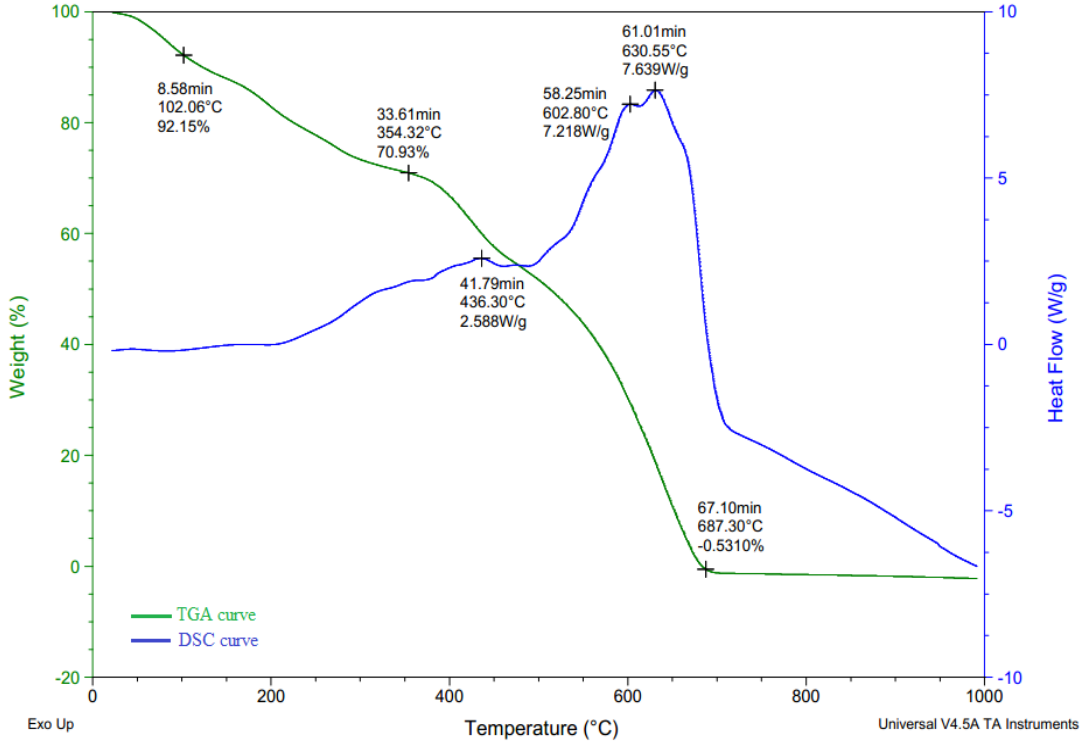

Fig 6.8: TGA/DSC thermogram of PEANI doped with HCl

It showed an initial weight loss of 7.85% up to 102.06°C which is due to the presence of moisture retained in polymer chains after vacuum drying. Second weight loss occurred in the temperature upto 354.32°C, due to the rearrangement or crosslinking of chains. On further heating, PEANI polymer gets completely decomposed into its moieties at about 687°C. It has been observed that this

decomposition temperature is about 50-80°C higher than PANI indicating that this polymer is thermally better stable than PANI (7-8). In DSC studies, we observed that the first transition occurs at 436.30°C with the heat absorption of 2.588 W/g which may be due to cross linking / breaking of small oligomers. The second and third transitions were seen around 600 to 630°C which are due to complete degradation of the polymer. The first step was not a glass transition temperature as no subsequent transition was observed when the same experiment was repeated twice in the temperature range of 25-435°C.

Thermal study of PEANI (doped with PTSA):

The TGA-DSC curves of PTSA doped PEANI is shown in Figure 6.9. The behaviour of PTSA doped PEANI appears to be more close to HCl doped polymer.

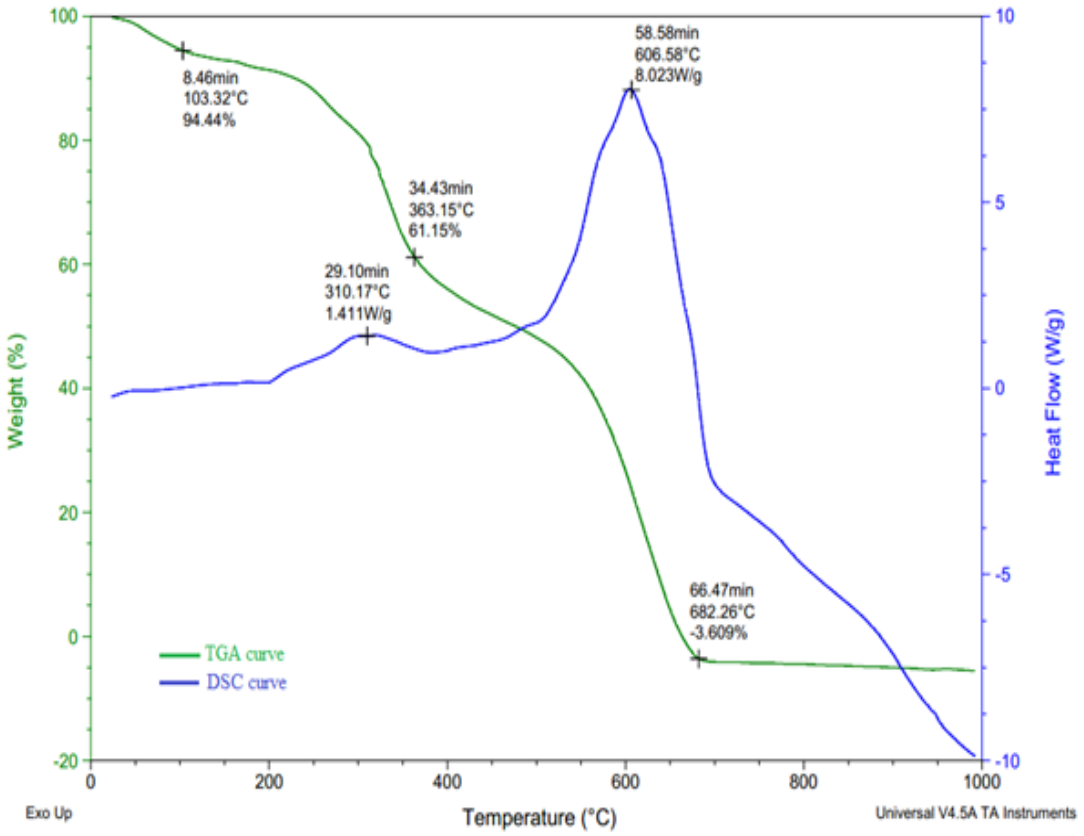

Fig 6.9: TGA/DSC thermogram of PTSA doped PEANI

First weight loss of 5.56% till 103.32°C is due to the presence of water molecules even after vaccum drying showing that material may be porous. Subsequent loss in weight upto 363.15°C may be due to bond cleavage / new bond formation and

decomposition of small oligomers retained in the polymer. The decomposition of the polymer completes at about 682°C showing further disintegration into its moieties. The negative weight loss may be due to some deadsorption occurring from the surface of aluminium oxide pan. In DSC analysis, an initial absorption peak was seen at 310.17°C, followed by transition at 606.58°C. These transitions must be related to chemical irreversible reactions such as cross-linking which involves bond cleavage followed by a new chemical bond formation (9-10).

Thermal study of PEANI (doped with sulphuric acid):

The TGA-DSC curves of SA doped PEANI is shown in Figure: 6.10.

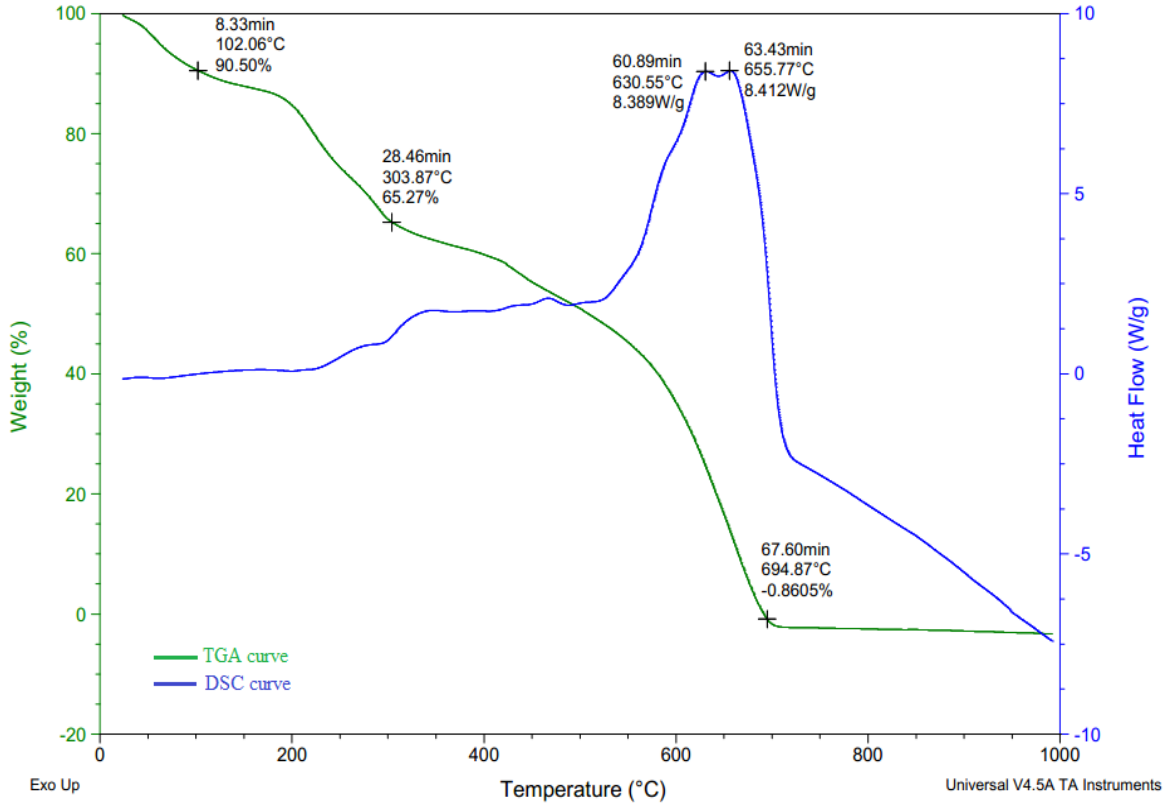

Fig 6.10: TGA/DSC thermogram of SA doped PEANI

TGA curve shows initial weight loss of 9.5% up to 102.06°C which is due to the presence of moisture in PEANI. This weight loss is higher than the Cl^- doped polymer as sulphuric acid has more affinity for water. Second weight loss (102.06-303.87°C) is due to the rearrangement or cross-linking, which involves bond cleavage or new bond formation and the decomposition of oligomers. The complete decomposition of the polymer took place at 694.87°C indicating still

more stable than Cl^- doped polymer. The DSC plots have split peaks at 630.55°C and 655.77°C with the heat absorption around 8W/g indicating certain transition at the decomposition temperature.

Thermal study of PEANI (doped with phosphoric acid):

The thermal analysis of PA doped PEANI showed three- step weight loss pattern as shown in figure 6.11.

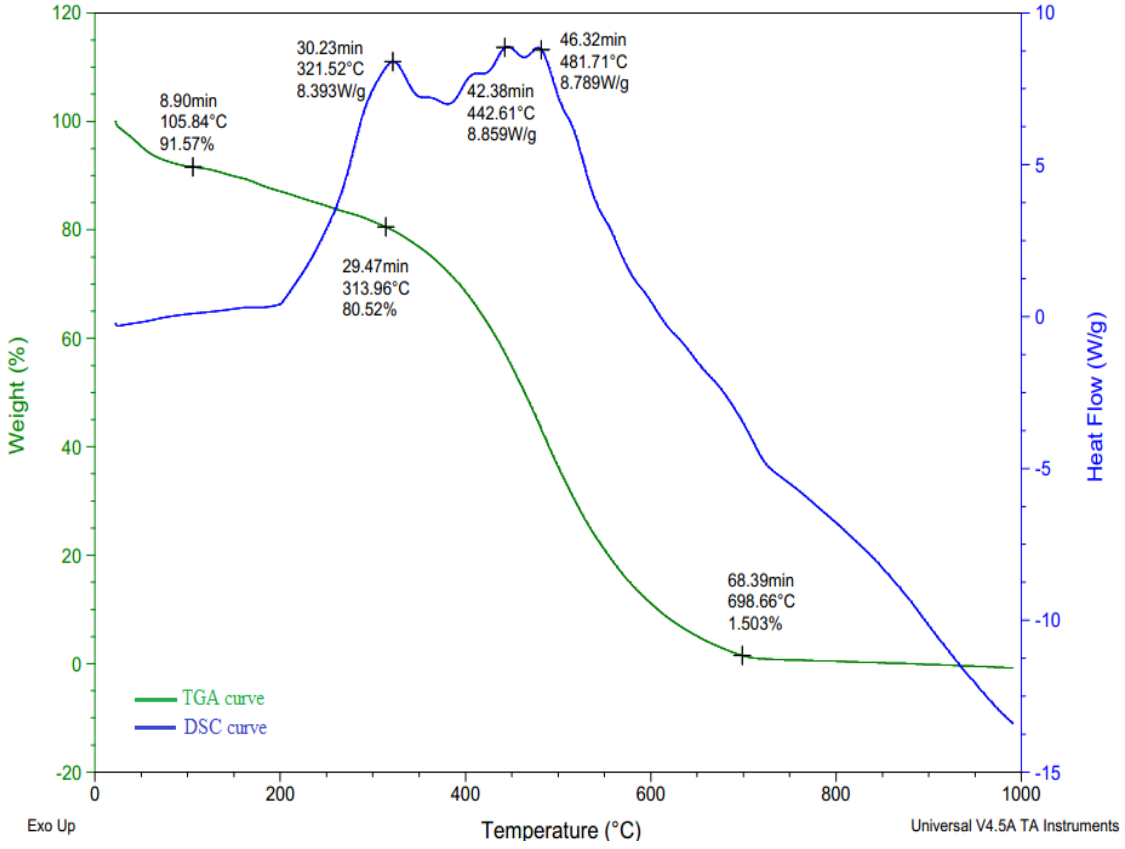

Fig 6.11: TGA/DSC thermogram of PA doped PEANI

The first weight loss which is upto 105.8°C is about 8.5% due to loss of moisture retained with polymer change due to porosity. The second weight loss due to decomposition of small oligomers occurs at 313.96°C. Further, complete disintegration of the polymer was complete at 698.66°C due to formation of its moieties which got converted to gaseous state and escaped with purged gas nitrogen. In DSC studies, first peak was seen at about 321°C whereas other twin

form peak was observed at about 440°C to 480°C which may be due to doping of anion of phosphoric acid.

From this study, it is concluded that:

1) All the polymers exhibit a three-step decomposition pattern as shown in table 6.4.

Table 6.4 TGA analysis of PEANI doped polymers

PEANI POLYMER	1st loss	2nd loss	3rd loss(complete disintegration)
PEANI A	102.06°C	354.32°C	687.30°C
PEANI B	103.32°C	363.15°C	682.26°C
PEANI C	102.06°C	303.87°C	694.87°C
PEANI D	105.84°C	313.96°C	698.66°C

2) All these polymers completely decompose at temperature more than 680°C, indicating better stability than polyaniline.

3) The amount of moisture retained in the polymers is around 6 to 8%, showing the hygroscopic nature which is due to the porous structure of the polymer chains.

4) There is possibility that small oligomers were also formed during synthesis which decomposed at about 300-400°C.

5) The DSC thermograms also confirm the absence of any glass transition and melting temperature for the polyaniline salt system.

Electrical Characterisation

The electrical conductivity of PEANI polymers (A, B, C & D) was measured using a two-point probe technique. The same amount of each polymer, approximately 0.030 g, was pressed into 0.8 cm diameter pellets. An electrical conduction phenomenon in conducting polymers depend on at least three factors contributing to the charge carriers mobility viz. single chain or intra-molecular transport, inter-

chain or between chain transport and inter particle contact. Current-voltage (I-V) scans were made from -5 to +5V for HCl, PTSA, SA, PA doped PEANI polymers and are shown in figures 6.12 to 6.15.

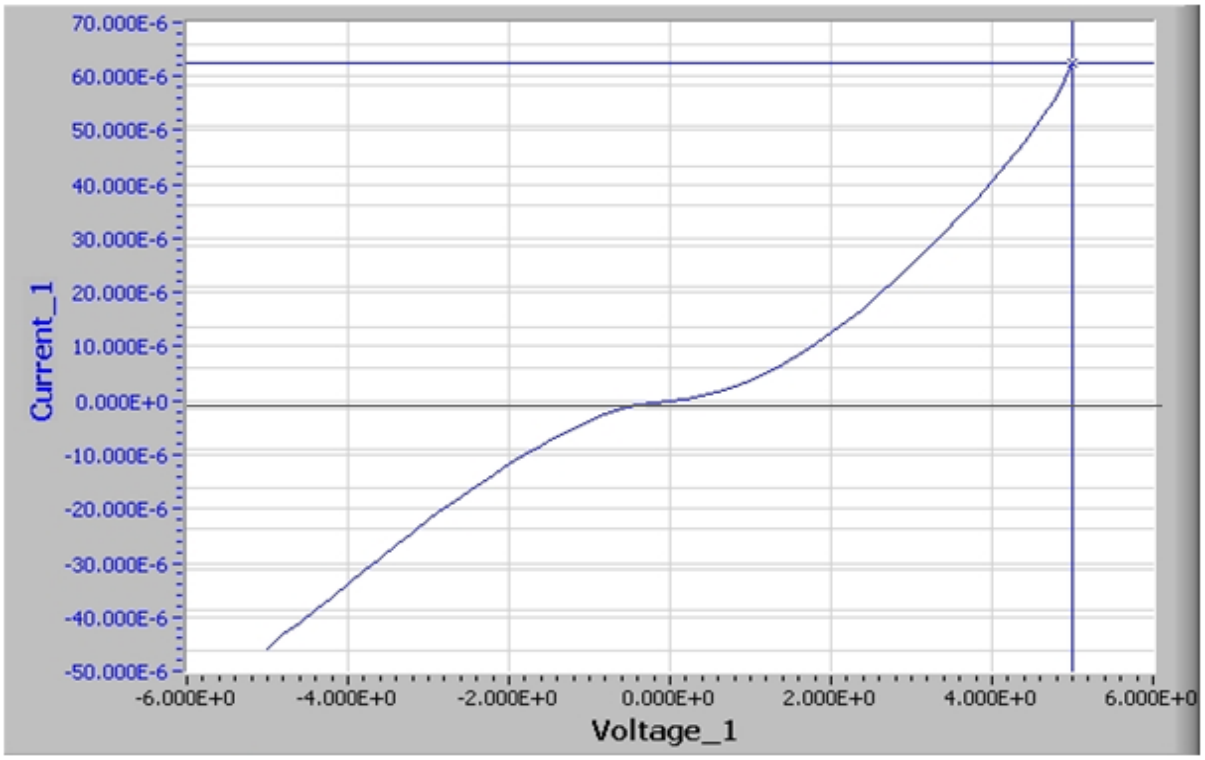

Fig 6.12: Characterstic I-V scan of HCl doped PEANI

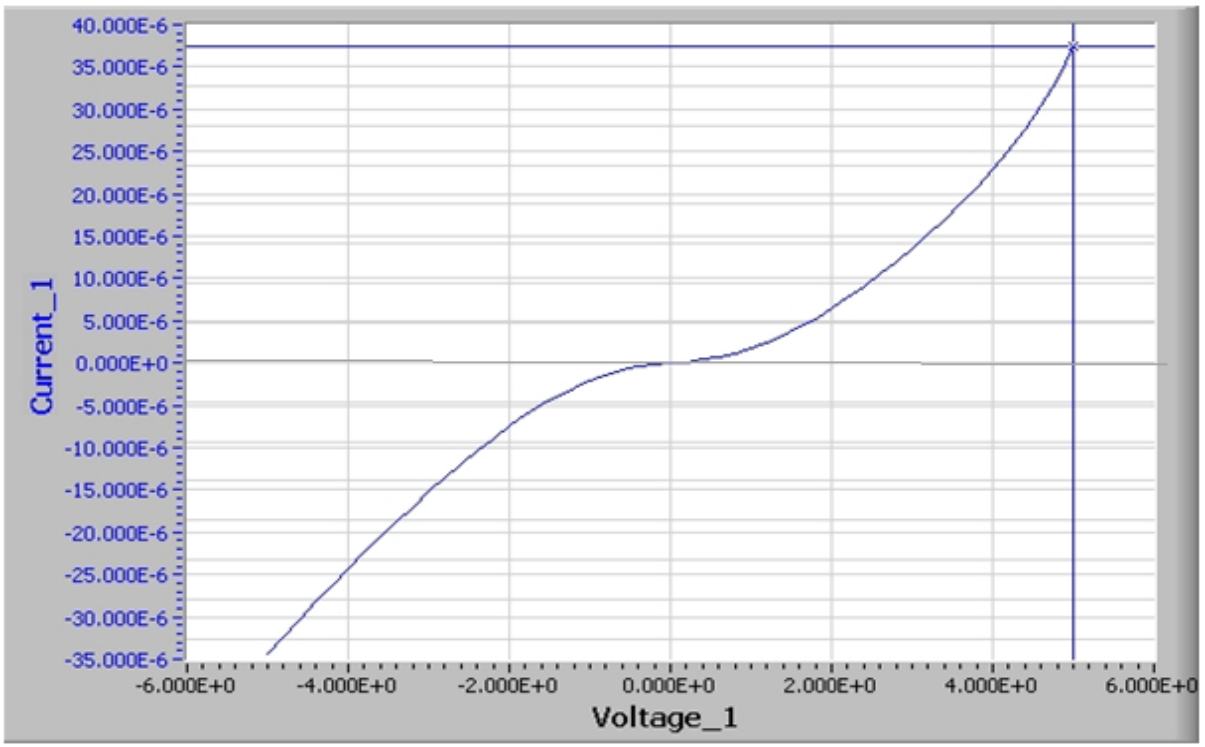

Fig 6.13: Characterstic I-V scan of PTSA doped PEANI

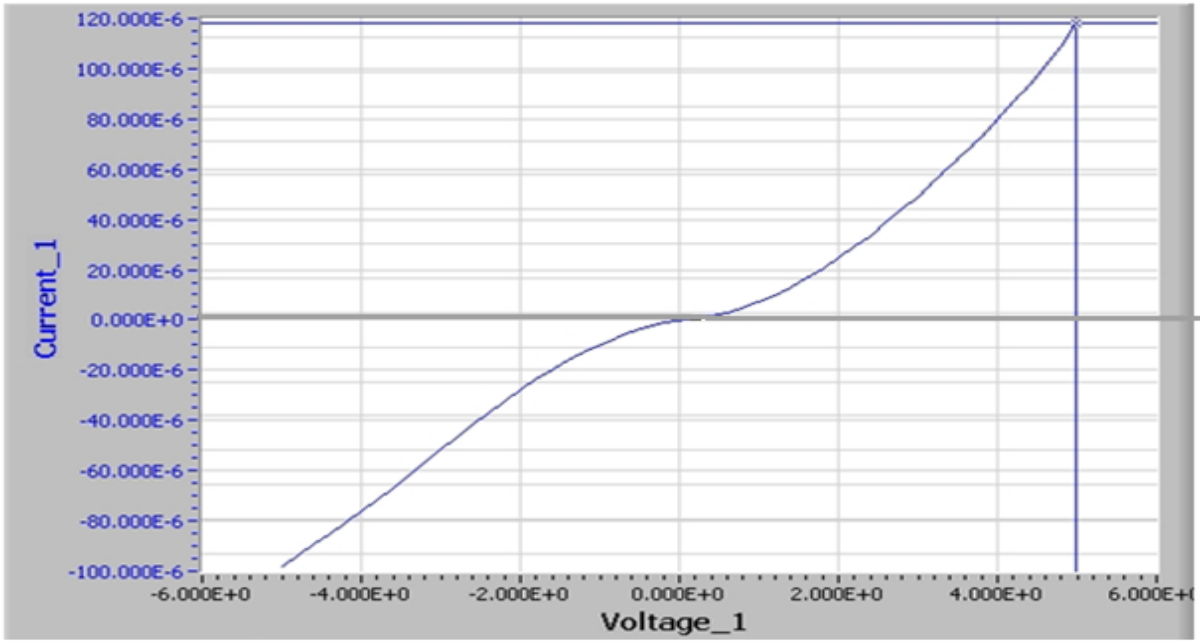

Fig 6.14: Characterstic I-V scan of SA doped PEANI

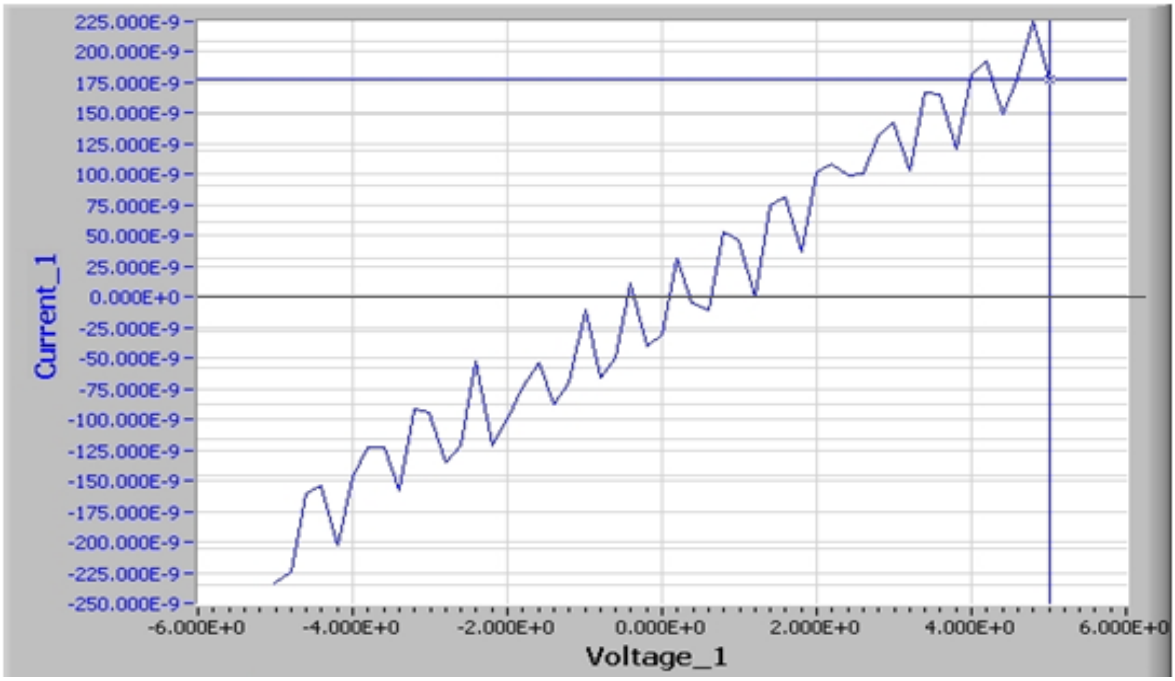

Fig 6.15: Characteristic I-V scan of PA doped PEANI

The values of measured current for HCl, PTSA, SA, PA doped PEANIs' are of the order of 62±1.5 µA, 48±1.8 µA, 118±2 µA and178±2 nA respectively. An electrical resistance or conductivity of each polymer was calculated at R.T. The conductivity σ of the polymer pellet can be given by σ = 1/ (π/ ln 2)*R*d, where (π/ln 2)*R is the pellet resistance and d the thickness of the pellet (11).

The conductivities of the prepared PEANIs' doped with HCl, PTSA, SA, PA were of the order of 13.2 μS/cm, 8.5 μS/cm, 26.2 μS/cm and 39.43 $x10^{-3}$ μS/cm respectively. The conductivities of different acids doped PEANIs' in ascending order is as following:

PA<PTSA<HCl<SA

These types of conductance data/materials may be useful for designing several sensitive devices and sensors.

6.3 CONCLUSION:

The study shows that the yield was 80 % indicating that the process of polymerisation was almost complete. The possible mechanism (12) for the growth of polymer is:

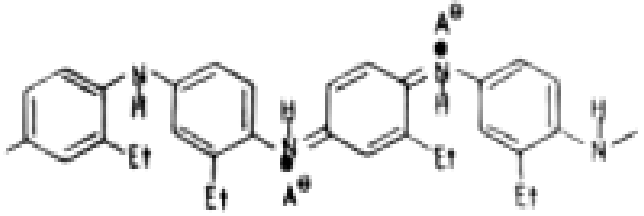

Scheme 1

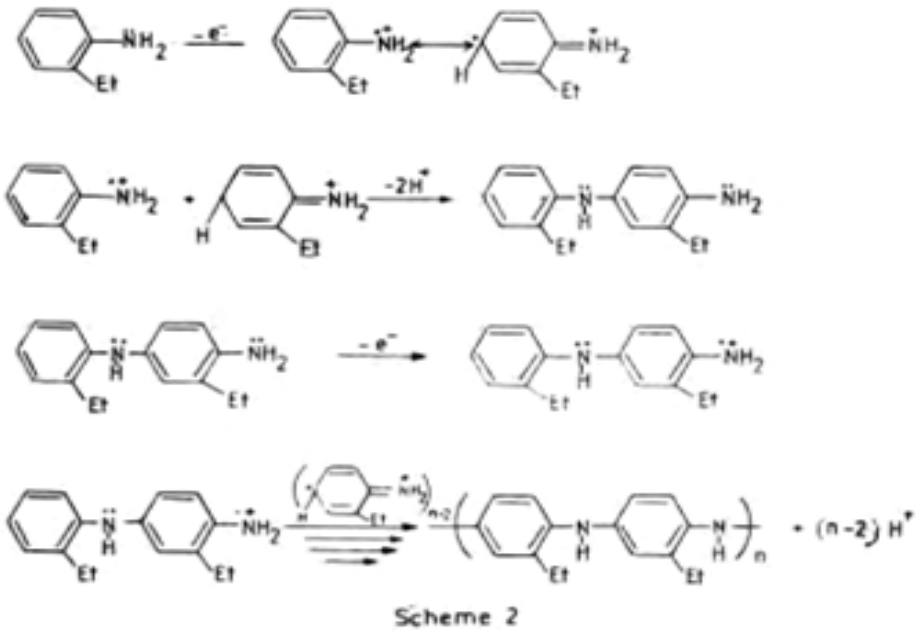

Scheme 2

Fig 6.16: Polymerisation Mechanism (adapted from reference 12)

From XRD studies, it is confirmed that the material is almost amorphous/partially crystalline with the diffraction peak obtained at about 23°.

Thermal studies show that almost same amount of moisture is retained in all the four polymers synthesised showing their hygroscopic nature due to the porous structure of the polymer chains.

FTIR studies confirm the signature of the polymer formation due to presence of bands of benzenoid and quinoid units.

There is small variation in the conductance values of all the four synthesised PEANI polymers A, B, C& D. However, these values are lower when compared with values of PANI (explained in Chapter 5). The lower conductivity relative to polyaniline may be explained by an increase of the interchain distance and diluting effect of the charge carriers caused by the presence of bulky ethyl group present on the nitrogen atom in the polymer.

SYNTHESIS AND CHARACTERIZATION OF POLYETHYLANILINE/SILVER NANOCOMPOSITES

This part of the chapter comprises of synthesis and characterisation of polyethylaniline/silver nanocomposite. PEANI/Ag nanocomposites were synthesised where PEANI was doped with PTSA, H_2SO_4 and PA. These nanomaterials have been named as E, F & G where these symbols represent different samples as under:

Sample E = PEANI with PTSA/Ag nanocomposite

Sample F = PEANI with SA/Ag nanocomposite

Sample G = PEANI with PA/Ag nanocomposite

The similar procedure was adopted for the synthesis of these nanocomposites however; explanation is presented for sample E which is explained below:

6.4 Synthesis of PEANI/Ag Nanocomposites using PTSA:

In a typical procedure,1mL of ethylaniline was dissolved in 5mL of ethanol in which 50mL of 1M PTSA acid solution was added and kept on ice bath to maintain the temperature between 0-5°C. Then, 5mL of 0.2M silver nitrate solution (containing 0.2g PVP) was added with continuous stirring. For polymerisation to occur, 2g of ammonium peroxydisulphate as an oxidant was dissolved in 10mL of water, ice cooled and mixed into above solution with constant stirring, followed with addition of 2mL sodium borohydride solution which acts as reducing agent for silver ions. The reaction mixture was stirred continuously and allowed to stand on ice bath till green coloration starts appearing. The reaction mixture was allowed to stand as such for complete precipitation. The green coloured residue formed was separated through centrifugation, washed with DI water till free from impurities and finally with ethanol. The residue was dried in vacuum oven at 60°C and stored for further studies.

6.5 Results and Discussion

Structural study (X-Ray Diffraction Analysis)

The X-ray diffractograms of powdered samples of PEANI/Ag nanocomposites using different dopant acids i.e. p-toluene sulphonic acid (PTSA), phosphoric acid (PA) and sulphuric acid (SA) are shown in figure 6.17

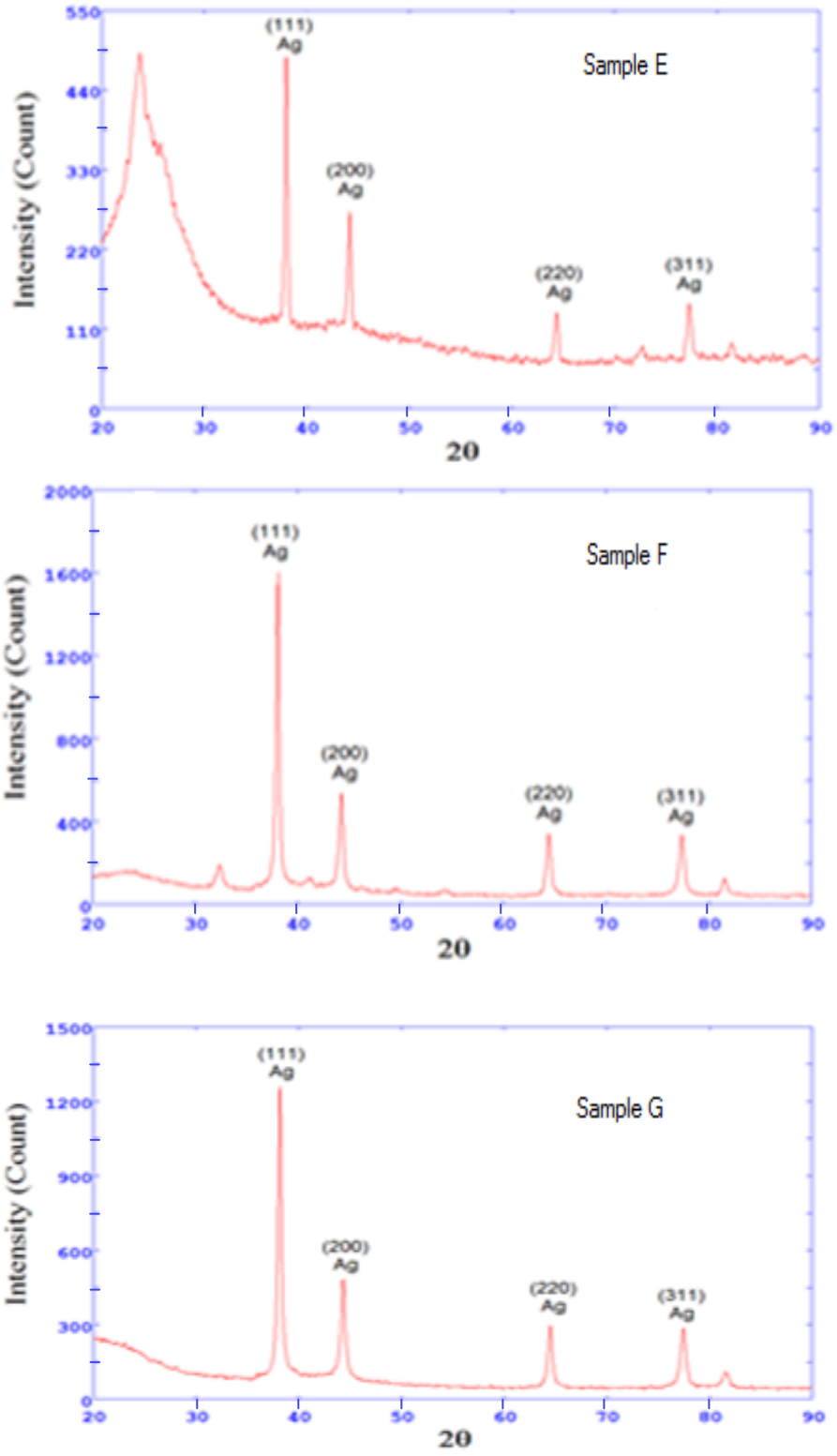

Fig 6.17: Individual XRD patterns of PEANI/Ag nanocomposites with different dopant acids.

The analysis of XRD patterns of PEANI/Ag nanocomposites with three dopant acids is summarised in Table 6.5

Table 6.5 Description of XRD peaks of PEANI/Ag nanocomposites using different dopant acids.

Name of Nanocomposite	2Θ(°)	d (A°)	Height	Area	FWHM	Bragg's reflection	Particle Size
Sample E	37.991	2.36653	494.7	7914.0	0.2720	111	30.88
	44.190	2.04790	273.2	5182.9	0.3230	200	
	64.362	1.44632	132.5	2650.9	0.3400	220	
	77.275	1.23369	144.0	3740.6	0.4420	311	
Sample F	38.070	2.36180	1612.8	28736.4	0.3060	111	27.46
	44.399	1.44558	340.3	7436.6	0.3740	200	
	64.366	1.23245	333.5	6670.4	0.3400	220	
	77.493	1.18014	124.7	2115.5	0.2890	311	
Sample G	38.161	2.35640	1260.1	21415.7	0.2890	111	29.08
	44.331	2.04170	482.7	8686.1	0.3060	200	
	64.486	1.44382	299.6	5987.7	0.3400	220	
	77.734	1.31471	1381.5	1329.0	0.1190	311	

The XRD patterns (figure 6.17) and its analysis (table 6.5) confirms the incorporation of silver nanoparticles in the composite and is well in agreement

with the literature values of AgNPs (JCPDS-04-0783). All the three PEANI/Ag nanocomposites showed diffraction peaks at 2Θ values of about 38°, 44°,64° and 77° whereas no such peaks were seen in individual XRD patterns (figures 6.1). These new peaks correspond to Bragg's reflections from (111,200,220,311) planes of Ag showing its presence in nanocomposites. All the peaks can be indexed to fcc metallic Ag and Scherrer equation resulted in an average particle size of 30nm.

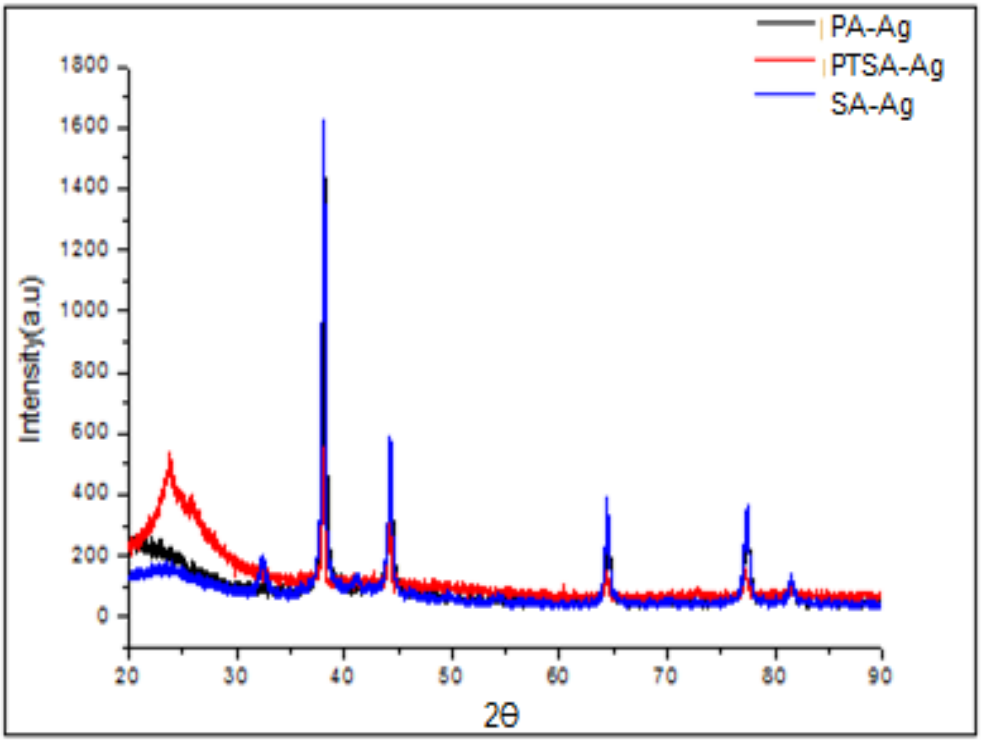

Fig 6.18: Overlay of XRD patterns of PEANI/Ag nanocomposites with different dopant acids.

The overlay of X-ray diffractograms of PEANI/Ag nanocomposites with different dopant acids show nearly similar pattern, with some variations in the intensity broad bands. This study confirms the incorporation of AgNPs in the polymer matrix resulting in the formation of composites having different dopants.

IR Spectral study of PEANI/Ag nanocomposites:

The FTIR analysis was performed in the 4000 to 400 cm^{-1} range for the following nanocomposites:

1) PTSA doped PEANI/Ag nanocomposite-Sample E
2) SA doped PEANI/Ag nanocomposite-Sample F
3) PA doped PEANI/Ag nanocomposite-Sample G

Figures 6.19 to 6.21 represent FTIR spectras of these nanocomposites and corresponding characteristic peaks are shown in the Table 6.6

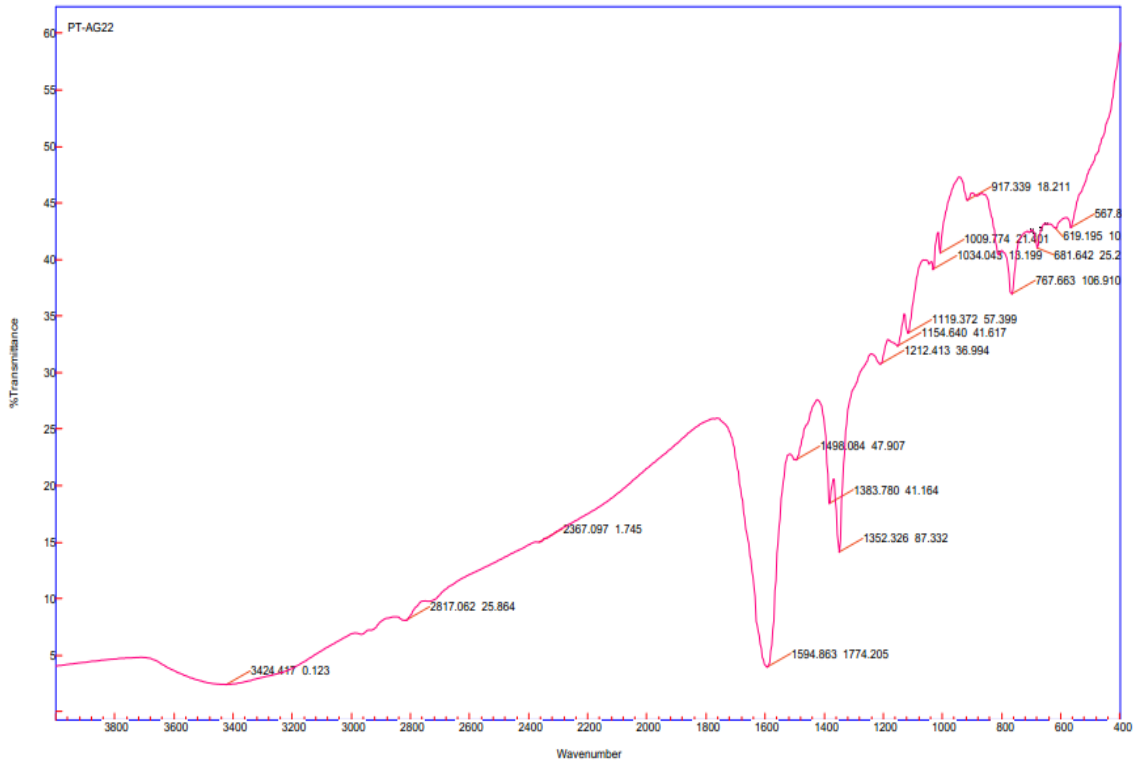

Fig 6.19: FTIR spectra of PTSA doped PEANI/Ag nanocomposite (Sample E)

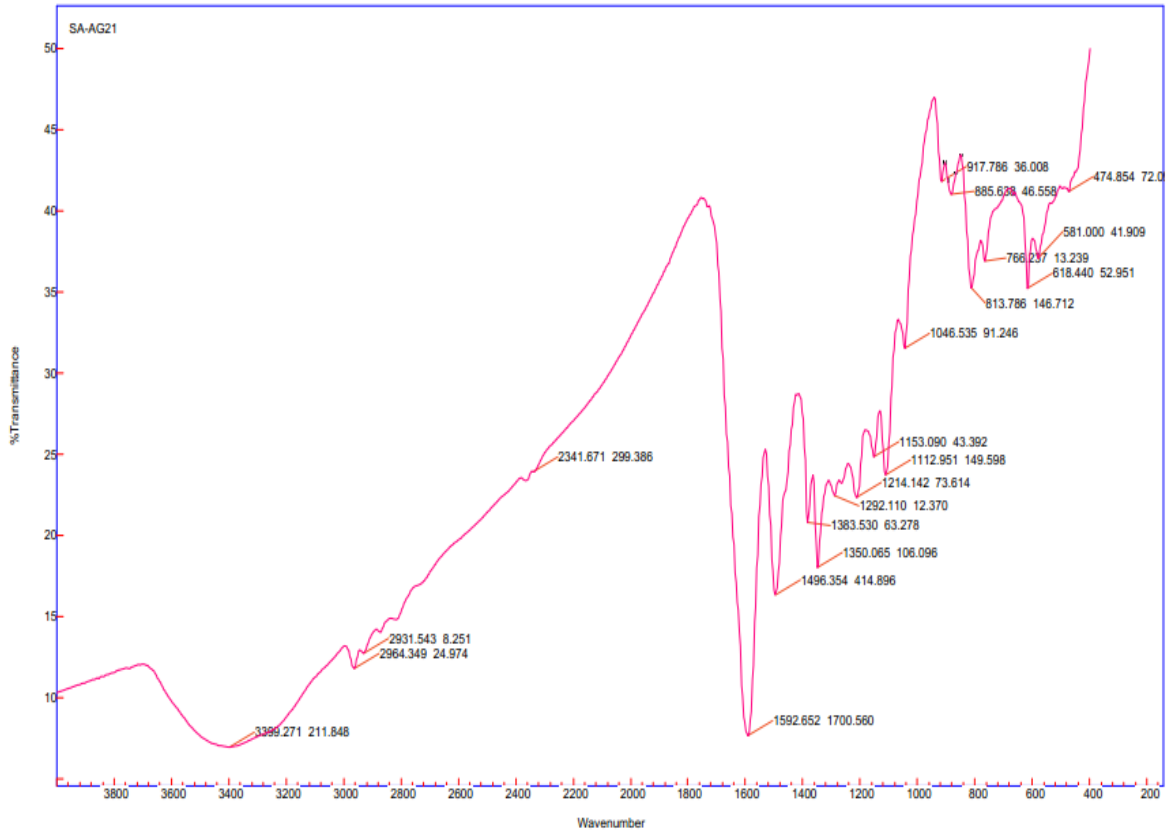

Fig 6.20: FTIR spectra of SA doped PEANI/Ag nanocomposite (Sample F)

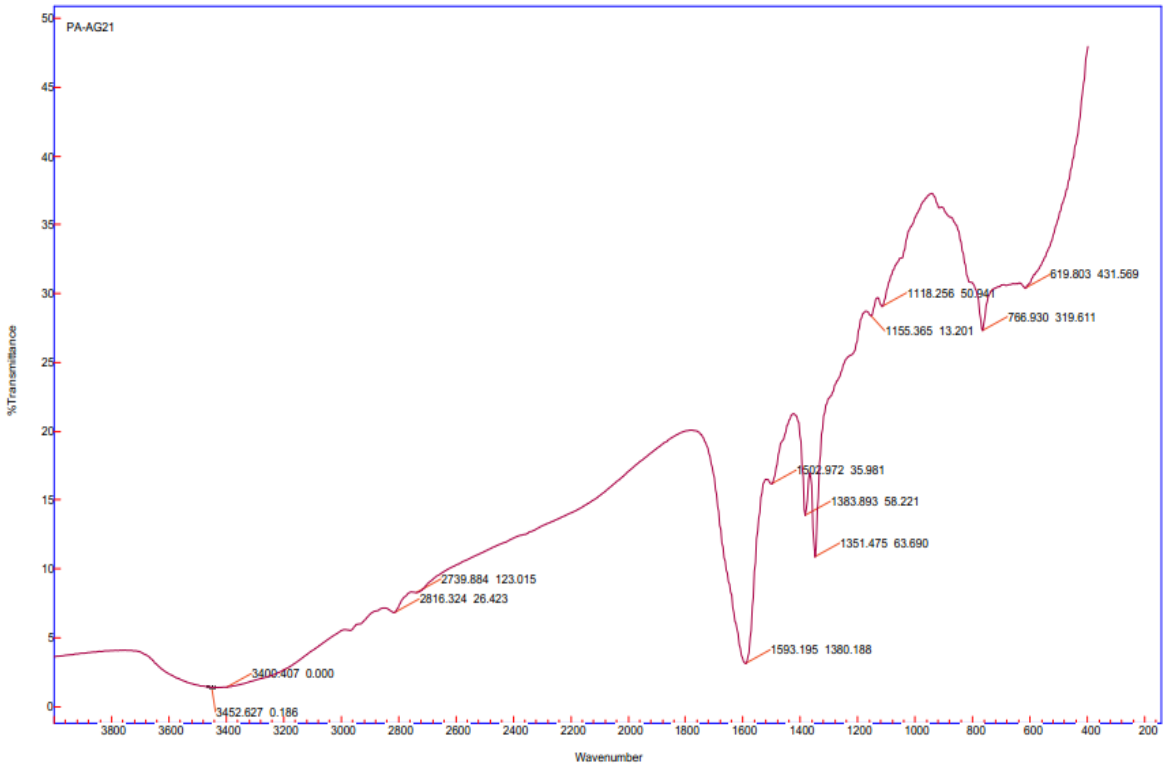

Fig 6.21: FTIR spectra of PA doped PEANI/Ag nanocomposite (Sample G)

Table 6.6: FT-IR absorption bands of PEANI/Ag nanocomposite using different dopant acids

	Sample E cm^{-1}	Sample F cm^{-1}	Sample G cm^{-1}
Quinoid	1594	1592	1593
Benzenoid	1498	1496	1502
C-H in-plane bending	1119	1113	1118
C-H out of plane bending	767	766	767
$C-N^+$ stretching vibration	1212	1214	1202
Paradisubstituted aromatic ring	850	813	816
C-H stretching of ethyl group	2817	2820	2816

The bands at 1594,1592,1593 cm^{-1} and 1498,1496,1502 cm^{-1} show the characteristic C=C stretching vibrations of the quinoid and benzenoid rings in the nanocomposites of PEANI/Ag doped with PTSA, SA & PA respectively. These peaks were observed at 1596, 1593, 1593 cm^{-1} and 1495, 1499, 1499 cm^{-1} for PEANI alone. The in-plane bending of C-H peaks in composites and PEANI were observed at 1119, 1113, 1118 cm^{-1} and 1119, 1107, 1114 cm^{-1}. The peaks at 775, 799, 766 cm^{-1} and 767, 766, 767 cm^{-1} are the characteristic to C-H out of plane bending in PEANI (Table 6.3) and its nanocomposites respectively. The peaks at 1200-1214 in the spectrum show the polaron structure of PEANI coming from $C-N^+$ stretching vibrations in the polymers as well as NCs. The region 800-850 cm^{-1} is characteristic of paradisubstituted aromatic rings indicating head to tail coupling of ethylaniline both in polymer and nanocomposite formation. The peaks due to C-H stretching vibration of the substituent ethyl group in the nanocomposites of PEANI/Ag doped with PTSA, SA, PA were observed at 2817,2820 and 2816 cm^{-1}(2-6).

The above results show that there is no structural change between PEANI alone and PEANI doped with Ag nanoparticles.

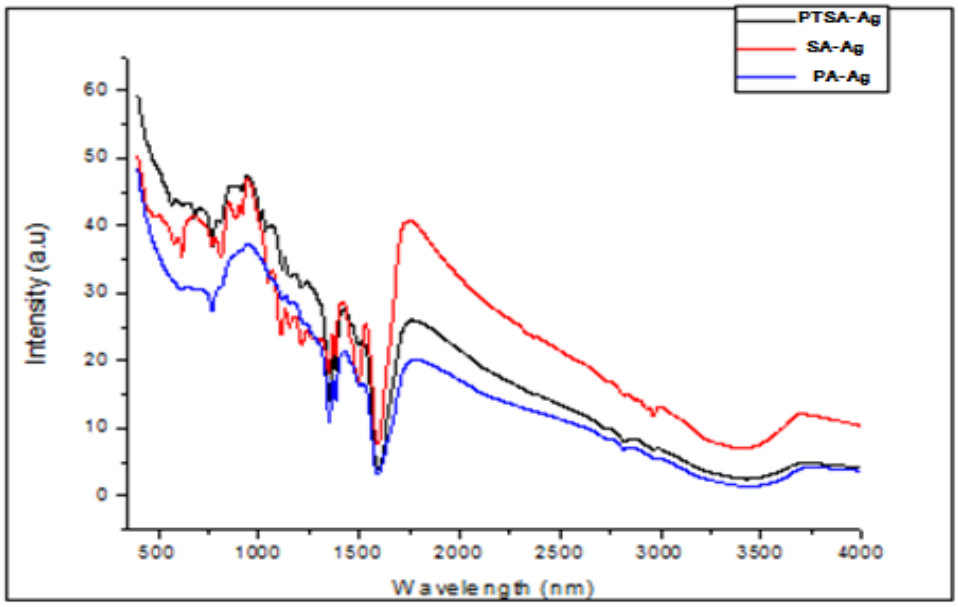

Fig 6.22: Overlay of FTIR spectra's of PEANI/Ag nanocomposites using different dopant acids (Sample E, F&G)

Thermal study (TGA-DSC Analysis):

The comparative thermal study of nanocomposites of PEANI/Ag (sample E,F&G) and PEANI polymers(sample A,B&C) was done. The analysis of thermograms from the figures 6.23 to 6.25 is given in table 6.7.

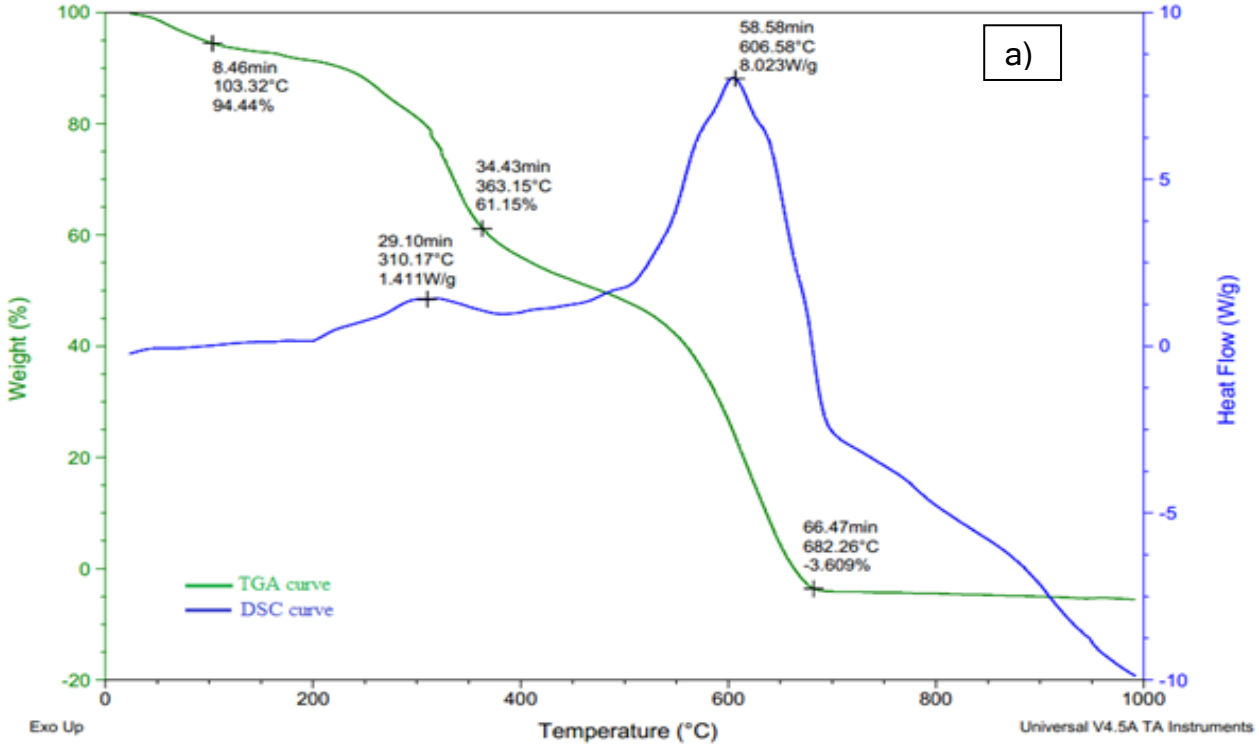

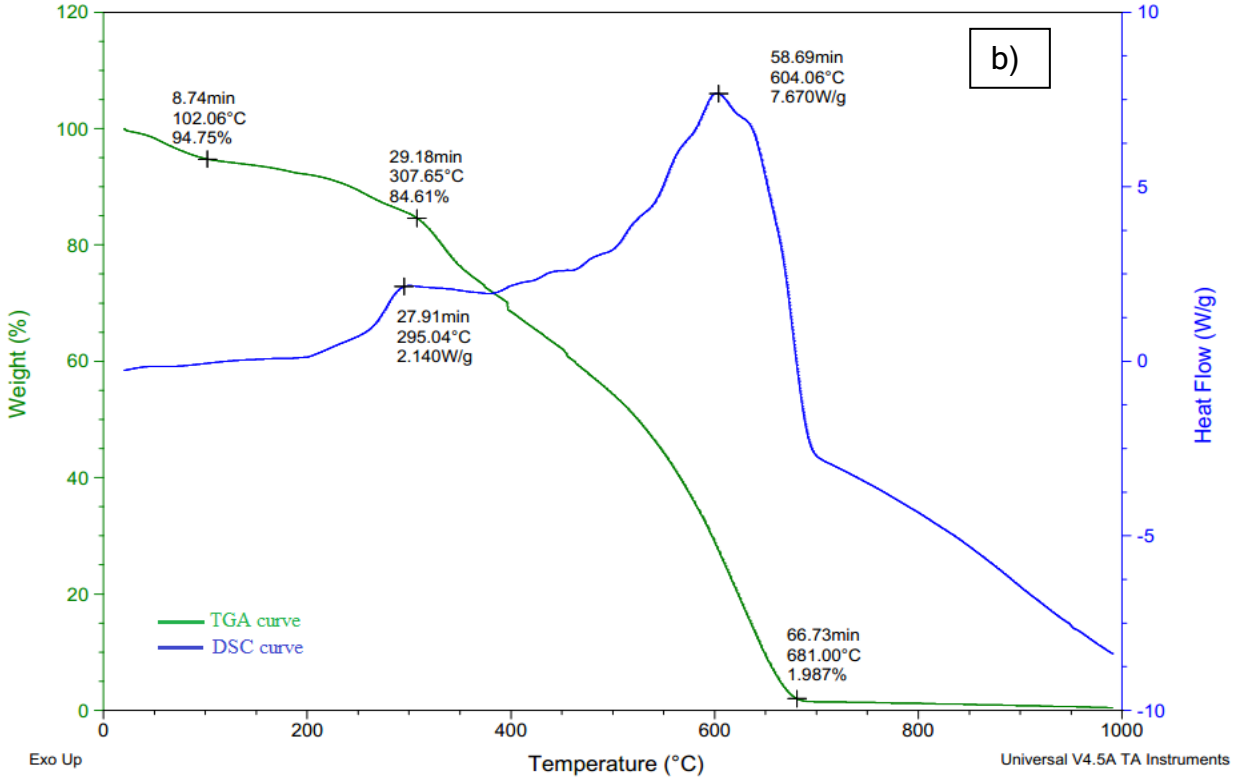

Fig 6.23: TGA/DSC thermogram of PTSA doped a) PEANI b) PEANI/Ag nanocomposite

PTSA doped PEANI and its nanocomposites with silver showed almost similar pattern for TGA as well as DSC studies. After the complete decomposition of polymer chains at 681°C, the residual amount of approximately 2 % retained is of silver nanoparticles entrapped within the polymer matrix. The study also shows that the presence of Ag NPs in the composites has not altered the thermal stability of the polymer. Moreover retention of moisture level in the polymer and its composite upto 110°C was similar.

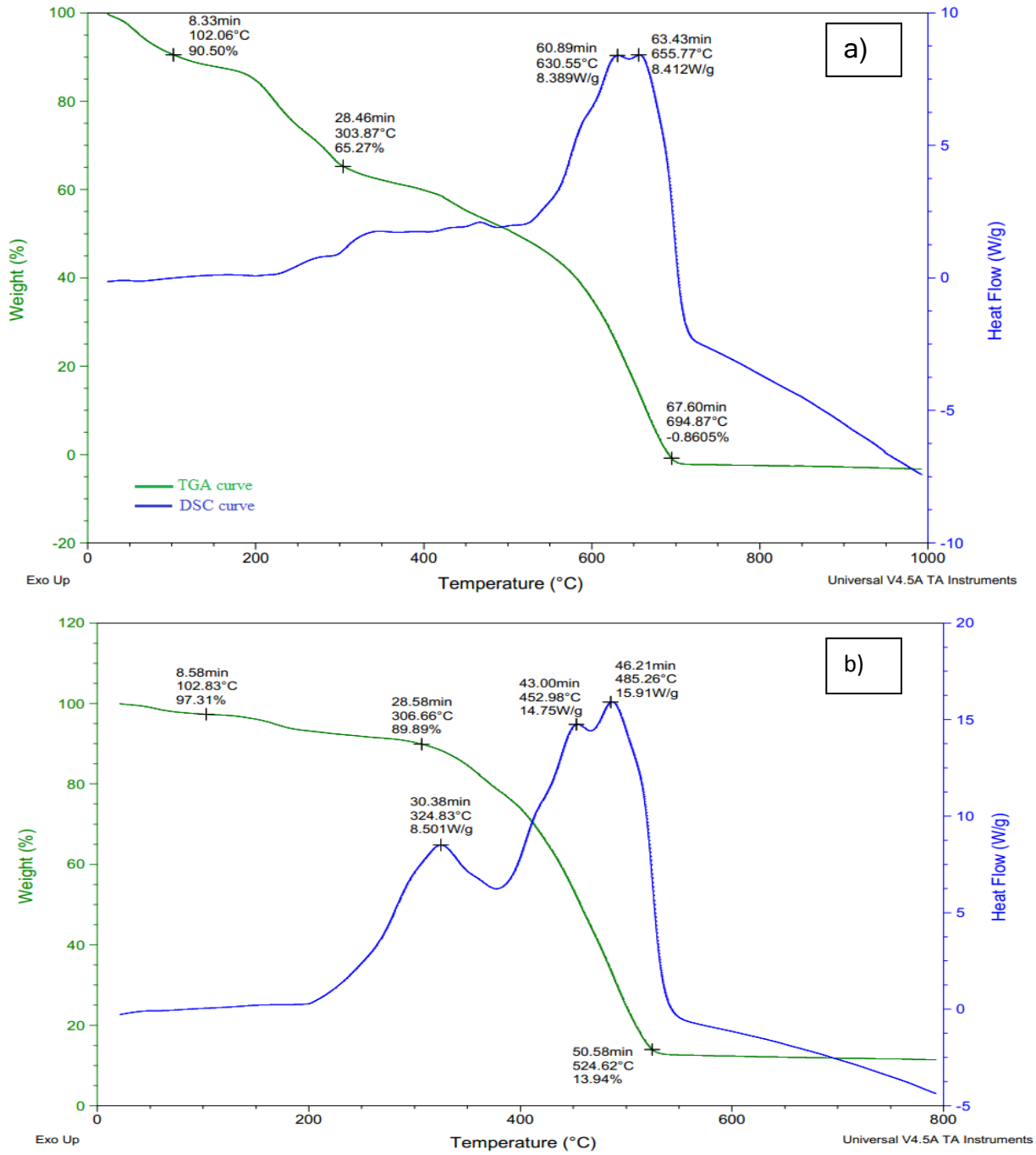

Fig 6.24: TGA/DSC thermogram of SA doped a) PEANI b) PEANI/Ag nanocomposite

This study shows that the composite doped with sulphuric acid has retained silver nanoparticles upto 13%, which is much higher than PTSA doped composite. Due to presence of large amount of silver NPs, the polymer network has weakened and decomposition of the composite is complete at 524.62°C showing that it is less stable than the parent polymer. In DSC plot, the first decomposition at 324.83°C is much sharper than that in the polymer, showing that small oligomers

may be formed where faster growth may be restricted by the presence of higher amount of Ag NPs.

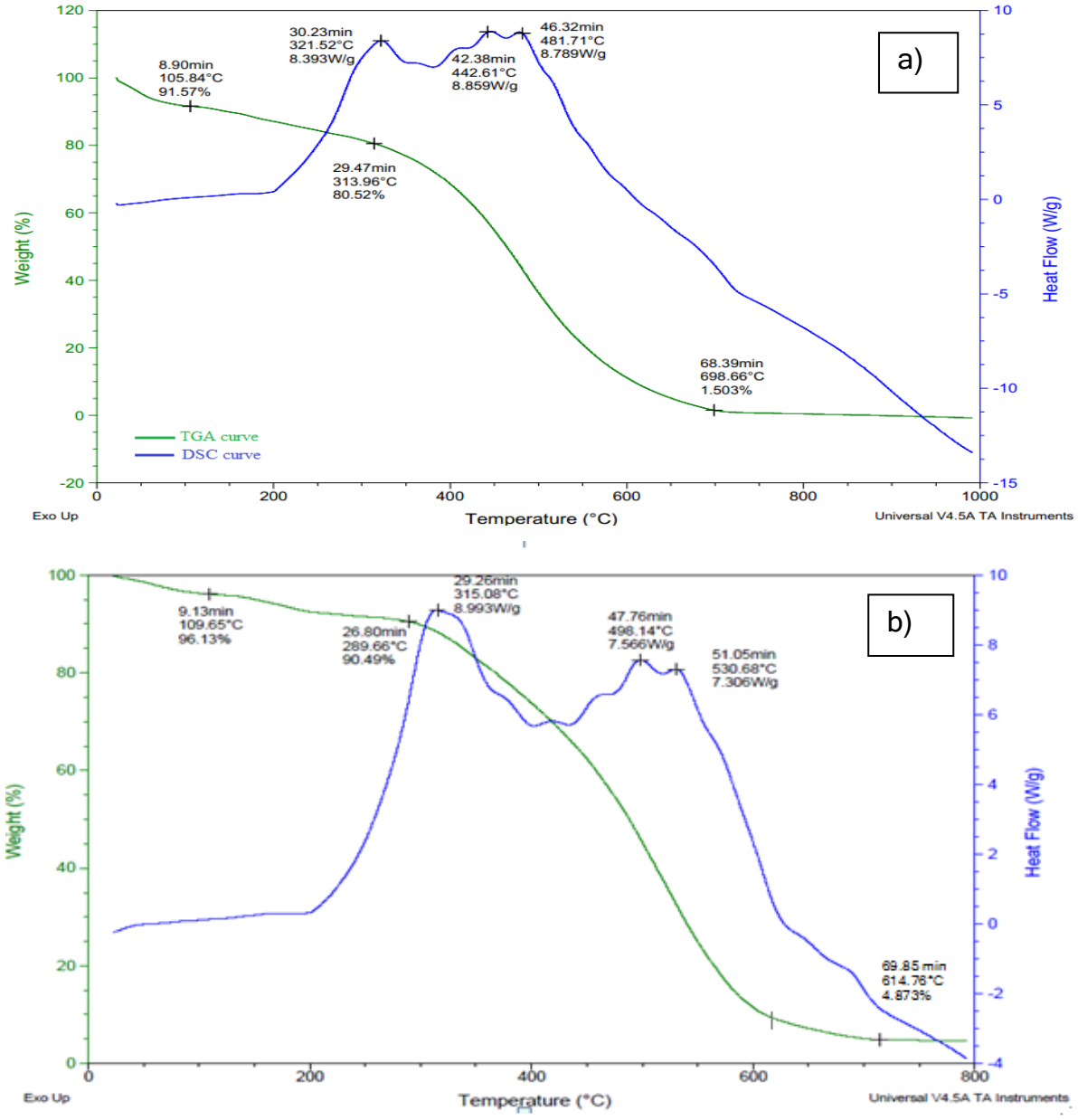

Fig 6.25: TGA/DSC thermogram of PA doped a) PEANI b) PEANI/Ag nanocomposite.

A similar pattern was seen in TGA and DSC plots of polymer alone and it's composite on doping with phosphoric acid. Around 5% silver nanoparticles were trapped in the composite polymer chains however; thermal stability has been somewhat lower than the PEANI polymer alone. The reason for the same may be large surface area of phosphate anions which increases the volume and weakens the bonding network of the polymer.

Table 6.7: TGA analysis of PEANI and PEANI/Ag nanocomposites

PEANI Polymers			
	1st step	2nd step	3rd step
SAMPLE B	103.32°C	363.15°C	682.26°C
SAMPLE C	102.06°C	303.87°C	694.87°C
SAMPLE D	105.84°C	313.96°C	698.66°C
PEANI/Ag Nanocomposites			
	1st step	2nd step	3rd step
SAMPLE E	102.06°C	307.65°C	681°C
SAMPLE F	102.83°C	306.66°C	524.62°C
SAMPLE G	101.83°C	331.89°C	614.76°C

From the study, we have concluded that PEANI/Ag nanocomposites exhibit a 3-step decomposition pattern similar to that of PEANI polymers. Secondly, PEANI doped polymers have a higher degradation temperature than PEANI/Ag NCs indicating that the presence of AgNPs have caused stress in the structure (7-10).

Electrical Characterisiation

The R.T. solid state current-voltage (I-V) scans made from -5V to +5V on pressed pellets using two-probe technique for PTSA and SA doped PEANI/Ag nanocomposites and are shown in figures 6.26 and 6.27:

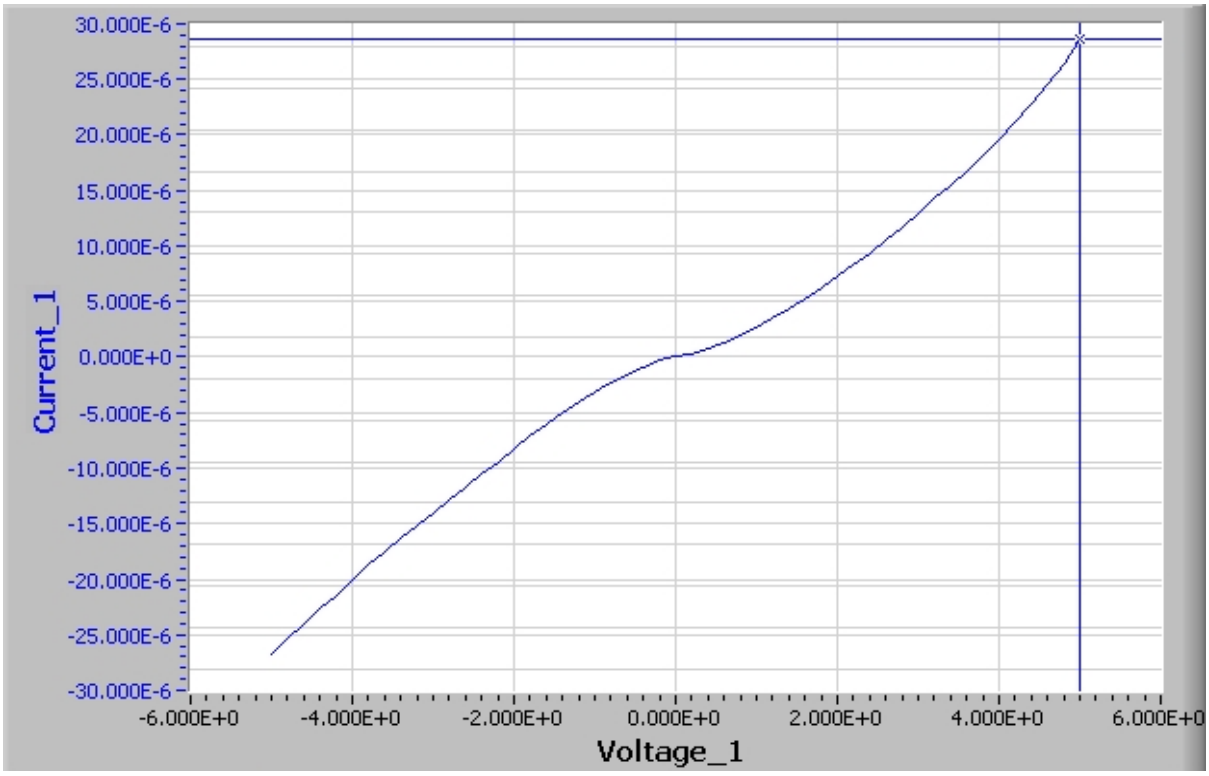

Fig 6.26: Characterstic I-V scan of PTSA doped PEANI/Ag nanocomposite.

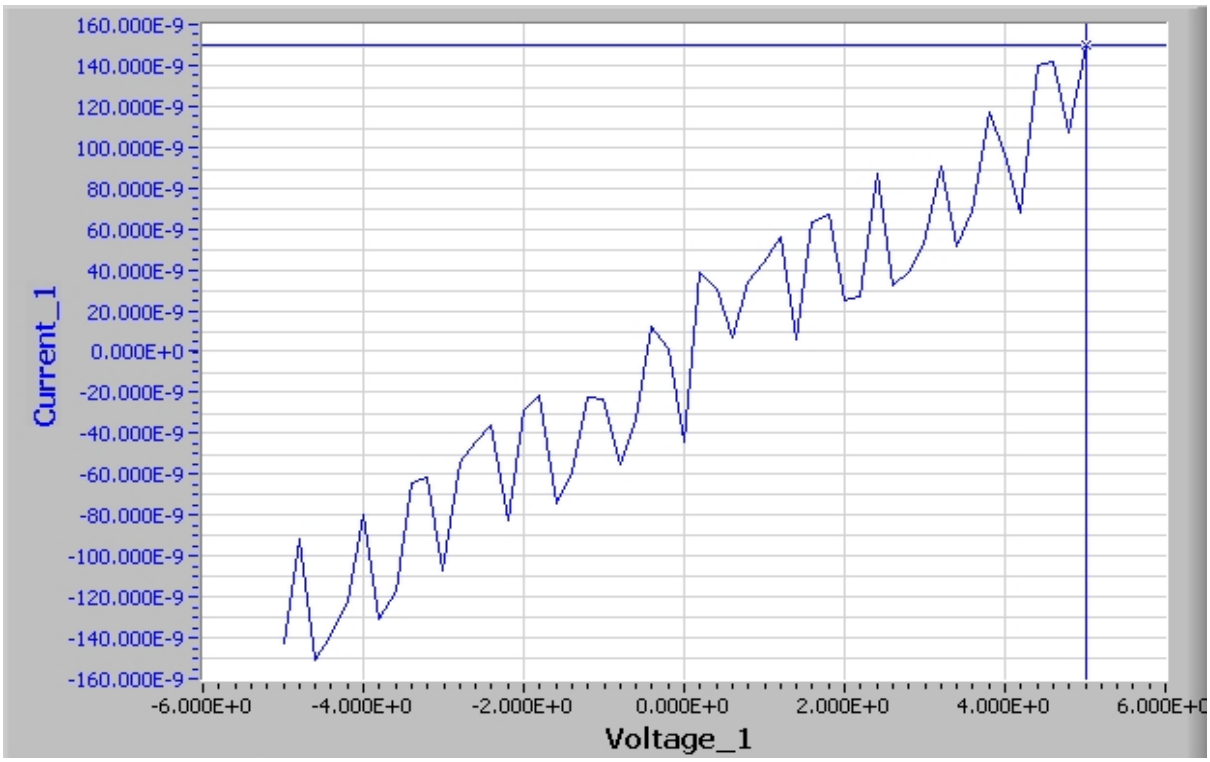

Fig 6.27: Characterstic I-V scan of SA doped PEANI/Ag nanocomposite.

The value of current for SA doped PEANI/Ag nanocomposite was observed of the order of 149nA. The value of current for PTSA doped PEANI/Ag nanocomposite was observed of the order of 28 μA and PA doped PEANI/Ag nanocomposite is almost insulating. An electrical resistance or conductivity of each nanocomposite was measured at room temperature using the two-point probe technique.

The conductivities of the prepared PEANI/Ag nanocomposites doped with PTSA and SA were 6.28 μS/cm and 33.3 x 10^{-3} μS/cm respectively. There is a drop in the conductance value of the composite in comparison to PEANI. However, in case of PANI/Metal nanocomposites, the conductivity value increases with the incorporation of metal NPs as compared to PANI alone. The reverse trend may due to the increase of the interchain distance and diluting effect of the charge carriers caused by the presence of bulky ethyl group present on the nitrogen atom in polyethylaniline. Consequently, the torsion angle between the repeat units is greater in substituted PANI (13-16). The same observation was seen for PEANI/Au nanocomposite which is explained in the next section.

Morphological Study (TEM Analysis):

The morphology of nanocomposites was studied from TEM images. Figure 6.28 (a to h) reveals the typical images of NCs as synthesized using different dopant acids.

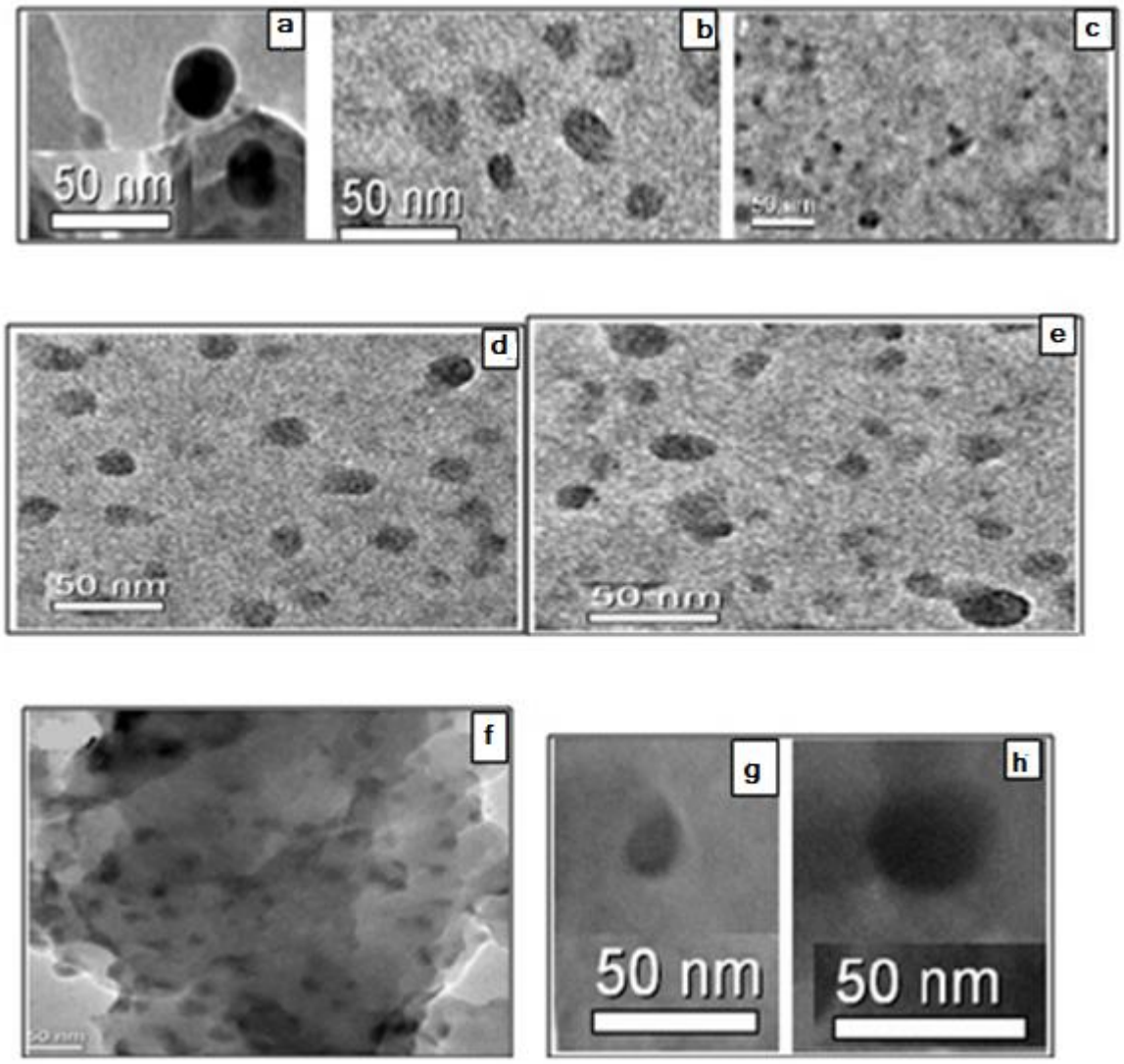

Fig 6.28: TEM micrographs of PTSA doped (a to c), SA doped (d-e), PA doped (f), PEANI/Ag nanocomposites, Indiviual particle of PTSA & SA (g-h) doped nanocomposite

It can be seen from the images that the dark spots correspond to Ag NPs while the light ones are PEANI. Most of the silver particles are not fully coated with PEANI but partly when radius is low. Consequently, there are dark lines or small spots appearing on the surface of PEANI particles. It is difficult to form perfect PEANI layers on the surface of AgNPs. On the contrary, PEANI appears to be forming irregular blocks which can be seen from the Fig 6.28 (f). It has been further confirmed that by increasing the amount of PEANI layer on the surface of AgNPs, it is easier to grow core-shell type of structure which can be seen in Fig 6.28 (g) and also clear from presentation in PEANI/Au NCs (section C). The size

of nanoparticles is less than 25nm, at some places with coating and some without coating.

6.6 CONCLUSION:

XRD and TEM studies confirm the incorporation of silver nanoparticles in composites.

Thermal study shows that as the amount of Ag NPs in the composite increases, stability decreases. In PTSA doped PEANI/Ag nanocomposite there is about 2% silver NPs, decomposition temperature remains unchanged whereas in case of phosphoric acid doped composite where Ag NPs are about 5%, it decreases by 80°C. However, if the content of Ag NPs is more than 10%, the decomposition goes down by 170°C in sulphuric acid doped nanocomposite.

In case of FTIR spectrual study of nanocomposites, finger prints of the polymer have been observed.

The electrical conductance of PEANI/Ag nanocomposite is different from that of PEANI polymer alone showing that they may not have similar behaviour towards electrical devices.

SYNTHESIS AND CHARACTERIZATION OF POLYETHYLANILINE/GOLD NANOCOMPOSITE

This part of the chapter comprises of synthesis and characterisation of polyethylaniline/gold nanocomposite using PTSA as dopant acid. The study was conducted with the addition of APS as oxidising agent for monomer and hydrazine hydrate as reducing agent for metal ions.

6.7 Synthesis of PEANI/Au Nanocomposite:

A representative procedure for the preparation of the PEANI/Au nanocomposite is as follows: To a glass beaker added a mixture (1mL of ethylaniline dissolved in 5mL of ethanol) in 25mL of 0.25M PTSA solution already placed in ice-bath. To this solution, 0.2g of PVP and 25mL of 0.025M chloroauric acid solution was added with constant stirring to make a uniform reaction mixture. Then, simultaneously added 5g of ammonium peroxydisulphate dissolved in 10mL of DI water along with 2mL of hydrazine hydrate with constant stirring. The reaction mixture was vigorously magneto-stirred for 1 hour maintaining ice bath temperature. The reaction product was allowed to stand for 24 hours at about 10°C. The green colored residue formed was separated by centrifugation, washed with DI water and ethanol and vacuum dried at about 60°C.

6.8 Results and Discussion:

Structural Study (X-Ray Diffraction Analysis):

The X-rays diffractograms of both PEANI and PEANIAuNPs composite is shown in Fig 6.29 a, b.

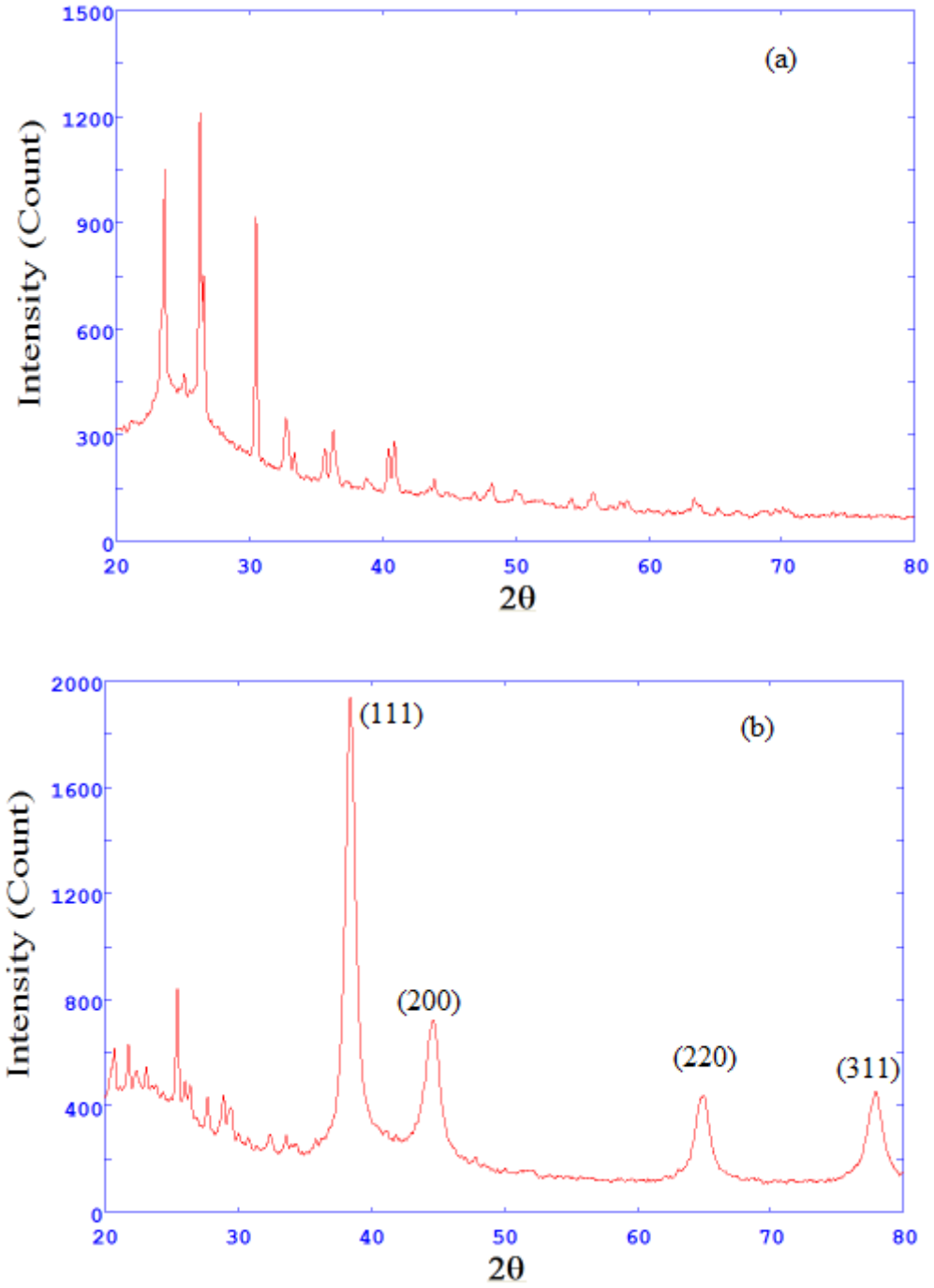

Fig 6.29: XRD patterns of a) PEANI, b) PEANI-AuNPs composite

As one can easily observe large X-rays peaks indicate that the PEANI is rather amorphous with a certain degree of crystallinity. The diffraction pattern is similar to that obtained by Andreia et al. The XRD of PEANI-AuNPs composite confirms the incorpration of AuNPs in composite. The composite of PEANI-AuNPs shows new diffraction peaks appear at 38.45°, 44.69°, 64.99°, 77.88° corresponds to Bragg's reflections from (111, 200, 220, 311) planes of gold in nanocomposite.

These diffraction peaks corresponds to fcc metallic gold. However, the diffraction peaks were broadened in contrast to bulk due to the surrounding environment of polymer chains. Using Scherrer equation, estimated size of AuNPs was found to be approximately 15 nm. In the nanocomposite, the PEANI also appears in a manner having low intensity indicating that the AuNPs have occupied significant space within the composite.

FTIR spectral study of PTSA doped PEANI/Au Nanocomposite

For FTIR spectrum, KBr dry powder was mixed with a test sample for making pellet for analysis. The infrared spectra of the PEANI and its composite with AuNPs are shown in Figure 6.30 a, b.

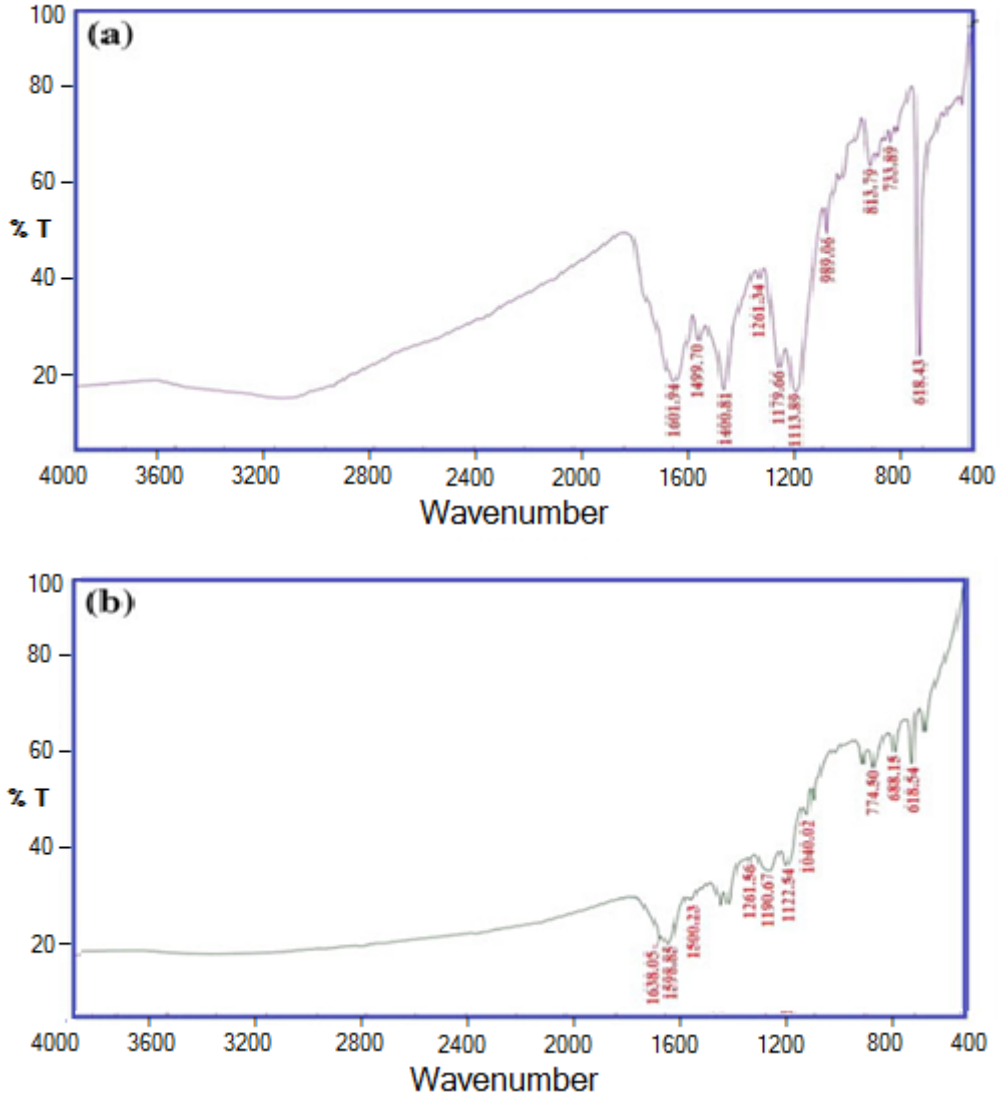

Fig 6.30: FTIR spectra of a) PEANI b) PEANI-AuNPs composite

The ring stretching (C=C stretching) of quionoid (N=Q=N) and benzenoid (N-B-N) forms were observed at 1601.94 and 1499.7 cm^{-1} in PEANI alone and at 1598.85 and 1500.23 cm^{-1} in composite of PEANI – AuNPs which are similar to absorption patterns in polyaniline. The strong absorption starting at 1600 cm^{-1} and extending to the near IR region shows the presence of free carriers in the polymer. The peaks at 1113.89 and 733.89, and 1122.54 and 774.5 cm^{-1} are the characteristic to C-H in plane bending and C-H out of plane bending in PEANI and composite respectively. The peak at 1,261 cm^{-1} in the spectrum shows the polaron structure of PEANI coming from C-N^{+} stretching vibration in the polymer as well as composite. The peaks from 813 cm^{-1} (2-substituted phenyl ring) indicating that the monomer units were linked to para position of the ring and a head to tail coupling of 2-ethylaniline occurred during the polymerization. The absorption band at 618 cm^{-1} is assigned to quinine diimine moieties. An absorption peak in nanocopmosite is at 1,638 cm^{-1} is of carbonyl (C=O) of PVP, however a shift in peak position from 1,661 cm^{-1} (PVP alone) to 1,638 cm^{-1} indicating a strong interaction of PVP with AuNPs present in polymer matrix. The study shows a slight shift in some of the peaks in composite over PEANI due to AuNPs in it (2-6).

Morphological Study (TEM Analysis):

Figure 6.31 reveals the typical TEM images of AuNPs-PEANI composite.

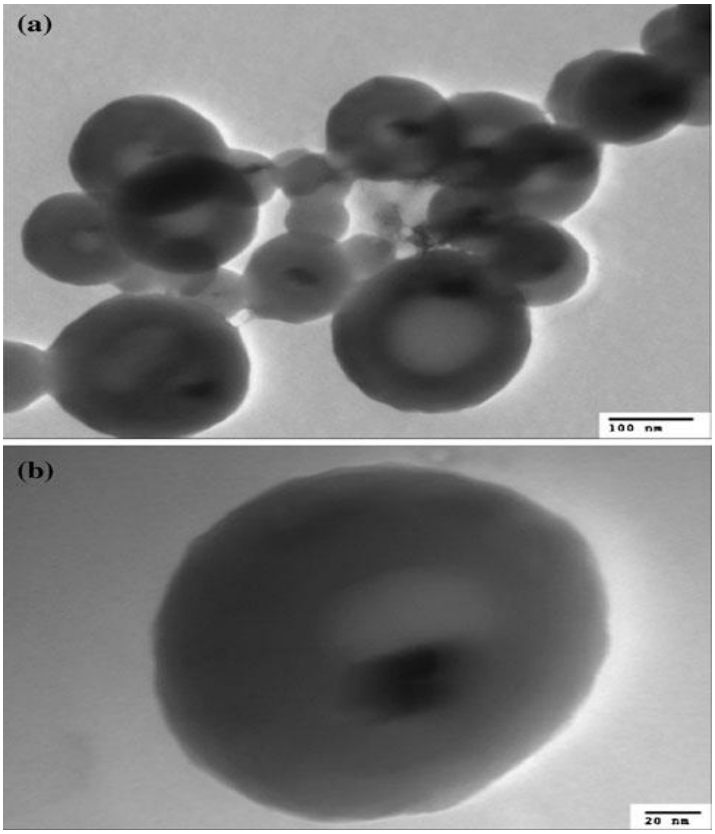

Fig 6.31: TEM micrographs of a) PEANI-AuNPs composite, b) Single core-shell particle

A close look into the the TEM micrograph indicates the formation of PEANI-Au core shell nanostructure with embedded AuNPs distinguishable by a dark core of AuNP surrounded by a white black shell of PEANI. However in some places overlapping of PEANI was observed resulting in dark spots due to continuous polymerization of PEANI over a period of time whereas formation of AuNPs is quick resulting in slow deposition of PEANI and bridges each other. The diameter of the shell varies from 20 to 150 nm.

Thermal study (TGA-DSC Analysis):

The thermal stability of polymers and their composites are very important for film formation and processability. The TGA-DSC curves of PEANI and PEANI-AuNPs composite are shown in Fig 6.32 a, b.

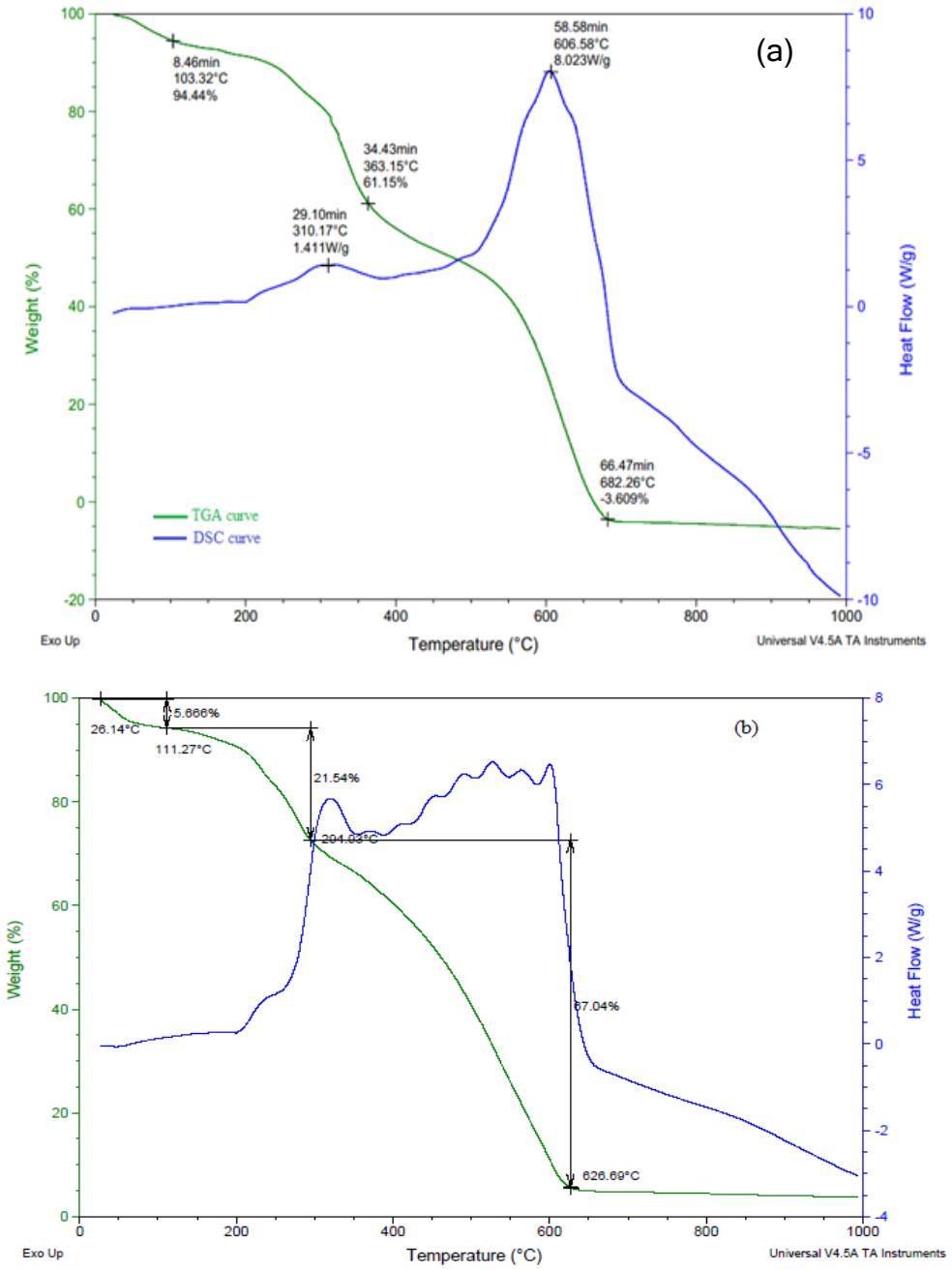

Fig 6.32: TGA-DSC thermogram of a) PEANI, b) PEANI-AuNPs composite

TGA of PEANI shows initial weight loss of 5.6 % up to 103.2 °C is due to the presence of moisture in PEANI. Second weight loss (from 103 to 363 °C) is due to the rearrangement or cross-linking, which involves bond cleavage or new bond formation. The complete decomposition of the polymer is around 682°C indicating that it is highly stable than aniline which completely decomposes around 600 °C. In the PEANIAuNPs composite, initial weight loss of 5.64 % is due to moisture and second weight loss is due to the decomposition of oligomers.

The composite completely decomposes at 626.6°C where polymer decomposes into moieties. The left out residue which is around 5 % was AuNPs. The decomposition of the polymer in the composite was lowered by 56 °C indicating that the presence of AuNPs has weakened the chain structure of polymer or caused stress in the structure. The DSC curve for PEANI shows one large and one small peak at 310.17 and 606.58 °C respectively. Though in our earlier reported results the decomposition temperature was observed around 800°C for PTSA doped PEANI polymer however on further study it was found to be 682°C which may be due to some impurities retained in the polymer during synthesis (17).

These processes are not glass transition because no second transition was seen in the rearrangement which involves the breaking of oligomers and new bond formation. This result may be due to the hydrophobic character of the ethyl substituents in the benzene rings. As the DSC curve of PEANI-AuNPs composite shows no exothermic peak indicating that the presence of AuNPs restricts the formation of oligomers and also may have acted as catalyst in the polymerization process (7-10).

Electrical characterisation

An electrical conduction phenomenon in conducting polymer depends on at least three factors contributing to the charge carriers mobility viz. single chain or intramolecular transport, inter-chain or between chain transport and inter particle contact. Current-voltage (I-V) scans were made from -5 V to 5 V for PEANI and PEANI/AuNPs composite as shown in Fig 6.33.

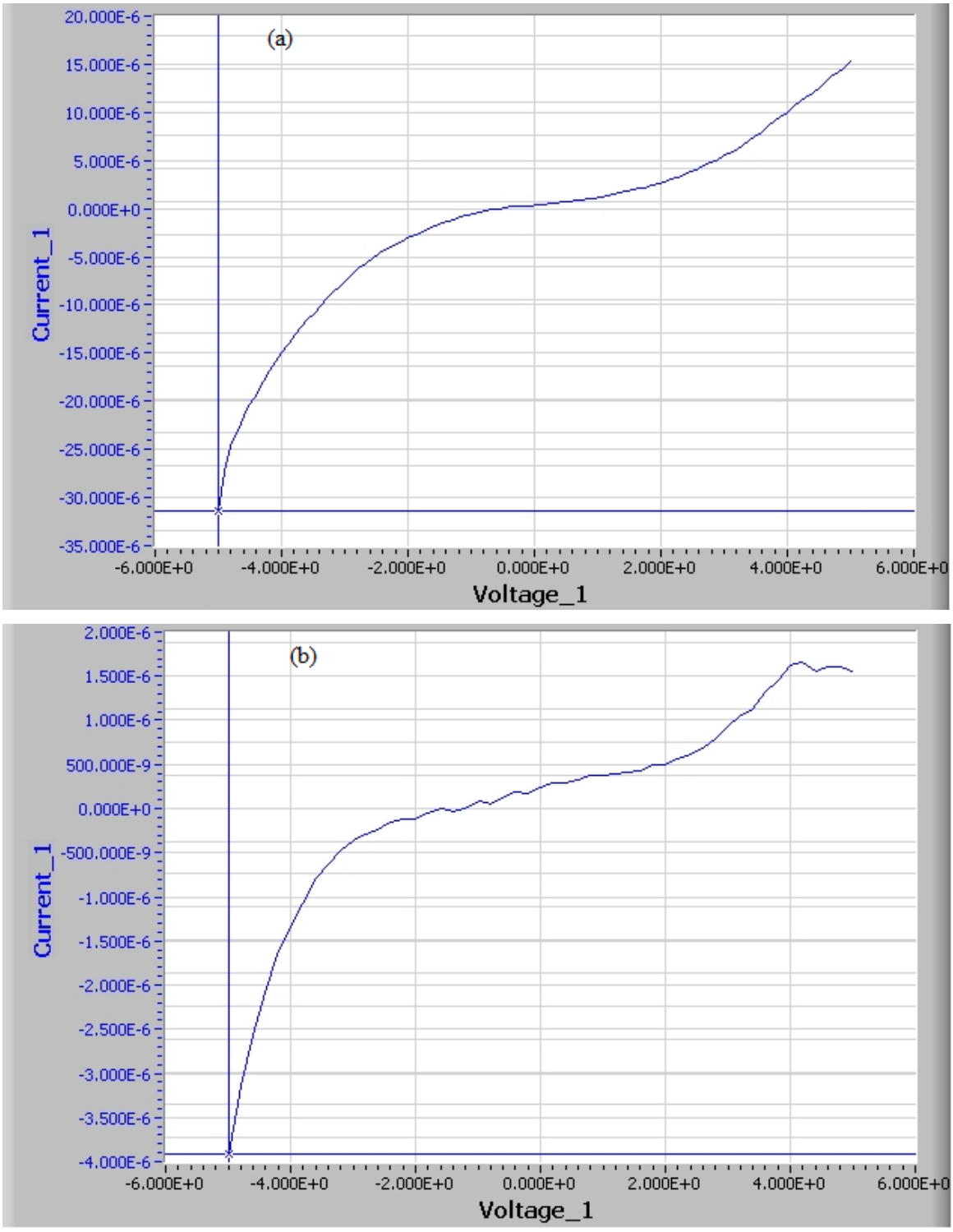

Fig 6.33: Characteristic I-V scans of a) PEANI b) PEANI/Au nanocomposite

The value of current for PEANI was observed of the order of μA. However in case of PEANI-AuNPs composite a drop of 10-15 % in current is observed indicating that the conductivity of composite has reduced in comparison to PEANI. Usually it has been reported that in the case of polyaniline/AuNPs composite the conductivity increases with the incorporation of AuNPs, but here

we got the reverse trend. The reason may be the steric effect of ethyl group that produces an increase in the torsion angle between the phenyl rings or due to low concentration of AuNPs as they are dispersed apart as seen in TEM image, as such they could not be able to participate in the conduction process.

6.9 CONCLUSION:

The structural confirmation of the synthesised PEANI/Au nanocomposite was sought by FTIR analysis. The presence of two bands in the vicinity of 1500 and 1600 cm^{-1} clearly showed that composite was composed of the amine and imine units, characteristic modes of polyaniline backbone. The data also suggested that electron-donating effect of ethyl substituent plays an important role.

The large peak in the X-ray diffractogram of PEANI indicates that PEANI shows a certain degree of crystallinity rather it is amorphous; however, PEANI-AuNPs composite shows more crystallinity and appears more ordered than PEANI alone.

TEM images showed the formation of core-shell nanocomposite having AuNPs of nearly 15nm as core surrounded by polymer shell.

TGA results showed that PEANI is more stable than polyaniline. As the PEANI-AuNPs composite decomposes at 622.6 °C as compared to PEANI which decomposes at 682.2°C indicating that the incorporation of AuNPs weakens the chain structure of polymer or causes stress. DSC results suggest that the presence of AuNPs restrict the formation of oligomers.

From the I-V studies it was found that conductance showed 10 % drop on addition of AuNPs, which may be due to steric effect or AuNPs presence at places distinct from each other. The AuNPs may act both as catalyst as well as filler in the process of polymerization.

REFERENCES:

1. A.L.Schemid, S.I.Cordoba de Torresi, A.N.Bassetto, I.A.Carlos, J.Braz.Chem. Soc. 11,317,2000
2. S.Vohra, M.Kumar, S.K.Mittal, M.L.Singla, J.Mater. Sci:Mater.Electron. DOI:10.1007/s10854-012-0933-0
3. A.Drury, S.Chaure, M.Kroll, V.Nicolosi, N.Chaure, W.J.Blau, Chem.Mater. 19,4252,2007
4. N.V.Natalia, J.Stejskal, M.Trchova, J.Prokes, M.Omastova, Eur.Polym.J. 43,233,2007
5. D.Anakli, S.Cetinkaya, Curr.Appl.Phys. 10,401,2010
6. X.G.Li, H.J.Zhou, M.R.Huang, J.Polymer Sci.A :Polymer Chemistry 42,6109-6124,2004
7. M.L.Singla, S.Awasthi, A.Srivastava, D.V.S.Jain, Sens.& Actuators A 136, 604,2007
8. K.Mazid, S.Awasthi, M.L.Singla, Sens.& Actuators A 135,113,2007
9. P.C.Painter, M.M.Coleman, Fundamentals of Polymer Science. Technomics, Lancaster, PA, 284,1997
10. S.Wang, Z.Tan, Y.Li, L.Sun, T.Zhang, Thermochim. Acta 441,191, 2006
11. J.Vivekanandan, V.Ponnussamy, A.Mahudeswaran, P.S.Vijayanand, Arch.Appl.Sci.Res. 3(6),147-153,2011
12. R.A.Misra, S.Dubey, B.M.Prasad, D.Singh, Indian Journal of Chemistry 38A, 141-149, 1999
13. H.Yin, J.Yang, Macromol.Mater.Eng. 297,203,2012
14. D.S.Lin, S.M.Yang, J.App.Polym.Sci. 98,1198,2005
15. Milind V.Kulkarni and Annamraju Kasi Viswanath, Polym.Eng.Sci. 47,1621-1629,2007
16. R.Shenhar, T.B.Norsten, V.Rotello, Adv.Mater. 17,657-669, 2005
17. S.Vohra, Narinder Singh,Susheel Mittal, M.L.Singla, J.Mater.Sci:Mater.Electron. DOI 10.1007/s 10854-013-1156-8

SUMMARY

The mixing of polymer and nanoscale inorganic particles has been recognized as a potential and economic method of producing new materials with better mechanical, electrical, optical and electrochemical behaviour and also with new functions. The present work reports the synthesis of such materials with reference to PANI & PEANI as conducting polymers and gold and silver as metal nanoparticles.

The first part of the thesis (Ch-4) describes synthesis of gold and silver nanoparticles by various methods and their characterisation for morphological, structural & optical properties.

Gold nanoparticles were synthesised using different reducing and capping agents. These reagents and their respective ratios helped in controlling size, shape and distribution of nanoparticles. Gold nanoparticles prepared by PVP as capping agent were smaller in size than those obtained with CTAB as capping agent. Due to small size, PVP capped gold nanoparticles can be used for medical applications like cancer treatment whereas CTAB capped gold nanoparticles can be used in optoelectronic devices. The size of the seed particles was 3-5 nm whereas AuNPs formed were having size varying from 10-25 nm depending upon the process of synthesis. Gold nanorods were also prepared by the seed growth process. The aspect ratio of gold nanorods can be controlled by varying the amount of gold nanoparticles seeds with respect to the gold precursor. The yield of nanorods obtained was about 7%. Hence high yield methods of nanorods synthesis should be worked out. The optical studies showed enhanced Surface Plasmon Resonance with nanorods as compared to nanoparticles which is due to scattering of light along short axis and long axis of the nanorods.

Silver nanoparticles (AgNPs) were synthesised by reducing silver ions using $NaBH_4$/ethylene glycol (reducing agents) in presence of PVP (capping agent). The size of AgNPs was less than 10 nm or more than 10 nm depending upon the reduction time and temperature. The prepared nanoparticles were characterised for their morphological, optical and structural properties.

The UV-vis spectra showed SPR band at about 430nm, which is considered to be the primary signature of AgNPs formation. The spectrum as a function of time was also recorded which showed rise in intensity without any change in the peak position. TEM analysis confirmed that the produced AgNPs were spherical in shape with diameter of 20-30 nm. The crystalline structure was investigated by XRD analysis. The obtained diffraction peaks indicated that the synthesised AgNPs were crystallised in fcc symmetry. The mean crystallite size calculated by Debye-Scherrer's equation was 25nm (Method A) and 38nm (Method B) respectively, which is comparable with the particle size as obtained from TEM analysis.

The next part of the thesis (Ch-5) is about synthesis and characterisation of PANI and its nanocomposites. PANI was synthesised in HCl medium using H_2O_2 for polymerisation and in the presence of $FeCl_2$ as a catalyst. PANI/Au and PANI/Ag nanocomposite were synthesised by simultaneous oxidative polymerisation of aniline and reduction of metal salt to form metal nanoparticles. These nanocomposites were characterised by FTIR, UV, TEM, SEM, XRD, TGA and the results were compared with polyaniline.

The characteristic FTIR peaks of PANI were found to shift to higher wave numbers in PANI/metal nanocomposites, indicating the interaction between polymer chains and metal nanoparticles. The TGA studies showed the greater thermal stability of the composites than PANI alone. The XRD pattern of the composites also showed the presence of metal nanoparticles with the polymer chains. The characteristic diffraction peaks of gold and silver in the diffractograms of PANI/Au nanocomposite and PANI/Ag nanocomposite respectively, confirmed the incorporation of metal nanoparticles in the polymer matrices.

The thin films of PANI and its composites were synthesised by spin coating method. The composites exhibited higher conductivity than PANI. It has been possible to cast the thin film of this material on ITO surface, which may find applications in switching devices, semiconductors and sensors.

In another study, nanocomposites of PANI/AgCl were synthesised by chemical polymerisation/precipitation in aqueous HCl solution using both aniline monomer

and $AgNO_3$ precursors in different molar ratios in PVP. The composite possesses improved stability than individual constituents, as PVP capped AgCl nanoparticles are acting nanofillers within polymer chains showing higher compactness in the polymer matrix. The electrical conductance values of the composite materials depend upon the AgCl nanoparticles level present in the composite, however when its level was more than 30% a reverse trend was found. Thus a new composite material can be synthesised with PANI and AgCl nanoparticles with different thermal and electrical behaviour. These composites can be used as semiconductor material and for building sensor array for measurement of conductance or impedance changes in complex beverages & drinks for the interpretation of physical and chemical behaviour following soft computing techniques.

A detailed study of new class of conducting polymers i.e. poly (2-ethylaniline) & its composites with silver & gold nanoparticles have been explained in Chapter 6. PEANI was prepared by oxidative polymerisation of 2-ethylaniline with different dopant acids (sulphuric acid, o-phosphoric acid, p-toluene sulphonic acid, hydrochloric acid). PEANI/Ag nanocomposites (using PTSA, SA, and PA dopant acid) and PEANI/Au nanocomposite (with PTSA as dopant acid) were prepared via in situ chemical synthesis route (simultaneous polymerisation and precipitation). The structural confirmation of the synthesised PEANI polymer was sought by FTIR. The strong absorption starting at 1600cm^{-1} and extending to the near-IR can be attributed to the presence of free carriers in the bulk polymer. The FTIR data of each composite indicated that the reduction of metal precursor occurs at the expense of the polymer. Thus the polymer is more oxidised in composite relative to polymer alone. In addition, bands associated with the nitrogen functional groups in the polymer shifted to higher energy, are consistent with the intrinsic linkage of the polymer and metal and an increase in the oxidation state of the polymer. XRD analysis of PEANI polymers indicated that the material is rather amorphous with a certain degree of crystallinity. Further XRD of nanocomposites confirms the incorporation of metal NPs in it. A more clear view of incorporation of nanoparticles was confirmed from TEM studies.

From the I-V studies, it was found that conductivity decreased on addition of metal nanoparticles. The nanoparticles may have acted as catalyst as well as

filler in the process of polymerisation. However, PEANI/metal nanocomposites maintain the conductivity of the polymer regardless of increasing oxidation state. The formation of PEANI/metal composites also influences the polymer thermal properties as the oxidation state increased. For example, the thermal, degradation of PEANI/metal nanocomposites started at lower temperatures as compared to PEANI polymer alone showing that composite is thermally less stable.But PEANI and its composite with metal NPs is thermally more stable than PANI.

In short, it is concluded that the results of synthesising the above said nanoparticles and nanocomposites suggest that they could be useful for several applications like semiconductor devices, coating, catalysis and many more with lot of scope in future study.

FUTURE SCOPE:

In my opinion there is a lot of further scope of future study in the areas covered in this thesis. The mechanism for increasing the conductivity in polyethylaniline (PEANI) by doping can be further studied. It may also be possible to enhance the conductivity of the PEANI/metal nanocomposite by increasing the concentration of noble metal nanoparticles. The nanocomposites can be grown with nanoparticles having different surfactants on their surface which will produce variable bio-devices. PANI & PEANI can be doped with carbon nanotubes to alter the conductance for semiconductor devices. In place of ethyl group, other hydrocarbons can be attached to make the polymer soluble in aqueous medium. Their composites with metals/metal oxides/metal chlorides can be synthesised. Number of thin films of differnt thickness can be grown and adsorption behaviour towards humidity sensors can be worked out. The study about the mechanical properties of PANI & PEANI composites is another important aspect for future scope of wrok.

LIST OF PUBLICATIONS

A: Publications in International Journals

1) Thermal and electrical behaviour of silver chloride/polyaniline nanocomposite synthesised in aqueous medium using hydrogen peroxide.
   Sujata Vohra, Manish Kumar, Susheel Mital, M. L. Singla
   Journal of Materials Science: Materials in Electronics DOI 10.1007/s10854-012-0933-0

2) Thermal stability and electrical characteristics of poly (2-ethyleaniline) -Au nanocomposite.
   Sujata Vohra, Narinder Singh, Susheel Mital, M.L. Singla
   Journal of Materials Science: Materials in Electronics DOI 10.1007/s10854-013-1156-8

B: Results Reported in Conferences

1) National Conference on Recent Trends in Material Science Research held on 3-5 September 2012 at NIT, Srinagar
   Topic: Synthesiss and Characterization of Gold/PANI Nanocomposite using Hydrogen peroxide

2) National Conference on Recent Trends in Material Science Research held on 3-5 September 2012 at NIT, Srinagar
   Topic: Synthesis of PANI/AgCl Nanoparticles Hyprid Molecule & its Thermal and Electric Behaviour

3) International Conference on Nano Sensors & Technology (ICNST) held on 28-30 October, 2010 at CSIO, Chandigarh
   Topic: Synthesis and Characterization of Gold and Silver Nanoparticles by Reduction Technique.